A RISK ANALYSIS METHODOLOGY FOR MICRO/NANO MANUFACTURING

YING KIT TANG

A thesis submitted in partial fulfilment of the requirements of the

University of Greenwich

for the Degree of Doctor of Philosophy

February 2012

DECLARATION

I certify that this work has not been accepted in substance for any degree, and is not concurrently being submitted for any degree other than that of Doctor of Philosophy being studied at the University of Greenwich. I also declare that this work is the result of my own investigations except where otherwise identified by references and that I have not plagiarised another's work.

_____

Ying Kit Tang
(Student)

_____

Prof. Chris Bailey
(Supervisor)

_____

Dr. Stoyan Stoyanov
(Supervisor)

ACKNOWLEDGEMENTS

ABSTRACT

This research concerns the development of a risk analysis and mitigation methodology for assessing the impact of uncertainties and complexity of the design requirements arising in new process and product developments in micro and nano manufacturing. The risk analysis methodology integrates different computational approaches for process and product analysis, including the reduced order modelling using design of experiments, risk analysis using sampling-based and analytical methods and optimisation techniques. The integrated risk analysis and optimisation methodology is applied to two applications: (1) the FIB sputtering process control, and (2) a flip chip design. Three different FIB processes using different ion sources were investigated in order to evaluate their process performance with respects to different process parameter uncertainties. A critical comparison of the process capability against the specification limits of different processes was studied.

As parts of the research, a new modified computational model is developed for a material sputtering process using focused ion beam (FIB). This model allows the analysis of micro- and nano-structures shape with the FIB machine controlled through multiple beam scans and different beam overlapping. The FIB model related studies also address the modelling requirements for including material re-deposition effects that occur during FIB milling. The model has been validated using an experimental test case. Good agreement is observed between the analytical shape using the model and the actual experiment. The validated model enhances the accuracy of the dwell time prediction. This approach overcomes the dependence of a trial-and-error approach of the process control in nano-manufacturing industry.

The proposed methodology is also used to address a design problem of a flip chip design. A novel method for the evaluation of the environmental impact of the flip chip design in a multi-disciplinary optimisation problem is proposed. The goal is to address materials constraints due to environmental regulations and to handle different types of requirements such as the reliability and cost. An optimal flip chip design reliability function is identified. The approach allows electronics manufacturers to consider the environmental impact amongst different design alternatives at an early stage of the design of the product before any real prototyping in order to reduce the total manufacturing life cycle.

PUBLICATIONS

Nine conference papers have been disseminated to cover the three focused researched areas mentioned above with associated findings and results.

Published Year	Authors and Paper Title
2008 Sep (Chapter 3, 5, 6)	Y. K. Tang, N. Sailesh, ''Risk Mitigation Framework for a Robust Design Process'', The 2nd Electronics System-Integration Technology Conference, 1-4 Sept 2008, London, UK
2008 Sep (Chapter 5)	Y.K. Tang, ''Risk Analysis and optimisation for models in Advanced Micro-system Electronics Manufacturing'', The 2nd Electronics System-Integration Technology Conference, 1-4 Sept 2008, London, UK
2008 May (Chapter 5, 6)	Y.K. Tang, ''Optimisation Methodology for Risk Mitigation in Advanced Micro-system Electronics Manufacturing'', International Conference on Engineering Optimization, 1-5 Jun 2008, Rio de Janeiro, Brazil
2006 Dec (Chapter 7)	Y.K. Tang, Decision Support Systems for Eco-friendly Electronic Product, The 8th International Conference on Electronic Materials and Packaging, Dec 2006, Hong Kong
2010 Apr (Chapter 5)	S. Stoyanov, Y.K. Tang, C. Bailey, R. Evans, S. Marson, and D.M. Allen, ''Modelling and Process Capability Analysis of Focused Ion beam'', The 32nd International Spring Seminar on Electronics Technology 2009, 13-17 May 2009, Brno, Czeh Republic
2010 (Chapter 5)	S. Stoyanov, C. Bailey, Y. K. Tang, S. Marson, A. Dyer, D. Allen and M. Desmulliez, ''Computational modelling and optimisation of the fabrication of nano-structures using focused ion beam and imprint forming technologies'', Journal of Physics: Conferences Series 253 (2010) 012008, doi: 10.1088/1742-6596/253/1/012008
2010 May (Chapter 3,4, 6)	S. Stoyanov, P. Rajaguru, Y.K. Tang, C. Bailey, J. Claverley, R. Leach, ''Reduced order modelling for risk mitigation in design of miniaturised/integrated products'', 33rd International Spring Seminar on Electronics Technology (ISSE), 12-16 May,2010, Warsaw, Poland
2009 May (Chapter 3)	P. Rajaguru, S. Stoyanov, Y.K. Tang, C. Bailey, J. Claverley, R. Leach, D. Topham, ''Numerical Modelling Methodology for Design of Miniaturised Integrated Products – an Application to 3D CMM Micro-probe Development'', 2010 11th International Conference on Thermal, Mechanical & Multi-Physics Simulation, and Experiments in Microelectronics and Microsystems (EuroSimE), 26-28 April 2010, Bordeaux, France
2008 Jul (Chapter 7)	C. Bailey, S.Stoyanov, Y.K. Tang, X. Xue, T. Tilford, ''Multi-physics modelling for the fabrication, packaging and reliability of micro-systems components'', The 8th World Congress on Computational Mechanics (WCCM8) and 5th European Congress on Computational Methods in Applied Sciences and Engineering (ECCOMAS 2008), 30 Jun - 4 Jul 2008, Venice, Italy

TABLE OF CONTENTS

LIST OF FIGURES

LIST OF TABLES

Chapter 1 Introduction

This chapter provides an overview of the research background about trends in micro-electronics manufacturing industry and miniaturised product manufacturing industry. The motivations of this research study, the aim and objective of the research of the work are presented.

1.1. Trends of Manufacturing Technology Development

Electronic products have developed very quickly nowadays especially in the area of computers, telecommunications, consumer electronics, cars. Emphasis on product miniaturisation has been the driving force in the research and development of the micro- and nano-structures and products. This trend has shifted the whole electronics industry from micro- scale to nano-scale. This motivates the developments in the field of avionics, bio-medical devices, heterogeneous systems, micro-fluidics, embedded test devices as well as in material sciences industries with the adoption of new materials. With the development of electronics packaging and production, manufacturing methods are capable of producing smaller and lighter products. Those advanced technologies are mainly driven by the market demand i.e. the customers. Moreover, some electronic products must be miniaturised for their applications in the

intended environment. Those electronic devices applications are subject to size constraints which have to be manufactured from micro-scale down to the nano-scale especially in medical and avionics devices. These demands and restrictions have driven the emergency of the use of nano-technologies. Therefore, developing the electronic devices, parts, components, and structures in micro- and nano- scale have become a huge target across the micro-electronics industry.

Miniaturised electronic products have stricter geometric specifications due to a smaller size. The accuracy to achieve precision has become a critical issue that can affect product reliability and functionality. New technologies and manufacturing methods have to be studied and developed to enhance accuracy issues. One of the prominent revolutions in the industry is the use of three dimensional processing manufacturing methods instead of planar techniques for the micro- and nano- structure. The use of micro and nano-scaled materials has also been investigated in conjunction with the technologies development. This manufacturing transition also means the old and sophisticated methods have to be revised, modified and replaced. Unfamiliar new manufacturing methods raise the challenges in maintaining the reliability and quality of the final products.

1.1.1. How Market Demands Motivate Technology Development

Products that can perform multi-functions would be welcome by the market. This is another driving force motivating the micro-electronics manufacturing industry to produce smaller products. Electronic products are moving towards an 'All-in-one' era. Printed circuit boards (PCBs) are required to pack more circuits into a product for more functionality. PCBs are designed as multi-layers which can accommodate up to

50 layers to embed more circuits. In short, the demands of enhanced functionalities in consumer electronics increase the complexity of product designs. As a result, product life cycle becomes more complicated and more value-added activities are necessary.

Consumer electronics are now under a tighter control from government legislation. Recently, environmental concerns are gaining more awareness in electronics industries. Sustainability becomes the main issue that governments address through legislations concerning the electronics production. Government has enforced the sustainability policy with legislations. Legislations have become a main driver to design for the environment due to the effect of European Union's directive on the Waste Electrical and Electronic Equipment (WEEE) [1] and the directive on the Restriction of Hazardous Substances (RoHS) [2]. Environmental considerations must be included to comply with WEEE and RoHS regulations. One of the most influential compliances by RoHs is that the use of the hazardous element Lead (Pb) has been prohibited by 2007. It affects the electronic products manufacturing process. Solder is used for interconnection in electronic packaging. The ban of numerous hazardous substances for interconnections has forced the industry to undergo an enormous lead-free evolution. This requires the use of new materials such as copper, gold and silver. Their associated processing techniques are also explored to meet environmental legislations. However, technical feasibility, reliability and costs become the subjects of interest for further study. In order to reduce the production cost, other technologies and materials are introduced. Adhesives and underfills have been developing with interconnection and joining effects that can replace the solder.

1.1.2. Key Manufacturing Challenges

The micro electronics manufacturing industry are facing the increasing demands from customers and government to meet the trend of miniaturisation, multi-functions and environmental issues. The micro-electronics industries are undergoing a transition period of manufacturing mode shifting from two-dimensional to three dimensional integration and product manufacturing. The industries are also facing new technologies, new product development and adoption of new materials. The electronic manufacturing technologies are still far from achieving 'optimum' among many other aspects like reliability, costs, environment and quality. Many other challenges arise including the followings:

- **Technical feasibility -** The new technologies demand much know-how knowledge from the practitioners and new materials require new processing techniques. Some process approaches can be technically infeasible due to unknown process behaviour and uncertain materials physical properties.

- **Mass production and high throughput -** Time is required for the manufacturing systems to switch to modified manufacturing approaches, new materials and resources for the new design. This leads to a lower process yield and efficiency.

- **Time to market -** Quicker time-to-market operations require shorter product life cycles on new product developments. Shorter development time means less time for intermediate stage and processing during life cycle.

- **Increased complexity -** Multi-functionality leads to the increased product complexity. Product layout has become more complicated. Internal component interactions have increased. The reliability testing and maintenance task have become more challenging.

- **Environment -** Environmental practice tends to cure and repair problems rather than impose preventive measures. Introducing quantitative analysis becomes necessary for environmental impacts estimation. However, the quantitative analyses concepts are completely new to engineers and researchers.

- **Reliability -** In performing reliability testing, the typical materials and their composition are well-tested for optimal process conditions. By contrast, the handling of new material alternatives is unfamiliar.

- **Costs** - With new technologies and manufacturing methods, new researches and developments are required. Hence, investments in terms of machines, equipments, human resources are indispensable. New materials are more costly to meet environmental standards and maintain product reliability level.

- **Achieve an optimum –** The industry aims to achieve low costs, environmental friendly and high reliability in order to fulfill the customer specifications. However, there are always trade-off among those requirements. Producing environmental friendly products involve a higher cost. Low cost production approaches cannot guarantee a reliable product. Electronic designs and manufacturing approaches must achieve a balance among all aspects called 'optimum'. To identify an optimum for multi-objectives task is complicated and can be impractical.

1.1.3. Uncertainties and Risk

The miniaturisation in size, multi-functional requirements and increased complexity in design are all the factors that result in higher demand of knowledge. However, knowledge about new materials processing, process and product are very limited at stages. Facing insufficient knowledge and historical data, practitioners typically know very little about any new technologies. The adoption of new materials and processes is

also associated with a significant decrease in the knowledge about their behaviour, quality, performance and reliability characteristics. Any random variations and stochastic behaviour of physical properties, such as manufacturing non-equivalent uniqueness in materials micro-structures and properties can turn out as uncertainty.

The risk described across the electronics manufacturing industries refers to the technological risk of achieving accuracy from targets in engineering problems. The target requirements that define the matrices of interests about a product design or a process performance are in terms of design and process parameters. Design risk refers to the accuracy to reach a target value of any design requirements under design variables uncertainties. Process risk means the failure to reach a target level of process performance. Because of the miniature nature in micro-world, the effect of any variations in variables can hugely increase the occurrence of product designs deviations or process performances scattered from targets i.e. output matrices of interests falling outside the acceptable specification limits causing defeats and failures. The risks caused by the uncertainties and variations are inherent in all engineering design problems. Mitigating the technology uncertainties and associated risk becomes an essential task.

1.2. Computational Analysis Tools in Design Stage

Computational power grows exponentially in the last century which offers a huge assistance to any industries. It eases the opportunity to achieve an optimum in product design, seek optimal process performances, and mitigate risk that are all ultimate targets in electronics manufacturing industry. This know-how knowledge must be

6

transferable across the whole process development team instead of solely the engineers. Any issues across the product life cycle involve various types of analysis tools, people and procedures. Essentially, all data flow and tools applied must be formulated and systemised into a general design practice allowing anyone to understand easily. The associated analysis tools are detailed as follows.

1.2.1. Computational Aided Design Tools

Component package design and parts manufacturing process in electronic manufacturing involved complicated procedures and careful observation. Computational capabilities coupled with emerging models offer significant advantages. Computational methods, in particular finite element techniques that represent engineered product, can forecast process behaviour and predict process responses. Computer modelling is now being used extensively to assist the area where experiments are impossible and too costly to perform. It enables examination and comparison of design alternatives efficiently. For instance, Finite Element Method (FEM) is a useful method that adopts computational analysis to assess reliability issues of materials. The use of simulation has also been proved helpful to study process behaviour so as to achieve any process and product improvement. Still, they are far from ideal. There are two limitations of computational models.

Model Errors – Models can facilitate understanding about process performance and its physics behind. However, models are not perfect to reflect the actual situations. The natural model discrepancies from reality are highly due to model errors. The errors are either induced from stochastic process behaviour of process parameters, or lack of understanding about the state-of-the-art knowledge.

Computational efforts - Limitations of computational resources and manipulation time are common in using computational aided design tools. The degree of freedoms of a design problem increases due to the increased design complexity and interactions. The underlying physics and mathematical equations applied to identify the solutions increases exponentially rather than linearly.

Product design, fabrication, packaging and assembly, testing, operational life and product disposal all need to be addressed in advance, at the early design stage, and in conjunction. It is understood that the cost of correcting mistakes at the late stages of product development can be of order of 1000 higher than the one at the early design stage [3]. Mistakes must therefore be addressed earlier rather than later. The use of conventional design practice involving in-situ testing and with the use of prototype should be minimal. Design and simulation toolsets with computational aided design are proved to be cost effective and helpful. They act as virtual prototype tools to understand about physics for design planning in the life cycle. Figure 1-1 shows the interactions between simulation toolsets and a product life cycle of micro-electronic products. The product life cycle begins from raw materials to end-products through stages including 3D processing, micro-assembling, packaging, and testing.
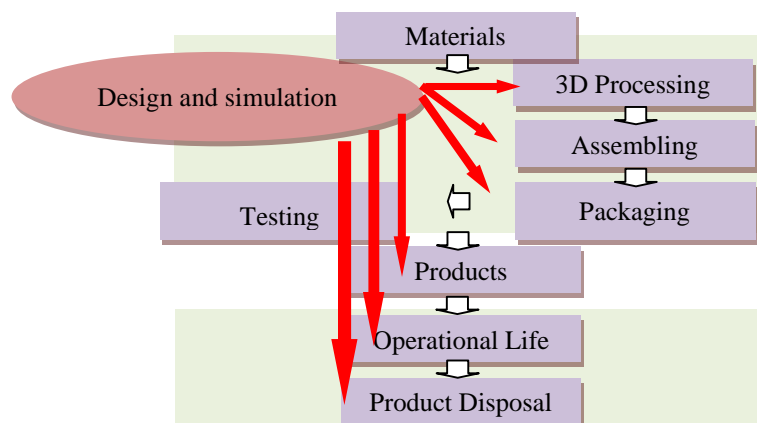
Figure 1-1 Role of design and simulations toolsets in the product life cycle

1.2.2. Optimisation Analysis for Engineering Problems

Optimisation is the process of choosing the design parameters which yield the optimum design. The process of yielding the optimal design is known as *design optimisation*. Optimisation explores the available limited resources in a manner that maximise utilities. It substitutes the traditional prototype oriented approaches using trial-and-errors methods. Optimisation provides quantitative analysis of the product design problems in terms of the quality and reliability according to customer specifications. Optimisation methods is utilised as follows. *Structural optimisation* can be applied to design of structure aiming to utilise the shape of products to reduce weight and usage of materials or improve process performances. *Topology optimisation* can be used to optimise material layout for a given set of loads and boundary conditions in a design space. It can be used in conjunction with finite element model. *Multi-disciplinary design optimisation* provides a routine to solve problems simultaneously which incorporates more than one discipline. Engineers often assume design problems to be deterministic. Deterministic optimum design allows no room for tolerances and is therefore associated with high potential of failure. *Reliability based design optimisation* is a probabilistic based approach which addresses uncertainties in design parameters, includes the evaluation of probabilistic constraints.

1.2.3. Risk Analysis

Risk mitigation involves risk identification and risk analysis which are used to understand and characteriser risk, and to forecast the risk impact. Risk identification can help identifying the key design variables, process parameters, process characteristics and product characteristics. A current study proposed by Thortons [4] is

widely used in avionic industries that focuses on using product reduction approach to identify the key characteristics of a product. However, Thortons ideas emphasise on solely product perspective. Engineers and designers are more interested in a quantitative assessment of risk to evaluate the degree of severity and how frequent do uncertainty affect the process performance. Risk analysis based on probabilistic theories has gained recognitions in recent research work. Its purpose is to explore how variations of a product or process parameters propagate into variations of the quality a product and process performance. NASA has conceptualised a framework to identify 'the failure margins' of a process based on models [5].

1.3. Motivations of Research

1.3.1. Methodology Integrates with Computational Tools

The challenges on manufacturing problems, new adoption of materials technologies have driven a computational framework of this research. Techniques such as computational modelling, design of experiment, reduced order modelling, risk analysis and optimisation analysis are well-established. They are commonly applied independently to evaluate a problem. These high level analysis are computational expensive for complex engineering problems which requires probabilistic and iterative analysis. Therefore, applying these tools interactively and dependently must be well-formulated in order to obtain problem solutions accurately and efficiently. In this research, a detailed methodology is proposed which integrates various techniques to address uncertainty and risk [6]. The methodology is used to address two application problems: (1) sputtering process with focused ion beam for micro-machining [7], and (2) a flip chip electronic package. Sophisticated tools established from specific fields

are brought into electronics and nano-manufacturing industries. The methodology is also applicable to other novel application problems.

1.3.2. Risk Mitigation Approaches Integrates with Reduced Order Model

The deterministic models have no allowances to deal with stochastic behaviour in most engineering problems. At the same time, many conventional approaches to address manufacturing process variations are dependent on historic data. These data are often impossible to obtain in new products and processes. Probabilistic models are required that can propagate the effect of uncertainty onto the process output or performances. Evaluation of reliability via probabilistic models are often computational expensive. Risk mitigation approaches which integrate certain probabilistic methods and reduced order models are developed to propagate uncertainty accurately and efficiently. Various types of reduced order models such as non-polynomial types are investigated. Analytical methods for risk analysis are also proposed to enhance efficiency of running subsequent optimisation analysis.

1.3.3. Better Focused Ion Beam Process Control and Uncertainty Propagations

Process control to estimate materials sputtering process using focused ion beam is investigated. The sputtering process are analysed in different ion beam scanning movements. In particular, a beam movement method is proposed that allows ion beam angle of incidence to be taken into account for sputtered depth variation. Another beam movement method and its associated number of cycle of scanning required for milling pre-defined shape are investigated. Beam overlapping which affects the materials sputtering are numerically formulated into a focused ion beam FIB model.

Consideration on re-deposition effects is integrated with the FIB model to enhance the accuracy on sputtered depth prediction.

Uncertainty in materials and process parameters variation can occur due to the stochastic behaviour and unknown process phenomena in focused ion beam process. The probability of failure and degree of scattering from target process performance requirements must be quantified. Appropriate risk mitigation approaches such as Monte Carlo Sampling methods must be incorporated into the process to propagate the impact of uncertainties. In order to enhance the process output evaluations in sampling methods, for instance, Latin Hypercube Sampling can be applied. To propagate the impact of uncertainties in a more efficient manner, reduced order models are suggested. For example, Kriging model is generated using interpolation techniques that can improve the accuracy of polynomial approximated reduced order models.

1.3.4. Environmental Considerations and Optimal Design in Flip Chip Package

As part of this research, the proposed computational methods are also used to evaluate product design of a flip chip. Bringing environmental issues quantitatively into consideration during product development has not been researched in literature so far. An innovated tool, Toxic Index (TI), is introduced to quantify the environmental hazard of compound materials. It has been used to demonstrate the Sn-Ag-Cu type (SAC) solder which is one of the essential materials in electronic packaging industries. The idea of index has been extended not only as an indicator for material environmental impact, but to qualify a component and the entire product. The Toxic Index is integrated in optimisation problem as a constraint or an objective. This proposed approach can help environmental authorities qualify relevant environmental

compliances. In industries, the Toxic Index can be used as a standard and can be applied to identify the optimal to meet any customer environmental requirements. The quantitative measure can motivate a new evolution to eco-products manufacturing in conjunction with the widespread qualitative management policies and standards.

Optimisation studies are focused on reliability and even cost analysis. What is lacking in the literature is a optimisation tool to quantify environmental characteristics of a product. In the research, an optimisation analysis that incorporates environmental evaluation for flip chip is presented to deal with impact of new emerging materials. Flip chip design optimisation problems in literature are focused on reliability requirements, costs and environmental impacts individually rather than a unified manner. A multidisciplinary optimisation problem is required in the early design stage. This motivates a flip chip design optimisation problem formulation unifying three aspects: reliability, costs, and environmental issues together. Responses evaluation in those aspects is obtained through finite element modelling and reduced order modelling via response surface models. A reliability assessment, an identified cost model, and an environmental model based on the Toxic Index are constructed. Such multidisciplinary problem is solved mathematically, to deduce the optimal design.

1.4. Aims and Objective of the Research Work

The aim of my research is to develop a risk analysis methodology and an associated computational framework which can aid the decision making process for fulfilling multi-objectives in micro-electronics manufacturing industries and nano-fabrication industries. The work aims to improve the design of miniaturised electronic products

and to facilitate the manufacturing process of the electronic products. A major effort is placed on the demonstration of the proposed methodology to real life problems and industrial applications. Two case studies: focused ion beam (FIB) material sputtering application and a flip chip electronics packaging application are researched and investigated. The research work has been divided into three main parts:

(1) Risk Analysis Methodology

Design a methodology based on computational modelling for predicting physical behaviours, process performances, and certain response of interests. The focus is placed on identifying a way to generate response efficiently. Reduced order modelling is suggested which integrates computational model and other computational approaches including design of experiment and response surface modelling. Techniques that allow quantification of the risk of achieving quality requirements and expected process performances are identified. Using uncertainty analysis and sensitivity analysis, design and process uncertainties are identified. Their impact on design quality characteristics and process performances of the fabricated products are characterised with statistical inferences. The objective of the computational analysis is to evaluate the capability of the any developed products and process when they expose to uncertainties. The methodology aims at identifying optimal design and process performance of advanced electronic products and their associated fabrication processes.

(2) Focused Ion Beam Process Control

Characterise the process control and performance of focused ion beam micro-machining which can be used to fabricate micro-engineered products. The application illustrates from process perspective that how the methodology can be applied to predict process behaviours and performances under the impact of process control uncertainties.

An investigation is primarily placed on the FIB milling process control by different modelling approaches in particular the depth variation that characterise the shape of pre-defined structures. A detailed computational FIB model is identified and integrated in the research. It provides a better understanding in the control of the advanced micro-machining process to model the time required to manufacture a shape. The objective is to validate the final shape produced at the predicted time against the pre-defined shape of product [8]. Certain important issues such as sputtering rate are also validated. Two important issues causing such a difference in FIB milling process: sputtering yield and re-deposition effect are further explained. The process control has been consolidated providing grounds for the secondary task: risk analysis on FIB process. Risk analysis is carried out with the introduction of process parameters uncertainties to assess the process capability and robustness. The computational methods are integrated to help understand process behaviour, process performance, product quality characteristics, and optimality of the micro-machining process [9] [10].

(3) Flip Chip Design/ Optimisation (Reliability, Costs and Environmental Impact)

Characterise the design considerations and identify the optimum of flip chip technologies to fulfil reliability and environmental requirements. The first application illustrates from product design perspective that how reliability, environmental and relevant requirements of a flip chip are assessed by computer modelling and how optimal design is identified. The key focus are on analysis of design considerations such as geometry and materials and their associated impacts with regards to reliability, environmental and the economical aspects of a flip chip package, Most importantly, this work aims at identification of an optimal design in one single multi-objective design problem. This helps provide decision support in selection of materials and design alternative. A new area regarding quantification of environmental impact is

demonstrated on the flip chip design. This numerical assessment provides a fundamental basis for optimising environmental impacts which has not been researched previously. The environmental assessment couples with the reliability and cost assessment. They formulate a single multi-objective design optimisation problem. Risk analysis is carried out to evaluate the design specifications with regards to design variables uncertainties to assess the product robustness.

1.5. Two Application Problems

Two applications problems were investigated. The suggested risk analysis methodology was demonstrated from two directions: A fabrication process perspective and a product design perspective providing holistic scenery for industry targets.

1.5.1. Fabrication Process using Focused Ion Beam Sputtering

The methodology and the associated computational tools have been used to characterise an industrial application where focused ion beam has been used for micromachining of fine features at nano-scales. This fabrication process has gained more popularity in micro-electronics manufacturing because of its strength to produce nano features efficiently for matching the current miniaturisation trends. However, the big challenges of this application to practitioners and engineers are the difficulties in controlling process parameters to achieve accuracy in shape. The focus of the work is to understand how to gain a precise process control and evaluate the risk of achieving final shape with accuracy when the process is exposed to uncertainties in reality.

Process capability will also be performed for assessing the robustness of the focused ion beam micro-machining process. In this work, a mathematical model is identified from the literature and further integrated to simulate the process. In particular, a desire shape profile in terms of several important process parameters is investigated to understand the process parameters impacts and the most important parameter towards the shape. The challenges for implementing this process that affect the final precise shape in reality are mainly due to two reasons. First reason is the difficulties to achieve the specified values in some process parameters due to randomness and other unpredictable factors. Secondly, relationships between the process parameters and output are not clearly understood as well as the key process parameters. Possibility and effect of hidden parameters cannot be ignored such as re-deposition effects in the process. To tackle these challenges and mimic the process in reality, uncertainties are potentially introduced into the process parameters and their associated impacts on process performance are studied. Sampling methods and analytical methods are carried out to identify the impacts of uncertainties within the risk analysis framework in our proposed methodology in forecasting the risk of obtaining the nano-feature pre-defined shape in terms of accuracy. Apart from evaluating one set of process set-up, different sources of ion beam like Gallium and Argon beam, and different process parameters values are used and fit into the model for comparison. Their process capability is evaluated by probability theories and statistic tools, to account for the stochastic process behaviour in reality in order to enhance the process robustness. Optimum process parameters and conditions among the available beam sources and materials are identified for the optimal process performances.

Since the mathematical model involves repetitive calculations in manipulating the sputtered shape, getting process responses from the model are time and

computationally expensive. Undertaking sampling methods to assess uncertainties seems impossible. Therefore, reduced order models are suggested in the methodology which enables fast evaluations of process responses. A limited number of process responses are first generated from the identified mathematical model. Then, design of experiment and response surface methodology are undertaken to formulate the reduced order model. This reduced order model does not only facilitate the sampling methods in risk analysis, but it has also been a helpful tool to subsequently perform the iterative optimisation task. The computer modelling and simulations have been validated against experimental test case studies in University of Cranfield. The findings from the modelling perspective are also well validated.

1.5.2. Flip Chip Design

The methodology and the associated computational tools have been demonstrated in an industrial application for electronics package assembling where a flip chip design is investigated for its optimised design. Flip chip design has been well recognised in particular for the miniaturised electronic products in electronic packaging industries. Researches and many reference books have covered the application of flip chip. Several other works have included the optimisation of a flip chip design. Our work has focused on two parts, (1) analysis of design considerations such as geometry and materials selection and their associated impacts with regards to reliability, environmental and the economical aspects of a flip chip design, (2) identification of an optimal design in one single multi-objective design problem. These two parts must be addressed in the early design and planning stage. Regarding reliability issues, interconnect fatigue (damage) in terms of design parameters geometry and materials property, subject to thermal loading are addressed.

Regarding environmental aspects, another area that has not been researched much in the past is numerical environmental analysis of a product design. The work illustrates an approach of how to quantify a flip chip design using the available environmental index for materials in literature, to justify the material selection decision for components and their environmental impacts. Simultaneously, costs issues of the flip chip package investigated above are also assessed. The assessment illustrates how the selected material affects the economical aspect of the overall design. A multi-objective task is required to evaluate the feasibility of assembling the investigated design in terms of costs, environment and reliability aspects. The highlight of this work is that all these considerations have been formulated as one design problem instead of a few single-objective design problems. This design problem is solved using the optimisation modelling to address the design problem objective, detailing the optimal design variables and conditions. Tools such as computational modelling, design of experiment and response surface modelling suggested in the risk analysis methodology are applied to solve the design optimisation problem.

A flip chip structure normally consists of the following components: a die, substrate, solder joints and underfills. A computational model which includes geometry consideration of the above components of a flip chip structure has been created. The interest of work here is to study the behaviour of the chip interconnects subject to applied thermal loading. The components react differently to this thermal loading since the materials property (elasticity) of each material is different. The thermal stress and strains induced under such thermal loads eventually causes damage/fatigue (mostly happen at solder joint) in package interconnects. Finite element method has been used to construct a model in order to simulate and predict the solder joint damage and to

identify how the damage is affected by parameters that define the flip chip geometry. The main focus is to assess reliability aspects by evaluating the thermal stress causing the damage with regards to the geometry of different components as well as their material properties and elasticity.

During the stage of materials selection, the investigated component materials forming the package do have their associated environmental impact. Fraunhofer IZM [11] have developed a Toxic Index (TI) to indicate the environmental impact of each material per unit mass. The toxic index of the component and overall package will change according to material ingredients as well as their weights which are governed by design parameters. The intention of the work here is to work out the toxic index of each component (various ingredients of materials) per package and also the toxic index for the whole package based on the toxic index of each material. Therefore, materials selection decisions can be justified using the toxic index of the whole package in terms of their environmental impact. This quantification approach provides a fundamental model for the subsequent design optimisation problem.

1.6. Contribution of the Research Findings

The significant contributions of the research findings are:

- **Methodology that characterises impacts of product/ process uncertainties**
  Risk mitigation strategies based on statistics probability theories are in use to tackle the process parameters uncertainties which leads to model errors and the deviated target process performances. Deviations are predicted in form of probability distribution such that process capability can measure how capable the process is.

- **Fast physics based reduced order modelling for risk analysis and optimisation**

  Conventional polynomial-based response surface approximations are used to utilise response prediction from intensive computational models for risk analysis and optimisation. Interpolations techniques are applied to construct reduced order models that enhance the accuracy of response evaluation.

- **Validated models for FIB processes**

  Computational modelling work about the focused ion beam process is validated with experimental case studies. Accuracy of FIB models can be enhanced by experiments Simulation refines experimental setup and improves experimental result. The work helps the experiment development at Cranfield University.

- **Multi-disciplinary optimisation of flip chip design**

  Optimisation methods are applied to identify the optimal design and process performance. Multi-disciplinary optimisation is used to demonstrate how to assess reliability and cost, in particular a novel way to assess environmental issues which have not been researched before. The researched environmental tool has entirely enhanced the efficiency of conducting a full life cycle assessment of a product.

- **Contributions to a decision support system**

  Certain theories and mathematical models work from this research work have been used to develop an in-house design supporting software –ROMARA [12].

- **Dissemination of research**

  Four conference papers as first author and five conference papers as the co-author were published.

1.7. Thesis Layout

There are eight chapters in this thesis and its structure is summarised by a flow diagram as shown in

Figure 1-2. In chapter 1, the research background is outlined about the challenges and the trends in the electronics and micro/ nano-manufacturing industries. The motivations in researching the application of focused ion beam for nano-structures fabrication and optimal design for electronics packaging are outlined.

In chapter 2, the researches for quantitative and qualitative risk assessment approaches in different fields in the literature are given. The developments and applications of associated computational modelling techniques and methods are reviewed. The overviews include (1) computation modelling, reduced order modelling, (2) risk mitigation and (3) optimisation analysis across application problems in different fields. Product design development and process control in the two industrial applications: (1) nano-structures fabrication process and (2) electronics design analysis are reviewed.

In chapter 3, the computational modelling and reduced order modelling, are firstly explained. The theory of finite element methods (FEM) and methods to construct a finite element model is briefly overviewed. The approaches to generate reduced order model through design of experiment and response surface methods are explained.

In chapter 4, the second part of the methodology- the risk mitigation framework is discussed. It allows to address parameter uncertainties and to evaluate the risk of not achieving pre-specified requirements. Risk mitigation comprises of sensitivity analysis

22

and risk analysis. Risk analysis is undertaken with the aid of statistical inferences and probability theories to propagate uncertainties during design and process development.

In chapter 5, a computational focused ion beam (FIB) model is identified and integrated to provide a better understanding to the control of the advanced FIB micro-machining process. The model has been used to predict the required time for manufacturing micro-structures using FIB. The model result is validated against experimental measurements from actual runs of a FIB system. Numerous important process parameters and their associated effects on the sputtered shape are identified, and further explained to improve a better process control.

In chapter 6, process parameter uncertainties are introduced into the validated FIB model of the FIB fabrication application. Uncertainties are propagated through the reduced order model. Risk analysis is executed based on the probabilistic evaluations. Results are used to mitigate the risk of not achieving the pre-defined shape. Finally, process capability indices are applied to characterise the robustness of this fabrication process with respect to customer requirements.

In chapter 7, a flip chip design application is demonstrated using the methodology. A procedural flow down illustrates how the optimal design can be identified. The emphasis here is on the numerical assessment of its environmental impacts to evaluate different design alternatives and select among various materials available.

Finally, a conclusion is given as a summary of the research work. Future work is discussed to extend and modify the current work as a holistic approach.

Chapter 1	Introduction	
Chapter 2	Literature review	Theories in the chapter applied to:
Chapter 3	Risk Analysis Methodology Part (1): Reduced order modelling	
Chapter 4	Risk Analysis Methodology Part (2): Uncertainty management	
Chapter 5	Application Problem (1): Simulation focused ion beam sputtering process control	
Chapter 6	Risk analysis on focused ion beam process with regards to parameter uncertainties	
Chapter 7	Application problem (2): Flip chip product design optimisation	
Chapter 8	Future work and Conclusion	

Figure 1-2 A flow diagram details the flow and structure of the thesis

Closure

In summary, this chapter has detailed the research background of the micro-electronics manufacturing industry and miniaturised product manufacturing industry. The overview includes the technologies trend and industry challenges. Different analysis tools and approaches were outlined. A methodology is required that can provide a procedural flows and computational analysis. From research prospective, the novelties are also outlined. Two applications problems are defined (1) a flip chip package design, and (2) materials micro-machining of focused ion beam sputtering process.

Chapter 2 A Review of Risk Mitigation Techniques and Micro/ Nano-Manufacturing

This chapter reviews risk assessment approach for product design development and process control. An overview of associated computational modelling approaches and optimal design identification are outlined. The current state of fabrication techniques using focused ion beam sputtering process for micro- and nano- products are also reviewed. The computational approach to design electronics products and to control process of fabricating miniature products is reviewed. The following areas were reviewed:

(1) the advances and development in risk mitigation techniques for uncertainties management and the associated application problems

(2) the role of computational modelling, response surface modelling, and optimisation techniques for the miniaturised products and fabrication processes

(3) the current statues of nano-fabrication technologies, the modelling work and studies in materials sputtering process using focused ion beam

(4) the advances in electronics packaging industries and how computational models are applied to evaluate the flip chip embedded IC packages

2.1. Concepts and Development of Risk Mitigation Techniques

2.1.1. Some Risk Management Concepts

Nowadays, risk-related issues become an important topic in every industry because of its inherent nature and influential impact. Risk was first considered and studied in the early 1980s. Kaplan and Garrick introduced a conceptual framework which defines risk into a 'set of triplets idea' and any risk assessment approach aims in addressing three basic questions: (1) What can go wrong? (2) How likely is it? and (3) What are the losses (consequences)? [13]. Modarres [14] had given his definitions on uncertainty: 'Uncertainty is a measure of the "goodness" of an estimate, uncertainty arises from insufficient knowledge'. The most suitable definitions of risk in this work closely link to NASA [15] contains three basic components around the triplet ideas proposed by Kaplan and Garrick. The three basic components and their definitions are as follows: (1) Scenarios, (2) Probability, and (3) Consequences. Risk is a function of both the uncertainty and damage [13]. i.e. Risk = Uncertainty + Damage. Risk is an integrated attribute from uncertainty and its consequences. Modarres expressed the view that *Risk Analysis* is the process of characterising, managing, and informing others about existence, nature, magnitude, prevalence, contributing factors, and uncertainties of the potential losses [14]. He also believes that risk assessment is a formal and systematic analysis to identify or quantify frequencies or probabilities and magnitude of losses to recipients. Uncertainty can generally be classified into two types: (1). *Aleatory uncertainty and* (2). *Epistemic uncertainty* [16] [17] [18] [5].

Aleatory uncertainty - This type of uncertainty is the physically variability which is inherent in a process. Uncertainties are induced due to the random variations and

stochastic behaviour in physical properties such as the manufacturing non-equivalent uniqueness in the materials or materials properties. ***Epistemic uncertainty-*** Uncertainties are induced when the understanding of the practitioners and decision makers about an approach or process is out of their boundary state of knowledge. No one can precisely predict what the outcome subject to scarce knowledge. This type of uncertainty is divided into three streams: (1) Parameter uncertainties, (2) Model uncertainties, and (3) Completeness uncertainty [19] [20].

2.1.2. Risk Analysis Approaches for Existing Industrial Processes

Risk analysis approaches have been developed for well established processes. To identify process and system failure due to the hidden uncertainty which could prompt into potential risk, Failure Mode of Effect Analysis (FMEA) has been used by the US Armed Forces since late 1940s [21]. It is commonly applied in current manufacturing processes and activities as an effective approach. FMEA is a traditional and powerful tool to investigate the probability, detectability, severity of failure for risk mitigation. The idea was based on collecting useful data by systematic documents and records through actual manufacturing activities. The entire or partial process flow can be fully captured such that defeats and process failures are identified [22]. After data and sample collections, statistical controls are applied for process control providing insight about process variability, failure and hidden problems due to (random) the common cause of failure. However, the shortcoming of using FMEA is that the whole process requires enormous data and sample collections through day-to-day observation. FMEA is limited to new developed technologies and processes which historic data is not available. Unknown knowledge on the process input, response, procedures and behaviour can hinder any data requisition about the process.

Quality Function Deployment (QFD) is another systematic method to identify system/design/ process weaknesses and strengths based on the voice of the customer [23]. It translates the customer's requirements, part characteristics, manufacturing operation, and production requirements into engineering languages aiming to eliminate failures, identify risk of not meeting customer requirements and improve process and design. QFD has to be implemented as a planning tool before a system FMEA is used as a quality improvement tool.

2.1.3. Risk Analysis Approaches for New Industrial Processes

Recently, researches have been focused on risk management in particular to handle risk of new processes/ products which are in development stage. Mitigation of risk for new processes is in the direction of developing both qualitative methods and quantitative techniques to ensure process robustness. Qualitative methods provide assistance to categorise risk related issues and group them into smooth flow down procedures. This helps the subsequent quantitative risk analysis to take place simultaneously.

2.1.3.1. Qualitative Risk Mitigation Methods

In recent years, significant work in the field of risk management has been carried out. Major risk management activities are well-suggested and documented by NASA. NASA ideas of Continuous Risk Management (CRM) and risk matrices [15] [24] are widely applied across different research institutions, companies and even government authorities for health and safety. A conceptual ring is used emphasising the flow of risk

management strategies. Risk Matrices are used as a tool to categorise, prioritise and assist risk communication activities. NASA emphasised on identifying the hazards having adverse consequences and estimating the probability of the occurrences, and evaluating the severity of consequences. Risk matrices are introduced to characterise such probability and severity of consequences of risk into different levels [24]. The levels are indicated by a Risk Assessment Code (RAC). RAC involves the assignment of a number from one to seven where number 'one' means the hazard leads to the most serious consequences and immediate action is required while 'seven' means the hazard has the lowest priority to be addressed. Similar concepts on the NASA matrices have also been examined elsewhere. For example, Maturity Capability Readiness Level (MCRL) indicator has been proposed based on a numeric indicator Technology Readiness Level (TRL) [25] [26] to evaluate how mature is the process. Similarity number is developed to characterise the risk level [27]. These tools aim to quantify the risk level of a particular technology.

Some other risk identification techniques are used to identify the 'key characteristics' (KC) during product development. Key characteristics are defined as 'a feature whose variation has the greatest impact on the fit, performance, or service life of the finished product from the perspective of the customer.' A more complete KC methodology was done by Lee and Thornton [4] aiming at breaking down a whole product into parts, sub-assemblies and components by flow down approaches. This method has been implemented by industrial leaders such as GM, Ford, Rolls Royce and Boeing to analyse car assemblies and aircraft manufacturing and maintenance [28]. The key characteristics about the whole product and the corresponding process are identified. Then the risk of failure to reach target performances and manufacturing specifications in critical parts due to variations can be identified. However, key characteristics

analysis requires a comprehensive analysis across every part and assembling procedure which is time and resources costly. For example, applying analysis on an aircraft assembly which includes many procedural interactions is difficult in reality.

2.1.3.2. Quantitative Risk Mitigation Methods

Another approach, Probabilistic Risk Analysis (PRA) is introduced as a risk quantification tool based on probability concepts. There are two major interpretations of probability: (1) Classical which is based on a limit of relative frequencies and (2) Bayesian which is based on a measure of degree of belief [5]. These concepts are employed based on statistical evidence in the PRA models that are constructed to reflect the random nature of the constituent basic events such as component failures. PRA is capable of characterising both the aleatory uncertainty and also epistermic uncertainty.

To capture the effect of uncertainty and variations, probabilistic models are used to describe the randomness of process observations instead of deterministic models in most engineering design problems. The challenges lie on how to propagate the effect of uncertainty into the process output or performances in an efficient manner. Uncertainty is presented in the form of probability distributions. Various methods can be used to identify the uncertainty impacts on process output. The commonly used method includes worst case analysis [29]. Regarding worst case analysis, variations on the variables on all assumed occurring at the worst scenarios in order to generate the most extreme value on process output. Such value can be found by first order Taylor series expansion. However, this approach tends to be too conservative. Using Taylor

series expansion is not accurate to estimate extreme conditions such as minimum and maximum of the performance.

Probabilistic distribution or process output can be generated through sampling method and analytical method. Monte Carlo Simulation (MCS) is a more comprehensive method which can improve the shortcoming of the approximation based method. Risk analysis is carried out based on MCS direct sampling method. The feasibility risk on construction cost of airports was evaluated by assigning probability distribution to input parameters [30]. However, running Monte Carlo Simulation on computational model like FE model is computationally expensive. The scatter ranges of input variables and their impacts on stress- strain values for lifetime estimation of a Chip Scale Package was investigated in [31]. This analysis combines the use of MCS with the Finite Element (FE) model demanding too much computational resources. Some modified Monte Carlo Simulation methods like stratified sampling methods have been proposed to improve the computational efficiency. Examples include Latin Hypercube sampling (LHS) [32] and orthogonal array sampling approaches [33]. These two work explains how samples are extracted in a reduced design space such that less samples are required to generate the output probability distribution. Even with these enhanced methods, sampling method is not affordable for complex design problems.

Running sampling based method on response surface model is an alternative method to replace taking direct sampling data on the full computational models. A LHS method was carried out to evaluate effect of variations of design parameters on its shape using a multi-quadric radial basis function [34]. LHS reduced the design space where samples are extracted to facilitate the identification of an optimal design in this study. In another study, response surface and MCS were used to investigate the stress

31

distribution in different material layers and sensitivity relationship between the major wire bonding parameters and the related stress value [35]. The approach greatly enhanced the efficiency of evaluating responses rather than analyses on finite element model. The cost to generate response surface model from its original model have to be considered. Obtaining accurate response surface models is another main challenge.

Analytical method involves calculation of the probabilistic distribution theoretically instead of extracting samples. One typical analytical method is the First Order Second Moment (FOSM) which calculates the mean and standard deviation of probabilistic distribution [36]. In this work, FOSM, Latin Sampling and Monte Carlo methods were used to propagate the uncertainty of a 3D vibration micro-probe [37]. The first order moment (mean) and the second order moment (standard deviation) are obtained to construct the output distributions. However, they are approximation based in which higher moments are truncated. For highly non-linear engineering problems, only taking lower moments are not sufficiently accurate to approximate the process outputs. Point Estimation Method further derives the skewness of probabilistic distribution [36].

Reliability based analysis is an analytical approach to perform uncertainty analysis which is widely used. In this type of analysis, a point in design space is identified relating to the probability of system failure which is defined by a limit state function. This point is called the Most Probable Point (MPP) or Reliability Index [38]. The limit state function of failure in a transformed co-ordinate system can then be approximated by first-order approximation. By assuming linearity, first or second order of Taylor series is used to estimate the probability at the MPP. These methods are known as first order reliability methods (FORM) and second order reliability methods (SORM) [39] [40]. Typical methods used to calculate the MPP include Performance Measure

Approach and Reliability Index Approach [41]. These analytical methods enhance the computational efficiency to obtain the probability of failure comparing to the sampling based methods. However, accuracy declines for addressing problems with nonlinearity.

During the last two decades, another reliability analysis method − Artificial Neural Network (ANN) algorithms are developed [42]. ANN requires no known relationship among variables. It can be used to construct a mapping from one multi-dimensional space to another multi-dimension space by learning through training examples. A vibration reliability analysis of turbine blade was investigated using combination of finite element method, artificial neural network, Monte Carlo simulation method and Latin Hypercube sampling method [43]. The study showed that ANN is more flexible and adaptable to access any continuous nonlinear function when compares to the sampling based methods through polynomials and analytical based methods.

These methods evaluating the process output probabilistic distributions can provide a good support for Reliability-Based Design Optimisation (RBDO) and quality engineering practices like Six Sigma Design. The optimal design and solution from RBDO can be assessed using process capability tool. Such design can be compared to the reliability requirements to verify whether it meets Six Sigma standard or not. There is an increase interest about non-probabilistic uncertainty modelling which can potentially overcome some of the limitations of the probabilistic approach and can handle in a better way "subjective" uncertainty (e.g. lack of knowledge about the modelling process). Examples are the evidence theory [44], fuzzy sets and possibility theory [45] and interval-based approaches [46].

2.1.4. Process Capability Modelling

After obtaining the probabilistic distribution, process capability ratio can be applied to quantify the process capability under the assumption that the probabilistic distribution is normally distributed. The objective of these indices is to reflect the standard deviations between the specification limits and their mean. For non-normal distribution, data is transformed with transformation matrices such as Box-Cox transformation [47] before calculating process capability ratios. A normalisation can be performed to check whether a normal distribution has achieved or not. By the Central Limit Theorem, increasing the sampling size can convert the non-distributed data in order to follow a normal distribution [48]. Another common way is to identify a well-known distribution which provides good fit to the obtained output data to assess the process capability. It is due to their simplicity and well established form allowing calculation of mean and standard deviation. For examples, Weibull distribution, is commonly used in accessing reliability of life time prediction in engineering problems [31].

2.2. The Computational Techniques in the Risk Analysis Methodology

2.2.1. Response Surface Modelling

Response surface modelling involves combination of mathematical and statistical techniques that are useful for developing, improving, and optimising processes. The objective of response surface modelling is to construct an explicit function (also regarded as response surface) which can closely fit known data points. Response surface can be constructed through two approaches: approximations and interpolation.

2.2.1.1. Approximations techniques: Regression analysis

Regression analysis has been used in many applications. Its objective is to identify the relationship between the dependent variables and one or more independent variables. There are three types of regression, linear, nonlinear parametric, and non-parametric.

Parametric (Linear Regression) - To address problems follows linearity, linear regression method such as ordinary least squares method, generalised least squares method, iteratively reweighted least squares, total least squares [49]. Least squares method is used to formulate a regression function in which the sum of the squared residuals is minimised. Ordinary least squares method is extended for different nature of problems and regression assumptions [50]. The regression approximations are not robust when outliers appear in the response variable (observations that do not follow the pattern of other observations) occur due to violations of these assumptions. Maximum likelihood estimation, least absolute deviation method and robust regression method are used in the presence of outliers [51]. Quantile regression, linear mixed models are other common techniques as the alternatives for linear type of engineering problems. Linear regression is useful for studying problems where data points are easily available from experiment or simulation. The limitation is that demand of data points increases enormously when the number of independent variable increases. Linear regression accuracy declines and the result is sometimes misleading when non-linearity relationships exist or are hidden in system.

Parametric (Nonlinear Regression) - Another parametric type of regression method – nonlinear regression can be used for problems with nonlinearity nature in responses. Nonlinearity is quite commonly seen in many reliability engineering problems that

lifetime can be well-fit with a Weibull distribution [52]. In parametric analysis, computing time of regression function is short as it possesses a known form. For instance, a second order polynomial consists of three terms such that only three regression coefficients are required. However, too many terms in a regression function may be weak or redundant to describe the relationship between the actual response and independent variables. To address the problems, (both forward and backward) stepwise regression can be used to extract the significant terms of describing the relationship [53]. Forward regression deals with additional significant terms through a repetitive term selection process until a good fit regression function is found. Backward regression is the opposite which refers to elimination of existing terms from a full model that contains all possible terms backwardly.

Non-parametric Regression - In non-parametric regression, a smooth function is usually developed with specifying a mathematical function and this smooth function is driven by the data themselves in the absence of any algebraic form function. Kernel regression, smoothing splines and LOESS regression are common non-parametric approaches to tackle problems with nonlinearity [54]. The non-parametric regression is able to deal with system with many independent variables. It does not require the specification of a function to fit all of the data in the sample. Thus it allows flexibility to complex process which theoretical model does not exist. However, non-parametric regression analysis demands large sampled data set in order to produce good models.

2.2.1.2. Interpolation and Extrapolation

Interpolation is a method of constructing new data points within the range of a discrete set of known data points. Linear and polynomial interpolation, piecewise constant

interpolation (nearest-neighbour interpolation) and spline interpolation are the widely used interpolation techniques because of their speed and simplicity. Neural network interpolation and radial basis interpolation [55] are added in the interpolation family. Radial basis functions interpolation is an interpolation method in which N set of basic functions are introduced for N data points. Each basic function is assigned with a weight representing each data points. The ultimate output function is a linear combination of all basic functions requiring each function passes through its data point exactly. Kriging interpolation has also gained a widespread use in spatial data prediction in the areas of mining and other geographic-related problems [56].

2.2.2. Applications of Response Surface Models and Applications of Optimisation Problems

Regression analysis has gained a widespread recognition in different industries because generating fast evaluation save the time and computational resources. A risk analysis methodology was suggested to evaluate the variations of process uncertainties through reduced order model included Kriging, polynomial and radial basis techniques. The methodology was adopted to illustrate a novel 3D vibrating micro-probe [57]. Regression models have been used for abstraction of finite element model to prediction stress, warpage, thermal strain in order to assess reliability [58]. In this work, a second order polynomial was adopted to evaluate the Focused ion beam micro-machining sputtering problems. Optimising the uncertainty of the process parameters was performed through the response surface model to characterise the deviation from target performances [9]. Response surface model can provide support to enhance efficiency of running optimisation which requires huge amount of response evaluations [59].

However, polynomial is restricted in its own form which may not reflect an accurate approximation especially on problems showing strong nonlinearity.

Kriging model commonly acts as a response surface model or reduced order model (synonymously called surrogate model) to predict process response for performing optimisation analysis. Its strength is to characterise data correlation distributed in spatial fields with limited number of observations. Kriging techniques can overcome shortcomings of polynomial-based response surface model for many complicated engineering problems which possess non-linearity and correlation between parameters. You [60] has adopted Kriging method on predicting integrated circuit performance. Hawe [61] investigated an optimisation using Kriging interpolation which was applied to an electromagnetic design problem. The accuracy of the Kriging model was discussed. Simpson [62] has compared Kriging methods against polynomial regression models for the multidisciplinary design optimization of an aero spike nozzle. Bang [63] optimised a jaw structure using the Kriging interpolation method. Husain [64] performed a shape optimisation of micro-channel heat sink through polynomial, Kriging and radial basis neural network methods.

2.3. Current Status of Nano-Fabrication Patterning Technologies

Nano-technology was first provided in 1959 by Richard Feyman [65]. The term "nanotechnology" was later defined by Norio Taniguchi in 1974 and developed extensively into engineering and academic fields for the last 20 years. The idea of nanotechnology is to control matters at a 1-100nm in at least one dimension and the creation of materials, devices and structures around this dimension. The significance of

this scale has been useful in a vast range of applications such as biomaterials, electronics and medicine especially to deal with the increasing demands for miniaturised products. Nanofabrication becomes a key to manufacture functional nano-devices and systems down.

In microelectronics industry, IC feature size is reducing at a rapid rate to couple with the trend of product miniaturisation. The semiconductor and microelectronics industry has been the main driver to push fabrication technologies to their dimensional limit. Nano-fabrication is already being applied in semiconductor manufacturing to enable IC with a minimum circuit feature of 32nm in 2007 [66]. Moreover, this kind of tiny IC chip must be produced in mass volume to satisfy huge demands in all kinds of electronics product in parallel with huge investment in production tools.

Optical lithography is the only technology capable of patterning over a hundred wafers per hour at this dimension. However, optical lithography incurred a high cost owing to its expensive tooling and equipments. In mid-1990s, nano-imprinting lithography was developed with same patterning capability but at a lower cost than the optical techniques. X-ray lithography is also a good alternative patterning technique because of its shorter wavelength than optical. Still, there exists difficulties to make X-ray masks and related manufacturing reliability issue for X-ray techniques remains a challenging part apart from cost and yield issues. Other nanofabrication technologies arise such as scanning probe system and molecular self-assembly. Scanning probe is simple to use and with low cost. However, the pattern area is small and speed is relatively low. Molecular self-assembly is targeted as a main future trend but it requires a guided control for useful patterning. Recently, photon-based lithography, electron beam and ion beam-based lithography, and reactive-ion etching have all been

studied and researched in contribution to next generation of nano-world. Electron beam and ion beam lithography has its strengths of high resolution and high flexibility. Focused ion beam has a widespread application in nanofabrication such as nano-features micro-machining, simple structures fabrication and ion lithography in semiconductor industry [66].

2.3.1. Modelling the Focused Ion Beam Sputtering Process

As part of the nano-fabrication, this part provides review of capability of micro-machining focused ion beam sputtering process, associated modelling work and experimental work. Research in the area of nano-fabrications using focused ion beam for micromachining of fine features and cavities at nano-scales are reviewed. This fabrication process has gained more popularity in micro-electronics manufacturing because of its strength to produce nano-features efficiently with high resolution when compared with the traditional chemical etching techniques.

The key and challenges of using this technique remain in shape accuracy of desired product its process control. Main researches and studies are focused on identifying a process control with regards to its process parameters to achieve accuracy in shape. Modelling work and experimental work have been carrying out in parallel. Numerous studies have been dedicated to modelling the FIB process behaviour in terms of depth variation control [67] [68] [69]. Other interests of process performances control from modelling perspective such as surface smoothness [70] and etching rate are also studied. Depth variation is the focus of interest as a process performance characterising the final shape corresponding to the pre-defined shape. Vasile *et al.* had modelled a

parabolic trough circular, a rotationally symmetric sine pattern, a sinusoidal pattern, and a dome convex shape on silicon Si(100)-type substrate in micrometers scale as shown at scanning electron microscopy viewing angles in Figure 2-1 [68]. Figure 2-1 shows: (a) a parabolic trough ion milled in Si(100), using a 10 mm×35 mm pixel pattern, (b) rotationally symmetric sine pattern ion milled in Si(100), (c) sinusoidal pattern ion milled in Si(100) on a 60 mm×330 mm pixel pattern, (d) convex dome based on a 15 mm diameter circular pattern.

(a)

(b)

(c)

(d)
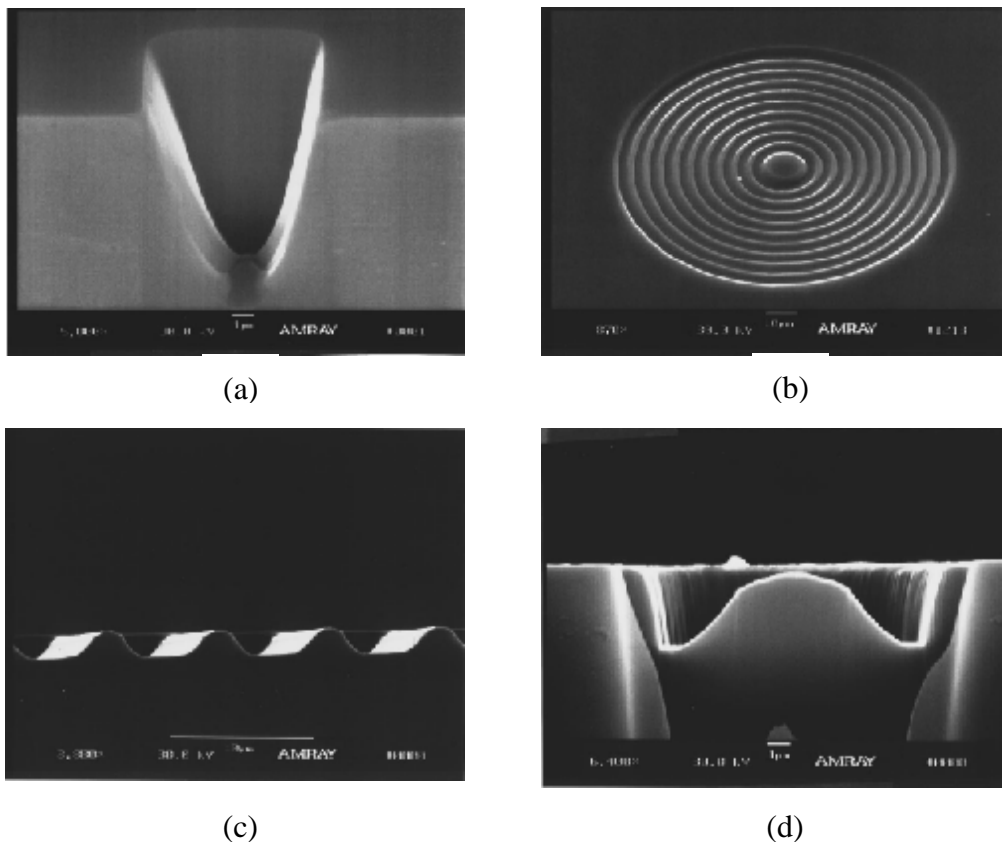
Figure 2-1 Different nano-patterns achieved by focused ion beam [68]

These shapes were modelled in the interests of depth profile and the final shapes shown above were then verified against predicted shape. A pixel scheme was introduced to define the geometry and characterise the beam movement. Analysis of process parameters were given by Vasile *et al.* [68] accounting for the effect of dwell time, pixel size and beam diameter on the depth variation. Experimental result has shown that the longer the dwell time, the deeper depth resulted. Correlation of pixel

size and beam diameter was also found to affect the ion dose at a pixel due to 'overlapping effect' in the ion distribution tail region between two adjacent pixels. However, in his work, overlapping were not addressed which showed an impact on depth variation. Re-deposition effect of sputtered materials was not considered which has an influential impact on the sputtered shape.

The mathematical model that relates the etched shape and the dwell times required to achieve a predefined shape using a numerous process parameters are initially investigated by Vasile *et al* (see Equation (2.1)) in [71] [72].

$$Z_{ij} = \iint \frac{\Phi(x, y)}{h} f_{x,y}(x_i, y_j) Y(E_0, a_{x_i, y_j}) t_{x,y} dx dy \tag{2.1}$$

In his model, a square pixel matrix is assumed which placed over the target surface. The sputtering model is discretised over each element of the pixel matrix so that ultimately a system of linear equations that relates the dwell times $t_{x,y}$ with the sputtered milling depth Z_{ij} at any pixel (i, j) is constructed. This system of equation then can be solved numerically. Vasile *et al* provided a well constructed structural approach to account for geometrical details of the pixels as a fundamental step to evaluate all pixel dwell time.

A similar depth model is developed by Fu [73]. Depth variation is expressed as a function of ion dose, dwell time and sputtering yield denoted by Equation (2.2).

$$D(x, y) = \frac{nlt}{2eps^2} \sum_i \sum_j \exp^{-\frac{(x-x_i)^2 + (y-y_i)^2}{2s^2}} \tag{2.2}$$

where $D(x, y)$ is the ion dose distribution, n is the number of scans, l is the beam current, t is the beam dwell time, e is the electron charge, s is the standard deviation

of the Gaussian distributions. x_i and y_i are the coordinates of the beam position stepped in x and y directions with a step size of dx and dy throughout the etching area.

$$Z(x, y) = \frac{1}{r} \times D(x, y) \times Y \qquad (2.3)$$

The depth profile of the shape $Z(x, y)$ is governed by ion does distribution as mentioned in Equation (2.3), atomic density of target material denoted by r as well as the sputtering yield Y which depends on parameters that affects ion-surface mechanical interaction like ion beam energy. The models capture all associated parameters in simulating the real process as a whole profile. This work provided an important understanding and a fundamental way to account for depth variation during the focused ion beam micromachining process.

Depth profile have been formulated as a function of process parameters such as sputtering yield, beam intensity profile, geometric pixel scheme, materials property and numerous process parameters. The key challenges for modelling FIB are how to control those process parameters to achieve a critical precision of the objective in the 'nano-scale' process. Many studies had investigated carefully on the sensitivity of these parameters individually. For instances, the relationship of sputtering yield and determined incident angle was identified in simulation and experimental test case for 2D structures fabrication in [74]. Long dwell time leads to deeper sputtered depth due to reduction of scanning number on pixels [75]. Aperture size, ion dose and flux distribution are included in a model by Fu *et al* [73]. System voltage, pixel spacing, scanning sequence are discussed in [76]. It reported that material removal rate increased when high voltage, large aperture size, short pixel spacing, and long dwell time. Some optimal conditions for FIB were also discussed [77]. A more complete study covered

the overlapping and re-deposition has been done which implement a two-Gaussian function to describe the intensity profile of ion distribution [78].

2.3.2. Modelling Various Beam Movements

One of the main differences between the methods of Vasile [71], and Fu [67] is the beam movement simulation. Shape is either achieved by milling 'vertical' block or 'horizontal' block that as depicted in Figure 2-2 (a) and Figure 2-2 (b). A parabolic shape is defined when numerous blocks are formed by two different beam movements over the surface pixels. Vasile adopted a single passing scheme, i.e. the ion beam would only pass each pixel once and stay long enough to make sufficient sputtering. In this way, the dwell time is varied among pixels to produce the final shape. Fu suggested a layer-by-layer approach where the ion beam moves repetitively across the pixels and remove materials through multiple passes. Layers are milled in sequence from top to bottom with multiple scans as shown in Figure 2-2(b). Dwell time are fixed and kept steady for each pixel throughout the entire process. Once the expected depth of the first slice (block) is complete, the beam restarting position moves inwards to the centre in order to allow milling of the second slice until the pre-defined geometry is obtained.

Vasile method is implemented under the assumption that pixel size must be small enough such that a flat line representation is used for a curve segment of parabolic wall with a small slope. However, varying the dwell time is practically not preferable due to limitation of the equipment control. Instead, Fu method is more preferable in real experiment. The angle of incidence of ion beam hitting the substrate is not captured as a plain surface is always obtained after each scan by the beam movement with fixed

dwell time. However, a small angle is always resulted when the ion beam move from one pixel to another. This small angle is proven as influential factor which affects the sputtering yield and hence the rate of materials removal. Similar work has been suggested by Kim [79], a slice by slice method with a helix path in order to reduce the re-deposition effect having the beam milled away the re-deposited materials immediately after they deposited instantly on the surface. Figure 2-3 illustrates the beam scanning path in top view for Vasile and Kim methods.

*Dash line indicates the intermediate shape
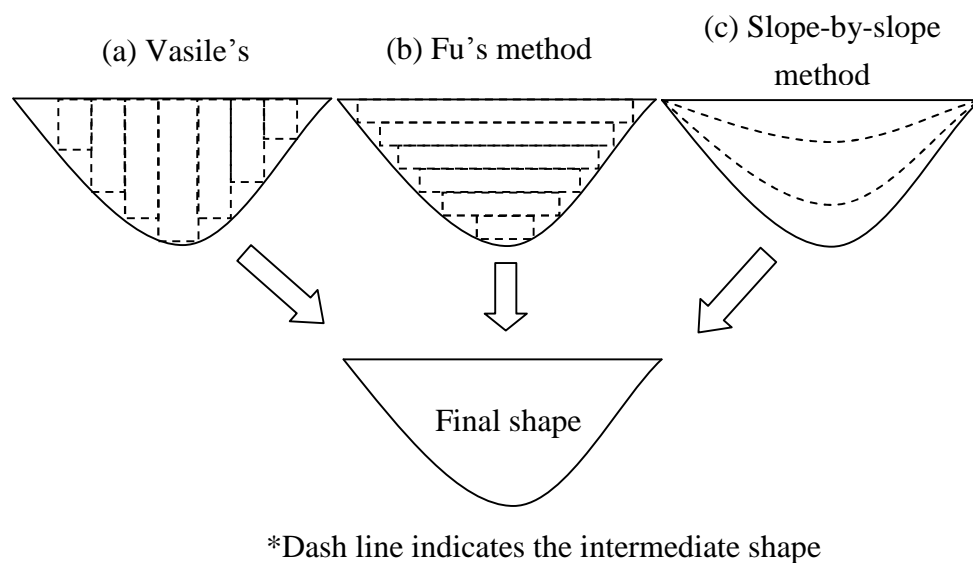
Figure 2-2 Shape achieved by different beam movement
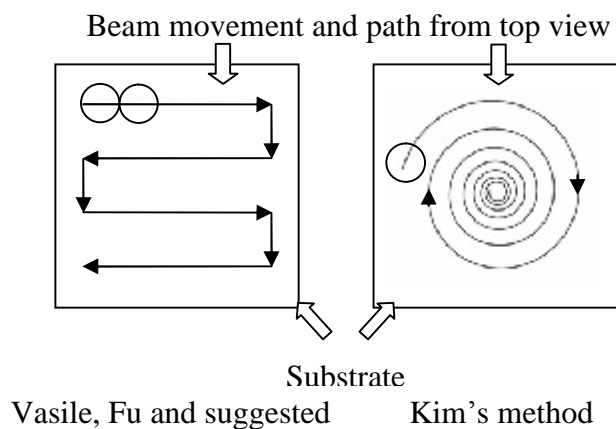
Figure 2-3 Top view of two different beam scanning paths

The FIB model in terms of beam movements is indicated by Figure 2-2(c). It is a modified method of Fu and Vasile method. A normal horizontal and vertical sequential path is used instead of the helix path. The initial dwell time is adjusted to create a slope/slice allowing ion beam angle of incidence to be taken into account for depth variation. Figure 2-4 shows how the angle of incidence is formed during the ion beam movement between pixel 1 and 2.
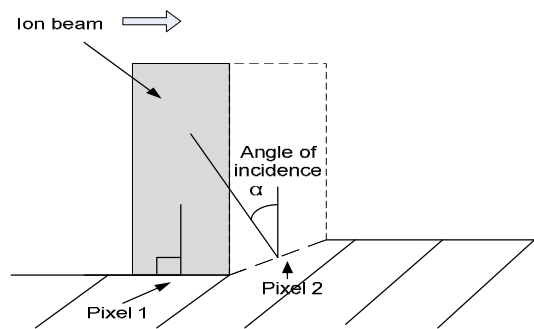
Figure 2-4 Incident of Angle is formed between pixels across the beam direction

2.3.3. Studies on Re-Deposition Effect

Another crucial issue which affects the accuracy in predicting the final shapes is effect of re-deposition. Some early work has described the occurrence and impacts of the re-deposition. It was found that re-deposition is most likely to occur on the sidewall near the root of the shape [80]. In the same study he found that re-deposited material will adhere to the sidewall of a 3D structure with an aspect ratio higher than 1, and deposited on the bottom causing a variation of milling depth for a structure with a low aspect ratio (normally smaller than 1) [80]. He then reported low ion energy and a smaller ion spot size can reduce the re-deposition effect on the sidewall in his other study [73]. Tseng [81] worked out a model to account for the volume of the actual re-deposition which has been taking into consideration during FIB model implementation in this work. Ishitani and Ohnishi [82] further modelled the sputtering and re-

deposition fluxes under assumption that the sputtered atoms are emitted according to a cosine distribution with regard to surface normal. Modelling for re-deposition and sputtering fluxes is also given in [83].

2.4. Trends and Development in Electronics Packaging Industries

Integrated circuit packaging technology has been advanced rapidly to further reduces the package thickness accommodate the miniaturisation trend of electronics products. There have been breakthrough and developments in electronic products in terms of product size. The flip chip application was a remarkable outcome of miniaturisation.

2.4.1. Integrated Circuit Assembly Technologies

Integrated circuit (IC) assembly is the first processing step after wafer fabrication. IC assembly is defined as the process of electrically connecting I/O bond pads on the IC the corresponding bond pads on the package [84]. Four interconnection IC assembly technologies: wirebonding, tape automated bonding (TAB), flip chip are explained in Figure 2-5. Flip chip advances were reviewed.
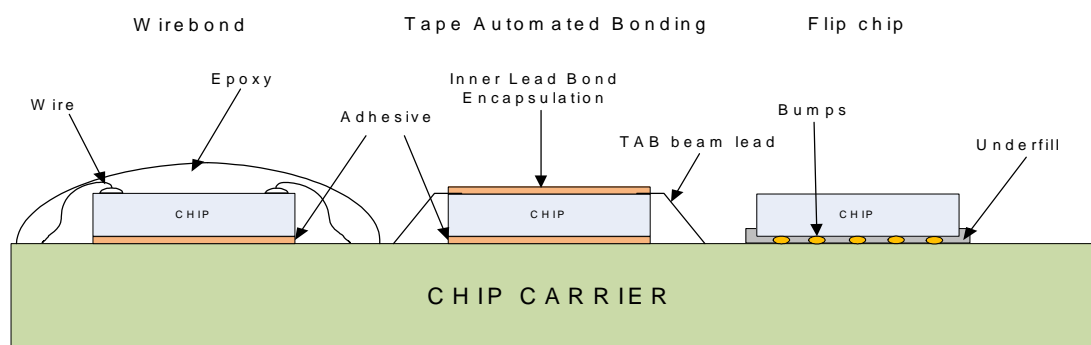
Figure 2-5 Four interconnection IC assembly technologies

Flip chip is one of the most remarkable breakthroughs in IC assembling technologies which achieves big improvements in reliability, productivity and cost reduction. It is an interconnection method between the IC and a chip carrier or substrate with the active face of the chip facing toward the substrate. Flip chip packaging involves four steps: past printing, chip bonding, reflowing, and underfilling and the process is illustrated in Figure 2-6. Solder are deposited onto the chip bumps in the final step of wafer processing of IC preparation and are flipped over to face towards the substrate. The bumps are aligned and stacked onto the corresponding metallised pads of substrate precisely. Solder bumps are liquefied during reflowing process to mount the IC and substrate together. Finally underfill is injected to encapsulate the flip chip [84].
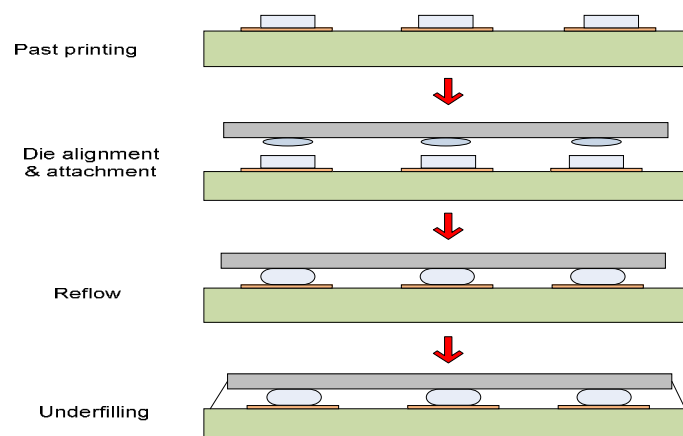
Figure 2-6 Flip chip assembling process with solder alloy

Flip chip is well-recognised and widely adopted which can be a replacement of wirebonding and TAB technology because it provides the shortest lead wire, that greatly reduces inductance, allows higher speed signals. Flip chip is much smaller than the carrier both in area and height which also allows higher density, greater number of I/Os. The merits of high I/Os, high electrical performance, high reliability makes flip chip as the most dominant IC assembly technologies in the 2000s.

2.4.2. Computational Modelling for Flip Chip Assembling

Computational modelling such as computational fluid dynamics (CFD), finite element method (FE) and finite volume (FV) method can provide valuable analysis to obtain solutions of engineering problems especially in electronics manufacturing industry. CFD has been employed to understand how air, water and fluidic flows and behaves. For example, CFD is used to analyse the behaviour of underfill. Underfill is dispensed to seal the chip and substrate at the final step of flip chip assembling process. Void, caused by unwanted air in the liquid, is a common of defeat that easily occurs when the underfill fills the space between chip and substrate. Flow of underfill injection process has been modelled [85]. It showed that underfill movement controlled by process parameters such as dispense head velocity, together with geometric parameters like stand-off height and solder mask thickness were the factors affecting void formation. Khor [86] has studied the void formation in terms of viscosity and pressure distribution of underfill with various injection methods using finite volume based CFD simulation.

Finite element method (FEM) is a numerical technique for obtaining solutions to different engineering problems. Engineering problems are often expressed as partial differential equations (PDE) or integral equations with boundary and/or initial conditions. However, analytical solutions to these equations may not always exist due to non-differentiable and non-integrable equations. Different numerical methods such as finite element, finite difference, finite volume, boundary element and particle method, can be used to address the problems. Computations of finite element analysis (FEA) enable evaluation of response in a physical system to certain imposed condition (loading) in engineering problems including structural, thermal, fluidic flow, electromagnetic or coupled multi-physics problems. Associated interests of responses

49

in electronics packaging industry include structural strength, structural distortion, effect of temperature changes on stress, fatigue and dynamic behaviour (vibration). Process performances during soldering process of different types of lead-free solder joints and underfill were reviewed. Fatigue formation is one of the important issues for product reliability improvement. Finite element model also plays an important role in material selection and determining the optimal process during the transition period from tin-lead solder to lead-free solder. However, the emergency of lead free solder like SAC solder demands careful investigations on the temperature control during reflow soldering process. Reflow temperature are required to adjust to $210^{o}C$ (melting point of SAC solder) to turn solder into 'liquidus' state. This temperature can cause damage to the substrate and die as the substrate CTE is much lower than that of SAC solder. Crack formation and defeat of SAC solder were studied by experimentally validated FEA model [87]. It was found that crack or flip chip warpage occurred due to the CTE mismatch between the substrate and solder joints. To reduce the effect of this CTE difference, underfill can be used as a buffer agent to compensate this difference [88]. Furthermore, FE model was constructed to investigate the relationship between crack formation and geometry parameters (standoff height, lower/upper contact angles of solder joints and materials) as well as material parameters (CTE, and Elastic Modulus). Thermal loading and their associated impact on thermal deformation was then identified among different lead-free solders and underfills [89]. This work [90] detailed the effect of shear parameters on shear strength at solder joints in the flip chip.

2.4.3. Reliability Assessment and Design Optimisation

Finite element (FE) method is a helpful tool to assist reliability study. Reliability is defined as the ability that an item can perform its required function under stated

conditions for a specified period of time [91]. Reliability testing has its importance in the study of fatigue formation and in the prediction of the life time of electronics products. Different reliability tests such as thermal, mechanical and moisture tests may be performed. The key consideration in design and manufacture is to ensure that the expected lifetime of the components is adequate for the application. Dynamics (transient) type of FE analysis is applied when loading is continuously applied for a certain period of time for electronic devices. Reliability testing have been performed on flip chip with the assistance of FE model such as drop-off and vibration test [92], humidity tests, and thermal-mechanical test to investigate devices.

In flip chip package involving the use of solder joints (or solder balls), fatigue damage is probably the most critical topic. Continuous cycle thermal loading were applied to investigate fatigue formation which shortens the life time of the package. This transient type of FE analysis was carried out both numerically and experimentally. It helped understand the solder joint crack and fatigue formation to deduce the life time of the package [93]. Accelerated thermal-cycle testing was mentioned to understand the dynamics behaviour [94]. Earlier work has identified that underfill follows a nonlinear material property and Sn-Ag-Cu solder possess a visco-plasticity material property. A hyperbolic sine law constitutive equation [95] denoted by Equation (2.4) for Sn-Ag-Cu has been employed. It detailed the inelastic strain rate in modelling fatigue formation under thermal cycle loading due to the visco-plasticity material properties. The constitutive equation (see Equation (2.4)) for the lead-free solder inelastic strain rate:

$$\dot{\varepsilon}^{creep} = A[\sinh(a\boldsymbol{s})]^n \exp\left(\frac{-Q}{RT}\right) \tag{2.4}$$

where $\boldsymbol{s}$ is the stress vector, R is the universal gas constant, T is the temperature

Equation (2.4) involves the following empirical values: $A = 277984s^{-1}$, $n = 6.41$,

$a = 0.02447 \times 10^{-6} Pa^{-1}$ and $Q = 6500R$. The values of the coefficients are given in [96] [97]. The work illustrated that the life (number of cycles to failure) of a single solder joint is predicted based on the accumulated creep strain and accumulated creep strain energy density. On the other hand, the effects of different design parameters and materials parameters on the thermo-mechanical reliability performance of solder joint flip chip are evaluated [98].

2.4.4. Environmental Impact Assessment

By July 2006, all manufacturers of electronic and electrical equipment sold in Europe must comply with the Directive 2002/95/EC of the European Parliament and the Council on the Restriction of the use of Hazardous Substances (RoHs) mandating the reduction of six hazardous substances [2], so as to protect human health and environment from the disposal of waste electrical and electronic equipment. Electronics manufacturing industry must incorporate environment management policy - 'Design for Environment' (DfE) in order to couple with worldwide trends towards 'Green Electronics'. Quantification of the environmental impact of design alternatives must be implemented. Two environmental impact assessments are commonly used in industry: *Life cycle assessment* and *Toxic Potential Indicator*. Different packaging technologies, through hole technology (THT), surface mount technology (SMT), chip size package (CSP) have been examined for their material content and have been evaluated with the toxic potential indicator [99]. The environmental prospects of solder material used on PCB during reflowing process are also evaluated [100].

Life Cycle assessment - Life Cycle assessment (LCA) is a widely accepted approach for detail environmental impact assessment for electronic products [101]. Environment standard such as ISO 14040 was published in 1997 to standardise life cycle assessment [102]. The challenges of using life cycle assessment arise as LCA does take a long time to perform a full analysis on electronic products due to many sub-assemblies involved, complexity of materials interactions and their proceeding process. Moreover, due to the lack of LCA software database, industry intended not to undertake LCA but use some simpler non-LCA method to assess environmental impact.

The Toxic Potential Indicator (TPI) - The Toxic Potential Indicator (TPI) published by Fraunhofer IZM in Germany is one of the non-LCA oriented assessment methods [11]. TPI is a numeric indicator which identifies the toxicity of materials by means of the Material Safety Data Sheet (MSDSs) [103]. The sources to determine this indicator is EU and Germany based according to the three areas: (1) Hazardous Substance Declaration (R-phrases), (2) Allowable Workplace Concentration (MAK) and (3) Water Pollution Classification (WGK). Item (1) depends on hazardous identification, stability, reactivity and toxicological information. Item (2) depends on exposure control and personal protection. Item (3) refers to Ecological information and disposal information. The information are gathered and extracted from MSDS. The final TPI value is derived by logarithmic aggregation calculation and modification of a scaling factor. TPI also covers indicator like energy demand during usage and production and recyclability. TPI is simple and cost effective to use. Most significantly, environmental impacts of materials for the entire electronic product are evaluated and analysed in early design planning stage rather than evaluation throughout the product life cycle.

Toxic Potential Indicator (TPI) has been introduced to assess the environmental impact of raw materials and only a few electronics and electrical products. For example, TPI has been computed for motorcycle [104] and personal digital assistant (PDA) [105] to evaluate the final product environmental impact. However, TPI is not widely applied to new emerging materials. Similar numerical index can be calculated for nano-materials-polymer in nano-technologies, and even for more complicated materials such as composite, alloy in electronics.

2.4.5. Cost Evaluation of Flip Chip Package

Environment laws prohibited the usage of traditional lead solder joint which gives rise to the lead-free solder such as Sn-Ag-Cu type (SAC) solder. The different materials incurred different costs and reliability requirements. These requirements on new materials such as SAC solder and adhesives are studied with the aid of constructing FE model. For instance, cost analysis is carried out to study the cost of the package assembly involving solder bump flip chip against wire bonding technologies [106] [107]. Cost analysis is only studied independently for the manufacturing costs of specific packaging technologies. However, studies on optimising costs of raw materials in maintaining certain reliability level for flip chip are not provided.

2.4.6. Multidisciplinary Optimisation

Flip chip package design considerations and packaging techniques have been researched for many years. Optimisation analysis has been carried out on flip chip design and manufacturing process in terms of reliability and costs. Design parameters are usually chosen and an *optimum* value is identified to minimise or maximise any

reliability and cost aspects subject to constraints according to customer requirements. Design evaluations and analysis such as thermal, electrical, structural and electromagnetic analysis are carried out independently. Optimisation is used to be performed with problem having a single objective. However, the current electronics packaging trends involves multiple disciplines. Multi-disciplinary optimisation is the key to manufacture a competitive new product. It allows designers to incorporate all relevant disciplines simultaneously since it can exploit the interactions between the disciplines. One example of multi-disciplinary optimisation work is illustrated by [108] which optimises criteria includes thermal, thermal strain, electrical, electromagnetic leakage, and cost, on a Ball Grid Array package design.

Closure

This chapter provides an overview of the methodology used in two industries: miniature product fabrication industries and electronics manufacturing industries. The following areas were reviewed:

- Concepts and development of risk mitigation techniques
- The latest researches of approaches in risk analysis methodology
- An exposition of current trend and development of nano-fabrication technology, an overview of the development and modelling studies in focused ion beam micromachining process
- Advances and developments in electronics packaging industries

Chapter 3 Reduced Order Modelling

This chapter details the development of risk analysis and mitigation methodology. The application of computational modelling is presented. A specific type of model using finite element method is outlined and how it helps understand the theory of solid mechanics. Material behaviour and its governing mathematical equations for elasticity and plasticity are discussed. The techniques of creating reduced order model through conducting the design of experiments and generating response surface are presented.

3.1. Risk Analysis Methodology and Reduced Order Modelling

The increased complexity of new miniaturised products and processes often makes real prototyping and testing difficult or expensive. Computational modelling can provide valuable insights into performance and reliability of products and generate knowledge on the optimal process control. These tools also play an important role in predicting process uncertainties, help achieving accurate target process performance and identifying optimal product design specifications.

The methodology objective is to integrate the latest advances in computational modelling, reduced order modelling, risk mitigation and optimisation modelling, using a detailed step-by-step approach. Engineer often assumes deterministic design and

process allowing no room for engineering tolerances and performances variations. However, in reality, these optimal specifications and design, from deterministic point of view, may not account for the risk of deviation from target requirements. Uncertainty and variation exist due to inherent uncertain nature in the design or process. They become more significant when we model the new processes and designs, and when adopting new materials. It is difficult and often impossible to control the existing variations in the micro-world. Therefore, design, process control and any associate computational modelling, require careful handling of uncertainty and respectively risk of not meeting defined requirements. To address these challenges, a methodology replying on certain techniques for analysis is required. The key concept of the methodology is in the integration of different techniques to provide a structured risk analysis and optimisation flow steps as shown in Figure 3-1. The methodology can be divided into three main building blocks: (1) Reduced order modelling, (2) Risk mitigation, and (3) Optimisation modelling. Three approaches can feed forward and backward data between as shown in Figure 3-1. It means data can be feed back to the other approaches to transfer of relevant data and results and to improve accuracy of the techniques and approaches.

(1) Reduced order modelling

Reduced order modelling comprises of two approaches: (1) Computational modelling and (2) response surfaces modelling. Design of Experiment is the required method which establishes the transfer of data between the two approaches. In a design (or process), design parameters and conditions must be first defined. Computational models can predict physical behaviour of micro- and nano- scale designs and the manufacturing processes. Experiments are used where possible to verify the

computational models and also can be used to enhance the model accuracy. Both computational models and experiments are time expensive to develop especially the case of complicated engineering problems. It is worthwhile to have a trade off between the fidelity and time. Therefore, response surface modelling can be applied to construct a reduced order model. Two methods are commonly used: (1) approximation method by regression analysis of response data and (2) interpolation for example by Kriging. Design of experiments must be carried out to provide limited number of design points to be evaluated with the computational models and used in the subsequent response surface generation. Additional DoE points may be added if necessary to improve the accuracy of the reduce order models. Their theories and application techniques are explained in chapter 3. The corresponding advantages and limitations will be discussed.

(2) Risk mitigation

Risk mitigation of two approaches includes: (1) Risk analysis and (2) Process capability modelling. These are explained in chapter 4. To understand any uncertainty and high risk-oriented issues in a process, sensitivity is often performed to identify the significant and critical design (or process) parameters during the process. After that, uncertainty data and distribution are specified and the developed reduced order model to characterise the process robustness by performing risk analysis. Both sampling and analytical methods can be employed to run the risk analysis. Since knowledge and historical data are very limited in new process which involves new materials, statistic inferences and theories are used to identify the probable failure region from the probabilistic perspective point of view. The ultimate aim is to identify the process capability when a design or process is exposed to uncertainties.

(3) Optimisation Modelling

The final building block of the methodology in Figure 3-1 is the optimisation modelling approach. In engineering problems, customer specifications are defined as objectives in terms of costs, process performances and quality characteristics. Any environment limitations or design limits are specified as constraints in order to formulate a design optimisation problem. Optimisation analysis is carried out using the constructed reduced model of the responses of interest. The formulated design optimisation problem is then solved mathematically to identify the 'optimum' design parameters or process conditions. In the presence of uncertainties, optimisation can also be used to identify optimal designs and processes.

In managing uncertainties, sampling methods, such as Monte Carlo simulation are undertaken to generate large number of response evaluations. Even with the assistance of computational tools, using high fidelity models such as finite element models in a Monte Carlo simulation become impractical and even impossible. Reduced order models are therefore developed in order to reduce the computational and time efforts. This methodology has been designed as a generic computational tool which can be implemented for both new advanced fabrications of new generated miniaturised integrated products as well as in novel micro- or nano-fabrication processes. It can be used for making assessment for other industrial processes and products to identify improvements and to increase the level of maturity of these technologies.
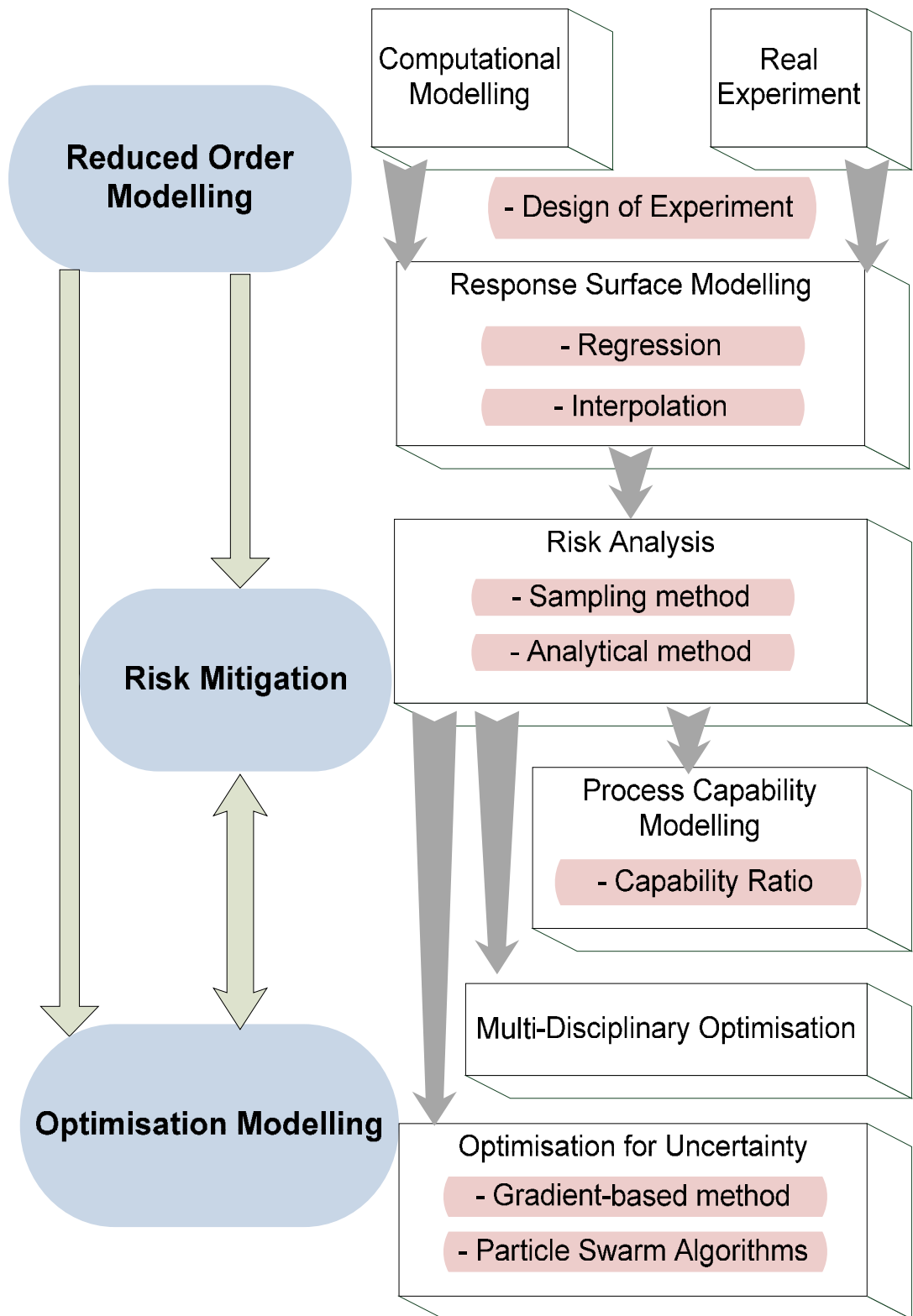
Figure 3-1 A risk analysis methodology for electronic products and fabrication process

3.2. Computational Modelling

Computational modelling is usually applied to problems with very high degrees of correlation between the physical and the mathematical aspects of a process with the aid of computers. The models explicitly realise most of the details and relationships on the design and process. Based on the degree of detail and the method selected, this could be a compute intense approach capable of predicting the responses of interest. Finite Element Analysis (FEA), Finite Volume Analysis (FVA) and Computational Fluidics Dynamics (CFD), are common techniques to build models for high fidelity analysis of a problem. Advantage of this type of model is the ability to characterise most of the details and relationships on the design and process input and output clearly and thoroughly. These models are able to compile millions analysis (handle by computational resources) which are unachievable by human hands processing. However, high fidelity analysis is computationally and time costly. In the following part, finite element models are constructed to demonstrate its capability and how finite element methods are used can help evaluate application problems.

3.2.1. Finite Element Method

Finite element method (FEM) is a numerical technique for obtaining solutions to different engineering problems. The finite element method first started in the 1960s which was applied on plane elasticity problems. The ideas behind the method was developed by Hrennikoff [109] and McHenry [110] who applied the method solving stresses in solids using one-dimensional elements. In particular, finite element model are constructed to gain knowledge and understanding in many aspects such as process behaviour and performances with respects to different materials physical property

61

subject to external loading like force and temperature change. The method is applicable to the problems of structural analysis, heat transfer, electromagnetic and fluid flow.

3.2.1.1. Procedures of applying finite element method

The finite element method always follows a standard step-by-step procedure.

(1) Understand the problem and make assumptions - It is essential to understand the physical nature of an engineering problem to presume analytical solutions do not exist that finite element method is required to derive a solution. Users must identify the geometry and degree of freedom, loading (static or dynamic type of thermo and structural loading), material model (linear elasticity or non-linear time dependent plasticity), and boundary condition of the problem. This helps identify appropriate mathematical model (such as truss model, plane stress model in 2-D, and axisymmetric 3-D stress and strain model) and making required assumptions.

(2) Discretise the continuum or solution domain into a mesh called finite element - The continuum of a problem is also called solution domain. The solution domain is discretised into many 'mesh' or finite elements. Interpolation functions are used to approximate the variation of the variables over each element. Polynomials are usually selected to approximate the shape function of the solution domain.

(3) Form element matrix equations – To form the matrix equation that represents each element after the finite element is defined. Each matrix equation expresses the properties of each individual element. One of the methods is Galerkin's method [111].

(4) Assemble all of the element matrices into a global problem matrix - The fourth step is to combine the matrices expressing the behaviour of the elements and form the matrix equations expressing the behaviour of the entire region. The global matrix is an expanded matrix by putting the individual matrix of each element together. The global matrix contains all nodes making up the computational mesh.

(5) Solve the global matrix system - The last step is to solve the above global matrix system which are formed by sets of simultaneous equations. The unknown nodal values of the variables are solved with the sets of simultaneous equations in the global matrix. Direct and iterative solvers such as Gaussin Elimination and Conjugate Gradient can be used. Newton-Raphson method can be applied to solve non-linear problems.

3.2.2. Structural Analysis on Solid Mechanics Problem

The method is applicable to structural analysis, heat transfer, electromagnetic and fluid flow. In particular, how finite element method is used to perform structural analysis a solid mechanics problem is discussed below.

3.2.2.1. Material behaviours

One of the important issues of structural analysis problems in solid mechanics is material behaviour characterised by elasticity, plasticity and rate dependent material behaviour. Material behaviour can be classified as: material linearity, rate independent material non-linearity and rate dependent material non-linearity.

Elasticity - The elastic material structure recovers and returns to its original shape when the load that deformed it is removed. The material can be classified as linear and non-linear. In linear situation, the stress is proportional to the strain that obeys the Hooke's law. Elastic materials do not dissipate energy when a load is applied and then removed. The following constitute equation (see Equation (3.1)) describes a linear material:

$$Stress = E \times Strain \qquad (3.1)$$

where E is the proportionality constant called Young's modulus or the modulus of elasticity of the material. In non-linear elastic material, the stress is not linearly related to the strain. The material deformation can still be recoverable after the load is removed.

Plasticity - Plasticity is defined as the material deforms and does not return to its original shape when the forces are removed. The deformation is permanent and energy in terms of heat is lost in the system. The term 'yield point' of a material is the stress at which plastic deformation begin. Prior to the yield point the material deforms elastically. Beyond this point a combination of elastic and plastic deformation occurs.

Rate dependent material behaviour - Time is taken into account to analyse the stress-strain behaviour of material during both elastic and plastic deformation. A visco-elastic material is said to follow rate dependent material behaviour which exhibits both elastic and viscous behaviour such that the material strain rate is dependent on time. It loses some energy when a load is applied and then removed. Visco-elastic constitutive laws describe the rate dependent behaviour of linear or non-linear elastic materials such as polymers, foams and rubber. Visco-plastic constitutive laws describe the rate dependent behaviour of linear or non-linear plastic materials such as metals. Materials exhibiting

visco-plastic behaviour are assumed to be rate independent below the yield point and rate dependent when the yield point is exceeded.

3.2.2.2. Equilibrium Equations

Figure 3-2 shows the stress and the body forces acting on each face of the cube in *x, y* and *z* directions. The body deforms due to the load. The deformation of any point at the body and the displacement vector is in Equation (3.2).

$$\{u\}=[u \ v \ w]^T$$

(3.2)

where *{u}* is the displacement vector in *x, y* and *z* directions
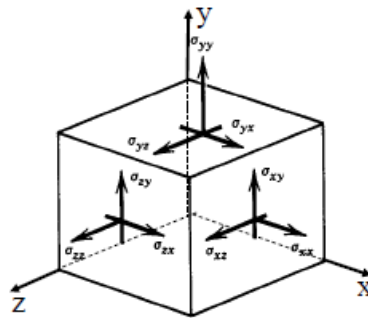
Figure 3-2 Stress and body forces acting on each face of the cube in *x, y, z* directions

The equilibrium equations that govern the conservation of force for a time independent static analysis are expressed as Equation (3.3):

$$\frac{\partial s_{xx}}{\partial x}+\frac{\partial s_{xy}}{\partial y}+\frac{\partial s_{xz}}{\partial z}=f_x$$

$$\frac{\partial s_{xx}}{\partial x}+\frac{\partial s_{xy}}{\partial y}+\frac{\partial s_{xz}}{\partial z}=f_y$$

(3.3)

$$\frac{\partial s_{xx}}{\partial x}+\frac{\partial s_{xy}}{\partial y}+\frac{\partial s_{xz}}{\partial z}=f_z$$

where s_{ij} and f_i are the components of stress and the body forces acting in the direction represented by i.

On a three dimensional body, stresses and elastic strain on the body is given by Equation (3.4) and Equation (3.5):

$$s = \begin{bmatrix} s_{xx} & s_{yy} & s_{zz} & t_{xy} & t_{yz} & t_{zx} \end{bmatrix}^T \tag{3.4}$$

$$e = \begin{bmatrix} e_{xx} & e_{yy} & e_{zz} & g_{xy} & g_{yz} & g_{zx} \end{bmatrix}^T \tag{3.5}$$

The strain to the displacement relationships can be represented via Equation (3.6):

$$\{e\} = \begin{bmatrix} \dfrac{\partial u}{\partial x} & \dfrac{\partial v}{\partial y} & \dfrac{\partial w}{\partial z} & \dfrac{\partial u}{\partial y} + \dfrac{\partial v}{\partial x} & \dfrac{\partial v}{\partial z} + \dfrac{\partial w}{\partial y} & \dfrac{\partial w}{\partial x} + \dfrac{\partial u}{\partial z} \end{bmatrix}^T \tag{3.6}$$

Stress relates to strain for linear elastic material (Hooke's law) in matrix (Equation (3.7))

$$\{s\} = [D]\{e\} \tag{3.7}$$

where the material matrix [D] in three dimensions are given by Equation (3.8):

$$D = \frac{E}{(1+u)(1-2u)} \begin{bmatrix} 1-u & u & u & 0 & 0 & 0 \\ u & 1-u & u & 0 & 0 & 0 \\ u & u & 1-u & 0 & 0 & 0 \\ 0 & 0 & 0 & \dfrac{1-2u}{2} & 0 & 0 \\ 0 & 0 & 0 & 0 & \dfrac{1-2u}{2} & 0 \\ 0 & 0 & 0 & 0 & 0 & \dfrac{1-2u}{2} \end{bmatrix} \tag{3.8}$$

where E and u are the Young's modulus and Poisson's ratio

For a solid mechanics problem, typical interest of using finite element method is to solve for the displacements of the mesh at the nodal points. This displacement result will be used to carry out further analysis during deformation such as calculation of different types of stress and strain at points within each mesh element.

3.2.2.2. Discretisation of solution domain

The geometric domain is first divided into many small sub-regions regarded as elements or mesh. The fixed points in the element defining their vertices are called nodes. All

elements are connected by these node points in the domain and on the boundaries. From

Equation (3.2), the displacement of the entire solution domain for a 3-D solid is:

$$\{u\} = \begin{bmatrix} u & v & w \end{bmatrix}^T$$

The displacement within the element is then assumed by polynomial interpolation using

the displacements at its nodes (nodal displacement) as Equation (3.9):

$$u^a(u,v,w) = \sum_{i=1}^{n_d} N_i(u,v,w)d_i = N(u,v,w)d_e \qquad (3.9)$$

where the superscript a stands for approximation, n_d is the number of nodes forming the

element, and d_i is the nodal displacement at the i-th node, which is the unknown need

to be compute and expressed in a general form of (Equation (3.10)):

$$d_i = \begin{bmatrix} d_1 & d_2 & \mathbf{K} & d_{n_f} \end{bmatrix}^T \qquad (3.10)$$

where n_f is the number of degree of freedom (DOF) at a node, for 3-D solids $n_f = 3$,

and d_1 d_2 $\mathbf{K}$ d_{n_f} are the displacement component $1, 2, \mathbf{K}, n_f$

The vector form of nodal displacement is given in Equation (3.11):

$$d_i = \begin{bmatrix} u_i & v_i & w_i \end{bmatrix}^T \qquad (3.11)$$

where u, v and w are the displacement in the x, y and z direction

The vector d_e is the displacement vector for the entire element as Equation (3.12):

$$d_e = \begin{bmatrix} d_1 & d_2 & \mathbf{K} & d_{n_d} \end{bmatrix}^T \qquad (3.12)$$

where d_1 d_2 $\mathbf{K}$ d_{n_d} are the displacements at node 1 to node n_d

N is a matrix of shape functions for the nodes in the element to assume the shapes of the displacement variations with respect to the coordinates. It has a general form of Equation (3.13):

$$N(u,v,w) = \begin{bmatrix} N_1(u,v,w) & N_2(u,v,w) & \mathbf{L} & N_{nd}(u,v,w) \end{bmatrix}$$ (3.13)

N_i is a sub-matrix of shape functions for displacement components at the ith node which is expressed as Equation (3.14):

$$N_i = \begin{bmatrix} N_{i1} & 0 & 0 & 0 \\ 0 & N_{i2} & 0 & 0 \\ 0 & 0 & \mathbf{O} & 0 \\ 0 & 0 & 0 & N_{i3} \end{bmatrix}$$ (3.14)

where N_{ik} is the shape function for the k-th displacement component (DOF) at the i-th node. The mesh element with various kinds of node can be used such as triangles, tetrahedral, and any other shape functions [112]. The above process describes how the solution domain is discretised. The displacement profile for each element is formed using polynomial interpolation with global coordinates of the element transformed into local coordinates. Element equations are then setup whilst satisfying the equilibrium equations. The equations obtained for each element are assembled with adjoining elements to form the global finite element equation for the entire solution domain. The global equation is solved for the entire displacement field.

3.2.2.3. Discretisation of Equilibrium Equation

Displacements are integrated with the equilibrium equations from (3.3) by (3.15)

$$\frac{\partial s_{ij}}{\partial x_j} = f_i$$ (3.15)

68

Numerous approximation methods such as Galerkin weighted residual procedure [111], can be applied to approximate the above equilibrium equations which expresses physical properties over each elements into a set of algebraic equations. The algebraic equations are then solved using matrix solvers and computer.

3.2.2.4. Solution procedures

In FEM, x in Equation (3.16) is obtained by assembling contributions from all the elements that are derived from the finite element discretisation of the equilibrium equations. Load and boundary conditions of the problem are specified. The linear system is then solved by matrix solvers and computers. The contributions of each nodal displacement nodes (u, v, w) from each mesh element and its adjoining mesh element are merged into a global matrix system for the entire solution domain as Equation (3.16):

$$[A]x = [B] \tag{3.16}$$

where $[A]$ is a banded systems matrix, containing the coefficients relating each degree of freedom, x is the vector containing all degrees of freedom, $[B]$ is the source terms

The objective in structural analysis problems is to solve displacement matrix in Equation (3.17) from forces F_i and coefficients K

$$F_i = KU \tag{3.17}$$

where F_i is the source term represents forces, K is the coefficients, and U represents displacement. The variable solved at this stage is displacement from the set of algebraic equations. Possible calculation can be different types of stress and strain at points within each mesh element during deformation.

3.3. Design of Experiments

The Design of Experiments (DoE) method is a useful tool to improve the products quality characteristics and process performances. It can be applied to understand the relationships between process variables and process output in characterising new or existing processes. DoE is usually implemented with other quality management tools that are associated with statistical process control to address the reliability and quality issues in product and process development. It is an efficient approach to achieve robust design and process, and to improve experimentation efficiency. Experiments are normally performed to explore some issues about a particular process or system. An experiment can be regarded as a test. The design of experiments is a test or a series of tests that the user can change the specific process variables to observe and study the underlying reasons for changes in the process performances.

Suppose a new unknown process is investigated which can be described by a function in the form of $Y = f(x, z)$, where x and z are process variables [design variables] (also known as the independent variables or input factors or input parameters) that affect process output [product feature]. Y (is also called dependent variable or response variable or output parameter) is the process output that measures process performances [quality characteristics]. The term inside the bracket is related to the terminologies from the product perspective instead of a process. ***Level*** is used to describe a process variable value used or tested in the experiment. Common synonyms are ***setting*** or ***test value***. For example, experiment of a two-level design indicates each process variable is set to either a *low* level (represented by '-') or a *high* level (represented by '+'). A ***design***

point is a point (data) which presents one set of combinations of the test value for each process variable and the corresponding process output. Common synonyms are known as *sample point* and *observation.* A *design space* refers to the possible options where multi-dimensional combination and interactions of design or process variables are found to fulfil design or process objective of a problem. Common synonyms are *sample space* (in the case of sampling) and *design domain.* A *design limit* refers to the boundary of the design space, also regarded as the minimum or maximum test value of a design or process variable. The term *un-scaled* is used to describe the true value of process variable with their units. The term *scaled* is used when a process variable domain is normalised within a particular region that unify each process variable unit. All process variables possess a common scale.

3.3.1. Application of Design of Experiments

In general, design of experiment is widely used in addressing engineering problems to reduce the overall costs of developing the products. Analyses using design of experiment are carried out to evaluate alternative designs and possibility of different materials. The reasons and advantages to perform a DoE are explained as follows:

- Process performances and product characteristics of product are improved via determining key design and process variables that influence the most to the quality characteristics and process performances.

- Unknown relationship and dependencies between process variables and output can be uncovered during the design development stage.

- Risk is quantified to improve manufacturability, reliability and robustness.

In engineering fields, the system and the relationships between the process variables and the process performances are often investigated. Considering a manufacturing process possessing two process variables x and z where n values on x and z are possible. Its process performance is denoted by Y. For example, a relationship between x and Y is governed by a curve in Figure 3-3 (a) and a relationship $Y = f(x, z)$ among x, z and Y is indicated by Figure 3-3 (b) respectively.

An example graph with x and z against Y

Y against x

(a)   (b)
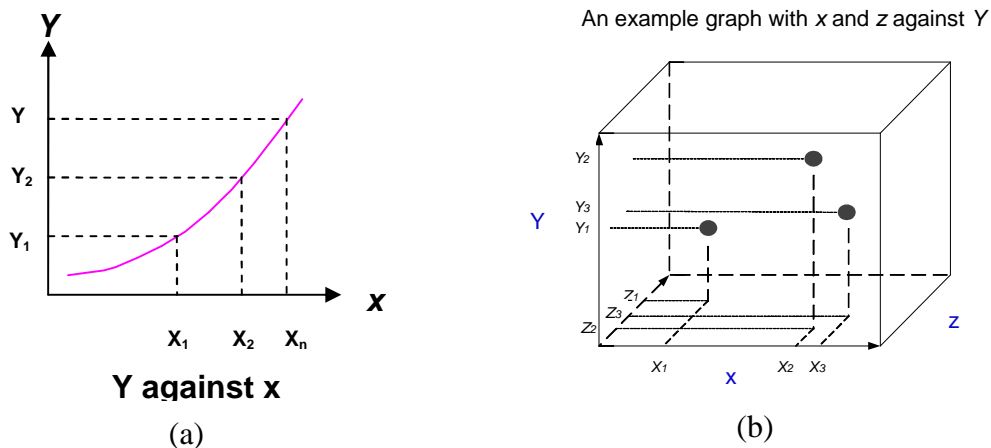
Figure 3-3(a) and (b) An example curve that summarise the relationship between x and Y, and the relationship $Y = f(x, z)$ among x, z and Y respectively

Let us assume the individual effect of process variable x on Y follows the curve shown in Figure 3-3(a). DoE can be used to achieve the following aims:

- Determine the value of Y when x is set to x_1, x_2, x_n or similarly, find what value x would result in a defined nominal value of Y

- Determine the range of x where Y is sensitive to variations in x

- By Figure 3-3(b), identify the most significant process variable that affects Y most

During a new process development, any unknown relationship between the process variables and process performances can be identified by graphs shown in Figure 3-3. However, manufacturing systems are complicated which associated with numerous

process variables and process outputs. For instance, the engineer may want to know how to set the value of x and z in order to achieve the desired nominal value of Y. There could be thousands of x value and z value combinations all providing different process output. It is costly, time consuming and impractical to run every combination as experimental test. Another huge challenge is which combination of x and z would be the best among all combinations in terms of cost, reliability and feasibility issues.

The effect of each process variable on the process output can be studied by undertaking DoE. Changes in the process variables may increase/decrease the process output and may have no effect. The effect of change in process output caused by the change in levels of a single process variable is called the main effect. DoE is applied to understand how each process variable x and z individually affecting the Y (regarded as main effect) as well as the interactions effect that x and z impose on Y in the above case. This can be done by undertaking a four trials experimental run. The objective is to observe the reactions on Y subject to change on x and z that is detailed as follows:

Trial	x	z	$x \times z$
1	-	-	+
2	+	-	-
3	-	+	-
4	+	+	+

In this design, the main effect of x is calculated by taking the average output of the runs with x at the plus (+) setting (runs 2 and 4) and subtracting the average output of the runs with x at the minus (-) setting (runs 1 and 3), Similarly, the main effect of Y is the average output for runs 3 and 4 - average output for runs 1 and 2. The interaction (joint) effect of two process variables is calculated by forming the product of the columns for

those two process variables, and then taking the average output of the runs with a plus setting in the interaction column and subtracting the average output of the runs with a minus setting in the interaction column. The interaction of x and z is calculated as the average output of the runs with $x \times z$ at the plus setting (runs 1 and 4) and subtracting the average output of the runs with $x \times z$ at the minus setting (runs 2 and 3). These details and results from the above three tests are also useful to derive what the most dominating process variables are that affect the response Y — individual effect of x, individual effect of z, and interaction effect of $x \times z$. Understanding the variability of Y with regard to variations on x and z is a fundamental step in improving process performances through adjustments of relevant process variables.

When dealing with experimental designs, it is required to scale the process variables with respect to their upper and lower limits (i.e. the maximum and the minimum values). One of the common ways to do the scaling is as follows:

$$ x_i = \frac{z_i - (max[z_i] + min[z_i])/2}{(max[z_i] - min[z_i])/2} \quad i = 1, \mathbf{K}, N \tag{3.18} $$

where z_i is the normal (un-scaled) process variable, x_i is the scaled process variable, and N is the total number of design points in the experimental design. The Equation (3.18) converts any process variables values from maximum to minimum into values between 1 and -1.

3.3.2. Different Types of Experimental Designs

Selection of DoE design refers to how to the method of choosing the representative process variable values so as to generate its process response. Process/design variable and response is specifically named as 'input and output factor' respectively. Many

different designs are available such as Full and Fractional Factorial Design, Central Composite Design, Latin Hypercube Design, D-optimal Design and Plakett-Burman Design. Each design has strengths and weaknesses [113]. Detailed description about different design can be found in [114]. Selection of any experimental designs is dependent on their capability to identify main and interaction effects of process variables on the process output according to resources constraints of running the experiment such as cost and time. A few typical and common designs will be described. The diagram presented by Figure 3-4 and Figure 3-5 are the examples to demonstrate experimental design with three process variables.

Nominal Design - A single point design referring to the central point in design space.

Plackett-Burman Design (Screening Analysis) - This design is particular useful and applied when experimental runs are very expensive. It is suitable for process variables with no interaction effects on process output. 2^n set of runs of experiments are required for a two-levels process where n is the number of process variables. The nominal design is used as a starting point, and for each process variable, two design points are generated: nominal design with lower limit and nominal design with upper limit.

Full Factorial Design - Full factorial experimental design is normally used when process variable interaction effects are presence and known. It is conducted after screening analysis tests and fractional factorial experimental design are carried out. This design is ideal for small number of process variables. For a two-level process, 2^n set of trial runs are required where n is the number of process variables. Figure 3-4 shows a three-variable full factorial design with a central point. Other points are taken from all the corners called factorial points. These factorial points are usually the upper limit and

75

lower limit of the variable domain. Process variables are varied simultaneously with two-levels at various combinations of their high and low levels. These designs allow us to estimate linear and two-level interaction effects of the process variables.
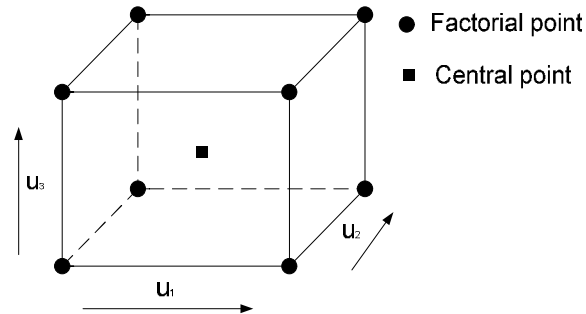
Figure 3-4 Full factorial design with the factorial points and central point

Fractional Factorial Design - Fractional factorial design is usually used as the first step to test the sources of variability of a process when only little knowledge is available and many process variables exist. It is a subset run of a full factorial experimental design. Fractional factorial designs offer a reduction in number of experiments without losing a lot of information. Fractional and full factorial designs are used when there is prior information about which process variables are important.

Central Composite Design - Central composite design uses the orthogonal table to perform the experimentation to determine the sample points of selected variables. It contains a fractional factorial design 2^n (levels are ± 1 and n is the number of input process variables) with a group of $2n$ axial points that allow for the estimation of curvature. In Figure 3-5, the first is a central composite design (CCD), where experiments are added to the factorial design after nonlinear behaviour is detected. The second is a modified CCD, called a face-centred cube design, where the added experiments lie on the faces of the space formed by the factorial design. In this experimental design, the treatment combinations are at the factorial points (upper and

lower limit) and the axial points. i.e. two of the variables are perturbed at a time and the third stays at the nominal value.
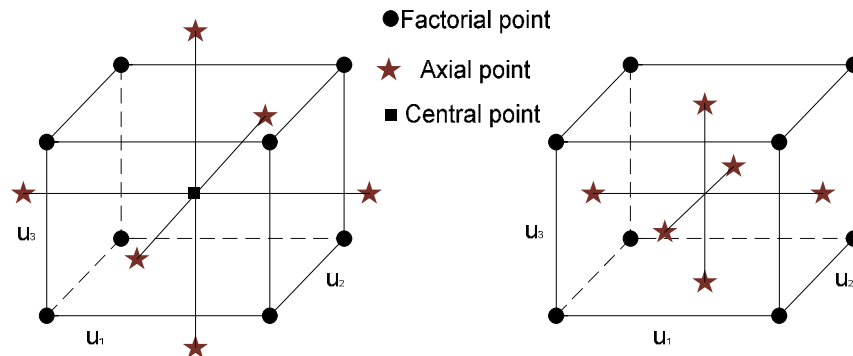
Figure 3-5 A typical central composite design & a modified face-centred cube design

A CCD is only effective for a rather small number of design variables. For practical purposes, especially with more than very few design variables, it could be useful to replace the factorial portion of a CCD with a fractional factorial design. The advantages of this design is, designs are rotatable (or nearly rotatable) and require only three levels of each process variable which is easy and simple to perform. These are three-level designs that allow us to estimate linear, two variables interaction and nonlinear effects of all process variables under study. They are used when there is prior indication of nonlinear behaviour or when a factorial experiment reveals the presence of nonlinear behaviour. They provide precise prediction of responses within the experimental region and are useful in identifying optimum conditions. It is worth mentioning that when a quadratic response surface model is fit to a composite design, the factorial points aim to estimating the linear terms and two factor interactions. In fact, the factorial points are the only points that contribute to the estimation of the interaction terms. The axial points contribute to estimating the quadratic terms. Without the axial points, only the sum of the quadratic terms can be estimated. The axial points do not contribute to the

estimation of interaction terms. The central point also contributes to the estimation of quadratic terms.

Latin Hypercube Design - The algorithm consists of two loops: For each of the n process variables, the range of the process variable is divided into m non-overlapping intervals on the basis of equal probability. From each interval one value is selected randomly with respect to the probability density in the interval. User has to specify the number of points (m). Random numbers are generated for each design variable between lower and upper bound user specified times. The specified number of points is selected from $n \times m$ number of points by permutation, where n equals number of variables.

In summary, undertaking design of experiments can provide understanding about the trends and dependencies between process variables and process outputs involved in the experiment. DoE also helps to study process and improve design robustness.

3.4. Response Surface Modelling

The approach was first introduced by Box and Wilson in 1951 [115]. The theme of response surface modelling (RSM) is to extract selected data points from a series of design of experiment to create an explicit approximation functions. Typically, approximations are constructed using lower-order polynomials. Other techniques for constructing response surface models are based on interpolation methods. For example, Kriging models are used and discussed. In this work, interpolation methods are generally more precise than the approximation ones as the response surfaces pass through all the data point. Evaluations of the response of interests (analyses) can be

obtained through either experiments or using computational models. The number of analyses in the design space undertaken depends on the approximation model. For instance, a first-order linear model requires the use of a factorial experiment or a fractional factorial design. Response surface modelling is used to characterise a product design or process where several input variables potentially influence the performance measure or quality characteristic (regarded as response). The input variables are called independent variables. The system or functional response is called dependent variables.

3.4.1. Approximation Method using Linear Regression Analysis

Regression analysis helps us understand how the value of the dependent variable changes when any one of the independent variables is changed, with the other independent variables remained changed. Regression function is constructed based on limited observed data points to approximate the true relationship between the response and independent variables.

3.4.1.1. Response surface generation using linear regression analysis

Regression model is a type of response surface approximation. It is an explicit function in the form of $\hat{y}(\mathrm{X}, b)$ which contains a vector of p regression coefficients. The objective of response surface model is to obtain estimators b, a vector of regression coefficients of the explicit function from N observations where $N \geq p$. Approximation errors must be taken into account between the actual and predicted responses at each data point. The approximation model can be represented by Equation (3.19):

$$y = \hat{y} + e = X b + e \tag{3.19}$$

where e is the vector of the difference between the actual and the predicted responses, X is the Model Matrix that based on the polynomial chosen, b is the vector of regression coefficients, y is the vector of true response function values, and $\hat{y}$ is the vector of predicted responses. The approximation errors e usually are in two types (1) random sampling errors, and (2) modelling bias errors that results prediction deviations from the actual responses. The Equation (3.19) here is valid under the errors assumption that observation is independently normally distributed with mean m and known variance s^2 [116]. All errors must have equal variance and the observations identically equal mean plus error. In reality, this assumption may not be true but it practically allows statistical evaluations on the approximation model. Consider a second order polynomial model (quadratic response surface model) in one independent variable, it is denoted by Equation (3.20) where estimators b_0, b_1, b_2 are assigned as the three unknown regression coefficients and x is the independent variable.

$$y = b_0 + b_1 x + b_2 x^2 + e \qquad (3.20)$$

3.4.1.2. Determine the estimator of regression model by least square method

The number of available data points should be more than the number of the unknown regression coefficients in general (i.e. $N \geq p$). Suppose that $N \geq p$ observations are available, a system of equations can be formulated from Equation (3.19) into a matrix-vector equation by Equation (3.21):

$$y = X b + e \qquad (3.21)$$

where y is a ($N \times 1$) vector of the real responses, X is a ($N \times p$) matrix of the regression parameters, b is a ($N \times 1$) vector of the regression coefficients, and e is a ($N \times 1$) vector of approximation errors. Consider an example of a quadratic response

surface model in one independent variable and N possible observations can fit to the model. A term called residue e where is defined as the difference between the actual and the predicted response value. Equation (3.19) may be rewritten in the matrix notation form as Equation (3.22) for a quadratic response surface model where

$$y = \begin{bmatrix} y_1 \\ y_2 \\ \mathbf{M} \\ y_N \end{bmatrix}, \quad X = \begin{bmatrix} 1 & x_1 & x_1^2 \\ 1 & x_2 & x_2^2 \\ \mathbf{M} & \mathbf{M} & \mathbf{M} \\ 1 & x_N & x_N^2 \end{bmatrix}, \quad b = \begin{bmatrix} b_0 \\ b_1 \\ b_2 \end{bmatrix}, \quad e = \begin{bmatrix} e_1 \\ e_2 \\ \mathbf{M} \\ e_N \end{bmatrix} \tag{3.22}$$

The *least square* method is used to estimate optimum value of regression coefficients b such that sum of the squared residuals (SSE) shown in (3.23) is minimised.

$$SSE = \sum_{i=1}^{N} e_i^2 \tag{3.23}$$

$$\begin{aligned} SSE = \sum_{i=1}^{N} e_i^2 = e'e &= (y - Xb)'(y - Xb) \\ &= y'y - b'X'y - y'Xb + b'X'Xb \\ &= y'y - 2b'X'y + b'X'Xb \end{aligned} \tag{3.24}$$

From Equation (3.24), since $b'X'y$ is a 1×1 matrix, or a scalar, and its transpose $(b'X'y)' = y'Xb$ is also the same scalar. To minimise the sum of squared residuals, the first derivative of SSE is set to zero in (3.25).

$$\frac{\partial SSE}{\partial b} = -2X'y + 2X'Xb = 0 \tag{3.25}$$

Then, from Equation (3.25) we have

$$X'Xb = X'y \tag{3.26}$$

Finally, the least squares estimator of b is obtained by multiplying the inverse of $X'X$ on both sides of (3.26), and we get

$$b = (X'X)^{-1}X'y \qquad (3.27)$$

Equation (3.27) is a solution of the least squares problem that is applicable to problems with the number of observations N and the p regression parameters in a response surface model where $N \geq p$.

Consider a problem with response $F(x, b)$ and m design variables. The general form of a second order polynomial reduced order model is expressed by Equation (3.28):

$$F(x, b) = F(x_1, x_2, ..., x_m, b_0, ..., b_{m,m}) = b_0 + \sum_{i=1}^{m} b_i x_i + \sum_{i,j=1}^{m} b_{i,j} x_i x_j \qquad (3.28)$$

x_i $(i = 1, \mathbf{K}, m), x_j$ $(j = 1, \mathbf{K}, m)$ are the design variables and b_0 is the vector of the model coefficients, b_i $(i = 1, \mathbf{K}, m)$ is a m-dimensional vector, and $b_{i,j}$ $(i, j = 1, \mathbf{K}, m)$ is a symmetric m-dimensional matrix, which have to be determined.

3.4.1.3. Pros and cons of polynomials and goodness-of-fit

Polynomial models are the most common empirical models for response surface methodology. Lower-order polynomial such as linear models and quadratic models have well-understood properties. They can flexibly cover certain number of design shapes. Moreover, they have a simple form such that they can be easily compiled computationally to perform quantitative analysis tasks such as optimisation. However, polynomial does have its limitations. The polynomial is constructed depending on the data points within the design space. It may provide a good fit if and only if the data points are bounded by the design space. It has a poor ability to predict response where the data points are beyond the design space boundary. Another limitation is that when polynomial models a more complicated problem in the reality, higher order polynomial

must be required which involves more number of variables. It demanded extensive amount of data for the increased number of variables which is impractical in reality.

The response surface is only an explicit approximation of a true response function. Using the response surface will inevitably lose some details of the true response function. The accuracy is hugely depending on the availability of data input and output and the how well-representing enough of the data points in the design space. There are numerical indicators to evaluate the goodness-or-fit of the approximated polynomials. Some common indicators are Standardised residual, Studentised residual, R-student residual and coefficient of variation. R-student residuals R^2 $(0 < R^2 \leq 1)$, also known as coefficient of determination, is commonly used to judge how accurate the approximation model is. The higher the R^2 value, the better fit the approximation model to the data points. In general, the approximation can be considered as fairly good if R^2 is achieved over 0.9. Another indicator adjusted R-student residuals (adjusted R^2) is generally considered to be a more accurate goodness-of-fit measure than R^2 [117]. After checking the relevant statistical (R^2) test, the effect of the regression equation is significant and highly relevant.

3.4.2. Interpolation Method using Kriging

Interpolation is a method of constructing new data points within the range of a discrete set of known data points which requires the predicted model passes through all the data points exactly. Interpolation using Kriging model is widely used to predict process response for performing optimisation analysis. Kriging originates from the field of geostatistics to predict responses for correlated data from a limited number of

experimental data in mining industry. The theory of Kriging was developed from the seminal work of its inventor, Danie G. Krige and further developed by Matheron [56]. Kriging is regarded as optimal interpolation that generates the best linear unbiased estimate at each location. It is applied to interpolate the value of a random field at an unobserved location from observations of its value at nearby locations to characterise spatial correlation. From Figure 3-6, spatial data distribution are observed at two points, point A and point B with known lag distance h between and known location vector s and vector $s+h$. Kriging is a geostatistics technique to interpolate any points at an unobserved location on the same spatial space based on the known observations at such as point A and point B and its correlation. A variogram $g(h)$ is first appeared and suggested by Matheron in 1962 in literature [118]. The variogram here is used for spatial prediction with respect to the lag distance h. In plotting the variogram against lag distance at some known locations by sample collections, we can understand how the variogram qualifies spatial correlations. Figure 3-6 shows variability is presence at those observations when variogram increases/ decreases with h. The variogram remains steady implies there is no correlation between the locations at such a distance h.
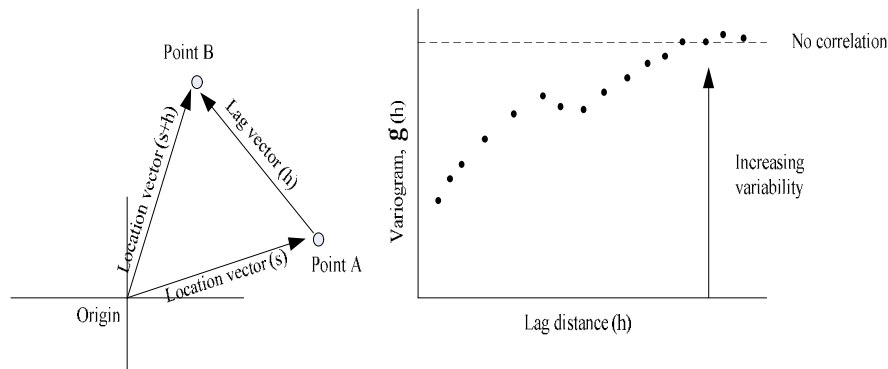
Figure 3-6 Spatial data distribution are observed at point A and point B, the right graphs relates the variogram plot to lag distance h between two points

The variogram $2g(\cdot)$ for distance h is defined by Equation (3.29) as:

$$2g(h) = E\{[Z(s) - Z(s+h)]^2\} \qquad (3.29)$$

$g(\cdot)$ has been regarded as a semivariogram. The variogram for lag distance h is defined as the mean squared difference of values by h in Equation (3.30):

$$2g(h) = \frac{1}{N(h)} \sum_{N(h)} [Z(s) - Z(s+h)]^2 \qquad (3.30)$$

where $N(h)$ is the number of pairs for lag distance h

3.4.3. Simple Kriging, Ordinary Kriging and Universal Kriging

Kriging refers to optimally predicting. Kriging interpolates the value $Z(s_0)$ of a random field $Z(s)$ at an unobserved location s_0 from observations $z_i = Z(s_i), \quad i=1,\mathbf{K},n$ of the random field at nearby locations $s_1, \mathbf{K}, s_n$. Let $\{Z(s) : s \in D \in \Re^d\}$ be a random function or process where D is a fixed subset of $\Re^d$ with positive d-dimensional volume, from which n data $(Z(s_1), Z(s_2), \mathbf{K}, Z(s_n))$ are collected at known spatial locations $\{s_1, \mathbf{K}, s_n\}$.

(1) Ordinary Kriging

Ordinary Kriging refers to spatial prediction under the two assumptions on mean and correlation error process.

- Model assumption (see Equation (3.31))

$$Z(s) = m + d(s) \quad s \in D, m \in \Re, and \ m \ unknown \qquad (3.31)$$

where $m \equiv E(Z(\cdot))$ is the deterministic mean structure and being *unknown*, and $d(s)$ is the correlated error process.

- Predictor assumption (see Equation (3.32))

$$\hat{Z}(s_0) = Z(s_0) = \sum_{i=1}^{n} l_i Z(s_i) \qquad \sum_{i=1}^{n} l_i = 1 \qquad (3.32)$$

85

where $\hat{Z}(s_0)$ is the Kriging estimator at unobserved location s_0, the coefficients of the linear predictor sum to 1 guarantees uniform unbiasedness. $E(Z(s_0)) = E(\hat{Z}(s)) = m$.

(2) Simple Kriging

Simple Kriging is one kind of Kriging where m is *known*, $m(s) = 0$ and the coefficients are not constrained to sum to 1.The optimal predictor $\hat{Z}(s_0)$ will minimise the mean-squared prediction error in Equation (3.33):

$$\sigma_e^2 \equiv E(Z(s_0) - \hat{Z}(s_0))^2 \tag{3.33}$$

over the class of linear predictors $\sum_{i=1}^{n} l_i Z(s_i)$ that satisfy $\sum_{i=1}^{n} l_i = 1$.

(3) Universal Kriging

Universal Kriging assumes an unknown mean model in $Z(s) = m + d(s) \quad s \in D, m \in \Re$, i.e. m is unknown and $d(s)$ is a zero mean intrinsically stationary random process with variogram $2g(\cdot)$. In Universal Kriging, a general linear trend model $m(s) = \sum_{j=0}^{m} l_j P_j(s)$ is assumed and the correlation error $d(s)$ can be quantified by a variogram. Hence, the Universal Kriging model can be defined as Equation (3.34)):

$$G(X) = \sum_{j=0}^{m} l_j P_j(X) + \sum_{i=1}^{n} g_i t_i \tag{3.34}$$

where $G(X)$ is the universal Kriging prediction model, X is the vector of the m design variables, $X = (x_1, \mathbf{K}, x_m)$, $l_j \; for (j = 0, \mathbf{K}, m)$ are the coefficients of the polynomials

$P_j(X)$ $for(j=0,\mathbf{K},m)$ and g_i $for(i=1,\mathbf{K},n)$ are the coefficients of the basic functions

t_i $for(i=1,\mathbf{K},n)$. The polynomials $P_j(X)$ $for(j=0,\mathbf{K},m)$ in this study are linear, i.e.

$P_j(X)=x_j$ $for(j=1,\mathbf{K},m)$ and $P_0(X)=1$. The basis function $t_i=j(|X-X_i|)$ is

called a variogram and has the absolute distance between point X and point X_i.

3.4.4. Determine Variogram Models

In geostatistics, the variogram $t_i=j(|X-X_i|)$ is a function characterising the degree of

spatial continuity of a data set or dependence of a random function. It is defined as the

expected squared increment of the values difference between locations point X and

point X_i. Instead of getting variogram through experimentations, many types of

variogram models are widely used in Kriging. A few common types of variogram

models are namely linear (Equation (3.35)), exponential (Equation (3.36)), spherical

(Equation (3.37)), Gaussian (Equation (3.38)) and power model (Equation (3.39)).

- Linear model

$$j_g(h_i) = \begin{cases} 0 & h_i = 0 \\ C_1 + C_2\|h\| & h_i \neq 0 \end{cases} \tag{3.35}$$

- Exponential model (valid in $R^d, d \geq 1$)

$$j_g(h_i) = \begin{cases} 0 & h_i = 0 \\ C_1\left(1-e^{-\frac{\|h_i\|}{C_2}}\right) & h_i \neq 0 \end{cases} \tag{3.36}$$

- Spherical model (valid in $R^d, 3 \geq d \geq 1$)

$$f_s(h_i) = \begin{cases} 0 & h_i = 0 \\ C_1\left(\dfrac{1.5\|h_i\|}{C_2} - 0.5\dfrac{\|h_i\|^3}{C_2^3}\right) & 0 < h_i \leq C_2 \\ C_1 & h_i > C_2 \end{cases} \qquad (3.37)$$

- Gaussian model (valid in $R^d, d \geq 1$)

$$j_g(h_i) = \begin{cases} 0 & h_i = 0 \\ C_1\left(1 - e^{-\frac{\|h_i\|^2}{C_2^2}}\right) & h_i \neq 0 \end{cases} \qquad (3.38)$$

- Power model (valid in $R^d, d \geq 1$)

$$j_g(h_i) = \begin{cases} 0 & h_i = 0 \\ C_1 + C_2\|h\|^l & h_i \neq 0 \end{cases} \qquad (3.39)$$

where $h_i = X - X_i$, C_1 and C_2 are the variogram coefficients, $C_1 \geq 0$ and $C_2 \geq 0$, and $0 \leq l < 2$ in the power model. The unknown coefficients in Kriging ROMs, $l_j(j=0,\mathbf{K},m)$, $g_i(i=1,\mathbf{K},n)$, and C_1 and C_2 are computed so that the error of variation of the predicted values in terms of linear combination of observed data is minimised [119]. The objective of Kriging interpolation is to predict unknown values from known data observed and minimises the errors at the predicted values that are estimated by distribution of observed data with fitting an appropriate variogram models.

3.4.5. Cross Validation to Compute Model Accuracy

Error estimation in Kriging is calculated by a process called cross-validation. Cross-validation is leaving one known response value out and estimating the prediction of that

response value by Kriging and we do this process to all known response values. The Kriging variance is also calculated for each Kriging prediction estimation. Let $y(x)$ be the observations from the real function and $\hat{y}(x_i)$ for $(i = 1, \mathbf{K}, m)$ be the Kriging predicted values at points $x_1, \mathbf{K}, x_m$. Four error estimators: mean deviation or mean error (Equation (3.40)), mean squared deviation or mean squared error (Equation (3.41)), mean squared deviation ration (Equation (3.42)), and relative mean error (Equation (3.43)), are calculated to evaluate the adequacy of the Kriging model.

(1) The mean deviation or mean error, ME is given by

$$ME = \frac{1}{m} \sum_{i=1}^{m} \left(y(x) - \hat{y}(x_i) \right) \qquad (3.40)$$

(2) The mean squared deviation or mean squared error, MSE, given by

$$MSE = \frac{1}{m} \sum_{i=1}^{m} \left(y(x) - \hat{y}(x_i) \right)^2 \qquad (3.41)$$

(3) The mean squared deviation ration, $MSDR$, computed from the squared errors and Kriging variances $s^2(x_i)$

$$MSDR = \frac{1}{m} \sum_{i=1}^{m} \frac{\left(y(x_i) - \hat{y}(x_i) \right)^2}{s^2(x_i)} \qquad (3.42)$$

(4) The relative mean error is given by

$$RME = \frac{1}{m} \sum_{i=1}^{m} \frac{\left(y(x_i) - \hat{y}(x_i) \right)}{y(x_i)} \qquad (3.43)$$

Since Kriging is an unbiased prediction method, ME should be close to 0. MSE should be as small as possible. If the model is accurate then the $MSDR$ should be close to 1. In summary, Kriging interpolation is a more precise method than that of regression approximation. Polynomial, one of the most popular methods is still widely used

because of its well known form and simplicity. The accuracy of both models should be evaluated before carrying out further task such as risk analysis and optimisation.

Closure

A specific type of computational model using finite element method is outlined and how it helps understand the theory of solid mechanics. The techniques to create reduced order model through conducting design of experiments and generating response surface are presented. Two response surface methodologies: approximation by regression analysis and Kriging interpolation are introduced.

Chapter 4 Risk Analysis Methodology: Risk Mitigation

This chapter demonstrates a modelling-driven risk analysis approach. The novelty is about its integration with other associated computational tools such as reduced order models and optimisation tools, in handling uncertainties involved in design and process parameters. In the analysis using Probabilistic Risk Analysis (PRA) approach, sampling and analytical method have both been adopted to propagate the uncertainties of quality/ performance metric of interests. Traditional statistics techniques can then be applied to evaluate the process performance and capability.

4.1. Risk Mitigation

Computational modelling can provide valuable insights into performance and reliability of products and generate knowledge on the optimal process control. However, in reality, these optimal specifications, from deterministic point of view, may not account for the risk of deviation from target requirements due to uncertainties in the design or process. Due to the emerging of risk, a deterministic optimal design is no longer suitable for modern industrial processes.. Mitigation the technology risk under limited knowledge becomes a major requirement to secure a successful development and insertion of the new technologies. A risk analysis methodology incorporates quantitative analysis is

introduced in this chapter: Probabilistic Risk Analysis (PRA) [5] , that are constructed to reflect the random nature of the constituent basic events such as component failures. A structured approach constitutes a conceptual flow and associated methods to characterise risk. Its main purpose is to quantify frequencies (probabilities) and the magnitude of losses. Risk management strategies, their break down and the integrated tools and methods is illustrated in Figure 4-1. The risk mitigation can be classified into three blocks. The first block includes sensitivity analysis which is used to identify the key process variables and the impact of variation of process variable. The second block includes risk analysis which accounts for the probability of failure when uncertainty is included in the process variables. Two methods are included namely sampling and analytical method. The third block uses process capability indice to characterise the output distribution from risk analysis. The objective of each block is depicted below.
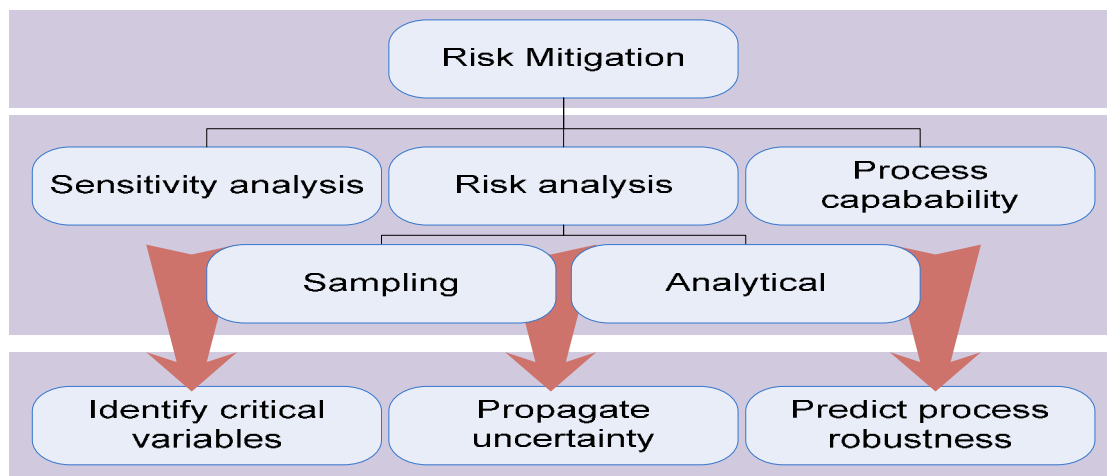
Figure 4-1 A hierarchy illustrates the risk mitigation framework

4.1.1. Understanding Variability and Uncertainty Using Sensitive Analysis

Variability of a process refers to the diversity in a well-recognised population. Uncertainty occurs in a poorly characterised population due to lack of knowledge about the process physical phenomenon. The process can possess either controllable variations

or uncontrollable variations due to common causes and special causes respectively. Variation due to common cause is often called 'natural behaviour' or 'randomness' of the process, caused by inherent variability in people, materials and environment. Natural variation induced from common cause and it affects all the process output. Unnatural or non-random variation is caused by special or assignable causes which are not part of the system. It does not affect all process outputs. Variations can be described by maximum and minimum value (i.e. tolerances) or described with a probability distribution through sample collections. Uncertainty and variability can both be described by a probability distribution which consists of mean, standard deviation and skewness.

Sensitivity analysis is used to study the impact of any variations of model input variables variations on the model output. Generally, a product/process metric of interest is defined to represent certain model behaviour. The model input variables are then varied such that the resultant changes on the model output can be observed. Sensitivity analysis is usually carried out based on an explicit function which represents the relationship between the model input variables and model output responses. Realisation of such function could be made through response surface generation. Therefore, DoE are necessary before sensitivity analysis and fit perfectly into the risk analysis methodology.

4.2. Risk Analysis

In most current manufacturing processes, variations can be observed and variability of a process is evaluated through sample collections on actual run of the system. During new design and process development, uncertainty exists due to the lack of knowledge about

the process. Engineers get more awareness on tackling uncertainty as well as dealing with variations. One of the common approaches to address the impact of uncertainty on the process output is *propagation of uncertainty*. Uncertainty distributions are programmed into a model to carry out risk analysis deriving the probabilistic distribution of process output uncertainty. The procedure is presented in Figure 4-2. Consider a process containing three process variables x_1, x_2 and x_3. The process performances are characterised by y which is expressed as a function of x_1, x_2 and x_3, i.e. $y = f(x_1, x_2, x_3)$. This function can be a response surface model or a full computational model.
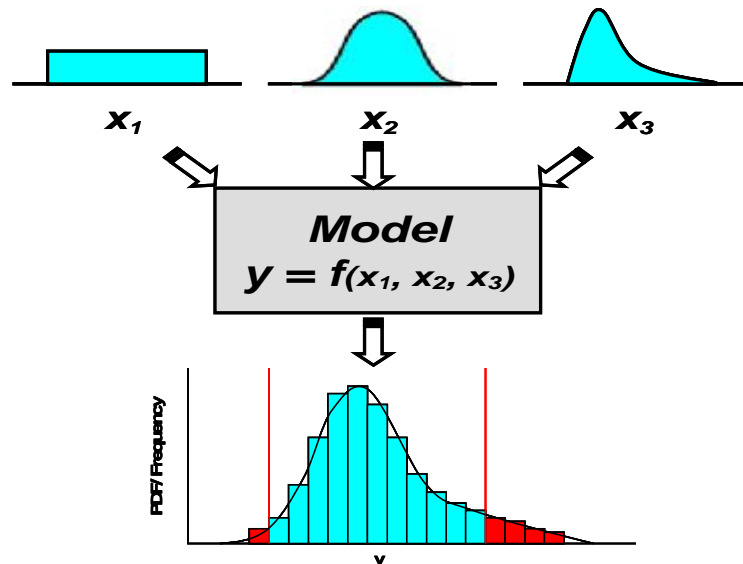
Figure 4-2 Uncertainty distribution are programmed into the constructed model

In reality, each of the process variables possesses a specified distribution of uncertainty. For example, x_1 has a uniform distribution, x_2 has a Gaussian distribution and x_3 has a Weibull distribution. These probability distributions are used as input for the model $y = f(x_1, x_2, x_3)$. The model output y is then generated as a probability distribution through two methods: sampling method and analytical method.

For sampling method, a random value is taken from each distribution of x_1, x_2 and x_3 respectively to form a *test value.* The corresponding value of *y* for this test value is computed via the model creating a *sample point*. Likewise, another test value is selected randomly to generate another sample point. The process is repetitive in order to generate thousands or millions of sample points. As a result, all sample points in terms of the frequency can be depicted as a histogram or a probability density function *(PDF)* as shown in Figure 4-2. The mean and deviation of this distribution can be calculated which propagates the interaction impact of any uncertainty in x_1, x_2 and x_3. Subsequently, *process capability* analysis is carried out based on the *PDF* that provides *confidence level* (also regarded as confidence interval, *CI*) with respect to customer specifications denoted by the region between two red lines. The *confidence level* does not give a value of the output variable *y* but it gives a percentage such that the process output is confidently comply with specifications. The passed samples can be described as *conformance* while the failed samples are described as *non-conformance*. For analytical method, no sampling is carried out. The probability density function *of y* is obtained by analytical calculation based on distinctive information of distribution x_1, x_2 and x_3 such as mean, standard deviation and skewness.

Sampling is a data collection process in which only a portion of data that is available (from the whole population) is collected. Sampling is often used to understand process variability since it is more cost, time and resources-effective than collecting all data from the whole population. Using statistical inference, conclusions can be drawn about variability of the sample data and other process output phenomena. Histogram, Pareto chart, control chart and scatter diagram, are graphical representation which helps presenting the data collected visually. Histogram is an estimate of the probability distribution of a variable. If the variable is discrete, the sample data is represented by

probability mass function while probability density function (*PDF*) is used for continuous data. The central tendency of *PDF* can be described by mean. Standard deviation measures how the sample data spread away the mean. For any symmetric distribution, the shape of *PDF* can be described by $m_Y \pm cs \quad c \in \Re$ where *c* describes the width of the distribution.

4.2.1. Analysis of Process Variability and Probability Distribution

4.2.1.1. Terminologies and definitions

Mean – The central tendency is usually measured by taking *Mean* and *Median*. The mean measures how and where the probability distribution is 'centred'. Mean is regarded as the average values of the populations or distributions. Median is defined as the 'middles' value that separates the lower and upper half of the population. Median is used instead of mean to describe the trend of distribution if the distribution is strongly skewed (distribution having a longer tail to the right than to the left or vice versa). Let X be a random variable which is continuous with a probability density function $f(x)$. The mean, or expected value of X, denoted m_x is:

$$m_x = E[X] = \int_{-\infty}^{\infty} xf(x)dx \tag{4.1}$$

where $E[X]$ is called *expectation* which is defined as a sum of all possible values of random variables weighted by the probability of each value occurrence, X can be a function and presented as $g(x)$ where $g(x)$ is a function of X.

Variance - Variability is measured by the quantity *variance* which tells us how 'wide' is the distribution spread out. Let X be a random variable with probability density function $f_X(x)$ and mean μ_X. The variance s_x^2 of X is defined by Equation (4.2):

$$s_x^2 = Var[X] = E[(X - m_x)^2]$$
$$= \int_{-\infty}^{\infty} (X - m_x)^2 f_x(x)dx \qquad (4.2)$$

Variance is sometimes computed as in Equation (4.3):

$$s_x^2 = E[X^2] - E^2[X] = E[X^2] - m_x^2 \qquad (4.3)$$

Standard deviation - Standard deviation and the square root of variance is denoted as s_x in Equation (4.4)

$$s_x = \sqrt{s_x^2} = \sqrt{Var[X]} \qquad (4.4)$$

A dimensionless indicator, *coefficient of variation* (u) is used to measure variability and the ratio of the standard deviation over the mean as shown in Equation (4.5):

$$u = \frac{s}{m} \qquad (4.5)$$

Covariance - In some circumstances, if more than one random variable exists and they influence each other, the quantity *covariance* is used to understand how strongly they are related to each other. *Covariance* depends on the units of the random variables involved and their variability. Let X and Y be random variables with joint probability distribution $f_{XY}(x, y)$. The covariance between X and Y is defined by Equation (4.6):

$$Cov[X,Y] = E[(X - m_x)(Y - m_Y)]$$
$$= \int_{-\infty}^{\infty} \int_{-\infty}^{\infty} (x - m_x)(y - m_y) f_{XY}(x, y)dxdy \qquad (4.6)$$

Covariance may also be computed as Equation (4.7):

$$Cov[X,Y] = E[X,Y] - E[X]E[Y]$$
$$= E[XY] - m_x m_Y \qquad (4.7)$$

Correlation coefficient - A dimensionless indicator *correlation coefficient* is commonly used to measure correlation between two variables. Correlation coefficient, R, $-1 \leq R \leq 1$ is defined as Equation (4.8):

$$R = \frac{Cov[X,Y]}{s_X s_Y} \tag{4.8}$$

The correlation coefficient is a useful tool to measure the linear dependence between X and Y. R will either be -1 or +1 if two variables are perfectly linearly related. If R is 0, it implies two variables are uncorrelated. Still X and Y can be dependent with each other on higher order of relationship. Note that R^2, $0 \leq R^2 \leq 1$ is regarded as coefficient of determination that is used to measure the goodness of fit in regression analysis.

4.2.1.2. Probability distribution

Discrete probability distribution - Let X be a discrete random variable. The set of probabilities assigned to each possible value of X i.e. $(x, f_X(x))$ is called a probability distribution. The sum of these probabilities over all possible values equal 1 where $f_X(x)$ is called the probability mass function of X. The subscript is to indicate what random variable is governed by the distribution. The followings (see Equation (4.9)) must be agreed.

$$
\begin{aligned}
&0 \leq f_X(x) \leq 1 \\
&\sum_{all\ x} f_X(x) = 1 \\
&P[X = x] = f_X(x)
\end{aligned}
\tag{4.9}
$$

Continuous probability distribution - Let X be random variable whose values are taken from real number $\Re$. We cannot characterise the probabilities of X values

straight away (since they are all essentially zero). The probability that X lies in the small interval between x and $x+dx$ is equal $f_X(x)dx$ where $f_X(x)$ is called the probability density function *PDF* of the random variable X. The term 'density' is used because 'density' must be multiplied by a length measure in order to get a 'mass'. In the continuous case, $f_X(x)$ is not a probability since it has units of probability per unit length. Probability is defined as the areas under the *PDF*, as the sum value of $f_X(x)dx$. The followings (see Equation (4.10)) must be agreed if it is a continuous distribution.

$$0 \le f_X(x) \le \infty \quad \textit{for all} \ -\infty < x < \infty$$

$$\int_{-\infty}^{\infty} f_X(x)dx = 1 \quad \text{i.e. implies area under } pdf \text{ is } 1 \tag{4.10}$$

$$P[a < X < b] = \int_{a}^{b} f_X(x)dx$$

4.2.2. Propagation of Uncertainty

In an engineering problem the inherent uncertainty of the process variables in the problem can be described by a probability density function (*PDF*) in a continuous case. The *PDF* can either be specified by user's assumption or generated through data observations/ samplings. Consider an example here. There is one process variable X with the process output Y in an engineering problem. Given that a random continuous process variable X with a known distribution (*PDF*) composed of many pairs of values $(x, f_X(x))$. The objective is to derive the probability density function from the known distribution of X. The relationship between X and Y is governed by a function $Y = g(X)$. This means that if a specific value $x \in X$ is taken, the value of Y, i.e. $Y = y = g(x)$, can be generated. In Figure 4-3, the probability X lies in the shown neighbourhood of x_1 is the area A_1. Y must lie in a corresponding neighbourhood of y_1 to have identical area (probability) as A_1. In the neighbourhood of x_2, the height of the

distribution of Y near y_2 depends not only A_2, but also the slope of the function $y = g(x)$ at the point x_1. As the slope of $y = g(x)$ at x_2 decreases, the height of distribution of Y must increase to maintain the equivalent area A_2. In this way, the height of distribution of Y can be defined from the area bounded by x and $f_X(x)$. Eventually, the distribution of process output Y can be constructed if the user specifies or assumes the *PDF* of process variable that characterise its uncertainty.
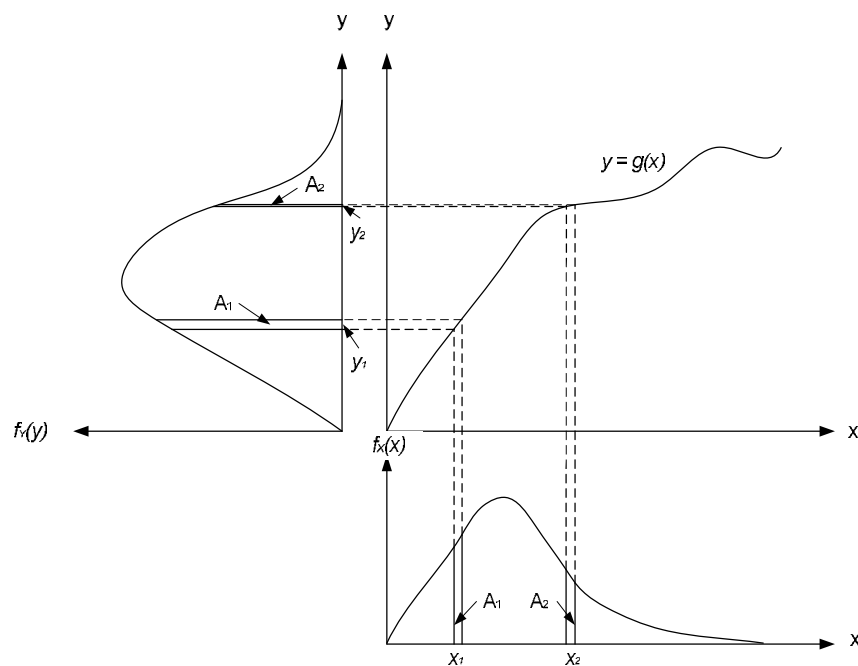
Figure 4-3 Probability density function of Y is derived from a known distribution x

The above example as shown in Figure 4-3 only illustrates visually how propagation of uncertainty with one single process variable to one process output using a simple graph presentation. However, a manufacturing process is much more complicated which contains more than one variable and each of the variable may possess its own uncertainty. In order to understand the propagation of the uncertainty and its impact on the process output, the *PDF* of process output can be generated through two methods: (1) sampling and (2) analytical methods.

4.2.3. Procedures to Perform Uncertainty Propagation

The procedure for risk analysis from the design and manufacturing process point of view using Monte Carlo simulation are detailed as follows. The procedures of undertaking risk analysis with sampling method can be described by the flow chart below in Figure 4-4.
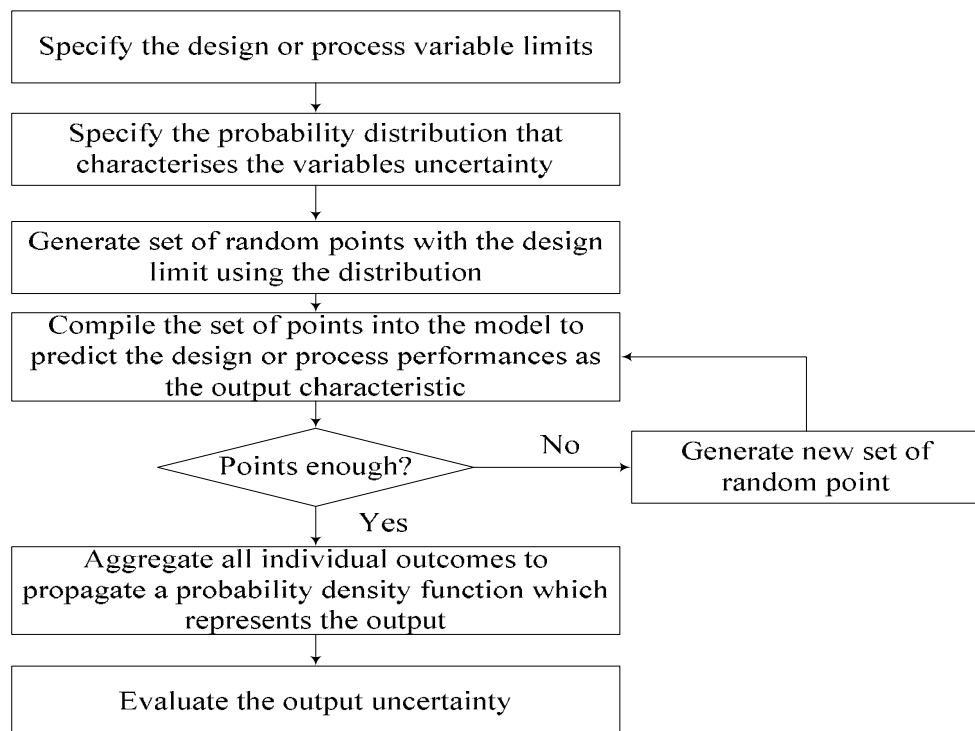
Figure 4-4 Procedure of undertaking risk analysis using sampling method

1. Specify the design limits of possible process variables (design points) in the sample space.

2. Generate design point randomly from the specified sample space using defined probability distribution. The spread and type of uncertainty distribution can be characterised by the specified mean values, and standard deviations.

3. Compute each deterministic design point into the model/ objective function for the design/ process performance prediction.

4. Aggregate the results of all the individual computation to propagate the process output distribution using any one of the suggested method, Monte Carlos or Latin Hypercube Sampling. The generated *PDF* should be with the response mean value and standard deviation

5. Evaluate with output uncertainty with capability assessment of the process behaviour with regards to the specification limits (customer requirements).

4.2.4. Sampling Method–Monte Carlo Sampling and Latin Hypercube Sampling

(1) Monte Carlo Sampling

The Monte Carlo sampling technique involves the random sampling of each input parameter's probability distribution within the model to produce many thousands of trials or scenarios. Variations are introduced into input parameter randomly to produce the distribution shape. Compiling the objective function using the random input parameters will give an outcome. Essentially, this process can be repeated by taking a new set of random input parameters. By running this process thousands time, a distribution of outcome can be obtained which does not only show the most likely outcome but a range of possible outcomes can be obtained. The most likely outcome is then given by a distribution curve known as the probability density function. The main advantage the techniques is correlations and other interdependencies between input parameters can be modelled. Also, the prediction of an outcome range rather than a deterministic value would enhance the capability of the system under input uncertainties.

(2) Latin Hypercube Sampling

The Latin Hypercube sampling selects *M* different values form each *N* random variables by following method. The probability distribution of each *N* random variable is split into *M* intervals on the basis of equal probability. One random value is selected from

each *M* interval based on the probability density function of the particular random variable. The selected *M* values from each random variable are paired to form an *M* by *N* tuplets. The next step involves the generation of *M* samples from *M* by *N* tuplets. The response function is computed from *M* randomly permuted variables in each interval provided no two samples have any input corresponding to the same interval. The advantage of this method is that random samples are generated from all the ranges of possible values, thus giving insight into the tails of the probability distributions of the response function.

4.2.5. Analytical method - First Order Second Moment Method (FOSM)

Analytical method can replace sampling method when data sampling is infeasible, however the mean and the standard deviation of distribution defining the uncertainties are known. Analytical can be used to construct the process output distribution based on the mean and the standard deviation. It provides an effective way to propagate the uncertainty of process parameters. One typical method is First Order Second Moment Method. FOSM is based on the first order Taylor expansion of the response surface function $Y = f(X)$, where $X = \{x_1, x_2, \mathbf{L}, x_n\}$, at the mean values of random variable X. By taking the first and second terms of the Taylor expansion, Y is truncated after the linear term and approximated as a linear function (hence "first order"). The modified expansion Y is used along with first two moments of the random variable X, to determine the values of the first two moments of Y (hence "second moment").

(1) First Order Second Moment Method (FOSM) for function of one variable

Let g is a function of one variable X, $Y = g(X)$, consider a Taylor's series expansion of $g(X)$ about m_X (Equation (4.11)),

$$Y = g(X) = g(m_X) + (X - m_X)\frac{dg}{dx}\Big|_{m_X} + \frac{1}{2}(X - m_X)^2 \frac{d^2 g}{d^2 x}\Big|_{m_X} + \mathbf{L} \qquad (4.11)$$

In first-order approximation, the first two terms in the Taylor's series are used, truncate the term after the linear terms, the mean (Equation (4.12)) and the variance (Equation (4.13)) are:

$$E[Y] \approx E[g(m_X) + (X - m_X)\frac{dg}{dx}\Big|_{m_X}] = g(m_X) \qquad (4.12)$$

$$Var[Y] \approx Var[g(m_X) + (X - m_X)\frac{dg}{dx}\Big|_{m_X}] = Var[X](\frac{d^2 g}{d^2 x}\Big|_{m_X})^2 \qquad (4.13)$$

This approximation regarded as *first-order second-moment (FOSM)* method is only accurate for small variability and small nonlinearity, because the nonlinear terms are truncated after the linear term. In second-order approximation, the first three terms of Taylor's series expansion are used, the mean (Equation (4.14)) and variance (Equation (4.15)) are:

$$E[Y] \approx g(m_X) + \frac{1}{2}Var[X](\frac{d^2 g}{dx^2}\Big|_{m_X}) \qquad (4.14)$$

$$Var[Y] \approx Var[X](\frac{dg}{dx}\Big|_{m_X})^2 - (\frac{1}{2}Var[X]\frac{d^2 g}{dx^2}\Big|_{m_X})^2 + E[(X - m_X)^3](\frac{dg}{dx}\frac{d^2 g}{d^2 x}\Big|_{m_X})$$
$$+ \frac{1}{4}E[(X - m_X)^4](\frac{d^2 g}{d^2 x}\Big|_{m_X})^2 \qquad (4.15)$$

The second-order approximation to the variance of Y requires the third and fourth moments of X while the second-order estimate of the mean is used along with the first-order estimate of the variance.

(2) First Order Second Moment Method for function of more than one variable

Let Y is a function of several variables X, i.e. $Y = g(X_1, X_2, \mathbf{K}, X_n)$, a Taylor's series expansion of $g(X)$ about the vector of mean $m = [m_1, m_2, \mathbf{K}, m_{X_n}]$: (Equation (4.16))

$$Y = g(m_1, \mathbf{K}, m_{X_n}) + \sum_{i=1}^{n}(X_i - m_{X_i})\frac{dg}{dx}\bigg|_{m} + \frac{1}{2}\sum_{i}^{n}\sum_{j}^{n}(X_i - m_{X_i})(X_j - m_{X_j})\frac{d^2g}{dx_i dx_j}\bigg|_{m} + \mathbf{L} \quad (4.16)$$

In first-order approximation, mean (Equation (4.17)) and variance (4.18) of Y are:

$$E[Y] \approx g(m) \quad (4.17)$$

$$Var[Y] \approx \sum_{i}^{n}\sum_{j}^{n}Cov[X_i, X_j][\frac{dg}{dx_i} \cdot \frac{dg}{dx_j}\bigg|_{m_X}] \quad (4.18)$$

If the variables are uncorrelated, the general form is expressed in Equation (4.19):

$$Var[f(X_1, X_2, \mathbf{K}, X_n)] \approx \sum_{i=1}^{n}(\frac{df}{dx_i})^2 Var[X_i] \quad (4.19)$$

where the first derivatives are evaluated at the mean values $(m_1, m_2, \mathbf{K}, m_{X_n})$.

Consider a function of two variables X and Y, truncating after first-order terms from Equation (4.20) of the Taylor series expansion about the mean values (m_X, m_Y) will give:

$$f(X,Y) \approx f(m_X, m_Y) + (X - m_X)\frac{df}{dx} + (Y - m_Y)\frac{df}{dy} \quad (4.20)$$

For a first order, the expected value (Equation (4.21)) is:

$$E[f(X,Y)] \approx f(E[X], E[Y]) \tag{4.21}$$

and the variance is given by Equation (4.22):

$$\begin{aligned} Var[f(X,Y)] &\approx Var[(X - m_X)\frac{df}{dx} + (Y - m_Y)\frac{df}{dy}] \\ &\approx (\frac{df}{dx})^2 Var[X] + (\frac{df}{dx})^2 Var[Y] + 2\frac{df}{dx}\frac{df}{dx} Cov[X,Y] \end{aligned} \tag{4.22}$$

Since X and Y are uncorrelated, variance is given by Equation (4.23):

$$Var[f(X,Y)] \approx (\frac{df}{dx})^2 Var[X] + (\frac{df}{dx})^2 Var[Y] \tag{4.23}$$

Recall Figure 4-2, the uncertainty of x_1, x_2, x_3 is specified with their individual mean m_1, m_2, m_3, variance $Var[X_1], Var[X_2], Var[X_3]$, as well as any correlation relationship indicated by co-variance. Using first-order second moment method, the distribution of Y with m_Y and $Var[Y_1]$ can be generated.

The advantage of using this method is that FOSM is rather efficient and simple for computation to account the effects of uncertainty of process variables. The drawback of the method is that the accuracy of the method deteriorates if second or higher order derivates of Y are significant since it uses only the first two moments of random variables instead of complete distribution information. Unlike sampling method, the method calculates analytically the mean and standard deviation which does not include the knowledge about the form of probability density function that describe the random variable. The skewness (third moment) and higher moments are ignored which are normally essential to describe a complex engineering process. Another limitation is, the method is applicable only under assumption that Y is normally distributed.

4.3. Process Capability Modelling

The two main purposes of process capability are: (1) measure the output variability of a process, (2) compare that variability with a user-defined specification or tolerant with respect to a *stable* process containing no unnatural variation. Output variability of a process in terms of *process control* can be determined by certain control charts [120] that usually presented as a histogram. This assistance statistics tools can be used only if process is 'in statistical control' which means the process has only random variation caused by common cause but not special cause [121].

4.3.1. Process capability Indices

Capability ratio C_p or C_{pk} is a simple arithmetic to compare the capability of a stable process to specification limits from the probabilistic distribution of process output. The purpose is to determine if the process is capable of providing performances or product 'well within' the customer specification. An acceptable region is a specified range by customers which is the difference between the upper specification limit *(USL)* and the lower specification limit *(LSL)*. Process range is defined as the total performances or product variation that characterise process variability. These terms and related statistical terms to describe the details of process output distribution in Figure 4-5.
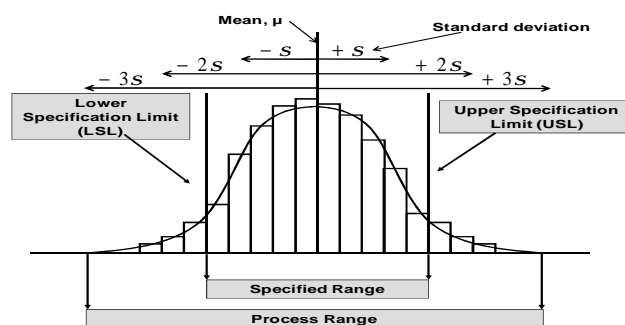
Figure 4-5 Terminologies and definition to describe a process output distribution

The ratio C_p measures the variability of the process relative to its specification limit and C_p is represented by Equation (4.24). Assuming the process is relatively normal distributed, the process range can be approximately to six standard deviations, i.e. $6 \times s$. The higher the C_p, the sharper the distribution, the more capable the process is.

$$C_p = \{ \frac{\text{Upper specification limit } (USL) \text{ -Lower specification limit } (LSL)}{\text{Process range}} \}$$
$$= \{ \frac{USL - LSL}{6s} \} \tag{4.24}$$

C_{pk} is similar to C_p while C_{pk} accounts also how centering the process is. C_{pk} is represented by Equation (4.25). C_{pk} is defined as the minimum distance between the process center (average output values) and either one of the specification divided by half of the process range. Higher C_{pk} implies a more centered distribution relative to average performance.

$$C_{pk} = \{ \frac{\text{Distance to the nearer specifiction limit}}{\frac{1}{2} \cdot \text{Process range}} \}$$
$$= Min\{ \frac{USL - m}{3s}, \frac{m - LSL}{3s} \} \tag{4.25}$$

In practical, the minimum requirement by most manufacturers is about $C_p = 1.33$. A process with $C_p > 1.5$ is considered as capable. Any process with $C_{pk} > 1.33$ is considered as highly capable. A six-sigma process is considered as an industry benchmark which demands high reliability requirement. It can be characterised by $C_p = 2$ or $C_{pk} = 1.5$. Before carrying out any capability assessment, the normality of the PDF must be checked first since assessment for normal and non-normal distribution are different. Some tests can be used to check assumptions of output distributions such

as stability test to study stability by I-MR chart, assumptions tests to study shape of distribution by normal probability plot, variance test to study the spread of distribution by Bartlett's Test or Levene's Test, and median or mean test to study centring of distribution by one-way ANOVA. To evaluate process capability with non-normal distribution, some methods like data transformation or identify a possible well established model which provides good fit to the data can be used.

Closure

Probabilistic risk analysis methods such as Monte Carlo Sampling, Latin Hypercube Sampling and First Order Second Moment method are presented to propagate the uncertainties of quality or performance metric of interests via the generated reduced order model. The probabilistic distribution is presented by histogram and is quantified by traditional capability tools to evaluate the process robustness and capability.

Chapter 5 Modelling of Focused Ion Beam Sputtering Process for Nano-structure Fabrication

This chapter details the micro-machining capabilities in the application of focused ion beam technologies and the computational modelling of the associated sputtering process. A computational focused ion beam (FIB) model that can be used for the control of different process parameters is presented. To improve the depth accuracy of a pre-defined shape, a modified form of model that includes additional process parameters - beam overlapping is experimented. Re-deposition effects are also discussed with the use of a re-deposition model. The FIB model is demonstrated by using a test case study. The optimal process parameters of a three dimensional micro-trench are accurately predicted using the FIB model. Model predictions are required to mill a micro trench using FEI-200 FIB system. Process parameters such as sputtering yield, beam overlapping and their associated effects are explained.

5.1. Applications of Focused Ion Beam Nano-Fabrications

Focused Ion Beam (FIB) has gained a widespread recognition in materials science. It is used as a tool/process to cut away and mill material from defined area or to deposit material onto it at micro and nano scale. Applications such as transmission electron

microscopy (TEM) for sample preparation, micro-structural analysis and cross sectioning offer high-resolution imaging in scanning ion microscopy. Other applications of the FIB technology also includes failure analysis and design modification for integration circuit fabrication [122] [123] [124], semiconductor doping or ion implantation, and lithography. Gas-assisted deposition to repair optical and x-ray lithography masks and modify integrated circuits is well developed over the last 25 years [125] [126] [127]. In this research, the main focuses are placed on the FIB milling capabilities. FIB milling possesses the attributes of direct, non-contact material removal, maskless, and high resolution nano- fabrication. Unlike the traditional etching processes with the use of masks that involves lengthy procedures, FIB allows the microscopic structure to be manufactured in mass volume and in a speedy way. The most attractive feature of the FIB is the ability of machining solid materials of any hardness with almost no materials restriction in the same time having no tool wearing. FIB high resolution potential offers processing capability of producing miniaturised prototype down to micro- and nano-dimension. Feature sizes are potentially as small as $0.1\mu m$. Industrial examples such as micro-surgical device, probe tips [69], and micro-mould are widely seen. Thus this potential has initiates a rapid development on ion beam fabrication and prototyping.

The main challenging in FIB applications relates to the control of the process parameters integrated with the surface morphology in materials science. The process involves ion-solid interaction such that the use of ion beam and its associated parameters must be well understood in order to create the precise shape. Previous FIB treatment are essentially a prediction of the geometry resulted from a given time. The time required can be predicted to mill a pre-defined geometry given a particular mode of

beam operation approach. The requirements for the FIB process at present are much more demanding than its original ion milling abilities. In particular, one of the critical controls required for FIB milling is the depth variation. This is an essential capability for the nanofabrication of 3D nano features, miniaturised objects, and masks and moulds for various Microsystems.

The main objective of this work is to further develop a computational model that can be used to simulate the milling of predefined shapes using focused ion beam (FIB) micro-machining process. A FIB mathematical model that relates beam milling dwell times to pre-defined shape using a pixel scheme for geometry charactisation is used. From process control point of view, the aim is to understand in advance the milling time at each pixel required to obtain the overall pre-defined shape of the micro feature. The effect of process parameters and their possible variations on the accuracy of achieving fabricated micro features are also studied. It is well documented that re-deposition of some material takes place during FIB milling. This will affect the milling shape and the targeted sputtered depth. A re-deposition model is also included in the modelling procedure in order to predict and understand the simultaneous effect of sputtering and re-deposition of material. The depth profile prediction (the process behaviour prediction) which includes the consideration of overlapping effect and re-deposition effect is based on Vasile *et al.* model. The re-deposition model is discussed so that more accurate predictions for pixel dwell time and milling depth are offered. Different modelling approaches are applied to various test cases study. The overlapping is considered to be one of the important parameters for process control. A modified modelling approach is proposed which implements the beam overlapping ratio into the FIB model.

Current implementation of the sputtering model allows the analysis of true three-dimensional shapes. A major aspect of the undertaken work is the FIB computational model (for material removal). A test case study of milling a micro trench with parabolic shape is investigated. In order to evaluate the accuracy of the model, model predictions for this test case are validated experimentally using a FEI-200 FIB system. Relevant results are presented and the differences between the predicted and actual shape are discussed. In addition to above FIB models, techniques and tools that are capable of providing evaluation of the influence of process parameters, process performance, product quality characteristics, and any risks associated with the sputtered depth as a result of parameter variations are also researched and implemented in the next chapter.

5.2. Simulation of Focused Ion Beam Micro-Machining Process

5.2.1. Principle and Fundamental Operations

Figure 5-1 illustrates the principle of operation for FIB as a bombardment of a target surface through high energy gallium Ga+ (or other) ions. As a result, small amount of material sputters in the form of secondary ions, natural atoms and secondary electrons. During the bombardment, gallium atoms are implanted in the first few nanometres of the sample surface. Beam current must be applied correspondingly. The typical simulation time ranges from seconds to few mintues for a nano-structure depending on its size. Low ion beam current requires longer time to produce a cut and to sputter the material. Therefore, reducing the time for FIB is a major issue. A possible strategy is a two-step milling process: (1) short time milling at high ion current, and then (2) fine and focussed beam with low current ion etching.
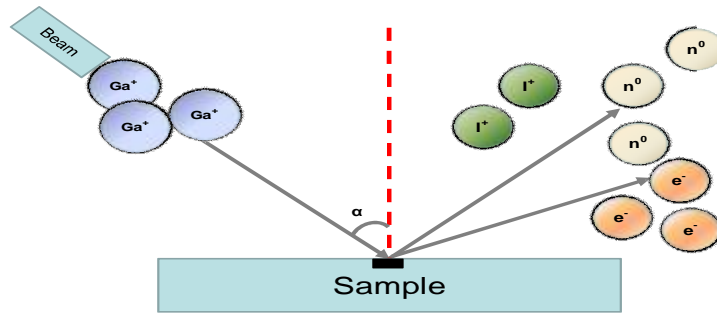
Figure 5-1 Particles sputtering

5.2.2. Pixel Scheme and Sputtering

In focused ion beam (FIB) milling, the ion beam sweeps across the surface of the target material, often in an iterative manner, and sputters small amount of material producing the desired shape of the feature. The sample surface is divided into a number of pixels *(i,j)* based on the size and shape of the final structure. Figure 5-2 details the location of a pixel layout over the target surface during beam movement. Two typical focused ion beam scanning sequences are illustrated in Figure 5-3(a) and Figure 5-3(b). Figure 5-3(a) shows the beam raster the target surface along the +*i*-direction. It moves up the j-direction, carries on another scan along −*i*- direction and so on. Figure 5-3(b) shows beam raster using a helix path. The advantage of this helix path is to reduce the re-deposition effect [128] by milling away the re-deposited materials immediately after they deposited on the surface.
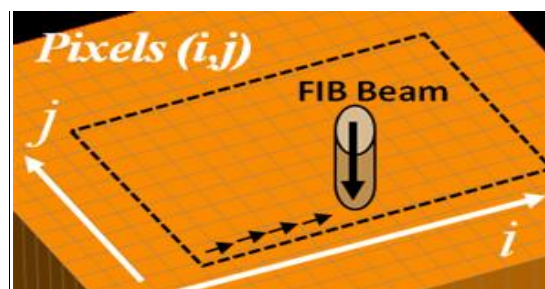
Figure 5-2 Ion beam on sample surface layout represented by pixels *(i, j)*
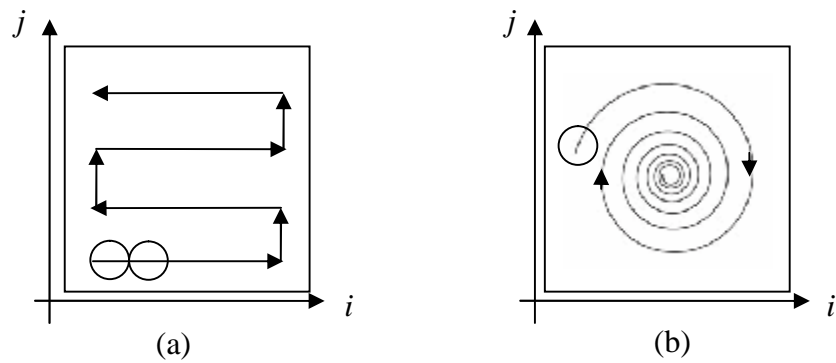
Figure 5-3 Two typical beam scanning sequences from top view

The time for which the beam stays on each pixel is known as the pixel dwell time. Longer dwell time corresponds to greater milling depth at that pixel. The milling depth (also considered as sputtered depth) of a pixel is defined as the vertical distance from the pixel's initial (previous) geometry to its final geometry as shown in Figure 5-4. Pixel size is among the number of the process control parameters specified through the actual FIB machine and can be changed according to the ion beam discrete movement steps. Each pixel has an associated milling depth. It is controlled by several parameters such as the ion dose, beam current, beam angle of incidence and pixel dwell time. A critical parameter for FIB is the sputtering yield. It indicates the rate of material removal and is primarily dependent on the beam angle of incidents and the beam energy.
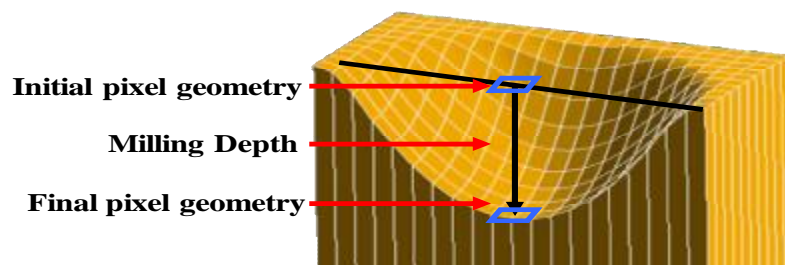
Figure 5-4 Pixel milling depth definitions on the target shape

The pixel milling depth of a small feature using FIB is usually performed by a number of scans. An repetitive processing provides better control and can achieve an accurate shape. It is necessary to include the actual angle of incidence of ion beam after each

scan which affects the sputtering yield. An example of a parabolic shape progression is given in Figure 5-5. For each scan, the pixel depths are estimated by using the specified pixel milling time. The total number of scans can be derived by the pre-determined milling depth. The associated total milling time required to produce the pre-defined parabolic shape can then be calculated.

Figure 5-5 Repetitive process to obtain a parabolic shape

5.2.3. Beam Operations

Beam operation determines the pixel dwell time. Dwell time is defined as the amount of time that the ion beam stays at a given pixel. It is a crucial parameter which determines the way how an initial shape progresses to the pre-defined shape. To fabricate 3D structures, the FIB users must decide a profile control in order to control the beam movement. In this thesis, the milling of a circular conical shape with its side view as shown in Figure 5-6 is considered.

Three methods are suggested by Vasile *et al* [71], Fu [67] and Kim *et al* [79]. Figure 5-6(a) shows the sequence of how the final shape is achieved by beam milling of the block one after another. One of the main differences between the modelling methods of Vasile, and Fu is the beam movement simulation. Shape is either achieved by milling vertical block or horizontal block as depicted in Figure 5-6(a) and Figure 5-6(b). A parabolic shape is defined when numerous blocks are formed by two different beam

movements over the surface pixels. Vasile adopted a single passing scheme, i.e. the ion beam would only pass each pixel once and stay long enough to make sufficient sputtering. In this way, the dwell time needed to produce the sputtered depth at each pixel is calculated as a function of sputtering yield, angle of incidence, beam energy, and intensity contributions from all other pixels through the use of the FIB model. Fu suggested a layer-by-layer method where the ion beam moves repetitively across the pixels and remove materials through multiple passes. In Figure 5-6(b), layers are milled in sequence from top to bottom with multiple scans. The dwell time are fixed and remains steady for each pixel throughout the entire process. Once the expected depth of the first slice is complete, the beam restarting position will be moved inwards to the centre in order to allow milling of the second slice and so on until the predefined geometry is achieved. Kim has modified Fu's method with a continuous slicing method. The ion beam raster the surface with a spiral scan with a vector path such as the one shown in Figure 5-3. It is noted that the FIB model compiled in this work demonstrates examples that refine a precise positional control over the pixel scheme does not cope well with the helix vector path in Kim's method.

(a) Vasile's method   (b) Fu's method   (c) Slope-by-slope method

*Dash line indicates the intermediate shape
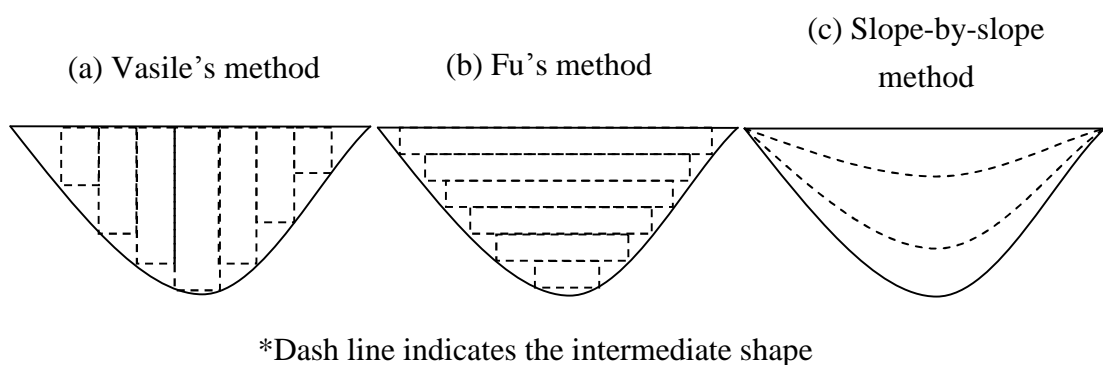
Figure 5-6 Different beam operations for milling a parabolic shape

In this research, a modified slope-by-slope method as shown in Figure 5-6(c) combines Vasile and Fu methods is investigated. It is a repetitive sweeping approach in which the dwell time is set in a constant increment step forming a set of dwell times along the pixels at i-direction. Then the same series of dwell time are applied on the same pixels along i-direction again after each scan. As a result, an initial slope can be produced in one scan and intermediate slopes are created in the next scan until the predefined geometry is achieved. The sputtering is carried out on the sputtered surface which is approximated as a stepwise slope with a gradient angle. This method can enhance the estimation of sputtering yield compared to a more inclined sidewall angle with a steep slope after scans.

5.2.4. Control of Milling Process Parameters

Process parameters or variables used to control the milling process includes material properties, beam diameter and beam intensity profile, beam current, ion flux, overlapping, pixel dwell time, and angle dependent sputtering yield. These variables are explained as follows.

(1) Material properties - The ion bombardment takes place between the ion and the target surface. Physical quantities such as the weight of the ion and atomic density of the target surface are influential factors affecting the collision cascades and hence the sputtering yield. Gallium (Ga), Argon (Ar), Xenon (Xe) ions are common ions amongst other metals ion sources. Ga-based is widely used because of its low melting temperature, low volatility and low vapour pressure with stable properties that it does not react with the material defining the ion ejection probe of the FIB apparatus [129].

(2) The beam diameter and the beam intensity profile – The beam intensity profile is another important factor that needs to be understood and addressed in order to obtain an accurate sputter depth in a milling process. Determining the beam profile is necessary since the pattern geometry is determined by many individual beams. Beam profile is basically governed by the basic parameter-beam diameter. Figure 5-7 shows a typical beam profile and the beam diameter in all experimental studies in this thesis is described by using the Full Width at Half Maximum (FWHM). Each beam ray has a beam intensity profile consists a distribution of ions instead of a uniform ray over the target surface.
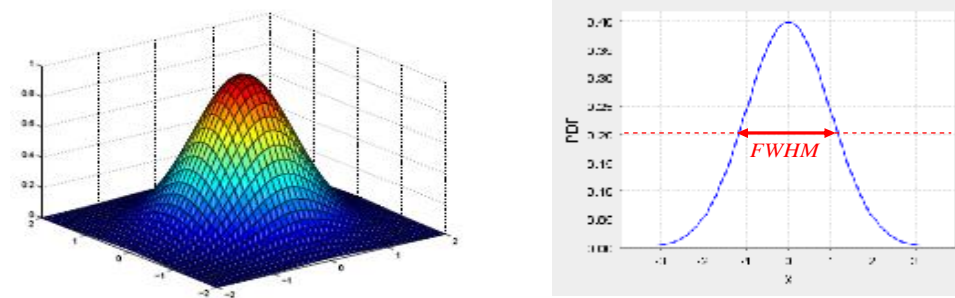
Figure 5-7 Beam diameter described by the Full Width at Half Maximum (FWHM)

A ray of ion beam with diameter equals FWHM can affect numerous adjacent pixels in the neighbourhood of the pixel. The beam profile usually overlaps in the tails of two neighbourhood distributions. The intensity distribution in this work is assumed to be a Gaussian bi-variate density function gives by (Equation (5.1)).

$$f_{x,y}(x_i, y_j) = (\frac{1}{\sqrt{2p}s})^2 e^{-\frac{r^2}{2s^2}} \tag{5.1}$$

where $s = \dfrac{FWHM}{2\sqrt{2}\ln 2}$ is the standard deviation of the distribution

To predict the precise expected shape, the beam intensity profile was measured by experiments in the past. Many researchers have selected a Gaussian distribution which is only a good fit for the centre of the distribution [130]. An exponential distribution profile is a better fit for the tails of the distribution. Some advanced studies by Assayag

[78] involve a two-Gaussian function may be used to describe the intensity profile, one for the centre region and another for the tails of the distribution.

(3) The beam current – The beam current is defined as the number of ions delivered to the target per unit time and can be controlled by the aperture position in the focused ion beam system. It is closely relates to the beam diameter and their relationships (with reference to a FEI 200 FIB system) can be checked from Table 5-1.

Table 5-1 Currents and the corresponding beam diameters for a FEI 200 machine

Ion beam current (pA)	1	4	11	70	150	350	1000	2700	6600	11500
Ion beam diameter (nm)	8	12	15	25	35	55	80	120	270	500

(4) Ion flux - Ion flux refers to the total number of ions that hit on the target area per unit time. The ion flux delivered from the beam to the target area is determined by the beam diameter and current. If the beam projected on the target area is exactly equal to the beam surface area, the ion flux delivered by the beam is given by Equation (5.2):

$$\Phi_b = \frac{I}{pR^2}K \tag{5.2}$$

where Φ_b is the ion flux that the beam carries, R is the radius of the beam, K is the number of charges in one ampere, and I is the milling current. If the ion flux projects on a pixel, the ion flux distributed over the pixel area will not be identical to the ion flux carried by the beam Φ_b. Let $\Phi(x,y)$ be the ion flux distributed across the pixel (ions/s cm^2) with pixel area A. The ion flux delivered on a pixel with area A can be found by Equation (5.3).

$$\Phi(x,y) = \Phi_b \frac{pR^2}{A} \tag{5.3}$$

(5) Pixel size - Pixel exists purely for geometric characterisation of the target surface. The pixel geometry is not fixed and changes according to the ion beam position. The pixel area A refers to the area formed by the rectangle of size $u \times v$ as shown in Figure 5-8. The pixel area is defined in a way that it depends on the beam overlapping. Therefore, u is dependent on the overlapping ratio while v equals the beam diameter D. For example, u equals half of the diameter in 50% overlapping, u equals (1-33%) i.e. two third of the diameter in 33% overlapping. During repetitive scanning process, pixel size increases slightly due to the surfaces becoming an incline slope. However, this increase can be negligible such that pixel size is assumed to be fixed throughout the repetitive scanning process.

(6) Overlapping - The beam overlapping is determined by the beam diameter and the overlap distance. It is assumed that overlapping occurs only in x direction and not in y direction during beam movement. The beam overlapping denoted by O_{ratio} is the ratio of *the overlapped distance w between two pixels* to the *beam diameter D* (overlapping=$\dfrac{\text{overlap distance}}{\text{beam diameter}}$) i.e. $O_{ratio} = \dfrac{w}{D}$. For example, an overlapped distance equals to the beam radius between two adjacent beam spots (centre to centre) are depicted in Figure 5-8. This example has a 50% overlapping. Here, a pixel contains part of its beam spot plus two half beam spots from the neighbouring beam spots. Therefore, the ion flux on one pixel with 50% overlapping is nearly double compares to the scenario of no beam overlap. The ion flux changes due to overlapping must be correctly captured for accurate sputtered depth prediction.
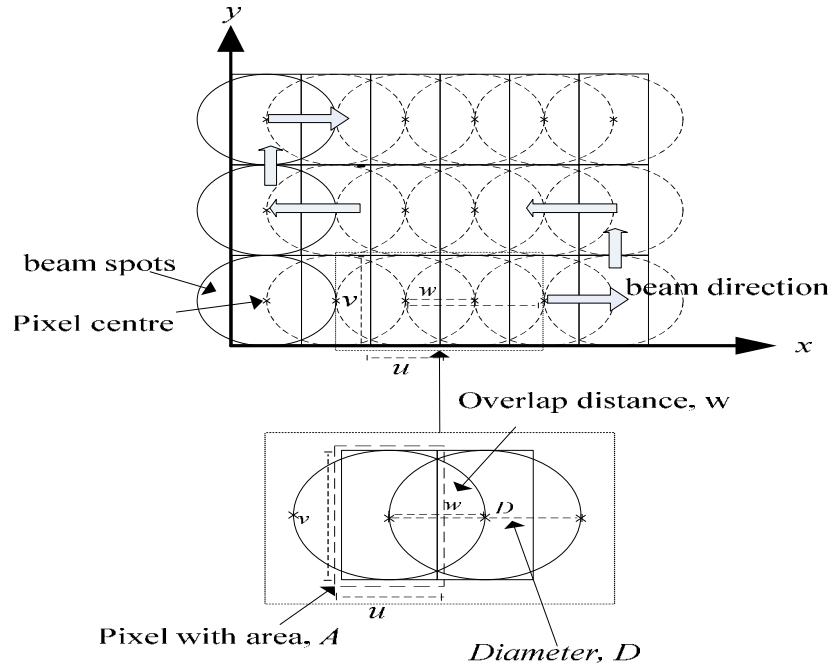
Figure 5-8 Beam spots having 50% overlapping between pixels and geometries

(7) Capturing ion flux for various overlapping scenarios - The ion flux that a pixel received is affected by the overlapping. It is different from the ion flux that the ion beam carries. An overlapping constant is developed which reflects the ion flux projected on a pixel due to overlapping from two adjacent pixels. Let A be the area of the pixel. If we take the area for no overlapping (overlapping equals 0%) as a reference area, $A_{0\%} = D \times D$ is shown in Figure 5-9(a). Figure 5-9(b) shows overlapping equals 33% where $w = O_{ratio} \times D$ i.e. $\frac{1}{3} \times D$. The pixel area shrinks into a smaller area due to overlapping equals $\frac{2}{3} A_{0\%}$. Figure 5-9(c) shows that overlapping equals 50% where $A_{50\%} = \frac{1}{2} A_{0\%}$. The relationship between overlapping ratio and pixel area is given by Equation (5.4).
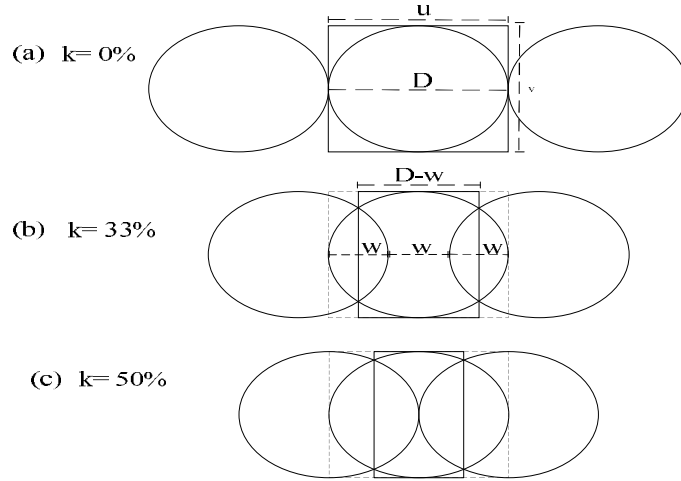
Figure 5-9 Beam spots having 0%, 33%, 50% overlapping between pixels

$$A_{overlap} = (1 - O_{ratio})A_{0\%} \tag{5.4}$$

From Equation (5.3), the ion flux delivers to a smaller pixel area due to overlap can be expressed by Equation (5.5).

$$\Phi_{overlap}(x, y) = k_{OV} \times \Phi_{0\%}(x, y) \tag{5.5}$$

where $\Phi_{overlap}(x, y)$ denotes the ion flux delivered from the beam to the pixel area due to the effect of beam overlapping, $k_{OV} = \dfrac{1}{1 - O_{ratio}}$ is regarded as the overlapping constant. k_{OV} is a overlapping related constant which governs ion flux delivered onto a pixel and defined by Equation (5.6). k_{OV} for some common overlapping scenarios are $k_{OV} = 1, 1.33, 1.5, 2, 4$ for 0, 25%, 33%, 50%, 75% overlapping respectively.

$$k_{OV} = \frac{1}{(1 - O_{ratio})} \tag{5.6}$$

(8) Pixel dwell time - Pixel dwell time is the time that the ion beam stays in one pixel and mills that specific pixel. The FIB model is capable of predicting the pixel dwell time. The next section (motivated example) will show how this can be done. However, generally, the pixel dwell time is dependent on the beam operation approach and can be adjusted (either constant or varied) during the milling process in a FIB system.

123

(9) Angle-dependant sputtering yield - With the use of the focused ion beam, the term -sputtering yield measures the efficiency of target material removal by the high energy beam. The data are essentially important to compile the depth variation during FIB process. Sputtering yield could be generated using experiments data, empirical formula compilation. One classical example is given by Equation (5.7) which is originally proposed by Yamamura [131].

$$Y(E_0, a) = Y(E_0, 0) \frac{e^{f[1-\frac{1}{\cos a}] \cdot \cos a_{opt}}}{(\cos a)^f} \tag{5.7}$$

where $Y(E_0, a)$ is the sputtering yield at ion energy E_0 and nominal angle of incidence α. The quantities f and a_{opt} are parameters to fit the experimental data. In addition, a_{opt} is the nominal incidence angle at maximum sputtering yield. Another way to obtain sputtering yield is to use Monte Carlo simulation software package such as SRIM (the stopping and range of ions in matter) [132] and TRIDYN (TRIM.SP Dynamical) [133]. SRIM has been widely used for predicting the sputtering yield for many different ions in a wide range of energies. TRIDYN is used to simulate the dynamical changes of the target composition during sputtering. Those data are well validated which shows good estimation of sputtering yield at low incident angles for the most of the common ion sources and targets such as Gallium-Silicon system. Sputtering yield is a function of the two parameters, incident angle a_{x_i, y_j} of the ion beam at point (x_i, y_j) and the ion beam energy E_0 as well as the type of ion source and target material. An intermediate incline surface is formed during the FIB iterative process. This incline surface varies the ion incidence angle and so as the corresponding sputtering yield. In order to get fast sputtering yield evaluations along the iterative milling process, the approximation and

interpolation techniques suggested in can also be applied to account for sputtering yield variation. It approximates sputtering yield as a function of beam angle and energy.

5.3. Mathematical Models

A FIB model ideally should capture various aspects of the nano-scale milling process such as sputtering yield, beam intensity profile, geometric pixel scheme, materials property and control of numerous process parameters. In the literature, numerous studies have been done in modelling the FIB process behaviour such as depth variation [67] [68] [69], surface smoothness [70], etching rate and sputtering with re-deposition [134]. Most of the work has been validated against experimental results. These theoretical models provide a profile to embed all the associated parameters in simulating the actual process. The model output is evaluated and improved based on the adjustment of these key process parameters in a process setup. The key challenge for modelling FIB is the controlling of parameters to achieve a critical precision of the 'nano-scale' process.

The mathematical model relating the etched shape and the dwell times required to achieve a predefined shape using a set of pre-defined process parameters was initially investigated by Vasile *et al* in [71] [72]. The model as given by Equation (2.1) is

$$Z_{ij} = \iint \frac{\Phi(x,y)}{h} f_{x,y}(x_i, y_j) Y(E_0, a_{x_i, y_j}) t_{x,y} dx dy$$

The Vasile model uses a square pixel matrix which placed over the target surface. The sputtering model is discretised over each element of the pixel matrix resulting to a system of linear equations that relates the dwell times $t_{x,y}$ with the sputtered milling

depth Z_{ij} at any pixel (i, j) is constructed. This system of equations can be solved numerically. Vasile *et al* provided a structured approach to account for the geometrical details of the pixels. This is a fundamental step for the evaluation of the total pixel dwell time required to achieve a pre-defined structure. The work particularly suits the FIB simulation in which the ion beam is operated with a single scan pathway. The main theme of the single scan pathway is to calculate the required pixel dwell time at different pixel in order to obtain the pre-determined sputter depth using the specified process parameters.

5.3.1. Computational Model Developed for Dwell time Prediction

As a major part of this research impact, a new process variable - beam overlap related constant k_{OV} T is specified. This new constant accounts for the beam overlapping behaviour which has not been included in the model studies in the past. Another process variable $n_{x,y}$, number of scans required for a complete milling, is added into the model.

It provides a novel way allowing model to match with the multiple beam movements in an actual operation of a FIB machine. Another important contribution of the FIB work in the thesis is that the accuracy of process control is further enhanced by integrating an established re-deposition model [81]. This model leads to a more accurate prediction for sputtered amount of materials at each pixel due to the re-deposition. The impacts of two important aspects, (1) beam overlapping ratio and (2) re-deposition, on the process output depth variation are explained theoretically in literature but not numerically. The mathematical model is discussed with regard to three different beam operation approaches in the following sections.

126

5.3.1.1. Model for ion beam operation with a single scan

If (x_i, y_j) denotes the centre of the pixel (i, j), then the sputtering at this pixel in terms of depth due to milling depth sputtered away (material removal) at that pixel can be expressed as Equation (5.8).

$$Z_{ij} = \int\int \frac{k_{OV}\Phi(x,y)}{h} f_{x,y}(x_i, y_j) Y(E_0, a_{x_i,y_j}) t_{x,y} dxdy \qquad (5.8)$$

where Z_{ij} is the sputtering depth at the point (x_i, y_j), $\Phi(x, y)$ is the ion flux for zero percent ion beam overlap at point (x_i, y_j) (cm^{-2}s^{-1}), k_{OV} is a beam overlap percentage related constant, h is the atomic density of the target material (atoms/cm^3), $Y(E_0, a_{x_i,y_j})$ is the sputtered yield (atoms per incident ion at point (x_i, y_j)), $t_{x,y}$ is the dwell time of the ion beam at point (x_i, y_j) in seconds, $f_{x,y}(x_i, y_j)$ is the ion beam density distribution function in two dimensions. The ion beam geometry is not uniform, however, is in terms of a density distribution $f_{x,y}(x_i, y_j)$. Generally, a Gaussian bi-variate density function is assumed for ion distribution and $f_{x,y}(x_i, y_j)$ is given by Equation (5.1).

The sputtered yield $Y(E_0, a_{x_i,y_j})$ is a function of the incident angle a_{x_i,y_j} of the ion beam at point (x_i, y_j) and the ion energy E_0 as well as the type of ion source and target material. Generally, the yield increases from perpendicular ion beam incidence to a maximum at angle 60° to 85°, and then rapidly decreases due to the strong reflection at grazing incidence [135]. The sputtering yield values can be computed through an empirical formula. The sputtering yield values can also be measured from experiment or

generated using software such as SRIM for particular ion source and target material under specified energy conditions by Monte Carlo binary collision simulation.

The double integral in the Equation (5.8) considers ion projected on all pixels at the surface. Let x_k and y_l i.e. (x_k, y_k) represents the mid-point of the pixel where the ion beam *focused at*. To calculate the dwell time t_{xy} at every pixel for Z_{ij}, the surface is discretised into $n_1 n_2$ pixels where n_1 and n_2 represents the number of subintervals on the x and y directions. The sputtering depth can be found by Equation (5.9).

$$Z_{ij} = \sum_{k=1}^{n_1} \sum_{l=1}^{n_2} \frac{k_{OV} \Phi(x_k, y_l)}{h} \times f_{x_k, y_l}(x_i, y_j) Y(E_0, a_{x_i y_j}) t_{k,l} \Delta x_k \Delta y_l \tag{5.9}$$

where x_i and y_j are the mid-point of the periphery pixels. $(i, k = 1, 2, \mathbf{K}, n_1; j, l = 1, 2, \mathbf{K}, n_2)$ and $A_{k,l}(i, j)$ is defined as Equation (5.10).

$$A_{k,l}(i, j) = \sum_{k=1}^{n_1} \sum_{l=1}^{n_2} \frac{k_{OV} \Phi(x_k, y_l)}{h} \times f_{x_k, y_l}(x_i, y_j) Y(E_0, a_{x_i y_j}) \Delta x_k \Delta y_l \tag{5.10}$$

The sputtering FIB models is discretised over each element of the pixel layout so that a system of linear equations is constructed as Equation (5.11) that relates the dwell times with the sputtering depth at any pixel (i, j).

$$[A_{k,l}(i, j)][t_{k,l}] = [Z_{ij}] \tag{5.11}$$

where $[A_{k,l}(i, j)]$ is a coefficient $n \times n$ matrix , $[t_{k,l}]$ is a $n \times 1$ vector of dwell times and $[Z_{ij}]$ is a $n \times 1$ vector of pixel milling depths. Equation (5.11) will give a set of $n = n_1 \times n_2$ linear equation in n unknowns. $[t_{k,l}]$ can be solved in this matrix system

when desired $[Z_{ij}]$ is specified using a known ion beam sources. The model presented in

Equation (5.9) can be applied to calculate time vector when milling depth is specified.

5.3.1.2. Model for ion beam operation with multiple scans in various dwell time

To further improve the process control of predicting the total milling time for achieving a more accurate shape, the changes of angle of incidence during multiple scans must be considered. The model considering multiple scans in various dwell time will be applied if the beam is operated under a slope-by-slope approach. Sputtering yield can be updated after each scan according to the current pixel geometries. The specified shape is then produced with multiple beam scans in the form of a *slope* rather than a flat *slice*. $Y(E_0, a_{x_i, y_j})$ changes accordingly to the updated pixel geometries. The updated pixel geometries after each scan can affect the beam angle of incidence and thus a new sputtering yield value must be evaluated. The FIB model from Equation (5.8) is modified. The number of scans as a new process parameter will be included to account for the milling depth and the milling depth is expressed as Equation (5.12):

$$Z_{ij} = \int\int \frac{k_{OV}\Phi(x, y)}{h} f_{x,y}(x_i, y_j) Y(E_0, a_{x_i, y_j}) t_{x,y} \cdot n_{x,y} dxdy \qquad (5.12)$$

where $n_{x,y}$ is the number of scans required at pixel (x_i, y_j) and $t_{x,y}$ is the pixel dwell time which is a user-predefined parameter.

5.3.1.3. Model for ion beam operation with multiple scans in constant dwell time

To improve control of sputtering depth, the FIB model from Equation (5.8) is modified. Pixel dwell time $t_{x,y}$ from Equation (5.12) is set constant for all pixels as a user-

predefined parameter in a FEI-200 FIB station. The required number of ion beam scans to sputter each pixel milling depth using a predefined dwell time. The model considering constant-dwell time will be applied if the beam is operated under a slice-by-slice approach. Number of scans is included in the explicit model. This modified model can be used to predict the number of scans required to achieve a predefined shape at a given (user-defined) constant dwell time.

5.3.2. Re-Deposition Model

The re-deposition proposed by Tseng [81] is limited to the complex shapes which contains irregular contour as accurate re-deposition amount is estimated according to pixel geometry location. However, this model is still worthwhile to be applied in order to calculate the re-deposited amount for some simple shapes.

In this sputtering process, part of the scattered atoms would re-deposit back into the sample surface. The effect of this re-deposition was proven an influential factor for depth variation prediction. A computational model for the volume of the re-deposited material across all pixels is investigated and integrated with the computational FIB model. Any model for depth prediction model would estimate a less depth than expected owing to this re-deposition effect. Fu [80] provided an analysis on scenarios where and how this effect happened and found re-deposition are likely to happen on the side wall of the fabrication structure. While the amount of ion flux that avoiding hitting the side wall was worked out in [136]. Tseng [81] later on worked out a model to account for the volume of the actual re-deposition which has been taken into consideration during FIB model implementation. Itoh [137], Ishitani and Ohnishi [82] further modelled the sputtering and re-deposition fluxes under assumption that the

sputtered atoms are emitted according to a cosine distribution with regard to surface normal. Modelling for re-deposition and sputtering fluxes is also given in [83].

Re-deposition happens when focused ion beam performs milling of high aspect ratio features where the milling depth is function of both sputtering and re-deposition phenomena. Another model that accounts for the re-deposition effects during FIB sputtering should be considered. A mathematical model accounts for the volume of the re-deposited material across all pixels in addition to the sputtering model outlined above. Both models are integrated. It is assumed that the amount of the sputtered atoms or ions from a source pixel cell (i, j) and then re-deposited onto another target pixel cell (k, l) is dependent on the relative locations between the two pixels and their own orientations. The re-deposited volume of material R_{ij} as function of the sputtered volume S_{ij} can be calculated from Equation (5.13) [137].

$$R_{ij} = \frac{F(b) - F(g)}{F(180^\circ)} S_{ij} \quad \text{where} \quad F(x) = \frac{pr^3}{3}[\cos^3 x - 3\cos + 2] \tag{5.13}$$

In Equation (5.13), b and g are the minimum and maximum angles that are measured from the centre of the source pixel cell (i, j) to any possible locations within the target unit pixel cell (k, l) respectively. For a cell (k, l) the re-repositioned volume can be found as the summation of contribution from all other source cells (i, j). This model assumes that the total re-deposited volume of material after the re-deposition is normal to the surface of the unit cell. The sputtered volume S_{ij} is calculated from the FIB sputtering model in Equation (5.8) from the sputtered depth and dimensions of pixels i.e. $Z_{ij} \times dx \times dy$. The sputtering direction of materials in the source pixel follows a cosine distribution. Figure 5-10 shows interpretation of sputtering and re-deposition as formulated through Equation (5.13). Note that an assumption is made that all particles

or ions are all energetic enough to re-deposit on the target pixel. The re-deposition model outlined above can be implemented and integrated into modelling procedure in particular for milling low aspect ratio features.
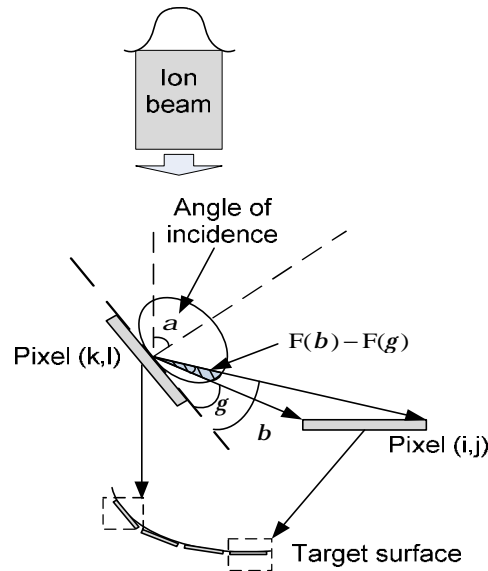
Figure 5-10 Sputtering direction of atom when the ion beam hits the target surface

5.4. Case Study One: The Milling a Two Dimensional Parabola

5.4.1. The Case Study

The aim of this case study is to apply the proposed model to predict the dwell times needed to mill a pre-defined parabola in a planar dimension. The study consists of moving an ion beam in a straight line producing a parabola with a given shape as depicted in Figure 5-11. The ion beam has a FWHM diameter of $55nm$ was swept across a 10×1 pixel array containing 10 pixels each of which has a pixel area $55nm \times 55nm$.
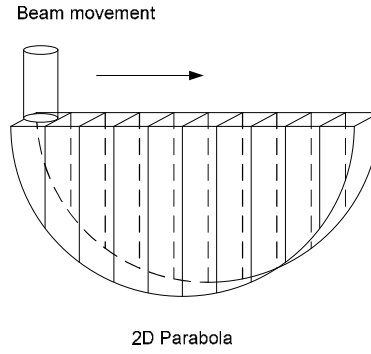
Figure 5-11 A two-dimensional pre-defined parabola obtained by the ion beam

(1) Geometrical Scheme of the Parabola

With the specified 10×1 pixel array which contains 10 pixels each with dimension $55nm \times 55nm$, the width and length of the parabola is 0.55 µm and 0.055 µm respectively. The target milling depth at the centre point equals the deepest milling depth of the parabola (denoted by Z_{centre}) is 0.2 µm. The target milling depths of all the pixel centres along the parabola are listed in Table 5-2. Let $Z_{t\arg et}$ be the target milling depth defined by Equation (5.14) for a two dimensional parabola:

$$Z_{t\arg et} = Z_{centre} - \frac{x^2}{4p}$$
(5.14)

where p is a constant governed by the width and target milling depth of the parabola. In this case study, $p = 0.0945 \times 10^{-6}$ and $Z_{centre} = 0.2\,mm$ at the centre point of parabola.

Table 5-2 Target milling depths at the pixel centres of the case study

Pixel	1	2	3	4	5	6	7	8	9	10
$Z_{t\arg et}(mm)$	0.038	0.102	0.150	0.182	0.198	0.198	0.182	0.150	0.102	0.038

(2) Implementation of Beam Operations

The pixel milling depth of this parabola feature was performed using a slope-by-slope multiple scans approach as shown in Figure 5-12(a). The milling depth which defines the shape is given by Equation (5.12). Dwell time was set with fixed increment and then decrement time steps among neighbouring pixels in one scan. The same set of pixel dwell time within one scan was used in the next scan to achieve the same slope surface. This repetitive approach provides better control and can achieve a more accurate shape because the approach accounts for the actual angle of incidence of ion beam after each scan that affects the sputtering yield. Figure 5-12(b) shows that the target surface before and after one scan and how the slope produced creates an angle of incidence a . The pixel geometry on the target surface changes after each scan and the ion beam induces a slight angle a with the updated pixel geometry.
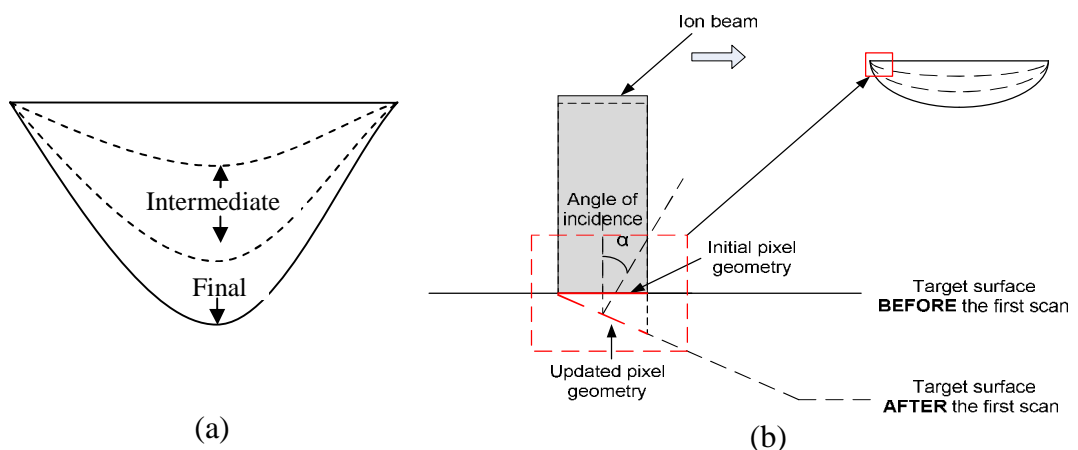
Figure 5-12 (a) A slope-by-slope multiple scans approach, (b) the target surface profile before and after one scan

In this case study, the ion beam was positioned initially at the first outermost pixel of the parabola central line x and that the dwell time at that pixel was t = 0.05 ms. The ion beam moves along the x direction as indicated in Figure 5-13 to the next adjacent pixel,

134

and so on. At every movement to a new pixel the dwell time was increased by an increment time steps of $\Delta t = 0.005$ ms until the centre pixel of the 2D parabola. The dwell time for the symmetric pixels with respect to the trench centre line is equal. Table 5-3 details the pixel dwell time used in the numerical calculations. Note that the pixel time of each pixel may be set to a different constant value.
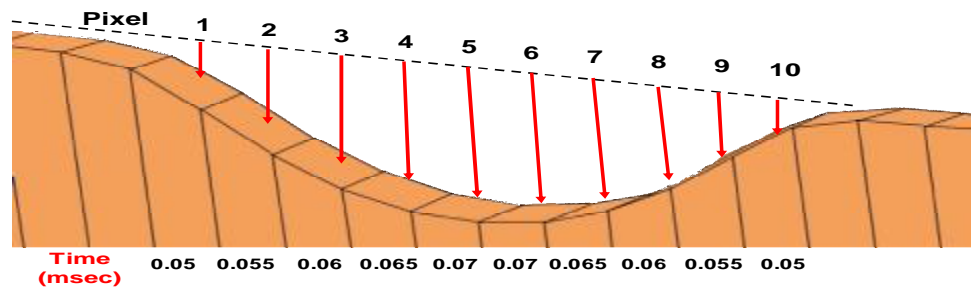
Figure 5-13 Pixel dwell time presentation on pixel 1 to pixel 10

Table 5-3 Pixel dwell time (msec) for each pixel in the 2D parabola representation

Pixel	1	2	3	4	5	6	7	8	9	10
Time $t_{x.y}$ (msec)	0.05	0.055	0.06	0.065	0.07	0.07	0.065	0.06	0.055	0.05

In the first scan of the milling the material removed after taken the above dwell time results to an intermediate parabola over a single row of pixels in the matrix. In the second scan, the intermediate slope is subjected to milling using the same set of pixel dwell times as that in first scan. This is repeated until the final desired milling depth is achieved. During the iterative procedure if the depth at a particular pixel has reached or exceeded the final depth required by the shape, this pixel will not be visited by the ion beam anymore in the remaining mill scanning. The ion beam continues to sputter material of those pixels only where the target milling depth has not been achieved yet.

The model predicts the number of FIB scans required The total milling time is controlled based on the fixed dwell times in Table 5-3.

5.4.2. Control of Process Parameters

The aim of this study case is to apply the proposed models to predict the dwell times needed to mill a pre-defined parabola. The interest of this FIB model is to translate the pre-defined geometry (depth Z_{ij} against the x, y-coordinate) into ion beam control coordinates (known as the pixel scheme). Z_{ij} is expressed as a function of time and other associated parameters defined by Equation (5.12). For the beam operation, a multiple scan with the mentioned dwell time listed in Table 5-3 is used with the model. The input of the model is the pre-defined geometric shape characterised by z_{ij} and other model process parameters such as ion flux denoted by $\Phi(x, y)$, beam intensity distribution profile by $f_{x,y}(x_i, y_j)$, angle and energy dependent sputtering yield function by $Y(E_0, a_{x_i, y_j})$ and mentioned dwell time $t_{x,y}$ at point (x_i, y_j). The model output will be the number of scans $n_{x,y}$.

The FIB material removal depends on a number of control parameters such as the ion dose, beam current, angle of incidence, pixel time and sputtering yield. The parameters explicitly observed are the angle of incidence, ion beam energy and pixel dwell times. The angle of incidence refers to the angle between the ion beam and the sample surface normal. The calculations presented here assume that the initial angle of incidence is 0 degrees (i.e. parallel to surface normal). After the first FIB sweep which causes some partial formation of the shape that needs to be formed, the ion beam will not hit anymore perpendicularly the target surface at the location of the individual pixels. The

angle of incidence on the target surface will change automatically (based on the geometry of the pixels which form the slope of the shape surface). It is taken in the model calculations for the subsequent FIB sweep. The ion beam energy assumed in the test case study is constant at 30 *keV*. The sputtering yield data for various angles of incident values and ion energy 30 *keV* for Ga ion beam is generated using SRIM software. Pixel dwell time varies from pixel to pixel as outlined above and illustrated in Figure 5-13. Pixel dwell time of first pixel = 0.05ms and pixel dwell time increment along the *x* direction is 0.005 *ms*. Overlapping for 0% is used i.e. k_{OV} =1. The two dimensional parabola Equation (5.14) is used in the modelling procedure to check if the final depth of the parabola at any pixel is already achieved at the current scan, i.e. if it is at or exceeds the target values in Table 5-2. A summary of simulation parameters is shown in Table 5-4 below.

Table 5-4 Specification of the focused ion beam micro-machining simulations

Target material atomic density	Silicon (atomic density $h = 5 \times 10^{22}$ atoms/cm^3)
Ion beam	Gallium (Ga$^+$)
Beam spot diameter	55 nm (Full Width at Half Maximum, FWHM)
Ion beam flux	$\Phi(x, y) = 0.72216e^{12}$ ions / μm^2 sec
Beam overlapping	0% (dx = 55.5 nm, dy = 55 nm)
k_{OV} for 0% beam overlap	1
Ion beam distribution	Gaussian bi-normal, with standard deviation 28.054 nm
Sputtering yield	$Y(E_0 = 30, a = 0^o) = 2.3982 \, atoms / ions$
Ion beam current	350 pA
Initial ion beam angle	0 degree
Ion energy	30 keV

5.4.3. Simulation Results

The number of scan of the beam required to complete milling the target milling depth is described by Equation (5.12). The predicted output can be used to compute the total milling time of all the pixels. The final shape is eventually achieved at the two centre pixel (pixel 5 and 6) after the 328th FIB scan which is the closest to our pre-defined shape tabulated in Table 5-5. Table 5-5 details the model predictions for the number of scans $n_{x,y}$ required to mill the pre-defined shape of a parabola.

Table 5-5 Number of scans required until the pixel target milling depth is reached

Pixel	1	2	3	4	5	6	7	8	9	10
Number of scans $n_{x,y}$	98	226	294	325	328	328	325	294	226	98

Table 5-6 and Figure 5-14 summarise the total milling time in second required to mill the pre-defined target milling depth ($Z_{target} = Z_{centre} - \dfrac{x^2}{4p}$) at each pixel of the 2D pixel slice. The overall evaluation of the required milling time needed to produce the entire parabola is calculated as the multiple of the number of scans at that pixel and its associated pixel dwell time.

Table 5-6 Total milling time required to mill the target milling depth

Pixel	1	2	3	4	5	6	7	8	9	10
Milling time(sec)	0.0049	0.0124	0.0176	0.0211	0.023	0.023	0.0211	0.0176	0.0124	0.0049
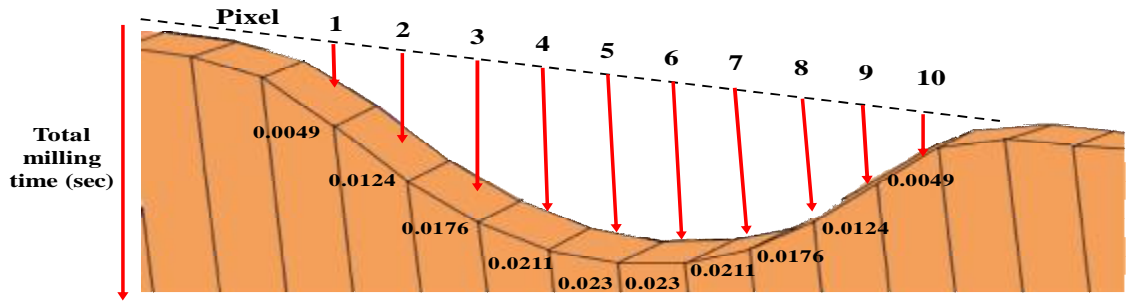
Figure 5-14 The total milling times (sec) required to mill the pre-defined shape

5.4.4. Discussion

The simulations result is generated from the FIB computational model. The development of the surface during intermediate scans: 1, 50, 98, 200 and 328 (final) scans are shown in Figure 5-15. The milling depth of the ten pixels centre after the first scan are indicated by '$*$', while the final shape, as shown by the solid line with '$\times$' in Figure 5-15. The other lines also details the intermediate milling depth (Z_{ij}) developed during various scans. For example, at 98th scan, the current milling depth is $Z_{ij} = 0.0384mm$ which has just exceeded the target milling depth $Z_{t\arg et} = 0.038mm$. From 98th scan onwards, the beam will not visit this pixel. It can be checked from Figure 5-15 that Z_{ij} of the first pixel centre does not increase anymore. The beam will then carry on milling the second pixel until target milling depth of all pixels are reached. For any discrete amounts of material removed, the depth at a pixel also changes in a discrete manner and exact value would be difficult to achieve in the general case.
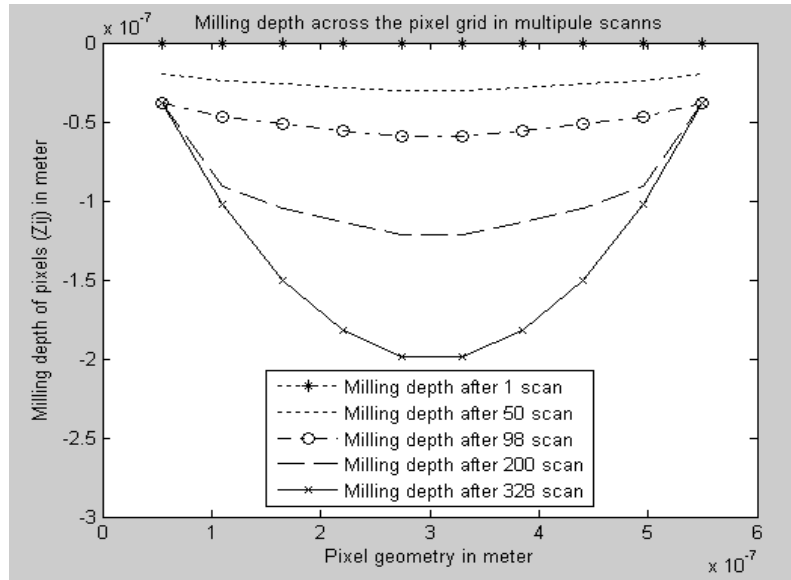
Figure 5-15 Milling depth developed in multiple scans at the pixel

Table 5-7 shows the model evaluation for the milling depth at each pixel (denoted by Z_{ij}) after the target milling depth is achieved. As evident from the table results, there are some small differences between the exact target depth values reported in

Table 5-2 and the pixel depths achieved as a result of iterative FIB sputtering. The ion beam stops milling at a pixel in the reaming scans once it is detected that the target depth at the present scan is achieved or exceeded. The milling depth will not be exactly the same as specified requirements (i.e. slightly smaller or bigger than the specified depth).

Table 5-7 The milling depth at the final scan obtained from the FIB model

Pixel	1	2	3	4	5	6	7	8	9	10
$Z_{ij}(mm)$	0.0384	0.1021	0.1502	0.1825	0.1985	0.1985	0.1825	0.1502	0.1021	0.0384

5.4.5. Contributions of the Modelling Work

The novel part of the model work is that prediction of number of scans required is considered in the model. This further improves the original FIB model developed by Vasile. The milling depth which defines the shape is captured within the mathematical model given by Equation (5.12) using a pre-defined constant set of pixel dwell time by controlling the number of ion beam scans. This repetitive scanning approach provides a better process control and can help obtaining a more accurate shape because the updated pixel geometry after each scan is used to calculate the actual angle of incidence of ion beam which affects the sputtering yield.

The mathematical model of FIB given by Equation (5.12) can be used as part of the proposed risk analysis methodology. It helps gaining knowledge about the importance of FIB process control parameters on process output parameters. It also helps make predictions for the process capability and forecast how uncertainties may affect the quality of the fabricated shapes. The mathematical models are compiled to build reduced order models together with design of experiments and response surface methodology. These approximated models are particularly useful for saving computational resources. They can be utilised for uncertainty analysis where large number of process evaluations are typically required. Existing uncertainties, e.g. the level of stability of the ion source with the stated energy, directly affect the performance or the process behaviour. They must be characterised and their effect must be taken into consideration. Methodology for risk analysis is proposed and demonstrated using the FIB milling process using assumed uncertainty data in the next chapter. Sensitivity

analysis can be carried out to understand the significance of the process parameters. Optimisation can also be undertaken to find out the optimal process conditions and product specifications to fulfill specified constraints for the FIB sputtering process.

5.5. Sputtering Yield Validation Experiment: Milling a Rectangular Block

After demonstration of the model approach, the model predictions are validated against the experimental work carried out in Cranfield University. The model predictions are validated with the experiments using a FEI 200 FIB machine as shown in Figure 5-16. The interaction and significance of this verification have facilitated the development of FIB surface geometry morphology for micro- and nano-structures fabrication.

Figure 5-16 The FEI 200 FIB system

Obtaining a reliable sputtering yield value is important in order to predict the dwell time for milling the pre-defined shape precisely. The objective of experiments here is mainly to validate one of the crucial parameters in FIB process: the sputtering yield, used (as a function of beam angle and energy) at the specified angle and energy in the experiment against the SRIM software. Sputtering yield for the initial models relies on sources such as FIB machine library and literature. Variation and uncertainties in the process parameters may cause a deviated sputtering yield value from expected. . Therefore, this

value should be verified using a separate experiment so that the validated value can be applied in subsequent experiment. Numerous experiments were performed using a trial-and-error approach to identify the relevant ranges and nominal values of certain process parameters leading to the basic shape such as a basic straight line and a volume block (the investigated case study here). The ranges of values were input back into the FIB model given by Equation (5.12). The preliminary results from models would also be useful to improve the experiments and vice visa. Few simple experiments can also be carried out to explore the uncertainties of some process parameters, like the current and beam energy.

5.5.1. Case Study for Sputtering Yield Investigation

The FEI 200 FIB system is used to set the milling of a simple boxed shaped feature. The purpose is to estimate the amount of sputtered material and understand the process parameters to obtain experimentally a value for the sputtering yield under a particular set of FIB process conditions. The sputtering yield values reported in the previous section is obtained from sources such as SRIM software, literature, and FIB machines' library. The sputtering yield value at a given beam angle and energy is calibrated priory to any experiments because it is one of the crucial parameters which affected the milling depth obtained. Experiments are carried out on target material (100-orientation) p-type Silicon, B doped wafer substrate using the FEI 200 FIB system. A rectangular block with dimension $10mm \times 5mm$ is specified to be milled as show by Figure 5-17. In the experiment, a 30 keV focused Ga+ ion beam is used to accelerate the incident ions. The beam diameter and current used is 55nm and 350 pA respectively. The dwell time is set to one microsecond. A 50 % beam overlap is used.
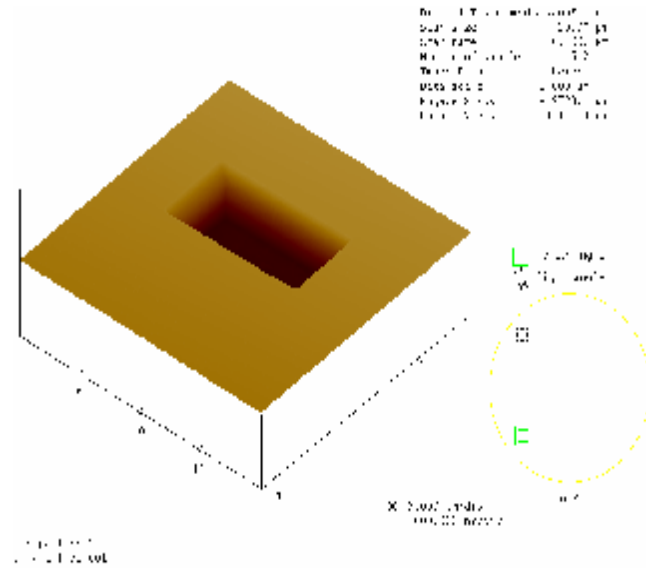
Figure 5-17 An AFM image of the milled structure

5.5.2. Experimental Results

Using the above process set-up, the ion beam raster across the surface and produced a rectangular block. Its dimensions and milling depth are measured to calculate the volume of sputtered materials. The sputtering yield is determined experimentally. Figure 5-18(a) shows an AFM image of the milled structure in top view. The three lines with arrows indicated the analysed sections. Figure 5-18(b) shows AFM image of the section analysis. The couple of arrows show the positions of the measured sputtered depth. From cross sections measurements it is observed that the actual milled feature is not very accurate box-shape but rather have linearly increasing depth along the long side of the box. The depth is measured as 1.03 μm. This depth variation ranges from 0.883 μm to 1.09 μm. This is most likely caused by not very accurate placing of the sample inside the FIB station priory to undertaking the experiment. The sputtered volume is 48.176 μm^3 (note: This calculation is from the cross section profile area 9.9537 μm^2 and average width of the box of 4.84 μm).

144

(a)	(b)
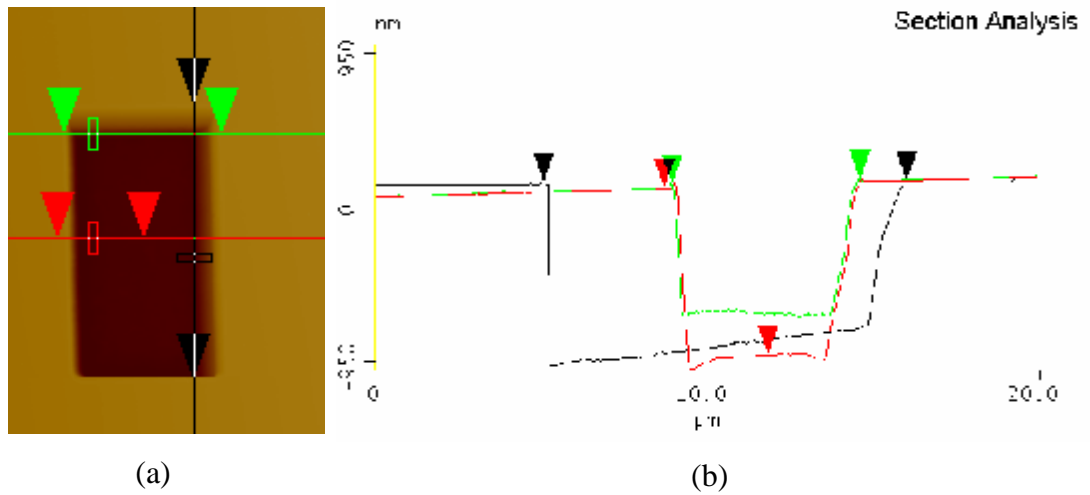
Figure 5-18 (a) showed an AFM image of the milled structure in top view and (b) showed AFM image of the section analysis.

5.5.3. Discussion

It is recorded that 460 seconds are required for milling the above volume. With time equals to 460 seconds and ion beam current equals to 350pA, the total amount of ions delivered to the sample is calculated to be 1.00488×10^{12} ions (this can be calculated by $I \times K \times T$ where I is the current, K is the number of ions in one unit current which equals $6.24150948 \times 10^{18}$, and T is the recorded time). The atomic density of the target material is $5 \times 10^{10} \, atoms / mm^3$. The sputtering yield from experiment can be calculated by Equation (5.15). The experimentally derived sputtering yield is found to be 2.397 atoms/ion. The process parameters and output are recorded by Table 5-8.

$$Sputtering \ yield \ [atoms/ion] = \frac{Atomic \ density \times sputtered \ volume}{total \ amount \ of \ ions} \qquad (5.15)$$

145

Table 5-8 Summary of parameters recorded and derived in the experiment

Ga+ ions delivered at given time	1.00488×10^{12} ions
Recorded depth	1.03 μm
Total time of milling	460 sec
Volume of sputtered material	48.176 μm^3

With ion beam angle of 0 degree and ion energy of 30 keV, the sputtering rate in the model is reported to be 0.3 μm^3/nC in the FEI 200 FIB machine library. The corresponding sputtering yield is 2.3982 atoms/ion. While the respective sputtering yield extracted from SRIM is 2.39 atoms/ion and the experimental value is 2.397 atoms/ion. It has verified that the experimental sputtering yield value agrees well with the mentioned value in SRIM software and the FIB machine library.

5.6. Case Study Two: A Three Dimensional Parabolic Trench

Focused ion beam micro-machining emerges as a crucial technology in producing different shapes in micro- and nano- scale in fabrication industries such as the micro-mould for injection moulding, and probe tips. Quite a few models and simulations (mentioned in chapter 5.3) have been developed recently trying to predict an accurate shape in the real manufacturing process such as Nassar and Vasile [71] work. Their modelling for dwell time prediction in one single scan is used in our FIB model which can establish a fundamental base for accounting re-deposition effect as a further step. Re-deposition effect modelling is discussed but not implemented at this stage. However, the FIB models given by Equation (5.12) have been validated against the experimental

work performed at Cranfield University. This FIB model can allow simulations in the early design stage to fabricate a micro-probe. The FIB model is applied to illustrate a parabolic trench fabrication as an example. The verified sputtering yield values i.e. 2.397 atoms/ion can also be applied in this section. The whole study aims at understanding how to gain a control on process parameters to predict the scans required and give the corresponding milling depth. Its principles have been outlined and explained in chapter 5.1-5.3. Motivated examples using this FIB mathematical model by Equation (5.12) to predict the total time required for milling different shapes such as a 2D parabolic shape in chapter 5.4. In this case study, a micro-parabolic trench is investigated.

5.6.1. Computational Modelling

The aim of the test case study is to apply the developed computational modelling procedure to predict the dwell times needed to mill a pre-defined micro-channel. Equation (5.8) is first applied to calculate the required time theoretically assuming the ion beam is operated under a single scan approach. However, a FEI 200 FIB machine is operated with a multiple scans approach. Predicting number of beam scans required for milling the defined feature is more preferable than pixel time prediction. Therefore, the FIB model outlined by Equation (5.12) is used which is capable to predict number of beam scans. The focus is to translate the pre-defined geometry (depth vs x, y-coordinate) into ion beam control coordinates (known as the pixel scheme) as a function of time and other associated parameters. The input of the model is the pre-defined geometric shape characterised by Z_{ij}. Other model process parameters such as ion flux is denoted by

$\Phi(x, y)$, beam intensity distribution profile by $f_{x,y}(x_i, y_j)$, angle and energy dependent

sputtering yield function by $Y(E_0, a_{x_i, y_j})$. The model output is the number of scans $n_{x,y}$.

5.6.2. The Case Study

(1). Geometrical Details of the Parabolic Trench and Pixel Layout

This study has focused on the case of producing a trench with a known size and using

pixel layout where an ion beam sweeps over a surface. Its isometric view, top view and

cross section is shown in Figure 5-19(b) and (c). The pixel layout details over the target

surface are listed in Figure 5-19(a).
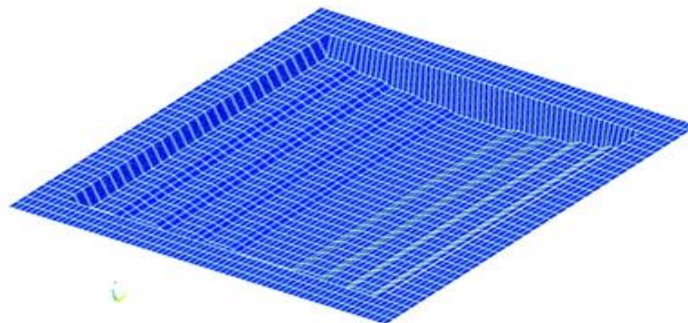
(a) Isometric view and pixel array
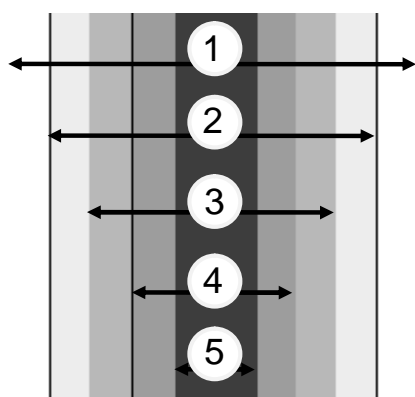
(b) Top view and pattern numbers
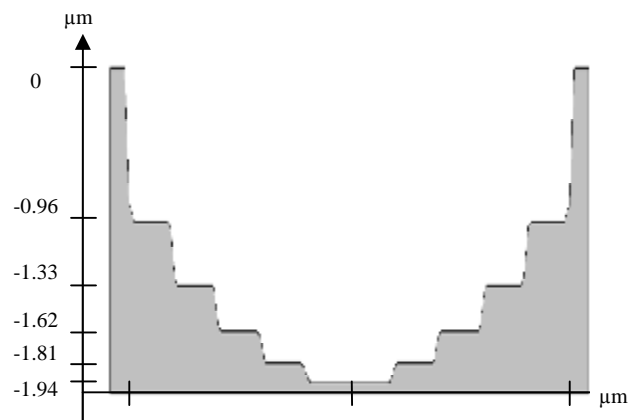
(c) Front view/ Cross section of the trench

Figure 5-19 The isometric, top and cross section view of a micro-trench

The pre-defined sputtered shape is a 3D stepwise parabolic micro-trench which has both width and length of 10 μm. The milled shape can be divided into five '*Patterns*', or can be expressed as five '*Parts*' i.e. *Pattern or Part 1 to 5*. '*Pattern*' refers to the horizontal divisions while '*Part*' refers to vertical divisions, across the trench cross section presented in Figure 5-20.
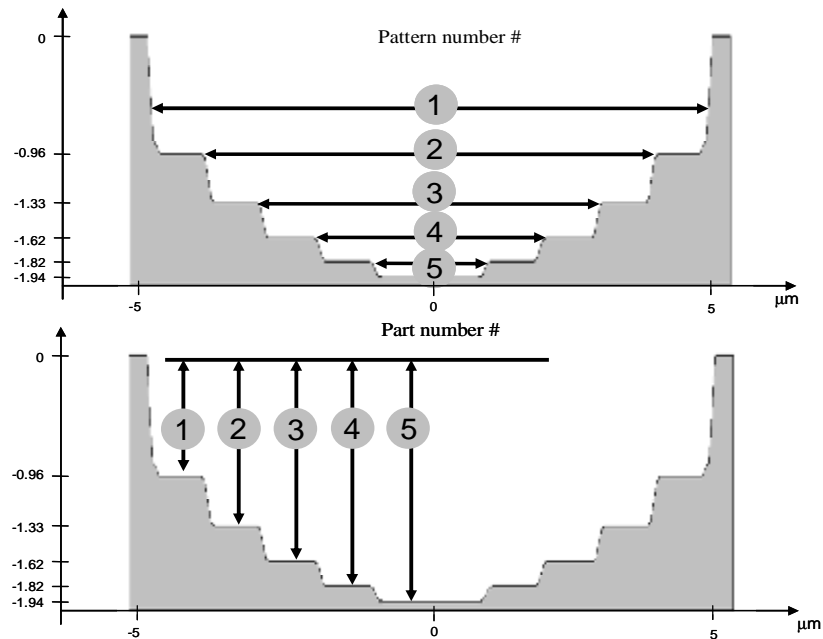
Figure 5-20 Terminologies of 'Pattern' and 'Part' across the shape

Each pattern has an expected total milling depth as illustrated by the y-axis of the front view in Figure 5-19. The total milling depth at any pattern is the incremental milling depth from the previous milling depth. For example, pattern '1' has a dimension of $10mm \times 10mm$ and milling depth of 0.96 μm. Pattern '2' has a dimension of $8mm \times 10mm$, a total milling depth of 1.33 μm or a milling depth increment by 1.33 - 0.96 = 0.37 μm from the milling depth of pattern 1. Pattern '5' has a milling depth of 1.94μm. Every single pixel shown in Figure 5-21 possesses same dimension of $55nm \times 27.5nm$. There are $182 \times 364, 146 \times 364, 110 \times 364, 72 \times 364$ and 36×364 pixels in pattern 1, 2, 3, 4 and 5 respectively. The pixels on patterns are listed in Figure 5-21.

149
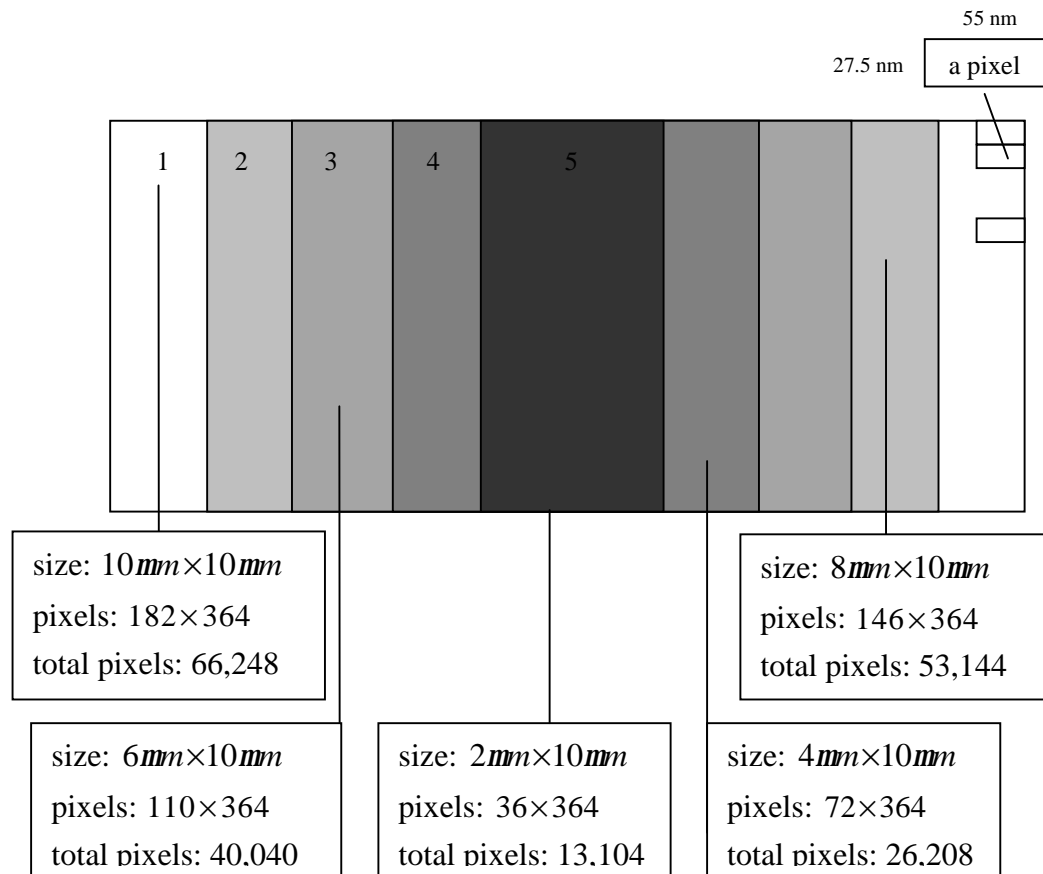
Figure 5-21 Pixel schemes details and pixel size across the surface in top view

5.6.3. Process Set-up and Parameters Control

In this study, a 30 keV focused Ga+ ion beam with diameter 55 nm (Full Width at Half Maximum) is used to accelerate the incident ions and raster across a silicon surface. The beam diameter and current used was 55nm and 350 pA respectively. A pixel area is $27.5mm\times55mm$. 50% beam overlapping is used. k_{ov} for 50% beam overlapping is 2. Sputtering yield is 2.3982 atoms/ion, the same as the calibrated yield in chapter 5.5.3.

(1) Determination of beam profile and ion flux - 50% beam overlapping is used. Due to this overlaps, the pixel size is adjusted to be 27.5 nm by 55 nm. An ion beam distribution with Gaussian bi-variate distribution with a standard distribution equals

27.86 nm is adopted. The above beam diameter will give a corresponding current of 350 pA (referring to Table 5.3-1). With current equals 350 pA and diameter equals 55nm, the ion flux of the beam Φ_b can be obtained by Equation (5.2), i.e.

$$\Phi_b = \frac{I}{pR^2} \times K ,$$

where Φ_b is the ion flux (ions/s cm^2), K is the number of charges in one ampere current, R is the Beam radius (meters), I is the milling current. With $I = 350\,pA$, $R = 27.5\,nm$, and $K = 6.24150948 \times 10^{18}$, Φ_b is calculated as 0.9195074×10^{20} (ions/s cm^2). When the ion beam carrying ion flux 0.9195074×10^{20} (ions/s cm^2) sweeps across a pixel, the associated ion flux delivered on a square pixel with an area $A = 55nm \times 55nm$ is calculated by using Equation (5.3), i.e.

$$\Phi(x, y) = \Phi_b \frac{pR^2}{A} ,$$

which gives $\Phi(x, y) = 0.722 \times 10^{20}$ (ions/s cm^2). The flux of ions receives at the surface of the target material depends on the beam overlapping. $k_{OV} = 2$ for a 50% beam overlap means ion flux that a pixel received is double i.e. $\Phi_{50\%}(x, y) = 1.44 \times 10^{20}$ (ions/s cm^2).

(2) Determination of sputtering yield from sputtering rate - The beam angle and beam energy to start the milling process in the model is 0 degree and 30 keV respectively. Sputtering rate (micrometer cubic per nano Columb) is found in the FEI 200 FIB system library at these parameter values for Ga + ion and silicon surface combination equals 0.3 µm^3/nC. This sputtering rate Y_r can be translated into sputtering yield by Equation (5.16). [138]

$$Y(E_0, a_{x_i, y_j}) = 96.4 \times \frac{r \times Y_r}{m} \tag{5.16}$$

where $Y(E_0, a_{x_i, y_j})$ is the sputtered yield (atoms per incident ion at point (x_i, y_j)), a_{x_i, y_j} is the incident angle of the ion beam at point (x_i, y_j) and E_0 is the ion beam energy, and where m is the mass in AMU, Y_r is sputtering rate in cubic microns/ nano Coulomb, r is the density of silicon. With $a_{x_i, y_j} = 0$, $E_0 = 30keV$, $m = 28.0855$, $r = 2.329g/cm^3$, $Y_r = 0.3mm/n$, therefore sputtering yield $Y(E_0 = 30, a_{x_i, y_j} = 0^o)$ is calculated to be 2.3982 atoms/ion.

5.6.4. Model Result of Dwell Time Prediction

All process parameters and geometric details are compiled into the FIB model by Equation (5.8) to predict the time required for each pixel to achieve its pre-defined total milling depth. This predicted time represents the pixel dwell time $t_{x,y}$ that the ion beam stays on each pixel. Table 5-9 and Figure 5-22 summarises the pixel dwell time prediction on each 'Part' to produce its expected total milling depth. For instance, pixel time 13706 µsec is required to mill any single pixel inside part 1 for a total milling depth 0.96 μm. Part 5 has the most depth, it takes 27905 μsec to achieve the 1.94 μm total milling depth. In Table 5-9, the pixel dwell time on part 1-5 is mentioned.

Table 5-9 Dwell time prediction for each pixel across part 1-5

Part #	1	2	3	4	5
Dwell time $t_{x,y}$ (μsec)	13706	19257	23403	26227	27905
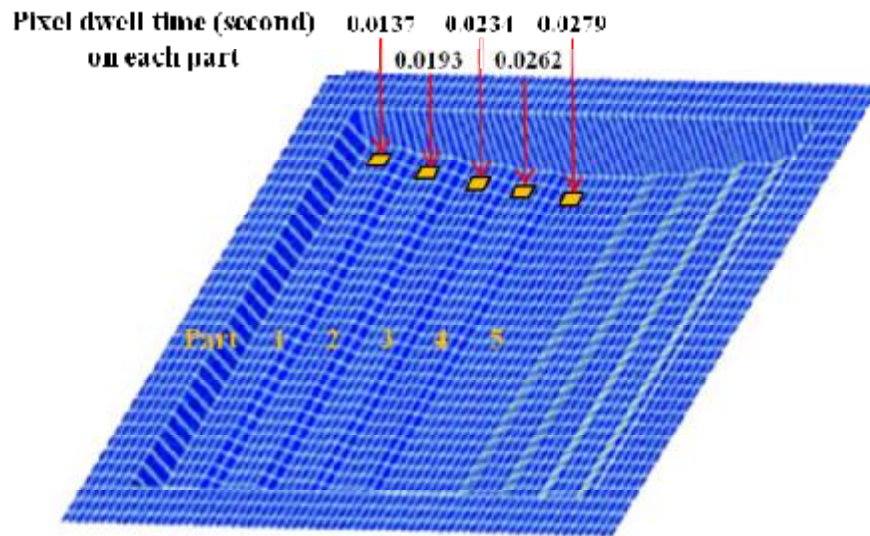
Figure 5-22 Pixel dwell time $t_{x,y}$ required on each pixel to mill its expected depth

5.6.5. Dwell Time Transformation

The model and experimental work adopted two different beam operation approaches: (1) a single scan with different dwell time and, (2) multiple scan with constant dwell time on all pixels. The ion beam raster across the target surface in a single passing scheme in model. The experimental work has adopted a multiple scan with constant dwell time due to the FEI-200 FIB system operation routine. A transformation on model output (pixel dwell time) is required such that the transformed dwell time becomes a feasible input for the FIB machine. Different milling depth is sputtered when pixels receive different number of scans over its respective pattern. The number of beam scans $n_{x,y}$ at any one pixel equals the model dwell time prediction $t_{x,y}$ on each pixel (from Table 5-9) divided by the fixed pixel dwell time t_c. A fixed dwell time, $t_c = 1\,m\sec$ on each pixel are defined in FIB system. The calculated $n_{x,y}$ required over each pattern, and the

153

number of pixels over the pattern area, are used to compute the incremental time T_{incre} required over each pattern area by Equation (5.17).

$$T_{incre} = n_{x,y} t_c N_{pixels} \qquad (5.17)$$

where T_{incre} is the incremental time for milling a pattern area, $n_{x,y}$ is the number of beam scans over respective pattern. t_c is the fixed dwell time defined in FIB system. N_{pixels} is the number of pixels over the pattern area that are listed in the third column of Table 5-10. The incremental time are listed in the last column of Table 5-10.

Table 5-10 Number of pixels on pattern and the corresponding incremental time

Pattern area #	Dimensions ($mm \times mm$)	Number of pixels N_{pixels}	The incremental time over pattern T_{incre} (sec)
1	10×10	182×364	908
2	8×l0	146×364	295
3	6×10	110×364	166
4	4×10	72×364	74
5	2×10	36×364	22

The incremental time is then summed up to get the total (cumulative) milling time for scanning the pattern area. The predicted dwell time from the model is transformed into an equivalent FIB set up for total milling time at each pattern as shown in the last column of Table 5-11. The last column in Table 5-11 specifies the cumulative time for milling the respective pattern area. Therefore, the total scanning time at any pattern is the incremental time from the previous milling time. For example, 908 sec is required to

mill the area of pattern 1; then milling the area corresponding to pattern 2 is 295 sec (the incremental time from the time set for milling over pattern 1).

Table 5-11 Number of beam scans from model and the FIB pre-set total milling time

Pattern area #	Model prediction: Number of beam scans over respective pattern $n_{x,y}$	FIB system set-up: Total (cumulative) time for scanning the pattern area (second)
1	13706	908
2	19257	1203
3	23403	1369
4	26227	1443
5	27905	1465

5.6.6. Discussions

The model first predicts the dwell time on each pixel, then number of scans required for achieving the pre-defined geometry. In this experimental study, the dwell time predicted from the model (known as the given time) are transformed as an input to set the dwell time for the FIB machine, as well as other process parameters listed below in chapter 5.6. At the mentioned number of scans over each pattern set into the FIB machine, the final shape (observed shape) obtained in the experiment is measured. The milling depth of each pixel is measured in each pattern. This measured milling depth will then be compared against our predefined milling depth of the parabolic trench in the model. The aims of experiments here are mainly to verify (1) the deviation of the predefined geometry against the final experimental geometry, and (2) sputtering yield used at the

155

specified angle and energy in the experiment against the values from SRIM software/ FIB machines library. The experiments will further be explained in chapter 5.7.

5.7. Experiment to Validate the Computational Model

The time prediction and the corresponding number of scans required are obtained to obtain a three dimensional trench with a pre-defined geometry from model by Equation (5.12). The predicted number of scans from the model is specified as a process input in FEI-200 FIB machine to obtain a final geometry. The experimental geometry was obtained at Cranfield University to validate the predefined shape of the model. However, re-deposition effect that affects the final shape is not included in this study.

5.7.1. Experimental Set-up

Experiments are performed on p-type Silicon, B doped wafer substrate to verify the FIB modelling result using a FEI 200 FIB system. A 30 keV focused Ga+ ion beam is used to accelerate the incident ions. The beam diameter and current used is 55nm and 350 pA respectively. This amount of current with beam diameter 55nm possesses an ion flux of $\Phi(x, y) = 0.722 \times 10^{20}$ ions/cm^{2}sec. A pixel area is $27.5nm \times 55nm$. 50% beam overlapping is used. k_{OV} for 50% beam overlap is 2. Other process parameters are all equivalent to the model set-up and summarised by Table 5-12. The beam scanning path in the FIB experiment is presented by Figure 5-23.
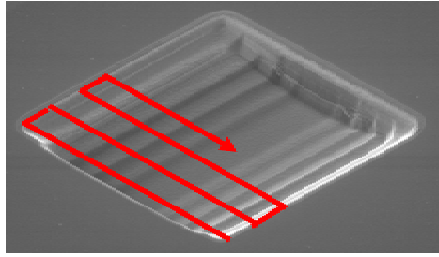
Figure 5-23 FIB beam scanning sequence for producing the trench feature

A multiple scan approach is adopted with pre-defined constant pixel dwell times that pixels are scanned in a controllable number of times. The defined patterns are subjected to different number of scans by controlling the total times of scanning the defined areas of the patterns.

Table 5-12 Pre-defined set of process parameters in the experiment

Target material atomic density	Silicon (atomic density $h = 5 \times 10^{22}$ atoms/cm^3)
Ion beam	Gallium (Ga$^+$)
Beam spot diameter	55 nm (Full Width at Half Maximum, FWHM)
Ion beam flux	$\Phi(x, y) = 0.722 \times 10^{20}$ ions / cm^2 sec
Beam overlapping	50% (dx = 27.5 nm, dy = 55 nm)
k_{ov} for 50% beam overlap	2
Ion beam distribution	Gaussian bi-normal, with standard deviation 28.054 nm
Sputtering rate	0.3 μm^3/nC
Sputtering yield	2.3982 atoms/ion
Ion beam current	350 pA
Ion beam angle	0 degree
Ion energy	30 keV
Dwell time	$t_c = 1\, m\sec$

5.7.2. Experimental Results

Milling depth of pixels on each pattern is measured and observed. A trench is produced using the FIB system from the experiment. Figure 5-24 shows the AFM image in the top view and the output data. The cross section of the milled structure is also examined. Figure 5.25 and Figure 5.26 show the output data and graphs from a cross-section analysis undertaken to obtain information for the actual shape that is produced in the experiment, and to evaluate the milling depths of the trench. The actual depth of the milled structured is measured. In Figure 5.25, the three sets of arrows from top to bottom on the upper graph show the positions of the measured sputtered depth and its cross sectional depth of pattern 5, 1 and 2. Their corresponding sputter depths are shown in the lower (cross section) graph and reported to be 1.959 µm, 1.017 µm and 1.32 µm respectively. Figure 5.26 shows the cross sectional depth of pattern 4 and 3 indicated by the first set and the second set of arrows from the upper graph as well as the output data and graphs. The measured depths are presented in the cross section graph and are reported to be 1.831 µm and 1.619 µm respectively. The accuracy of the measurement is ±0.03 µm.
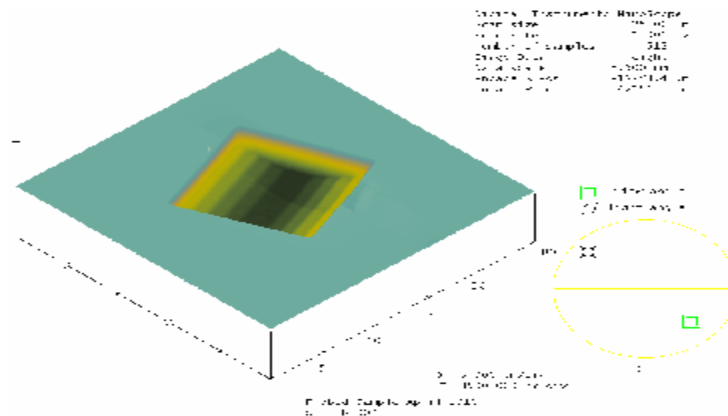
Figure 5-24 AFM image of the fabricated structure in the top view
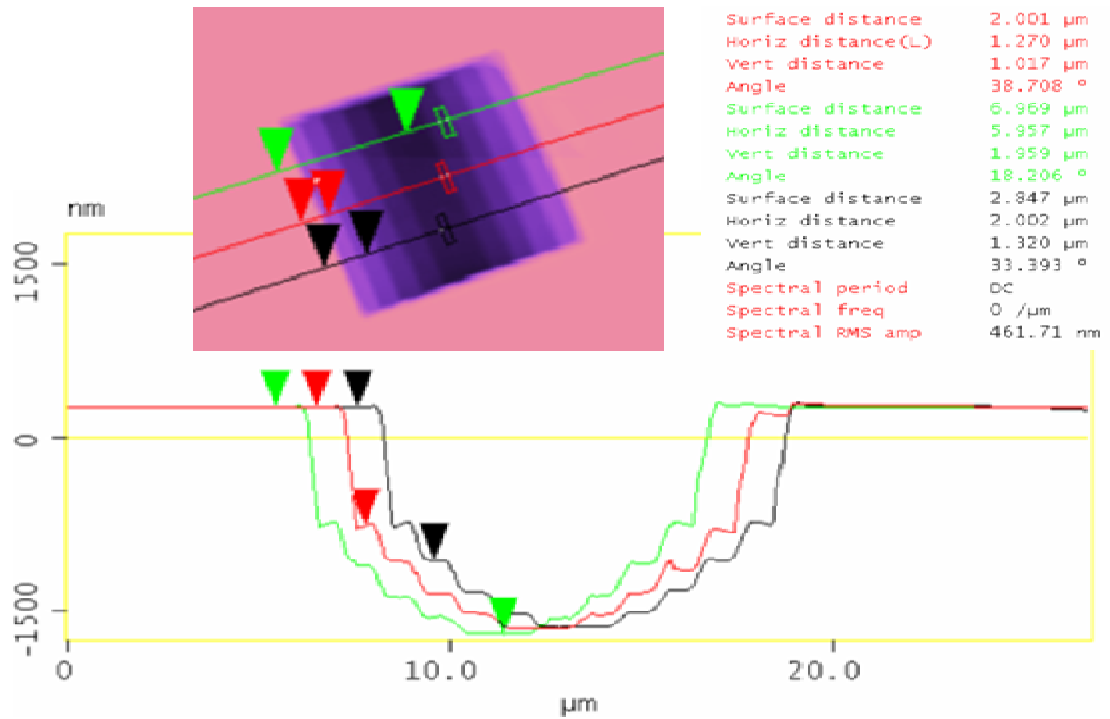
Figure 5-25 Cross sectional analysis of the sputtered trench on pattern 5, 1, and 2
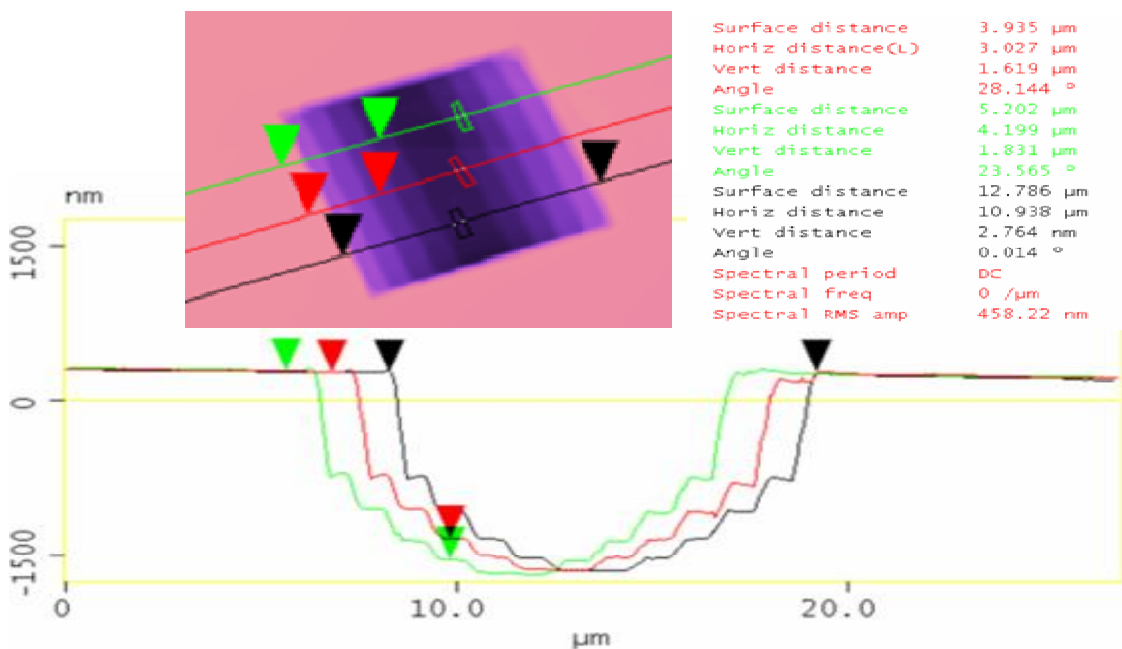
Figure 5-26 Cross sectional analysis of the sputtered trench on pattern 4 and 3

5.7.3. Discussion

Table 5-13 summarises the (1) the pre-defined shape used in the computational model, and (2) the measured cross sectional depth from the shape produced in the experiment using FIB set up based on the model predictions. The cross sectional depths across five patterns obtained from FIB model are verified against that the measured values from the experiment. The percentage errors between the model and experimental values are derived and listed in the table.

Table 5-13 Comparison between model and experimental data for depth variation

Pattern	1	2	3	4	5
Set Z values from FIB model (mm)	0.96	1.33	1.62	1.81	1.94
Z measured (mm) $\pm$ 0.03 from sectional analysis	1.01	1.32	1.61	1.80	1.96
Difference in model and experimental cross-sectional depths (%)	5.0	0.8	0.6	0.5	1.0

The data in Table 5-13 shows that there is a very good agreement between the intended shape as analysed with the model and the actual experiment (see also Figure 5-27). Only at the level of the first topmost step the difference in depth between the model and the experiment is larger (5%). This can be possibly due to a measurement related error and possibly deviations from the expected milling parameters at the topmost layer of the target material in terms of material composition. The errors may arise due to the inaccuracy to capture precise process parameters values due to parameters uncertainties. The depth at all other subsequent steps defining the cross-sectional profile is extremely well predicted. The percentage errors are less than one percent. At the centre line of the

trench the model predictions associated with depth 1.94 *mm* compare with the measurement of 1.96 *mm* for the actual obtained shape experimentally. The model validation study has demonstrated that the FIB computational model can be used as a powerful tool to predict how to set the FIB system in order to accurately achieve the desired shape without using a trial-and-error approach. It is critical to use accurate model input data related to the process parameters as variations do always exists, and in particular in relation to the sputtering yield value. The impact of re-deposition is not prominent and influential for affecting the final shape obtained here due to the high aspect ratios of the shape feature [80]. Additional computations accounting for re-deposition effect must be considered in the scenarios of low aspect ratios product shape.
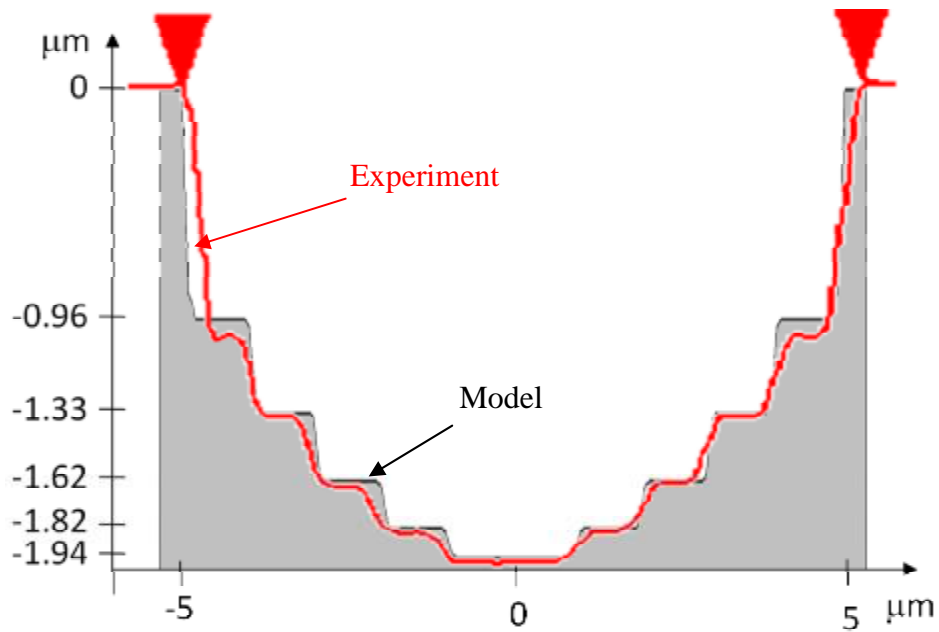
Figure 5-27 Model vs. experimental cross-sectional profiles

Closure

A few mathematical model that can be used to predict pixel dwell times, or number of FIB scans required to mill predefined shapes have been developed. Important process parameters are explored and explained through the explicit model. Accuracy of the model is also enhanced by addressing the accuracy of process parameters such as obtaining a validated sputtering yield. The models are then applied on predicting shape of a 2D parabola, a rectangular block and a 3D parabolic trench with different beam operation approaches. Finally, the procedure has been implemented and tested successfully on the test case study of milling a micro-trench with parabolic cross-section. There is a very good agreement between the intended shape as analysed with the model and the actual experiment. In most of the pattern area over the parabolic trench, the model prediction for depth is having less than 1% deviation from the experiments. For example, in the test case, the centre line of the trench the model predictions associated with a depth 1.94 mm compared with the measurement of 1.96 mm for the actual experimentally obtained shape. The work does not only help how to gain a precise process control, but it also helps evaluate the risk of achieving final shape with accuracy when the process is exposed to uncertainties in reality (as a future work). As a result, research and study on focused ion beam application can move towards robustness. Optimisation can be undertaken to minimise the deviations of shape prediction, and maximise process capability.

Chapter 6 Risk Analysis on Focused Ion Beam Sputtering Process

In this chapter, the simulation-driven methodology is demonstrated using the validated focused ion beam model from the previous chapter. Uncertainty propagation of two process variables: angle and energy on process output- milling depth are demonstrated by means of the response surface model. An optimisation problem is also outlined and identification of the optimal process performance is presented.

6.1. Risk Mitigation for Variability and Uncertainty in Manufacturing Processes

The risk analysis methodology development mainly addresses the risk of achieving process performance and design specifications. The novel aspects include:

- Conventional statistical analysis approaches for risk analysis based on Monte Carlo simulations enhanced with approximate but more efficient analytical methods such as First Order Second Moment method;

- Risk analysis integrated with reduced order models for product/ process analysis;

- Adopting non-polynomial reduced order models within the response surface approach for generating reduced order models.

In order to illustrate the process capability of the FIB materials sputtering process, a risk analysis methodology integrated with other computational methods is proposed in this thesis. Risk analysis of the FIB process is a new area which has not been studied much before. Integration of the computational tools as the proposed methodology is an important novel outcome of this research study. The risk mitigation can provide a novel strategic way to help understand the impact of uncertainties involves in the use of FIB related technologies.

Focused ion beam (FIB) sputtering capability is widely used to mill fine structures with pre-defined shape at micro- and nano-scales. The challenge of achieving the pre-defined shapes depends on whether process parameters can be well controlled to predict the response precisely. However, uncertainties always come along with the process variables and have significant effects on the process performance and reliability. In this chapter, process variable uncertainties are introduced and their impact on performances are quantified their impact on performance. Recalling the risk analysis methodology as shown in Figure 3-1 such that computational modelling characterises sputtering yield and milling depth in terms of two investigated process variables: beam angle and energy and other process variables. A reduced order model is constructed using various response surface techniques. The analysis of the design and performance in terms of risk of failure, capability of satisfying specification limits are examined for three FIB processes with three various ion sources. The FIB process scenarios are demonstrated with the risk analysis methodology comprising reduced order modelling and risk analysis. Kriging interpolation is used to investigate the focused ion beam sputtering process explained as in Figure 6-1.
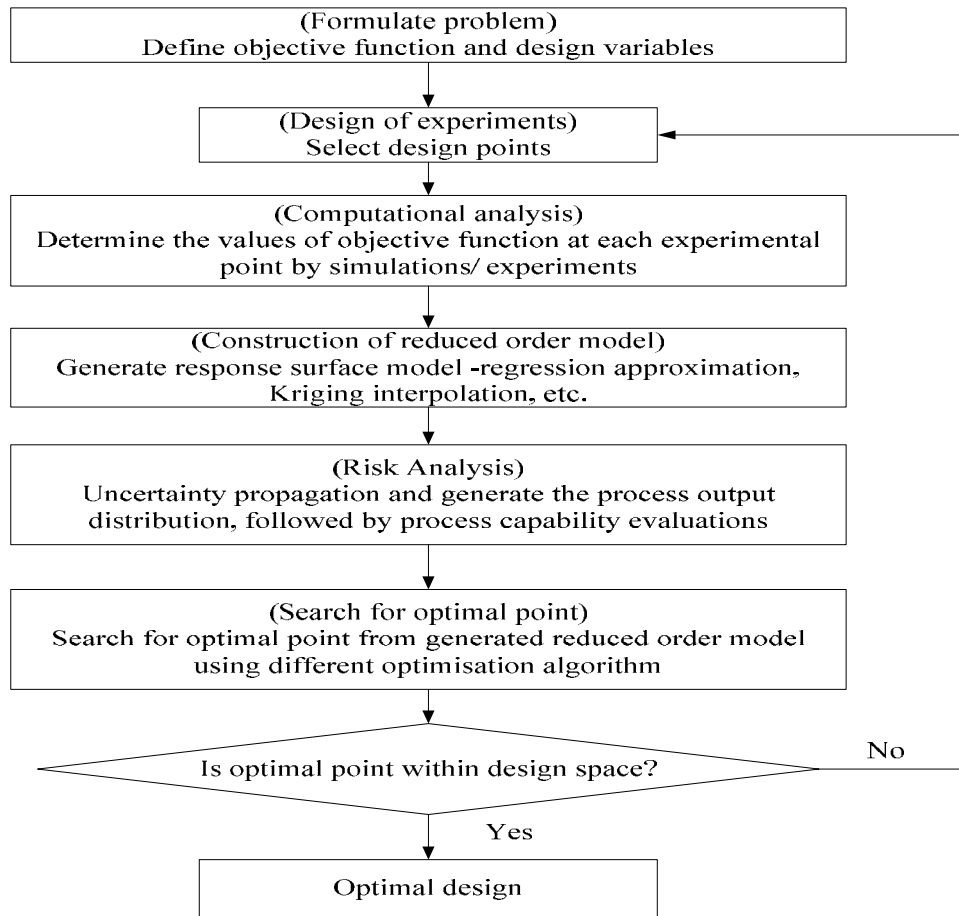
Figure 6-1 A procedural flow representation of the risk analysis methodology

(1) Identify process setup, process inputs (i.e. process variables we can vary to achieve different objective function), and process output (process performance metrics).

(2) Use Design of Experiments (DoE) to define different sets of process inputs.

(3) For each DoE point in step 2 above asses the process output response values (model or real experiment can be used)

(4) Use DoE process response values to build reduced order model (ROM) by fitting the DoE data with different numerical techniques.

(5) Perform statistical risk analysis and calculate process capability using defined specification limits.

(6) Undertake numerical process optimisation.

6.1.1. Application of the Methodology

This chapter consists of two main sections. The first section is to characterise the relationship of sputtering yield, angle and energy by reduced order model. The constructed reduced order model (ROM) can facilitate the sputtering yield extraction avoiding SRIM and experiment and it also be used for sensitivity analysis to identify significant process variables (presented in chapter 6.1-6.3). The second section is to explore the risk analysis and optimisation modelling (presented in chapter 6.4-6.7) based on the identified validated FIB model. To understand the physical behaviour of focused ion beam milling process, computational modelling followed by design of experiments are undertaken according to the risk analysis methodology which is shown in Figure 3-1. Two separate design of experiments (DoE) were considered in order, i.e. (1) relating the angle and energy – sputtering yield and (2) relating the angle and energy – milling depth.

In the first DoE, sputtering yield values can be extracted through empirical formula or experiments. Here, the details are obtained via simulation-based software SRIM which is well validated by means of experiments and literature. In the second DoE, milling depth is manipulated through the validated FIB model governed by Equation (5.12). To account for the variability of the sputtering process, regression models that relate angle, energy and sputtering yield are used to identify the main effect, and the interaction effect of the process variables on the process performances. Sensitivity analysis were carried out based on the regression model, as an important step for subsequent milling depth analysis and understanding the FIB process behaviour.

In the second DoE, another response surface model: Kriging model is used to characterise the relationship between *angle, energy* and *milling depth*. Kriging interpolation methods are applied to enhance the accuracy of reduced order model to predict the milling depth. In order to account for the parameter uncertainties and their impact on the process milling depth during the FIB process, risk analysis is carried out. Sampling method and analytical method are applied via the developed reduced order models (ROM) instead of the FIB computational model in order to generate many evaluations of milling depth in the sample space. Three ion beam sources, Argon, Xenon and Gallium ions, have been used to compare and quantify the process variable uncertainties that can be observed during the milling process. The evaluations of the milling depth take the uncertainties and variations of angle and energy into account and are used to identify their impact on the reliability and quality of the fabricated structure. Finally, an optimisation based design task is formulated to identify the optimal process conditions, by varying the process variables, so that certain quality objectives and requirements are achieved and imposed constraints are satisfied.

6.2. A Reduced Order Model for the Sputtering Yield

6.2.1. Design of Experiments

Several experiments concerning for the ion bombardment process were designed. It is used to establish the relationship between the yield value with respects to *angle* and *energy*. Let x_1 be the continuous process variable *angle of incidence*, x_2 be the continuous process variable *beam energy*, Y_{spu} be the process output which characterises

the process performances *sputtering yield.* Values of x_1 and values of x_2 generate a value of Y_{spu}. A few representative design points are selected in the design space depending on the chosen experimental design. The design points are scaled from -1 to 1 and their corresponding design limit is $x_1 \in [0^\circ, 80^\circ]$ and $x_2 \in [10keV, 50keV]$. A Central Composite Design (CCD) Experimental design is chosen. It requires at least nine design points for a 'two-process variable' problem. The design points are selected at the boundary and midpoint of the design limit in the design space as shown in Figure 6-2.
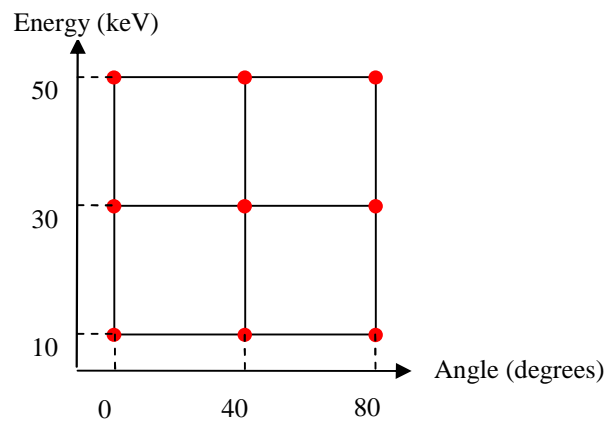
Figure 6-2 Design point selection using Central Composite Design

Materials, physical properties and process variables values x_1 and x_2 for one set-up are specified in the software SRIM (the stopping and range of ions in matter) to generate a value of sputtering yield [132]. Then a few representative design points are chosen to formulate a design of experiment table. One example of experimental setup is detailed in Table 6-1. It demonstrates an ion bombardment process using Xenon ion beam. Table 6-2 is the design of experiment tables for Central Composite design. It summarises the sputtering yield generated using Xenon ion beam in SRIM.

Table 6-1 Materials, physical properties and process variables values

SRIM simulation	
Ion used	Xenon ion
Ion Weight	Mass (amu) 131.904
Sample surface	Silicon (Mass in amu: 28.08, Atomic density: 5×10^{22} atoms/cm^3)
Incidence angle x_1	60 degree
Beam energy x_2	20 keV
Sputtering yield Y_{spu}	7.66 atoms/ion
Number of runs	1000

Table 6-2 DoE summarises the sputtering yield using Central Composite Design

DoE trial run number	Incident angle	Beam energy	Incident angle (degree)	Beam energy (keV)	Sputtering yield (atoms/ion)
1	-1	-1	0	10	2.04
2	-1	0	0	30	3.16
3	-1	1	0	50	3.34
4	0	-1	40	10	5.17
5	0	0	40	30	7.11
6	0	1	40	50	7.53
7	1	-1	80	10	24.08
8	1	0	80	30	39.08
9	1	1	80	50	46.64

6.2.2. A Polynomial Reduced Order Model

The Process response-sputtering yield Y_{yield} is expressed as a function of the process variables x_1 and x_2. A scaled second order polynomial model is constructed using DoE (CCD) table in Table 6-2 by linear regression. The regression model is given by

Equation (6.1) where the regression coefficients are detailed in Table 6-3. For example, $b_1 x_1$ becomes the linear term where b_1 describes a linear effect of the variable x_1. $b_{12} x_1 x_2$ is called the interaction term and $b_{12} x_2{}^2$ becomes a quadratic term.

$$Y_{yield}(x_1, x_2) = b_0 + b_1 x_1 + b_2 x_2 + b_{12} x_1 x_2 + b_{11} x_1{}^2 + b_{12} x_2{}^2 \qquad (6.1)$$

Table 6-3 Regression coefficients for the polynomial response surface models

Regression Coefficient	Central Composite Design
b_0	7.7
b_1	16.88
b_2	4.37
b_{12}	5.315
b_{11}	13.12
b_{12}	-1.65

The coefficient to determination R^2 of the above approximation is found to be 0.98499 while the adjusted R^2 is reported to be 0.93996. The coefficient of variation is 0.2220127. From the statistical tests, the constructed polynomial has indicated a good approximation, i.e. both R^2 and the adjusted R^2 are above 0.9.

6.3. Sensitivity Analysis of the Ion Bombardment Process

The effect of each variable, namely the linear, interaction and quadratic effects, on the process output can be determined by the regression coefficient of the approximation polynomial. Sensitivity analysis is another way to identify the significance of angle and energy on the sputtering yield. It is performed on the reduced order polynomial in order to identify which process variable can cause a higher degree of variations on the process

performance. The effects of any algebraic terms in Equation (6.1) can be deduced by extracting the average sputtering yield of the associated terms with the scaled level being set at '-1', at '0', and at '1'. Table 6-4 details the level setting of linear terms, interaction term and quadratic term. The main effect of the variable angle is the differences of average sputtering yield values between the level setting of x_1 at '-1' and at '0'. These differences are denoted by the slope of graph presented in Figure 6-3. The slope indicates the significance of the associated effect of process variables. The higher the slope, the more significance it is.

Table 6-4 The scaled level setting of terms showing effects of angle and energy

DoE trial number	x_1	x_2	$x_1 \times x_2$	x_1^2	x_2^2
1	-1	-1	1	1	1
2	-1	0	0	1	0
3	-1	1	-1	1	1
4	0	-1	0	0	1
5	0	0	0	0	0
6	0	1	0	0	1
7	1	-1	-1	1	1
8	1	0	0	1	0
9	1	1	1	1	1

Main effect of angle x_1 is determined by extracting the average of sputtering yield with scaled angle at '-1' level setting (i.e. the average of sputtering values in trial run 1, 2 and 3), at '0' (trial run 4, 5 and 6), and at '1' (trial run 7, 8 and 9), the corresponding average yield against angle is plotted in Figure 6-3(a). Similarly, main effect of energy can be deduced from the graph in Figure 6-3(b). To identify interaction effect of the term $x_1 \times x_2$, the multiple of their level settings can be checked from the fourth column in Table 6-4. Interaction effect of angle and energy is determined by the average

sputtering yield between trial 1 and 9 (term level setting at '1'), the average sputtering yield among DOE trial 2, 4, 5, 6 and 8 (term level setting at '0') and the average sputtering yield between trial 3 and 7 (term level setting at '-1'). The slope of the interaction term is plotted in Figure 6-3(c).
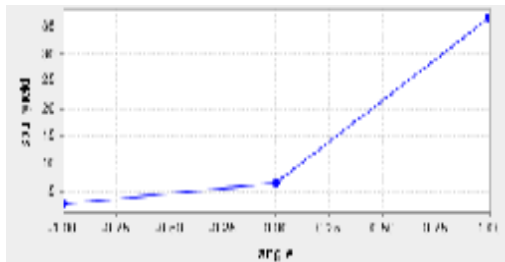
(a) angle vs sputtering yield   (b) energy vs sputtering yield
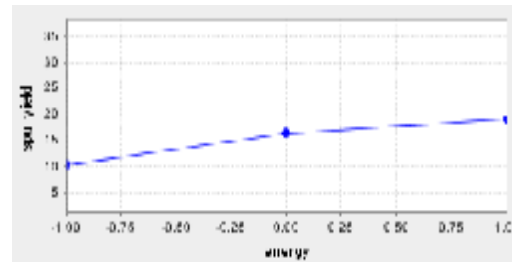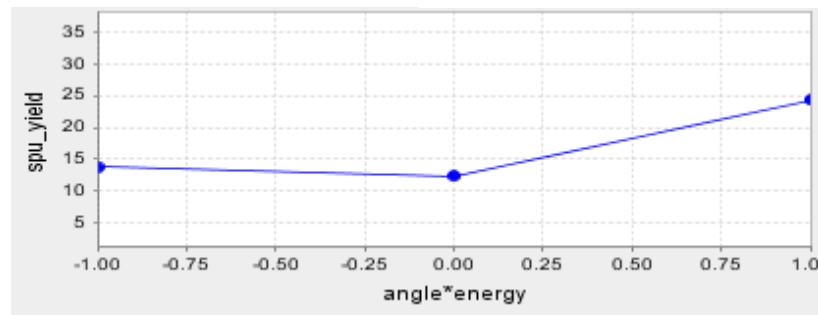
(c) 'angle × energy' vs sputtering yield

Figure 6-3 Relationships of single and interaction process variable against the process response - sputtering yield

To summarise from Figure 6-3, sputtering yield is more sensitive to change when variations impose on main effect of angle. Quadratic term cannot be estimated here. The term level setting of at '-1'. x_1^2 and x_2^2 cannot be determined from Table 6-4 due to the reason that x_1^2 and x_2^2 are always positive. There does not exist a slope between the high level '1' and low level '-1' setting. However, the quadratic term effect can be determined by evaluating the regression coefficient (in Table 6-3).

The degree of each process variable impact on the process output is quantified by the regression coefficient of each term (linear, interaction and quadratic term). The

regression coefficients are compared directly in a scaled design space which possesses a common scale. For any unit change of a variable, the effect of the related terms will be magnified by their regression coefficients. The regression coefficient effect on the process output value with respect to the constant term is presented in Figure 6-4. The x-axis denotes term number $0, 1, \mathbf{K}, 5$ which refers to regression coefficient of polynomial reduced order model with respect to the constant term. The y-axis denotes the corresponding sputtering yield Y_{spu}. The significance of each term can be determined by the absolute length of the bar which refers to the regression coefficient in Table 6-3. A negative bar means that increasing the process variable results a decrease in the process output. From Figure 6-4 , linear term x_1 has the highest impact on Y_{spu}.
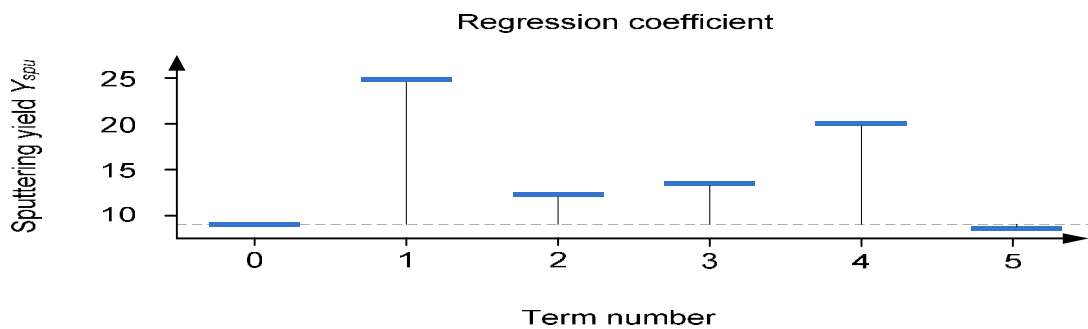
Figure 6-4 The regression coefficient effect to the constant term

6.4. Risk mitigation –Risk Analysis

6.4.1. Process Problem Definitions

The objective of this study is propagate the uncertainties in the focused ion beam process using the validated FIB model as described in section 5.6 by using the probabilistic based risk analysis detailed in chapter 4. Uncertainties are introduced into the two process parameters: *beam angle of incidence* and *beam energy* to forecast the

uncertainties of milling depth in terms of probabilistic distribution. Those small variations can cause process performance and quality characteristics deviations- *milling depth* from specification – *predefined shape*.

6.4.2. Computational Modelling

A modelling procedure is introduced in chapter 5.7 to predict and number of scans needed to mill pre-defined micro-structures at a given pixel dwell times. This can be used to derive the total milling time of scanning the pattern area. The input of the model in Equation (5.12) is the pre-defined geometric shape characterised by Z_{ij}. The model predicts the number of beam scans on each pixel for achieving the pre-defined geometry. The corresponding total milling time is then computed on each pixel. This total pixel time predicted from the model (known as the given time) are used as a process input, along other process parameters. The pre-defined sputtered shape investigated here is the same to Figure 5-19: a 3D stepwise parabolic micro-trench which has both width and length of 10 μm.

6.4.3. Process Set-up and Design of Experiments

In this study, three focused ion beam of Gallium, Argon and Xenon cation beam with diameter 55 nm (Full Width at Half Maximum) were used to accelerate the incident ions and raster across a silicon surface. Two process variables are examined: (1) beam angle with a nominal value 35 degrees and (2) beam energy with a nominal value 30 keV. The defined trench geometry is used as a process input. The process variables are the same as the experimental setup in section 5.7.1. Pixel dwell time ($t_{x,y}$) for producing such 3D trench are predicted at the nominal values for the beam angle (35 degrees) and energy

(30 keV) from FIB model. $t_{x,y}$ predicted at the nominal value from part 1 to part 5 are

listed in Table 6-5. Sputtering yield $Y(E_0 = 30\,keV, a_{x_i,y_j} = 35^o)$ expressed as a function

of beam angle and energy is 4.08 at the sixth row in Table 6-7.

Table 6-5 The model prediction for pixel dwell time $t_{x,y}$ in the three FIB processes

Pixel on Part #	1	2	3	4	5
Gallium FIB Pixel dwell time (sec)	0.008359	0.011494	0.014106	0.015760	0.016892
Argon FIB Pixel dwell time (sec)	0.012787	0.017715	0.021578	0.024108	0.025840
Xenon FIB Pixel dwell time (sec)	0.005874	0.008137	0.09911	0.011074	**0.011869**

These dwell time in Table 6-5 are now specified as the process inputs. At these given

dwell time, altering the two process variables will change milling depth Z_{ij} (defined as

the process performance metric of interest) at each part or pixel of the produced trench.

Sputtering yield varies accordingly and dwell time are kept the same to Table 6-5. On

each of the pixel over the pattern area, we can obtain a *deviated milling depth* by

varying the two process variables. For simplicity, **the centre pixel of pattern 5** is

focused to illustrate how to obtain the deviated milling depth by varying the two process

variables at the given time 0.011869 *sec* for Xeon ion. The process will be repeated to

identify the *deviated milling depth* for Gallium ion and Argon ion as well. Let x_1 be

process inputs beam angle, and x_2 be the beam energy. Let Y_{depth} be the process outputs

characterised by *milling depth*. DoE can be carried out using a limited identified design

point (a series of combination values of two process variables- angle and energy here) in

a two dimensional design space. Central composite design (CCD) is used to generate

nine design points for Argon, Xenon and Gallium FIB process while four additional design points are added in the Gallium FIB process based on a factorial design applied to a reduced, in terms of variable's range, inner design sub-space. The process performance, milling depth Y_{depth}, on these design specifications or points are computed through our FIB model. The design points are scaled from -1 to 1 i.e. $ang, E \in [-1,1]$ and their corresponding design limit is $x_1 \in [10°, 60°]$ and $x_2 \in [20keV, 40keV]$. All process variables are required to be transformed to scaled values in any type of DoE and ROM generation. The DoE points, associated sputtering yield and other process variables are compiled into FIB model to obtain the milling depth prediction. Let us illustrate the milling depth Y_{depth} on the *centre bottom pixel* of the trench as a demonstration in Table 6-6 for the Argon FIB), Xenon FIB and Table 6-7 for Gallium FIB. The same milling depth calculation can also be done on other pixel to get the deviated milling depth for the whole structure.

Table 6-6 The DoE - sputtering yield and milling depth using Argon and Xenon FIB

Design point	x_1	x_2	Argon		Xenon	
			Y_{spu} (atoms/ion)	Y_{depth} (μm)	Y_{spu} (atoms/ion)	Y_{depth} (μm)
1	-1	-1	1.68	1.066	2.43	0.856
2	-1	0	1.5	1.070	2.94	0.954
3	-1	1	1.35	1.086	3.1	0.994
4	0	-1	2.68	1.911	5.18	1.624
5	0	0	2.52	1.940	5.82	1.940
6	0	1	2.48	1.980	6.4	2.197
7	1	-1	8.14	5.990	14.46	4.827
8	1	0	7.8	6.044	16.17	5.361
9	1	1	8.46	6.110	17.76	5.836

Table 6-7 The 13 DoE points, sputtering yield and milling depth using Gallium FIB

Design point	x_1	x_2	Y_{spu} (atoms/ion)	Y_{depth} (μm)
1	-1	-1	1.97	0.925
2	-1	0	2.15	0.967
3	-1	1	2.22	1.001
4	0	-1	3.63	1.660
5	0	0	4.08	1.940
6	0	1	4.22	2.022
7	1	-1	11.84	5.634
8	1	0	12.99	6.056
9	1	1	13.3	6.280
10	-0.5	-0.5	2.16	1.017
11	-0.5	0.5	2.39	1.126
12	0.5	-0.5	7.30	3.443
13	0.5	0.5	7.84	3.694

6.4.4. Reduced Order Modelling

Reduced order models (ROMs) are generated with explicit approximate function or interpolated function to characterise the relationship between process variables and FIB process performance metric- milling depth. Let Y_{depth} be the milling depth in microns. Although it can be obtained through full detailed FIB model, response surface modelling is a more efficient approach to generate fast FIB evaluations which facilitate the risk analysis and optimisation. Two types of ROMS (1) polynomial reduced order

model and (2) Kriging reduced order model are illustrated for Argon, Xenon FIB and Gallium FIB respectively.

6.4.4.1. Polynomial ROM

For a quadratic respond surface, the coefficients of such a model are computed using least square approach to provide the best fit of the DoE data to evaluate the process performance metric. The generated polynomial reduced order models of the FIB response- Milling depth using the nine DoE points listed in Table 6-6 for Argon FIB (see Equation (6.2)) and Xenon FIB (see Equation (6.3)) are defined as follows. The Gallium FIB ROM in Table 6-7 is also derived in Equation (6.4).

$$Y_{depth}(Ar) = 1.94 + 2.487x_1 + 0.0348x_2 + 0.025x_1x_2 + 1.617x_1^2 + 0.006x_2^2 \quad (6.2)$$

$$Y_{depth}(Xe) = 1.94 + 2.203x_1 + 0.2864x_2 + 0.2177x_1x_2 + 1.217x_1^2 - 0.0293x_2^2 \quad (6.3)$$

$$Y_{depth}(Ga) = 1.94 + 2.497x_1 + 0.1807x_2 + 0.1426x_1x_2 + 1.619x_1^2 - 0.09897x_2^2 \quad (6.4)$$

where Y_{depth} = milling depth, x_1 = angle, x_2 = energy

It is essential to carry out the goodness of fit test which summarise the discrepancy between observed values and the values obtained through the model. Two indicators Coefficient of variation (CV) and the adjusted Coefficient of Determinations (Adjusted R^2) are used to measure the accuracy of the above polynomials reduced order model and how well they fit the DoE data. Table 6-8 details the coefficient of variation (CV) and Adjusted R^2 of the above polynomial ROM for the milling depth prediction in FIB process. The measure shows the coefficient of variation is at a tiny order and Adjusted R^2 equals one which is very accurate for the milling depth prediction.

Table 6-8 Coefficient of variation and Adjusted R^2 of ROM of three processes

	Argon FIB	Xenon FIB	Gallium FIB
Coefficient of variation (CV)	4.95 x 10^{-13}	2.647156 x 10^{-13}	3.893878 x 10^{-13}
Adjusted R^2	1	1	1

6.4.4.2. Kriging Reduced Order Model

Kriging is a method of interpolation. It predicts unknown values from data observed at known points and minimises the error at the predicted values that are estimated by distribution of observed data. The generated Kriging reduced order models for milling depth prediction in Gallium FIB using the thirteen DoE points listed in Table 6-7 are defined as follows (Equation (6.5)):

$$Y_{depth} = 3.040 + 2.497 x_1 0.1897 x_2 + 1.382 \times \sum_{i=1}^{13} g_i \times \left(\frac{1.5 \times h_i}{1.743} - \frac{0.5 \times h_i^3}{1.743} \right) \qquad (6.5)$$

where $h_i = \sqrt{\left(x_1 - (x_1)_i\right)^2 + \left(x_2 - (x_2)_i\right)^2}$ and $i = 1, \mathbf{K}, n$ (n = 13, number of DoE points) and g_i is summarised in Table 6-9. Y_{depth} = milling depth, x_1 = angle, x_2 = energy

Table 6-9 Kriging model coefficients for γ_i

i	$(x_1)_i$ [scaled]	$(x_2)_i$ [scaled]	g_i
1	-1	-1	-0.6628
2	0	-1	-0.5898
3	1	-1	-0.4271
4	-1	0	0.7924
5	0	0	0.09855
6	1	0	0.7924
7	-1	1	-0.4271
8	0	1	-0.5898
9	1	1	-0.6628
10	-0.5	-0.5	0.4557
11	-0.5	0.5	0.3825
12	0.5	-0.5	0.3825
13	0.5	0.5	0.4557

6.5. Uncertainty Propagation of Milling Depth

In FIB manufacturing process, uncertainties can exist due to (1) lack of understanding about the process such as re-deposition effect, and (2) random variations and stochastic behaviour in physical and parametric properties. For example, the random variations to deliver specified process parameters such as beam angle and current. The uncertainties like types (2) – uncertainties in process inputs would propagate to affect our process outputs. Failure of predicting these uncertainties and variations could lead to product characteristics, process performance and behaviour falling beyond the tolerable specification limits. Therefore, risk analysis is employed to assess uncertainty in performance/quality characteristics and associated product or manufacturing capability.

There are two common types of risk analysis techniques: (1) sampling method and (2) analytical method. Monte Carlo and Latin Hypercube methods are used in the study. The analytical method presented is the Mean Value First Order Second Moment (FOSM). In Figure 6-5, it shows how input uncertainty distributions are programmed into the constructed model to generate a probabilistic distribution for evaluation uncertainty in performance. x_1 and x_2 are the two process inputs in terms of uncertainty distribution. The process performances are characterised by y which is expressed as a function of x_1 and x_2, i.e. $y = f(x_1, x_2)$.
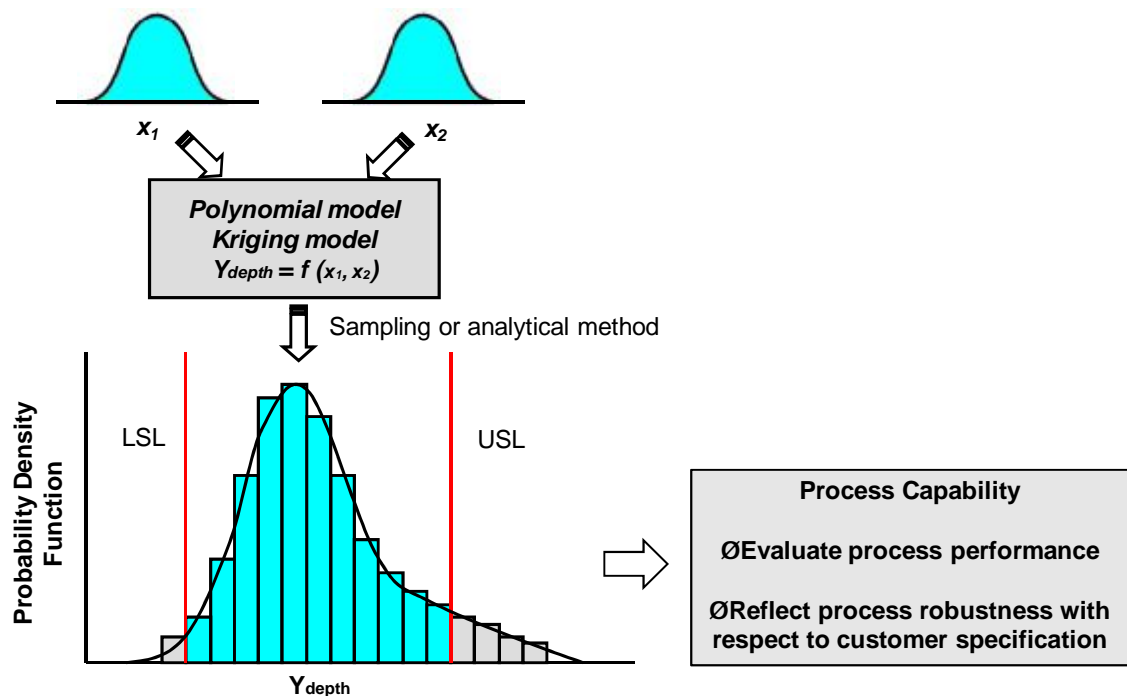
Figure 6-5 Input uncertainty distribution are programmed into the constructed model to generate a probabilistic distribution for evaluation of uncertainty in performance

Let x_1 and x_2 be the two process variables angle and energy. Let Y_{depth} be process output which characterises the process performances *milling depth* in the FIB process. x_1 and x_2 both have their own defined uncertainties following Gaussian distribution respectively. Many design points (sample points) from the specified distribution are

selected and compiled into the realised ROM, i.e. $Y_{depth} = f(x_1, x_2)$ to generate Y_{depth}

where Y_{depth} is the process performance. After performing the risk analysis using any one

of the methods, a probability density function (PDF)/ histogram can be obtained that

characterises the uncertainties of Y_{depth}. Then process capability concepts can be used to

evaluate such a *PDF* to determine the actual process capability with respect to the

customer requirements.

The model can actually be either the polynomial ROM or Kriging ROM to characterise

$f(x_1, x_2)$. Note that x_1, x_2 and Y_{depth} are now no longer a deterministic value. They

become a distribution. According to the procedures explained in Figure 6-5, the steps

and appropriate input and procedural flow are outlined as follows:

(1) Specify design limit for x_1 and x_2, process variables limit are as follows:

	Variable limit	Scaled limit
Beam angle x_1	10 to 60 degrees	-1 to 1
Beam energy x_2	20 to 40 keV	-1 to 1

(2) Specify uncertainties distribution on x_1 and x_2. Uncertainty distribution is assumed

to be normally distributed with mean and standard deviation listed as below.

	Mean [unscaled value]	Standard Deviation [unscaled value]
Beam angle x_1	0 [35 degrees]	0.015 [0.375 degrees]
Beam energy x_2	0 [30 keV]	0.01 [1 keV]

(3) Sampling points generation to produce the specified distribution in step 2. Those sample points can be compiled into any of one ROM for the milling prediction. Kriging ROM as Equation (6.5) is applied here.

(4) Aggregate the results of all the computations (1000000 manipulations are set for Monte Carlo Sampling and 1000 manipulations are set for Latin Hypercube Sampling) to propagate the process output distribution using any methods: MCS and LHS. Analytical method - FOSM based on pure mean and standard deviation calculations to construct the distribution are also illustrated.

(5) Evaluate with output uncertainty with capability assessment of the process behaviour with regards to the specification limits (customer requirements). Process capability index C_p and C_{pk} can be used in the case showing output distribution normality. Upper specification limit (*USL)* and lower specification limit (*LSL)* should be defined by user.

(6) User defined USL and LSL for sputtering yield in this test case

	Upper specification limit (USL)	Lower specification limit (LSL)
Milling depth	1.85	2.03

6.5.1. Probabilistic Distribution of Milling Depth

Risk analysis results are presented in forms of process output probabilistic distribution. To demonstrate the calculation procedure for risk analysis in *Gallium FIB*, the following uncertainty of the FIB input process variables is assumed. Uncertainty distribution is assumed to be Gaussian distributed for beam angle and energy with

standard deviations 0.375 degrees and 0.1 keV, mean value 35 degrees and 30 keV respectively. The milling depth at the centre pixel is the performance metric of interest. Process output evaluation is undertaken at the nominal or mean values of the process input variables. Kriging reduced order model are now involved in undertaking risk analysis methods comprising of Monte Carlo Sampling methods, Latin Hypercube Sampling methods and Mean Value First Order Second Moment (FOSM) analytical methods. Any beam angle and energy samples from their defined distributions are compiled into the Kriging ROM to generate milling depth distribution (PDF). The milling depth distribution predictions with regard to each estimation method are shown in Figure 6-6 (a), (b) & (c), respectively. The graphs show the shape, the centre and the spread of the distribution. For example, a Gaussian distribution is formed from 1000000 samples resulting a mean value 1.942 and standard deviation 0.03757. This represents how much variations of milling depth are deviated from mean value (see Figure 6-6(a)). In Figure 6-6(b), the graph is obtained by taking 1000 samples using the Latin Hypercube Sampling method, while Figure 6-6(c) is obtained from analytical method FOSM. The statistics regarding the mean and standard deviation of the milling depth distributions from all methods are listed in Table 6-10. The mean and standard deviation from all methods are of a tiny difference for this case. When a customer specification limit is defined, process capability ratio can quantify how 'well' the output variable falls to the target or the process tolerances.
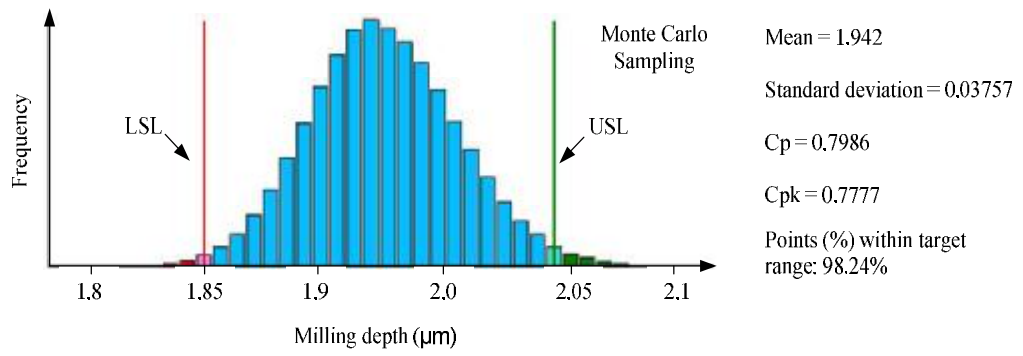
(a) Milling depth distribution estimated by Monte Carlo Sampling method
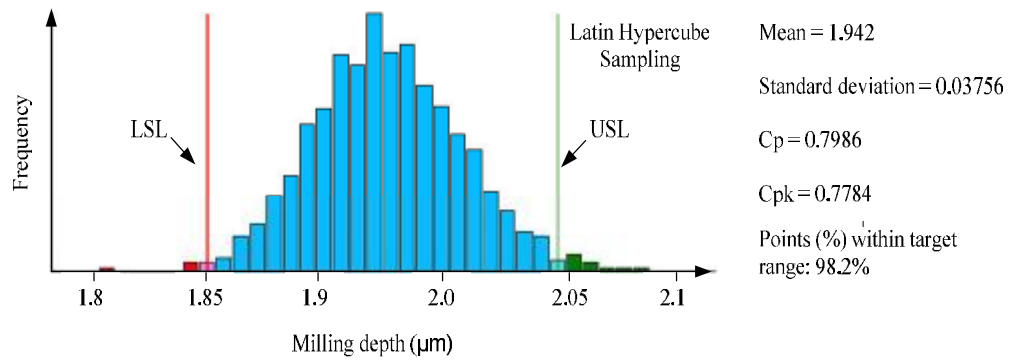
(b) Milling depth distribution estimated by Latin Hypercube Sampling method
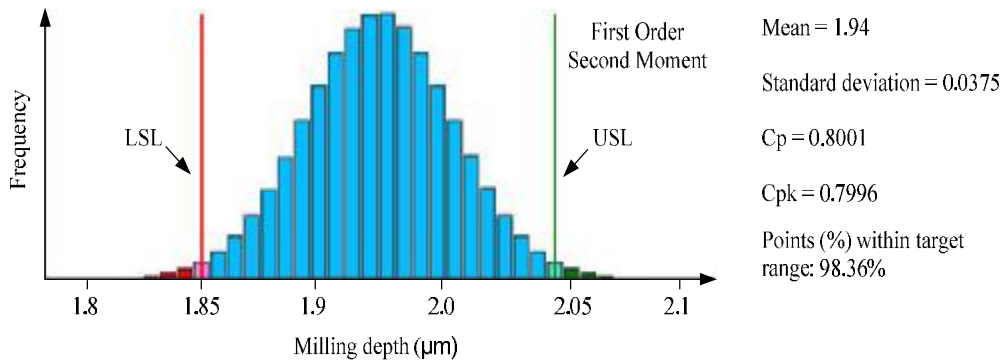
(c) Milling depth distribution estimated by FOSM analytical method

Figure 6-6 Gallium FIB: Comparison of the three milling depth distributions via Kriging ROM

Table 6-10 Details (the mean and standard deviation) of milling depth distribution

	Monte Carlo	Latin Hypercube	FOSM
Mean [Milling depth in μm]	1.942	1.942	1.94
Standard Deviation	0.03757	0.03756	0.0375

In general, sampling based methods tend to provide better output estimations than the analytical FOSM method, but sampling methods are more computationally expensive. In this study all methods provide similar estimates for milling depth distribution. Therefore, in the following optimisation analysis under uncertainty (chapter 6.7), the probabilistic design quantities can be evaluated with FOSM instead of Monte Carlo to speed up the iterative optimisation process.

6.6. Process Capability Evaluation

Capability ratio C_p and C_{pk} are used to compare the capability of a process to the specification limits. It evaluates the probabilistic distribution of the performance metric (milling depth). C_p has been defined by Equation (4.24) and C_{pk} has been defined by Equation (4.25). Let us look at the risk analysis result where milling distribution are estimated from Monte Carlo method via Kriging reduced order model for Gallium FIB. LSL= 1.85 μm and USL= 2.03μm are assumed. From the graphs and associated statistics beneath in Figure 6-6(a), we can observe that under the specification assumptions being made, the Gallium FIB has a process capability $C_p = 0.7986$ and $C_{pk} = 0.7777$. The regions below the lower specification limit and above the upper

specification limit indicate the amount of non-conforming samples. These samples should be rejected as they exceed the system or process tolerances. Another conclusion can be drawn from the C_p value that this process is considered as not capable enough with C_p below 1.5 or C_{pk} below 1. From the graph, only over 98.24% of the milling depth values predicted fall within the specification limits with the Gallium FIB.
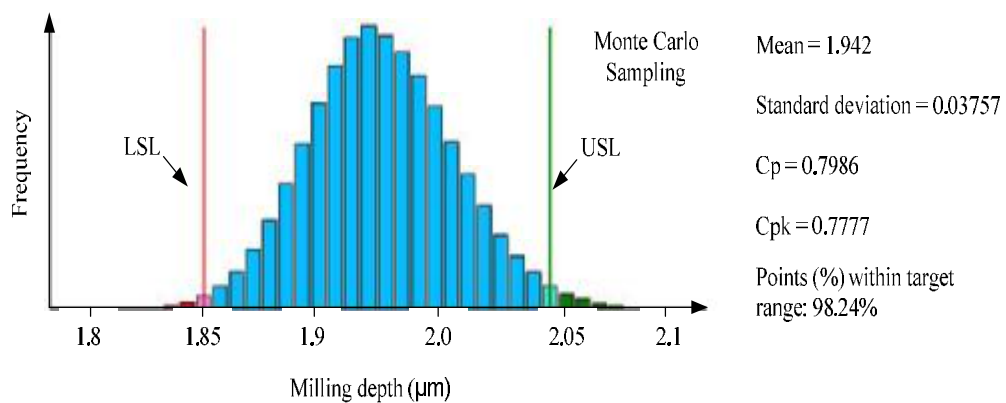
Figure 6.6(a) Gallium FIB: Milling depth distribution estimated by Monte Carlo sampling method through Kriging ROM using 1000000 samples

The significance of the certainty percentage tells the engineer how capable your process is in comparison to specified limits. 98.24% points within target range is far from meeting a typical engineering goal of industry 'design for six sigma' which requires long-term production defect levels below 3.4 defects per million opportunities (DPMO). i.e. A six sigma process is one in which 99.99966% of the products manufactured are statistically expected to be free of defects. The preferred sigma level for industries is 4.8 and is considered ideal for any industry. The usual standard sigma level used is 3.5. The percentage of points within target range and the DPMO are detailed in Table 6-11 [139].

Table 6-11 Process conforming percentage and DPMO level

Sigma level	Percentage of points within target range	Maximum allowable defects in Defects per million opportunities (DPMO)
1	31%	697632
2	69.20%	308537
3	93.320%	66807
4	99.3790%	6210
5	99.977%	233
6	99.99966%	3.4

6.6.1. Case Study 1– Addressing Uncertainty for Argon and Xenon Beam

Using the C_p and C_{pk} indicator/tool, two other FIB processes Argon FIB and Xenon FIB under different degree of process variable uncertainties are investigated. The key objective in this test case is to illustrate their process capability comparison under various degrees of uncertainties. Argon FIB is possessed a lower uncertainty in angle but a higher uncertainty in energy than those of Xeon FIB. One would interest what the process capability be which is superficially unpredictable for these scenarios. Again, the following uncertainty of the FIB input process variables is assumed: (1) *Argon FIB:* Gaussian distribution for incidence angle and energy with standard deviations 0.375 degrees and 0.1 keV respectively. (2) *Xenon FIB:* Gaussian distribution for incidence angle and energy with standard deviations 0.5 degrees and 0.05 keV respectively.

Risk analysis using Monte Carlo Sampling method is carried out via the polynomial reduced order model representing Argon FIB (Equation (6.2)) and Xenon FIB (Equation (6.3)). LSL= 1.85μm and USL= 2.03μm are assumed. From the graphs and associated statistics beneath in Figure 6-7(a) & (b), under the data assumptions being made, the

Argon FIB has higher process capability ($C_p = 0.8032$) compared with the Xenon FIB

($C_p = 0.6797$). Over 98.38% of the milling depth values predicted with the Argon FIB

fall within the specification limits while for Xenon FIB process, only 95.84% will meet

the specification requirements. The difference of C_p is due to the assumption made that

uncertainties in process variables angle of Xenon FIB is higher than Argon FIB. Any

real data from reality about the actual uncertainties for the two processes could fit back

into this process capability determination approach.
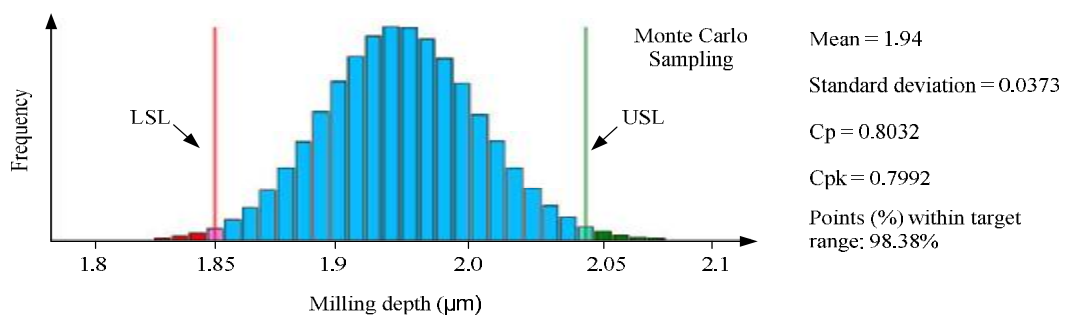
(a) Argon FIB: Milling depth distribution estimated via polynomial ROM
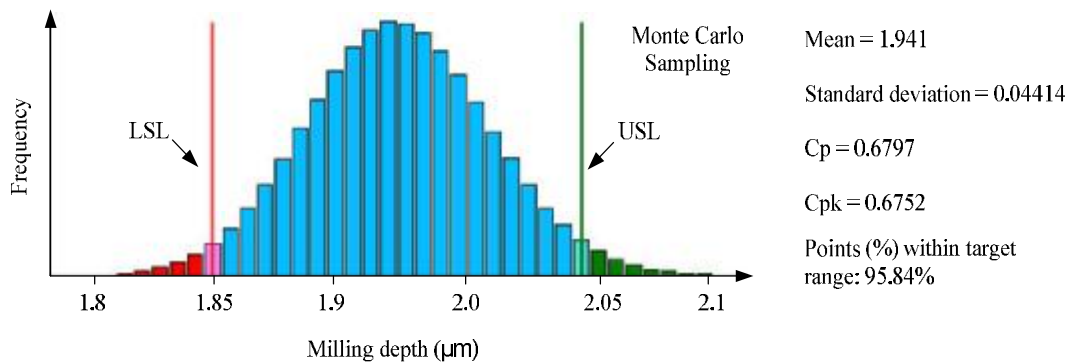
(b) Xenon FIB: Milling depth distribution estimated via polynomial ROM

Figure 6-7 Comparison of Risk analysis results for Argon FIB and Xenon FIB

6.6.2. Case Study 2– Comparing Polynomial and Kriging Models

The aim of this case study is analysing any differences on risk analysis result of using

Polynomial ROMs against Kriging ROMS. Take Gallium FIB as a demonstration, the

same process variables uncertainties distributions are defined. The same specification limits, LSL= 1.85μm and USL= 2.03μm, are assumed. Risk analysis is performed based on Monte Carlo method using both polynomial ROMs (Equation (6.4)) and Kriging ROMs (Equation (6.5)). Their results are shown by Figure 6-8(a) and (b) respectively. However, the sigma (standard deviation) of the milling depth distribution and the process capability ratios obtained are different between two runs. The process capability ratios C_p obtained from polynomial ROMs result (C_{pk} = 0.7952) are higher than Kriging ROMs (C_p = 0.7777). Process capability is overestimated in polynomial ROMs.

Monte Carlo Sampling

Mean = 1.94

Standard deviation = 0.0373

Cp = 0.7992

Cpk = 0.7952

Points (%) within target range: 98.33%

(a) Gallium FIB: Milling depth distribution estimated via polynomial ROM

Monte Carlo Sampling

Mean = 1.942

Standard deviation = 0.03757

Cp = 0.7986

Cpk = 0.7777

Points (%) within target range: 98.24%
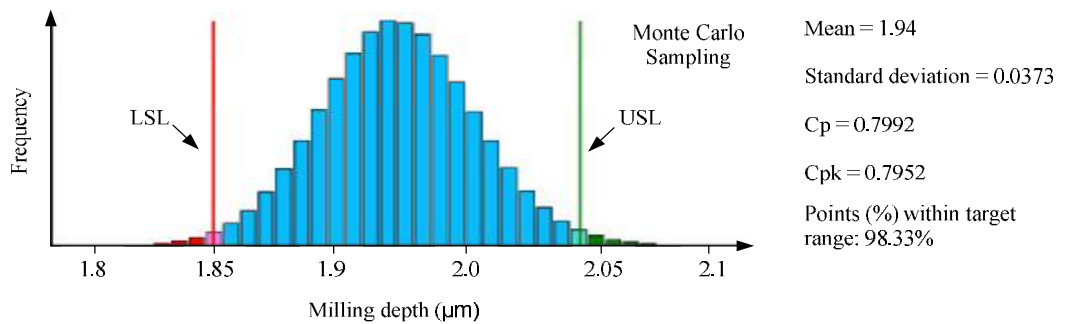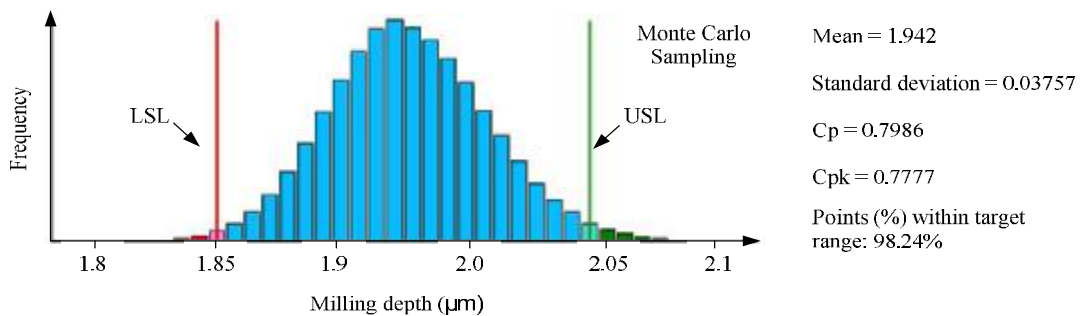
(b) Gallium FIB: Milling depth distribution estimated via Kriging ROM

Figure 6-8 Gallium FIB: Comparison of results via Polynomial and Kriging ROM

From the above two graphs, it is difficult to judge polynomial ROMs or Kriging ROMs provides better result. However, in terms of both models physical definitions, polynomial model is only a response surface approximation to fit the DoE/observed

data which includes errors. Kriging is an interpolation method which the response surface model absolutely passes all the DoE or observed data point. Kriging model is more reliable over the polynomial model. This test case also illustrates the significance of ROM accuracy and how well it represents the real high fidelity process. High discrepancy between the ROM and full high fidelity model can affect the accuracy of subsequent risk analysis and optimisation result.

6.6.3. Case Study 3– Investigating the Impact of Uncertainty in the Design Space

From the sensitivity analysis result, beam angle is a more dominant variable to beam energy. The main objective here is to uncover how uncertainties/ variations of the key process variables taken at various regions within the design boundary, exert different degree of impacts on the process performance metric. Since milling depth is dependant and directly proportional to sputtering yield, the relationship of milling depth against beam angle should also follow the one between the beam angle and sputtering yield. Their relationships between the beam angle and sputtering yield can be represented by Figure 6-9 [131]. It is observed that angle value moving from 10 degrees towards 60 degrees would result a sharp sputtering yield increase.
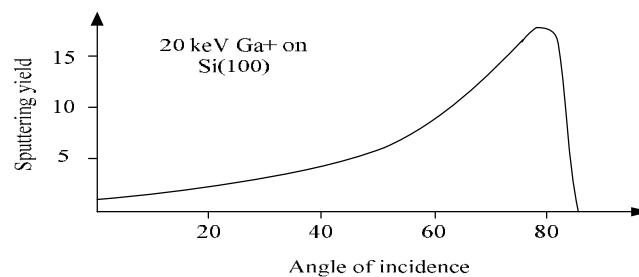
Figure 6-9 Sputtering yield is plotted against incident angle for Gallium FIB

Take Gallium FIB as an example, uncertainty distribution is assumed to be Gaussian distributed for beam angle and energy with standard deviations 0.375 degrees and 0.1

keV respectively. Three discrete set of risk analysis are undertaken separately about three design points. Design point (1): angle = 10 degrees, energy = 30 keV, design point (2): angle = 35 degrees, energy = 30 keV, and design point (3): angle = 60 degrees, energy = 30 keV. Risk analysis is then undertaken based on Monte Carlo method using via Kriging ROMs (Equation (6.5)). Three individual milling depth probabilistic distributions are obtained. Table 6-12 detailed the distribution statistics regarding mean and standard deviations of distributions. Standard deviations of the milling depth distribution are the highest at angle mean value 60 degrees. It is found that standard deviation increases when risk analysis takes place continuously from angle mean value 10 to 60 degrees in the design space. It implies that the predicted milling depth values will fall further apart from the central values and hence a less capable process is resulted. The resultant milling depth obtained has a higher deviation when sampling takes place at higher angle mean values. This is because angle increases nonlinearly with sputter yield i.e. slope of the sputtering yield curve increases as shown in Figure 6-9. In conclusion, same degree of input uncertainties exerts various impacts at different design regions on the dominating process/design variables. Some regions tend to be more sensitive to variations. Uncertainties will propagate more impact on process performance inducing a bigger failure margin or deviation from the desired values.

Table 6-12 Mean and standard deviations from risk analysis result

	DoE point 1 [angle= 10 degrees, energy= 30keV]	DoE point 2 [angle= 35 degrees, energy= 30keV]	DoE point 3 [angle= 60 degrees, energy= 30keV]
Mean [Milling depth in μm]	1.051	1.942	6.045
Standard Deviation	0.01921	0.03757	0.05728

6.7. Optimisation the Deviation of Milling Depth under Process Uncertainties

To understand the impact of risks may not be enough for engineers to achieve a robust design. It is necessary to exploit an optimal product design, performance and process condition to fulfill the objectives of a manufacturing system. These objectives may be across different disciplines such as reliability, accuracy, cost, as well as environment. At the same time it is important to satisfy the requirements specified by customers without violating any criteria and constraints.

In this section, the design problem is aimed to identify a combination of beam angle and beam energy for the Gallium FIB process such that the standard deviation of the milling depth representing product characteristics/ process performance is minimised. In this task the process variables is assumed to follow Gaussian uncertainty distributions, i.e. defined with mean values of angle x_1 and energy x_2 denoted by m_{x_1} and m_{x_2} while $m_{Y_{depth}}$ represents the mean value of milling depth uncertainty distribution with respective standard deviations. An order pair (x_1, x_2) forms a sample point within their specified uncertainty design space with standard deviation 0.375 degree and 0.1 keV respectively (see 7(c) and 7(d)). Sample points are propagated via the objective function i.e. the reduced order model, to obtain a surface which contains the milling depth values with variations.

An optimisation problem is formulated for this FIB process. Its objective (see 7(a)) is to find the values of m_{x_1} and m_{x_2} so that they minimise the milling depth variations $s_{Y_{depth}}$ (see 7(b)), characterised by the standard deviation, subject to the constraint that the

mean value of milling depth $m_{Y_{depth}}$ cannot exceed 2.02 µm (see 7(e)). Both m_{x_1} and m_{x_2} are bounded by their design space limit (see 7(c) and 7(d)).

Find m_{x_1} and m_{x_2} s.t.	7(a)
Minimise $s_{Y_{depth}} = \sqrt{E[Y_{depth}^2] - m_{Y_{depth}}^2}$	7(b)
Subject to:	
$10° \le m_{x_1} \le 60°, \quad where \ s_{x_1} = 0.375°$	7(c)
$20 \, keV \le m_{x_2} \le 40 \, keV, \qquad where \ s_{x_2} = 0.1 \, keV$	7(d)
$m_{Y_{depth}} \le 2.02 \, mm$	7(e)

The task is solved using optimisation routines, particle swarm optimisation algorithm [140]. During optimisation, the objective value (milling depth standard deviation) is evaluated through the FOSM method via the Kriging ROMs by Equation (6.5). Monte Carlo could also be used, but the process is more computational expensive and time consuming. The minimum standard deviation of the milling depth in the case of the Gallium FIB is found to be 0.0378748 µm. At the optimum, the beam angle and the beam energy are 32.698 degrees and 29.68 keV respectively. This result, which here is obtained purely by mathematical means using the developed modelling methodology, is a design rule for FIB micromachining.

From Figure 6-9, sample points taken from the regions $x_1 \in [30°, 60°]$ tend to be more sensitive to those uncertainties or variations when compare to the region of $x_1 \in [10°, 30°]$. The uncertainties will propagate higher standard deviation on process performance/ product characteristics resulting a bigger failure margin from the desired milling depth. Taking a smaller x_1 mean value would lead to a minimised milling depth deviation. However, the advantage of taking a higher x_1 mean value can speed up the process to obtain the specified milling depth. At the same time, this would lead to a

higher deviation from expected shape. A constraint is imposed here that the mean value of milling depth cannot exceed a specified requirement. The solution to the objective: find x_1 and x_2 to minimise the standard deviation of milling depth is no longer obvious.

Process parameters uncertainties do affect failure margin of the process performances. In fact, the risk of achieving accuracy in milling depth under imposed constraints requirements are solved by optimisation routines. Similar study can be done such as maximising the process capability. The test case provides knowledge to achieve robustness FIB process rather than the deterministic optimal process identification which shows a weakness under certainties in real world.

Closure

The chapter has outlined the how to quantify the process variability and uncertainty in terms of focused ion beam technologies control for predicting shape of pre-defined structures in nano-scale. Sputtering yield values with respect to two process variables, *angle* and *energy,* are extracted from SRIM forming representative design points. Design of experiment is then performed based on these design points to formulate a response surface model through techniques like Kriging interpolation. Evaluation of sputtering are made easier to specify into the realised FIB computational model as a process variable, to characterise the depth variation. This type of reduced order model is significant for allowing fast evaluation of process output without losing much accuracy of the original model. This strengthens the efficiency of undertaking Monte Carlo type risk analysis. Uncertainties in two variables are introduced in form of probability distribution. Risk mitigation methods suggested like sampling and analytical method are used to propagate the uncertainty distribution of the milling depth. Process capability

indices are used to quantify this distribution to determine the process robustness due to process uncertainty and variability with respect to specification requirement. The procedures have been applied on FIB problems with various sources for comparison. The optimisation task has helped identified the optimal values in angle and energy such that the predicted shape has the least variations under certain specified constraints.

Chapter 7 An Optimal Design of Flip Chip

The chapter details an electronics packaging application - flip chip design in micro-electronics industry. The risk analysis methodology and the associated computational tools are demonstrated to derive an optimal package design in terms of product environmental evaluation during the design stage. An innovative way of using an environmental indicator, the Toxic Index, to perform a quantitative assessment of the product design on the environmental impact is also developed. Risk mitigation evaluation on the design is also provided.

7.1. Flip Chip Design Requirements

In the flip chip packaging process and in general, cost is normally regarded as the most important aspect for micro-electronics manufacturing industry. The actual design of the products is also extremely important issue. Engineers try to reduce their costs while in the same time ensuring the reliability of the product will not be compromised. Environmental considerations must be included to comply with their regulations. Legislations and customers are the main drivers to design for environment as the environmental performance of the electronic product is gaining more awareness. A

green product may require new technology which can result in increased cost of the products. At the same time, reliability cannot be neglected in the industry. Reliability modelling which helps to maximise life span of products plays an important role. Finite Element Modelling and Analysis can be used to predict deformations, strain and stress in the modelled system. Simulation predictions can be used to assess the reliability by observing damage in materials and to relate to life-time.

Having faced such a multi-dimensional task, a *multi-disciplinary optimisation* problem is established to aid optimal decisions with respect to various types of criteria as oppose to a single objective. With this tool a design engineer can simultaneously account for product or process performance (e.g. reliability and life time), design, cost (fabrication, materials, labour, shipping and disposal) and environmental requirements (eco-friendly designs and easy to dispose).

7.1.1. Optimisation Modelling

In this chapter, the approach described above is illustrated with a traditional product fabrication-Flip Chip Packaging. The key here is to understand the cost, environment impact, reliability aspects and also their combined effect in order to derive an optimal product design in an optimal process conditions. Objectives and constraints on cost, environment and reliability must be set up and included into a single design problem. Optimisation modelling enables us to find the solution to this problem which is regarded as the optimal design. The theme here is optimisation interacts amongst cost, environment and reliability as presented in Figure 7-1.

Figure 7-1 Optimisation matrix regarding reliability, environment and cost aspects

The methodology integrating various computational tools has been applied to help understanding the new advances technology in micro-electronics manufacturing industry. In particular, an electronics product life cycle is often complicated that demands quick and absolute solutions to any problems. The computational tools in the risk analysis methodology can assist deriving such a solution especially in the early design stage of the product. The optimisation analysis would provide sufficient quantification analysis of the product for product design problems in terms of the quality and reliability, according to customer specifications.

7.1.2. Materials Concerns in Flip Chip Technology

During flip chip assembly process, underfill materials are applied to protect the bumps from moisture of other environmental hazards, and provide additional mechanical strength to the assembly. Another issues dealing with solder bumps connections on a die stacked onto organic substrate is, underfill can compensate the thermal expansion differences between the chip and the substrates. Most of the substrates possess a large coefficient of thermal expansion (*CTE*) around 20-30 ppm/^{o}C) while silicon chip is about 3ppm/^{o}C. Such *CTE* mismatch can induce a large shear strain in solder balls that can cause fatigue and reduce the package life time. Thus, underfill can be served as a buffer by coupling the thermal mismatch into bending of substrate [88]. A typical flip

199

chip consists of three parts: an IC chip, a substrate and materials connecting the chip bumps with the substrate pads. IC ship is made of silicon wafer. A substrate is a combination of flex, glass, ceramic, epoxy, and organics like FR4. Two general types of materials joining the IC and substrate are either in form of solder alloy or electrical conductive adhesives. The following explains the latest trend of materials in a flip chip package.

Lead based solder - Tin- lead solder has been used in the electronics packaging industry for more than 50 years. Tin-lead solder is widely applied in electronics packaging industry because of its low costs and its low melting point physical property facilitating solder reflow process to take place. There are many types of tin lead solder in which two common types are Sn63/Pb37 and Sn60/Pb40 widely applied in interconnection process. The traditional tin-lead solders Sn63-Pb37 is the most popular solder due to its low melting point around $183^{o}C$ which is very preferable during reflow process. It has 'eutectic' property allowing direct transformation from solid to liquid without an intermediate state

Lead-free solder - Lead-free solder project was initiated in United States and followed by European Unions, Japan from 1900-1997. Mass product production firstly began in Japan from 1998 by Panasonic MD Compact player using lead free solder in reflow and wave soldering process [141]. Common type of lead free solder alloys based on tin, silver, and copper (SAC alloys). Many alternate tin lead solder arises such as Sn-Ag-Cu (SAC) solder alloy and Sn-Cu solder. All solder concentrations are by weight percentage. The melting point of SAC based solders are around $210^{o}C$ to $230^{o}C$ which are higher than that of traditional eutectic tin lead solder - 63Sn37Pb (melting point is $183^{o}C$). Due to higher melting point of SAC based solder alloys, extra temperature and

pressure are required in the reflow process and wave soldering process which could increase the costs and cause damage to substrate. Tin silver indium and tin-zinc alloy posses a lower melting point but incurred a higher material costs. Tin-copper alloys have a lower cost but it possesses high melting point 221°C. Apart from costs considerations and manufacturing control of using lead free solder alloys, reliability issues have been studying in gaining more understandings about the use of lead free solder materials.

7.1.3. Computational Modelling in Reliability Assessment

Virtual prototyping based on design optimisation is a powerful approach to maximise the reliability of electronic packages and products [142]. The life cycle of the electronic products is usually very complex and with the continuing miniaturisation of the electronic packages and utilisation of new materials there is a real danger how reliable are the developed products. Computational mechanics has become very important in analysing the response of the electronic packages and systems. Finite Element Modelling and Analysis can be used to predict deformations, strain and stress in the modelled system. Simulation predictions can be used to assess the reliability by observing damage in materials and to relate to life-time. The developed decision support system in this study uses software modules for FEA (ANSYS [143]) to make predictions for reliability of different flip chip designs.

With the continuing trend for further miniaturisation of the electronic components and devices and the utilisation of new materials (lead-free solders, underfills, encapsulates), there are real concerns about the reliability level of the products. A major aspect of concern is the reliability of solder joints. In particular, the *CTE* miss-match between

substrate and die in flip chip packages combined with the small joint dimensions makes the interconnects quite vulnerable under thermal cycling. The failure mode of interest is the thermal fatigue of solder joints. A careful design of such packages is critical to ensure minimised fatigue damage in solder interconnects.

Virtual qualification of the electronic packages and products is practiced nowadays widely to provide knowledge on the behaviour and response of the designed systems. Finite Element Analyses are conducted in this study to characterise the thermo-mechanical response of the flip chip package under thermal cycling. The technology provides fast and efficient approach to investigate different design options. Inelastic transient simulations are required to capture the time dependent creep deformations of solder joints. The modelling steps which also combine the usage of statistical and approximation techniques are explained in the following sub-sections.

7.2. Test Case Investigation on a Flip Chip Package: Reliability Assessment

This work investigates the design of a flip chip package where two design parameters are allowed to vary. The design variables are the underfill which can be chosen among several available materials and the flip chip stand-off height *SOH* (respectively solder joint volume). Changes in the design variables have impact on reliability of solder joints under thermal cycling, cost of materials used to assemble the package and also have effect on the level of environmental impact. Having particular cost and environmental impact requirements, the design task is to identify the optimal flip chip specification so that the requirements are met and the reliability of the package is maximised. The

assessment procedures and calculations of the flip chip package with respect reliability, cost and environmental impact are presented in the next sections.
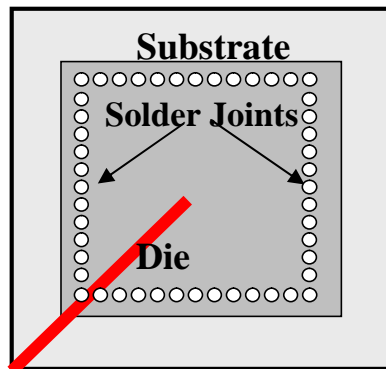
Figure 7-2 Schematic outline of the flip chip

Figure 7-2 shows the schematic outline of the flip chip package. The flip chip assembly has 48 solder bumps arranged peripherally and the bump pitch is the same on all sides, equal to approximately to 457 µm. The space between the chip and substrate is filled with underfill encapsulant. Some important geometric dimensions of the nominal package (initial geometric design) are listed in Table 7-1. The stand-off height (distance between chip and substrate) for the nominal flip chip design is 160 microns. This design parameter will be subject to investigation here and will vary as a result of changes in the solder joint volume used to assemble the package.

Table 7-1 Geometry parameters of the initial flip chip model

	Model
Die dimensions (mm)	6.3 x 6.3 x 0.6
Stand-off height (10^{-3} mm)	160
Substrate thickness (mm)	1.5
Pad diameter (10^{-3} mm)	150
Cu-Ni pad thickness (10^{-3} mm)	35
Bump pitch (10^{-3} mm)	457
Number of bumps	48

7.2.1. Flip Chip Model using Finite Element Method

The detailed procedures of constructing a model using finite element method could be tracked back in chapter 3. In the test case, the objective is to identify the damage of flip chip internal structures subject to thermal cyclic changes using a damage model. To investigate a flip chip package, a high fidelity type model using finite element analysis was first constructed. It aims to identify how the design variables namely, solder joints stand-off height (*SOH*), Young's Modulus and the Coefficient of Thermo Expansion impact on the reliability of solder joint in a flip chip package under thermal cycling.

The first step in the modelling procedure is to have representation of the package in terms of finite element model. In this study a two-dimensional (2D) model of the package is used. The planar model captures a cross section of the package along the diagonal; hence, the solder joint at the corner of the package is represented in the model. The existing symmetry in that plane is with respect to the centre of the package (i.e. half of the diagonal plane is modelled). The planar model is developed in this way based on existing knowledge that the critical (most damaged with respect thermal cycling fatigue) solder joint of this package is the one at the corner. Figure 7-2 illustrates the flip chip component and the bold line indicates the modelled part from centre of the package to the corner point. The 2D finite element model is shown in Figure 7-3. Detailed view of the corner solder joint captured in the model and corresponding mesh is also provided. The pad on the substrate consists of two layers, copper and nickel, and the pad on the die side is nickel. This detail has been included in the model.
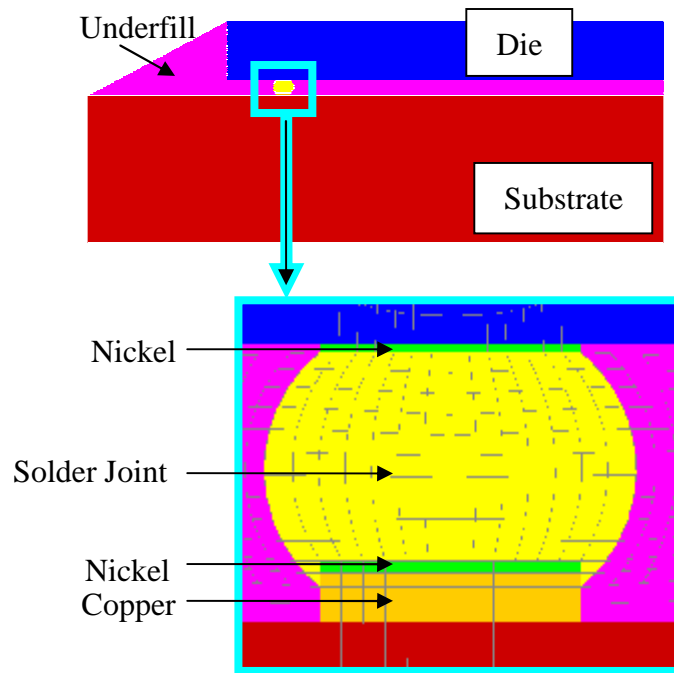
Figure 7-3 Finite element model of solder ball flip chip package

The solder used in this package is lead-free Sn-3.5Ag-0.7Cu (SAC) solder. In this analysis the solder material is assumed to behave as a visco-plastic material. All other materials used in the package are modelled as elastic materials. Solder is also modelled with temperature dependent properties. The material properties are listed in Table 7-2. Note that the underfill in this table refers to the nominal design of the flip chip package.

Table 7-2 Flip chip material properties

	CTE (10^{-6}/^{o}C)	Young's Modulus, E (GPa)	Poisson ratio, n
Substrate	16	24	0.2
Cu pad	17.3	115	0.31
Nickel	13	207	0.31
Sn3.5Ag0.7Cu (SAC)	22 at -25C 25 at 125C	58 at -25C 30 at 125C	0.40
Si (Die)	3	113	0.29
Underfill (Nominal design)	45	4.5	0.25

7.2.2. Analysis and Results from the Damage Model

Thermo-mechanical analysis of the flip chip package using finite element method predicts package deformation and stress under imposed thermal cycling conditions. The thermal cycle lasts for 1 hour and consists of four stages: ramp up from -25°C to 125°C for 15 minutes; hold at the higher temperature for 15 minutes; ramp down to -25°C for 15 minutes; and finally hold at -25°C for 15 minutes. The analysis output response of interest is the accumulated inelastic (or creep) energy density in the solder material per thermal cycle. This quantity is used as a reliability measure for solder joints and will refer to it as the damage. The maximum value of damage in the solder ball is denoted by D. The higher the damage D, the less reliable the flip chip is, and vice versa.

The following constitutive equation for the lead-free solder inelastic strain rate as given by Equation (2.3) is used in this study,

$$\dot{\varepsilon}^{creep} = A[\sinh(a\mathbf{s})]^n \exp\left(\frac{-Q}{RT}\right)$$

where $\mathbf{s}$ is the stress vector, R is the universal gas constant, T is the temperature; Equation (2.3) has the following empirical values: $A = 277984s^{-1}$, $n = 6.41$, $a = 0.02447 \times 10^{-6} Pa^{-1}$ and $Q = 6500R$. The values of coefficients are given in [96] [97]. The general calculation procedure for solder joint damage using accumulated inelastic energy density per thermal cycle W_p , is based on the following formula from [97]

$$Wp = \sum_{\Delta t} \frac{\sum_{i=1}^{N} \int_{Vi} \mathbf{s}(\Delta e^{creep})dV}{\sum_{i=1}^{N} \int_{Vi} dV} \tag{7.1}$$

In Equation (7.1), the outer sum is taken over the time steps Δt that cover a full thermal cycle, N is the number of elements used to calculate the creep energy density in the so-called critical volume, V_i is the volume of the i-th element, s is the stress tensor and Δe^{creep} is the tensor of visco-plastic strain increment for Δt. Usually a critical volume is a fairly thin layer of most affected elements for the critical (most damaged) solder joint, i.e., those with the highest values of the damage. In this study calculation is simplified and a criterion is used for solder joint damage D, the maximum element value of accumulated energy density in the solder ball per thermal cycle instead of Equation (7.1). For simplicity, in order to obtain a stabilised (constant) prediction from analyse for accumulated energy density, three thermal cycles are simulated. The damage value D is then obtained for the third cycle. The highest damage in solder joint is predicted at the interface with the die. Figure 7-4 shows the damage levels across solder ball at the end of a thermal cycle for the nominal flip chip package.
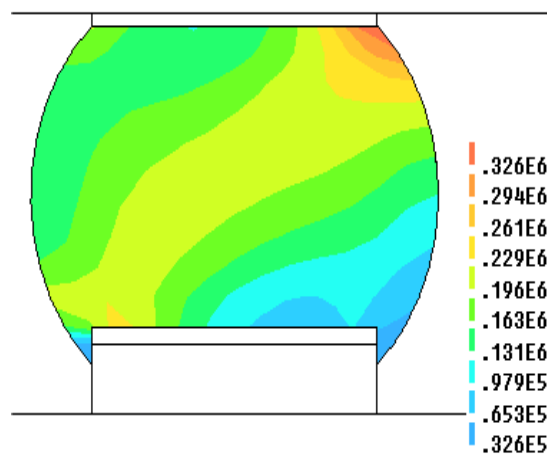
Figure 7-4 Accumulated creep energy density at the corner solder ball after three cycles

7.2.2. Design of Experiments (DoE)

The outlined above computational modelling is in essence approach for virtual qualification of a system. In this study the computational model is used to qualify the reliability of the package with respect to thermal fatigue of solder joints [144]. The output analysis value, the solder joint damage *D*, can be used to observe reliability of solder joints (higher value – lower reliability and vice versa). In general, the damage can be used subsequently into life time models. The optimisation of the investigated flip chip package is investigated with respect to variations of solder joint stand-off height (i.e. volume of the solder balls) and the applied underfill material. In this case the underfill properties which would be required are the Young's modulus (*E*) and the coefficient of thermal expansion (*CTE*) of the underfill. The constant Position's ratio for the selection of the available underfills are assumed. The focus is to predict the flip chip reliability as function of three design parameters: Solder joint stand-off height (*SOH*), Underfill Young's Modulus (*E*), and Underfill Coefficient of Thermal Expansion (*CTE*).

The experimental design used in this study is the Central Composite Design (CCD). For the three parameter design space (*SOH, E, CTE*) the number of design points is 15. The design space is defined in the following ranges: (1) Solder joint stand-off height $SOH \in [100, 220] mm$, $Underfill\ E \in [2,7] GPa$, and $Underfill\ CTE \in [25,65] ppm/c$. At each of the 15 DoE points finite element analysis is undertaken and the relevant prediction for solder joint damage *D* is obtained. Table 7-3 shows the 15 DoE points and the prediction for damage *D*.

Table 7-3 DoE data and the prediction for damage *D*

Design Point	*SOH* (μm)	*E* (GPa)	*CTE* (ppm/C)	Solder Damage *D* (MPa)
1	100	2	25	0.474
2	220	7	65	0.681
3	100	7	65	0.831
4	220	2	25	0.274
5	100	7	25	0.150
6	220	7	25	0.142
7	100	2	65	1.069
8	220	2	65	0.744
9	100	4.5	45	0.466
10	220	4.5	45	0.381
11	160	4.5	25	0.165
12	160	4.5	65	0.844
13	160	2	45	0.481
14	160	7	45	0.424
15	160	4.5	45	0.440

The information from DoE simulations is used to construct a response surface to the predicted data. A full quadratic polynomial is used to fit by least squares method the solder damage predictions at the 15 design points in this study. The polynomial is based on scaled values of the three design variables in the range [-1,1] (see Table 7-4).

Table 7-4 Scaling of design variables limits

	SOH	Young's Modulus, *E*	*CTE*
Un-scaled limits	[100, 220] μm	[2, 7] GPa	[25, 65] $10^{-6}/^{\circ}$C
Scaled limits	[-1, 1]	[-1, 1]	[-1, 1]

7.2.3. Response Surface Modelling

Let x_1 be the design variable *SOH*, x_2 be the design variable *E*, and x_3 be the design variable *CTE* and m =3. From Equation (3.28), the polynomial which can be used to assess the damage $D(SOH,E,CTE)$ of the flip chip solder joints (as a function of the normalised values of the three design variables *SOH, E* and *CTE*) in the form of Equation (7.2). Table 7-5 detailed the reliability model coefficient of Equation (7.2).

$$
\begin{aligned}
&D(SOH,E,CTE)\\
&= D(x_1,x_2,x_3)\\
&= b_0 + b_1 x_1 + b_2 x_2 + b_3 x_3 + b_{12} x_1 x_2 + b_{13} x_1 x_3 + b_{23} x_2 x_3 + b_{11} x_1^2 + b_{22} x_2^2 + b_{33} x_3^2
\end{aligned}
\qquad (7.2)
$$

Table 7-5 Reliability model coefficients of Equation (7.2)

Coefficient	b_0	b_1	b_2	b_3	b_{12}	b_{13}	b_{23}	b_{11}	b_{22}	b_{33}
Value (10^{-3})	424	-76.8	-81.4	296.4	45.9	-33.4	19.4	3.6	32.6	84.6

The mathematical model by Equation (7.2) for reliability assessment of the flip chip package will be exploited in chapter 7.5 to solve the flip chip design optimisation problem. The goodness-of-fit tests shows that the R^2 is 0.986, and adjusted R^2 is 0.952. It proves that the second order polynomial model provides a good fit to approximate of the 15 data points as $R^2 \geq 0.9$ is considered as good approximation. The generated Kriging reduced order models are defined as follows (see Equation (7.3)):

$$
Y_{depth}(\times 10^{-3}) = 0.56 - 0.086 x_1 - 0.096 x_2 + 0.28 x_3 + 0.017 \times \sum_{i=1}^{13} g_i \left(\frac{1.5 \times h_i}{3.464} - \frac{0.5 \times h_i^3}{3.464} \right) (7.3)
$$

where $h_i = \sqrt{\left(x_1 - (x_1)_i\right)^2 + \left(x_2 - (x_2)_i\right)^2}$ and $i=1,\mathbf{K},n$ (n =15, number of DoE points)

and g_i is summarised in Table 7-6. Y_{depth} = milling depth, x_1 =angle, x_2 =energy

Table 7-6 Kriging model coefficients for γ_i

i	$(x_1)_i$[scaled]	$(x_2)_i$[scaled]	g_i
1	-1	-1	-11420
2	0	-1	-596.8
3	1	-1	-1857.9
4	-1	0	-6187.7
5	0	0	3361.4
6	1	0	-6762.9
7	-1	1	-9703.5
8	0	1	5055.1
9	1	1	15596.6
10	-0.5	-0.5	4767.9
11	-0.5	0.5	4971.5
12	0.5	-0.5	-8635
13	0.5	0.5	14231
14	0.5	0.5	-2469.6
15	0.5	0.5	-649

For cross validation, Mean Error is found to be 0.036 and Mean Squared Error is 0.08.

7.2.4. Risk Analysis on the Flip Chip Package

Let x_1, x_2 and x_3 be the three design variables *SOH, E* and *CTE*. Let Y_{Damage} be design responses which characterises the reliability *solder joint damage D* in the flip chip package problem. x_1, x_2 and x_3 all have their own defined uncertainties following Gaussian distribution respectively. Many design points (sample points) from the specified distribution are selected and compiled into the realised ROM, i.e. $Y_{Damage} = f(x_1, x_2, x_3)$ to generate Y_{Damage} where Y_{Damage} is the process performance.

After performing the risk analysis, a probability density function (PDF)/ histogram can be obtained that characterises the uncertainties of Y_{Damage} . Then process capability concepts can be used to evaluate such a *PDF* to determine the actual process capability with respect to the customer requirements. The model is Kriging ROM to characterise $f(x_1, x_2, x_3)$. Note that x_1, x_2 and x_3 and Y_{Damage} are now a distribution. According to the procedures explained in Figure 6-5, the input and procedural flow are as follows:

(1) Specify design limit for x_1 and x_2 , process variables limit are as follows:

	Variable limit	Scaled limit
SOH x_1	100 to 220 μm	-1 to 1
E x_2	2 to 7 GPa	-1 to 1
CTE x_3	25 to 65 ppm/C	-1 to 1

(2) Specify uncertainties distribution on x_1 , x_2 and x_3 . Uncertainty distribution is assumed to be normally distributed with mean and standard deviation listed as below.

	Mean [unscaled value]	Standard Deviation [unscaled value]
SOH x_1	0 [160 μm]	0.1 [6 μm]
E x_2	0 [4.5 GPa]	0.05 [0.125 GPa]
CTE x_3	0 [45 ppm/C]	0.05 [1 ppm/C]

(3) Sampling points generation to produce the specified distribution in step 2. Those sample points can be compiled into Kriging ROM for the *Damage* prediction

(4) Aggregate the results of all the computations (10000000 manipulations and 10000 manipulations are set for Monte Carlo Sampling (MCS) and Latin Hypercube Sampling

(LHS)) to propagate the process output distribution using any one of the suggested method or both: MCS and LHS. Analytical method - FOSM and point estimation based on pure mean, standard deviation and skewness calculations to construct the distribution are also illustrated.

An example of risk analysis result for distribution of Damage (*D*) estimated by LHS method is indicated by Figure 7-5. Based on the assumed uncertainties data on design variables, the C_p and C_{pk} are found to be 0.9682 and 0.8919 respectively. Any higher degree of uncertainty values in *CTE* would decrease the C_p values sharply as *CTE* is the most dominant design variables in the study. 3.2% of samples fell outside the tolerances limit that should be rejected. Again, any uncertainty data from industry can fit into the risk analysis approach to evaluate the distribution of *Damage*. Table 7-7 details the statistics of mean and standard deviation obtained from the histogram for other risk analysis methods. The point estimation method further calculates the skewness of distribution. Both set of results from sampling and analytical method are very close to each other.
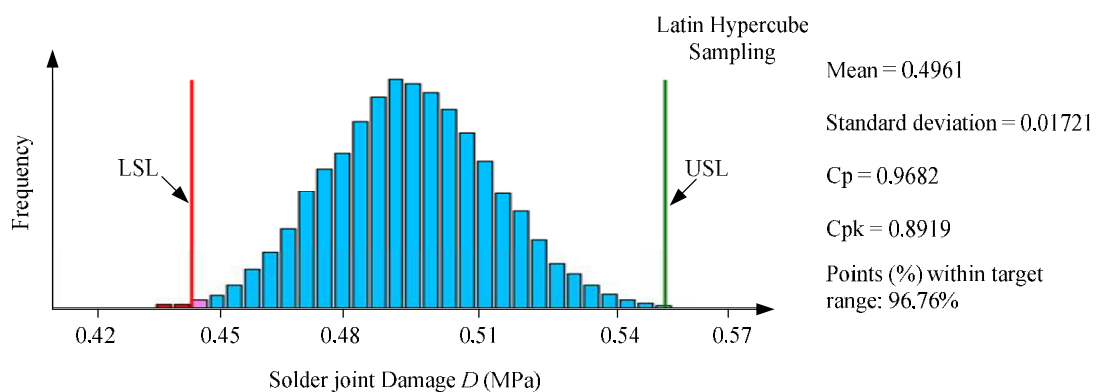
Figure 7-5 Distribution of Damage D estimated by LHS method through Kriging ROM using 10000 samples

Table 7-7 Details of the statistics generated different methods

	Monte Carlo	Latin Hypercube	FOSM	Point Estimation
Solder joint Damage D [µm]	0.4961	0.4961	0.496	0.4961
Standard Deviation [µm]	0.01729	0.01721	0.01729	0.01729

7.3. Environmental Assessment

The objective of this environmental assessment is to quantify the degree of material environmental impact. The emphasise has been placed on constructing an approach to optimise the flip chip package in terms of environmental constraints which can derive a design rule for material selections in the industries. Due to the imminent effect of legislations by WEEE and RoHS, several hazardous substances are prohibited. Environment laws prohibited the usage of traditional solder joint giving rise to the lead-free solder such as Sn-Ag-Cu type (SAC) solder. Subsequent influential changes have been brought into the manufacturing process. Those changes have induced a big deal of technical issues owing to the modified methods as well as the use of new materials. The emergency of new advanced technologies is an inevitable result of accounting for environmental issues during the manufacturing process and product development.

Environment performance with new materials of the flip chip package is also one of the key aspects in the design process. Environmental optimisation strategies must be used for the robust developing flip chip packaging technology. Environmental constraints are one important criterion which must be satisfied. Since the whole life cycle analysis of electronic products is so complex, the environmental performance of each process is

evaluated by individual environmental modular approach [145]. Environmental aspects are arising from toxic potential of raw materials, energy profile of raw materials, manufacturing processes and products, and recycling potential. The modules of materials toxic potential will be demonstrated. This work illustrates how the toxic potential of two types of materials, SAC solder and underfill in the flip chip package is accessed by the Toxic Index (*TI*). The evaluation result is then manipulated in the optimisation model.

7.3.1. Toxic Index

Undergoing the whole life cycle assessment of electronic product is time consuming and complicated. Therefore, a simpler environmental assessment tool - Toxic Index (*TI*), for each material is used to indicate its potential threat to the environment. A numerical indicator is assigned to each material according to its ecological impacts on a scale from 0 to 100. '0' is the least harmful to the environment whereas '100' has the maximum impact on environment. The rating for the materials in this study are interpreted based on the research findings by the Fraunhofer Institute for Reliability and Microintegration (IZM) for Toxic Potential Indicator (IZM-*TPI*) [146] [147]. The Toxic Index (*TI*) using the literature values of the IZM-*TPI* can be applied to investigate the environmental properties of the materials used in the products.

7.3.2. Toxic Index of Flip Chip Materials per Unit Mass

The Toxic Index *TI* for underfill and solder material in the flip chip package is a function of both *TI* of the material itself and the mass of each material used in the package (more material causes higher damage to environment). The amount of material

215

in the package is a function of solder joint stand-off height *SOH* in the flip chip package. Note that the data in Table 7-8 details the physical property SAC solder and underfills for the nominal flip chip package with *SOH* = 160 *μm*. In the design problem *SOH* can vary from 100 to 220 *μm*, for each particular design the actual amount of material is different and is a function of *SOH*. Higher *SOH* is equivalent to bigger solder balls and more solder material per package. Also, higher *SOH* results in bigger gap between substrate and die, such design requires more underfill material.

The volume of a single solder joint is calculated using the solder joint *SOH*. For example, for nominal design solder ball stand-off height of 160 *μm*, the volume is $6.08 \times 10^{-12} m^3$. With SAC density = 7380 *kg/m³*, by $Mass = V \times r$ where $V = SOH \times A$, where r denotes the density, V denotes the volume，A denotes the surface area of solder and *Mass* denotes and mass of each SAC solder. The mass of each solder joint for nominal design *SOH* is calculated as see Equation (7.4). Since there are 48 solder joints in the package, the total mass of 48 SAC solder joints in the nominal flip chip package is $2.15 \times 10^{-6} kg$.

$$
\begin{aligned}
Mass &= 6.08 \times 10^{-12} m^3 \times 7380 kg / m^3 \\
&= 4.49 \times 10^{-8} kg
\end{aligned}
\tag{7.4}
$$

Table 7-8 Solder and underfill material for nominal package.

Material	Nominal values of *SOH* (μm)	Volume $(10^{-10} m^3)$	Density (kg/m^3)	Mass $(10^{-6} kg)$
48 SAC solders	160	2.92	7380	2.15
Underfill (1 to 9)	160	127	1200	15.6

After working out the mass of the 48 SAC solder joints as function of solder joint stand-off height *SOH*, the *TI* for all amount of SAC material in flip chip is calculated. The

SAC composition used in this package is based on 95.8% tin (Sn), 3.5% silver (Ag) and

0.7% copper (Cu). The *TI* for Tin, Silver and Copper material per kilogram is taken

from literature and detailed in the second column in Table 7-9 [145]. Therefore, the *TI*

for the solder material can be calculated on these compositions and the *TI* for each of

these materials by simple multiplication.

Table 7-9 Toxic Index (*TI*) for nominal flip chip design (*SOH*=160μm)

Material	*TI* (1/kg) $TI_{(per\,unit\,mass)}$	*TI* (per flip chip package) $TI_{(per\,package)}$
Tin (Sn)	1200000	
Silver (Ag)	37800000	-
Copper (Cu)	16000000	
SAC solder (Sn-3.5Ag-0.7Cu)	2483800	5.35
Underfill 1	500000	7.8
Underfill 2	700000	10.92
Underfill 3	1500000	23.4
Underfill 4	1200000	18.72
Underfill 5	1000000	15.6
Underfill 6	800000	12.48
Underfill 7	930000	14.46
Underfill 8	1100000	17.11
Underfill 9	1350000	21.00

Multiplying the *TI* of Sn per unit mass (kg) from Table 7-9 with its mass fraction in the

SAC solder will give the *TI* contribution of Sn denoted as $TI_{Sn\_95.8\%}$ in the SAC solder.

Similarly, the *TI* of Ag and Cu as contributions to the overall *TI* of SAC $TI_{Ag\_3.5\%}$ and

$TI_{Cu\_0.7\%}$ are also calculated in Equation (7.5) respectively.

$$\begin{aligned} TI_{Sn\_95.8\%} &= 1200000 \times 0.958 \\ &= 1149600 \\ TI_{Ag\_3.5\%} &= 37800000 \times 0.035 \\ &= 1323000 \\ TI_{Cu\_0.7\%} &= 1600000 \times 0.007 \\ &= 11200 \end{aligned} \tag{7.5}$$

Summing these three *TI* contributions in Equation (7.6) will give us the *TI* for SAC solder joint as composition. *TI* for SAC is 2483800 per kg (listed in second column of Table 7-9. In the calculations, the *TI* unit for the material is one per kilogram.

$$\begin{aligned} TI_{SAC} &= TI_{Sn\_95.8\%} + TI_{Ag\_3.5\%} + TI_{Cu\_0.7\%} \\ &= 2483800 \end{aligned} \tag{7.6}$$

The *TI* per kilogram for the nine underfills is also listed in the second column of Table 7-9. Once the *'TI per kilogram'* of SAC solder and underfills are obtained, their *'TI per package'* can be calculated based on the amount of solder and underfills (which is expressed as a function of *SOH*) used in the package.

7.3.3. Toxic Index of Flip Chip Material per Package

For any particular flip chip design, the actual *TI* for SAC per package is derived based on the solder amount used in terms of mass which is also expressed as a function of *SOH*. The *TI* of each material per package (the third column *TI* per package in Table 7-9) is equal to its total mass (the last column in Table 7-8) multiplied by the *TI* of each material per unit mass (the second column in Table 7-9). The calculation of *'TI per package'* is given by Equation (7.7).

$$TI_{(per package)} = Mass_{total} \times TI_{(per\, unit\, mass)} \tag{7.7}$$

where $TI_{(per\,package)}$ is the *TI* per package, $TI_{(per\,unit\,mass)}$ is the *TI* per unit mass and $Mass_{total}$ is the total mass of the material. The *TI* of SAC material per package is detailed in Equation (7.8). For example, for the nominal flip chip design (solder ball *SOH*=160 microns), the volume of the 48 SAC solder joints $= 2.92 \times 10^{-10} m^3$, density = 7380 kg/m^3 and the mass of the 48 SAC solder joints is $2.15 \times 10^{-6} kg$. Using the *TI* data for SAC (*TI* = 2483800 per kg), the *TI* of SAC material per package is calculated to be 5.35.

$$
\begin{aligned}
TI_{SAC(per\,package)} &= 48 \times Mass_{SAC(total)} \times TI_{SAC(per\,unit\,mass)} \\
&= 2.15 \times 10^{-6} kg \times 2483800 \; kg^{-1} \\
&= 5.35
\end{aligned}
\tag{7.8}
$$

The *TI* of underfills material per package is detailed in Equation (7.9). Similarly, for the nominal design solder ball *SOH* = 160 μm, the volume of underfill is found to be $127 \times 10^{-10} m^3$. The density of underfill is 1200 kg/m^3, hence the mass of the underfill in the nominal package is $15.6 \times 10^{-6} kg$. Again, knowing the *TI* for underfill (e.g. *TI* = 500000 per kg), the *TI* of the underfill for the package is calculated to be 7.8.

$$
\begin{aligned}
TI_{underfills(per\,package)} &= Mass_{underfill} \times TI_{underfills(per\,unit\,mass)} \\
&= 15.6 \times 10^{-6} kg \times 500000 \; kg^{-1} \\
&= 7.8
\end{aligned}
\tag{7.9}
$$

Other material properties for SAC solder and nine underfill materials is summarised in Table 7-10. The last two columns of the table provide information on the material properties of the underfill, the Young's Modulus *E* and the coefficient of thermal expansion *CTE*.

Table 7-10 Materials properties of nine underfills materials

Material Sn-3.5Ag-0.7Cu	Young's Modulus E (GPa)	CTE (ppm/C)
Tin (Sn)		
Silver (Ag)	Defined in Table 7-2	
Copper (Cu)		
SAC solder		
Underfill 1	3.0	35
Underfill 2	4.5	48
Underfill 3	2.0	50
Underfill 4	2.5	62
Underfill 5	7.0	28
Underfill 6	5.0	40
Underfill 7	5.5	26
Underfill 8	6.5	32
Underfill 9	6.5	28

7.4. Cost Assessment of Flip Chip Package

Factors that affect the costs in micro-electronics manufacturing industry have to be identified. Cost can be related to cost of raw materials, processing, assembly, labours and equipments. In this study the cost of materials is considered only but any other cost can be considered in the same manner. The cost of solder and underfill is assessed only because the amount/cost of these two materials vary as a result of variations in the design variables (SOH and underfill choice). The amount per package of rest of the materials is constant, hence the cost is fixed and will not be influenced by package

design changes. The cost aspect for the investigated package materials form specific requirements that are incorporated into the design problem.

The mass of solder and underfill material is a function of the design variable solder joint stand-off height *SOH*. Higher solder joint *SOH* corresponds to bigger solder joints and bigger gap between the silicon die and the substrate. Hence, more SAC solder materials and underfill would be required. Nine underfill materials are available for selection. Material cost is different for each material. Therefore, the cost for underfill material per package depends simultaneously on (1) design geometry - solder joint *SOH* (cost is directly affected by the amount of used material), and (2) selection of the underfill material (actual cost of different underfill materials). Equation (7.10) describes how material cost is calculated.

$$C_{(\$ per\ package)} = Mass_{total} \times C_{(\$ per\ unit\ mass)} \qquad (7.10)$$

where $C_{(\$ per\ package)}$ is the material cost per package, $C_{(\$ per\ unit\ mass)}$ is the cost per unit mass and *M* is the total mass of the materials

For example, material cost of 48 SAC solders is $0.00402. It is calculated from unit cost of SAC $18.7/kg multiplied by the total mass of SAC per package i.e. $2.15 \times 10^{-6} kg$. Similarly, the cost of underfill is also obtained. Mass of the solder joint and underfill can be found in the last column of Table 7-8. The cost of solder and underfill material for a flip chip package with stand-off height 160 microns is demonstrated in Table 7-11.

$$
\begin{aligned}
C_{SAC(\$ per\ package)} \\
= \$18.7/kg \ \times \ 2.15 \times 10^{-6} kg \\
= \$0.0402 \times 10^{-3}
\end{aligned}
\qquad (7.11)
$$

Table 7-11 Material cost for solder and material per kilogram and per package

Material	Material cost $C_{(\$\,per\,unit\,mass)}$ (\$/kg)	Material cost per package (nominal flip chip, SOH=160µm) $C_{(\$\,per\,package)}$ (\$ 10^{-3})
Solder SAC	\$18.7	0.0402
Underfill 1	\$132	2.06
Underfill 2	\$97	1.51
Underfill 3	\$88	1.37
Underfill 4	\$120	1.87
Underfill 5	\$105	1.64
Underfill 6	\$124	1.93
Underfill 7	\$103	1.60
Underfill 8	\$99	1.54
Underfill 9	\$93	1.45

7.5. Optimisation Problem

Engineers try to reduce the costs while in the same time ensuring the reliability of the product cannot be compromised. There is always some trade-off between cost and eco-friendly aspect of the product. Green products usually require higher cost of materials and processes. Less cost production does not guarantee reliable product. To identify the optimal design in each aspect in individual study is possible but entirely inefficient. Therefore, *Multi-disciplinary optimisation* is employed to investigate this complicated design problem involving numerous objectives area. Multi-disciplinary optimisation provides a routine to solve problems simultaneously which incorporates more than one discipline in a more efficient way.

This study investigates the design of a flip chip package where two design parameters are allowed to vary. The design variables are the underfill which can be chosen among several available materials and the flip chip stand-off height *SOH* (respectively solder joint volume). Changes in the design variables have impact on reliability of solder joints under thermal cycling, cost of materials used to assemble the package and also have effect on the level of environmental impact. For example, mass of solder joint and mass of underfill employed in the flip chip package are dependent on solder joints *SOH* (respectively the gap between substrate and die). Changes in solder joints *SOH* would directly affect the amount of solder and underfill material (i.e. the mass) used in a package. Subsequently, the changes in the amount of materials required to assemble a single flip chip has direct effect on the package cost and level of environmental impact.

From chapter 7.2, 7.3 & 7.4, three models have been developed to assess reliability, environment and costs issues in terms of design variables and other design consideration including a mathematical model which is capable to predict the damage in solder joints. The damage *D* is obtained as a function of the package design variables, the *SOH* and underfill material.

7.5.1. Formulations of the Design Problem

Having particular cost and environmental impact requirements, the design task is to identify the optimal flip chip specification so that the requirements are met (see (7c) to 7(g)) and the reliability of the package is maximised. The design problem for this flip chip requires identifying optimal solder joints stand-off height (*SOH*) (see (7a)) and selection of underfill among nine available materials (see (7h)). The objective is to

minimise the solder joint damage D (see (7b)). The two design variables are factors that have impact on reliability, cost and environment impact associated with the flip chip.

The flip chip design problem is defined as follows:

Find SOH and select a suitable underfill from the set of available underfills s.t. (7a)

Minimise $D(SOH, E, CTE)$ (7b)

where

$$D(x_1, x_2, x_3)$$
$$= b_0 + b_1 x_1 + b_2 x_2 + b_3 x_3 + b_{12} x_1 x_2 + b_{13} x_1 x_3 + b_{23} x_2 x_3 + b_{11} x_1^2 + b_{22} x_2^2 + b_{33} x_3^2$$

Subject to:

$$TI_{SAC(per\ package)} < 6.5$$ (7c)

where $TI_{SAC(per\ package)} = 48 \times TI_{SAC(per\ unit\ mass)} \times SOH \times A_{SAC} \times r$

$$TI_{Underfill(per\ package)} < 16$$ (7d)

where $TI_{underfill(per\ package)} = TI_{underfill(per\ unit\ mass)} \times SOH \times A_{underfill} \times r$

$$C_{SAC(\$\ per\ package)} < \$5 \times 10^{-5}$$ (7e)

where $C_{SAC(\$\ per\ package)} = 48 \times C_{(\$\ per\ unit\ mass)} \times SOH \times A_{SAC} \times r$

$$C_{underfill(\$\ per\ package)} < \$2 \times 10^{-3}$$ (7f)

where $C_{underfill(\$\ per\ package)} = C_{underfill(\$\ per\ unit\ mass)} \times SOH \times A_{underfill} \times r$

$$100mm < SOH < 220mm$$ (7g)

$$Underfill \in [1,2,3,4,5,6,7,8,9] \ as\ given\ in\ Table\ 7\text{-}10$$ (7h)

where $TI_{(per\ package)}$ and $C_{(\$\ per\ package)}$ denotes the toxic index and cost per package respectively, $TI_{(per\ unit\ mass)}$ and $C_{(\$\ per\ unit\ mass)}$ denotes the toxic index and cost per unit mass respectively, r denotes the density of materials, A denotes the surface area, D denotes the damage, CTE denotes the coefficient of thermal expansions, E denotes the Young's Modulus and SOH denotes the stand-off height.

Note that the solution of this problem is not trivial. For example, an underfill might be environmental friendly (low *TI*) but expensive, and vice versa. There could be a trade-off between material environmental impact and cost. The decision is even more complicated because solder joint stand-off height has impact on reliability and at the same time it affects the amount of material used in the package, hence affect the package *TI* and cost. Underfills affect on the other side the reliability of the package through their material properties.

7.5.2. Optimal Design Evaluation through Design Optimisation

To account for all existing interactions between the factors of interest in the design process, all requirements for reliability, environmental impact and cost are formulated as an optimisation problem. This problem can be solved using optimisation methods, and the solution will account for all imposed constraints and objectives. Note that there could be many more requirements than those used in this problem, hence the complexity of the interactions may be much more extreme. Any additional requirements can be added in the design problem formulation without any limitation.

VisualDOC [116] optimisation software package is used to solve the problem. The stand-off height is defined as a continuous design variable while the underfill variable is discrete and can take value from 1 to 9 (corresponding to the underfill number in the selection set). VisualDOC performs the assessment of the specified flip chip design and provides the required values for objective (damage of solder joints), constraint functions (cost, *TI*), the design specification for assessment, (the values of the design variables *SOH* and underfill choice) and the associated values for solder damage (i.e. reliability),

cost and *TI* associated with that particular design are calculated. The calculations undertaken exploit the equations and data explained in characterised by the reliability reduced order model, *TI* environmental model, and the cost model.

7.5.3. Discussions

The design optimisation problem has been solved using non-gradient optimisation technique because the design problem includes a discrete variable, selection of an underfill among nine available choices. Non-gradient techniques are applied to identify the global minimum.

The following optimal solution of the problem has been derived and identified:

- *SOH* = 164 microns;

- Underfill 5

The optimised objective (solder damage) for this optimal flip chip design is ***0.168 MPa***, and the imposed requirements are satisfied. From those constraints the requirement for underfill *TI* per package is the one becoming active at the optimal design solution (i.e. has value at the imposed limit, *TI* = 16). Therefore, any further reduction of the damage in solder joint which can be achieved by further increasing the *SOH* above 164 microns will involve the violation of that constraint (*TI* will exceed the limit of 16 as a result of more underfill material corresponding to the increased *SOH*).

The optimal solution shows that the best solution of the design problem is not based on extreme values of *SOH* (i.e. at the specified limits) and does not involve the underfills with lowest cost or TI. This is because those underfills are not good for reliability. Underfill 5 is the one which can minimise the damage in solder joint to greatest extend while providing the required eco-design specification and fits into the cost restriction.

Closure

This study has focused on how requirements on three different design aspects - for reliability, cost and environmental damage can be formulated into a design problem which then can be solved using multidisciplinary design optimisation techniques. Demonstration of how reliability of a flip chip package solder joints can be assessed has been described. The package evaluation with respect to environmental impact using Toxic Index definitions and cost of materials has been also presented. The design of a flip chip package has been successfully optimised by varying two design variables: solder joint stand-off height *SOH* and Underfill material (nine choices). At the optimal design the damage of the solder joints has been minimised while requirements for eco-design and cost have been satisfied. The risk analysis methodology investigated in this application study is generic and can be used for range of design problems in microelectronics packaging and product development. There is virtually no restriction on what and how many requirements that define environmental impact and cost are specified in the design task. Reliability of the product is also part of the design problem. Defining and solving the design problem as an optimisation problem provides the opportunity to use efficient and powerful optimisation techniques to find the solution of the design task. It allows us to account for complex interactions that may exist between key product aspects. This environmental is convenient and cost effective when compared to full life cycle assessment for evaluation of environmental impacts of materials and components. This novel multi-disciplinary approach addressing environmental issues can also assist decisions on new materials selection among all design configuration alternatives. It provides an effective and efficient way when comparing to the trial-and-errors approach.

Chapter 8 Conclusion and Future Work

8.1. Conclusion

A risk analysis and mitigation methodology is developed to assess the impact of uncertainties and complex design requirements for new processes and product development in micro/nano manufacturing. The novel methodology integrates computational modelling of the industrial process, reduced order modelling through the design of experiments and response surface modelling, risk analysis, process capability and optimisation techniques. The associated tools have been applied and demonstrated for the following two applications: (1) Control of the focused ion beam (FIB) sputtering process, and (2) Reliability, cost and the material requirements of electronics package design. In the first application, risk mitigation has been successfully applied to address the impacts of the process parameters variations on the process performances. The statistical analysis provides a useful tool to accurately estimate material removal in the FIB sputtering process. The proposed method can be applied to any other new manufacturing process where accuracy of process control is important and when uncertainties are defined.

A computational model for estimating FIB milling dwell times to achieve pre-defined shape was validated with an experimental test case. Different influential factors such as re-deposition effect and ion flux distribution across geometric pixel layout were discussed. This study includes a control profile, which relates the materials sputtering rate to the depth variation, in terms of several process parameters, including dwell time, sputtering yields, angle and energy, and the desired shape geometrical details. A modified FIB model is derived taking account of the beam *overlapping ratio* on the material sputtered depth, the required number of beam scans across the target surface to achieve the pre-defined shape through fixed dwell time operations for real FIB stations. The theoretical milling depth prediction is shown to be below 5 % deviations from the experimental results for the micro-trench test case. The number of scans from the model also agrees well with the experiment. The model shows good accuracy and was applied to two problems in risk analysis and optimisation analysis.

The risk analysis methodology is applied to the FIB sputtering process. Three different FIB process were evaluated using different ion source, Gallium, Argon and Xeon ion that the process parameters- beam angle and beam energy have different degrees of variations. The uncertainties on these sample points were propagated into the proposed reduced order model. As a result, the degree of impacts on process performance on the associated sample points were captured and presented by histograms. Statistical process control tools such as process capability ratio have been applied to evaluate the process performance with respects to the defined specification limits. The risk of not achieving process targets was identified. Different reduced order model were also investigated in the risk analysis methodology. Interpolation Kriging reduced order model was presented in FIB process to replace the conventional polynomial approximation reduced order model. The accuracy of process performance evaluation can be improved.

In the second application, the focus is placed on the reduced order modelling to generate fast analysis of responses for the optimisation task. The risk of fulfilling certain specifications is presented in a multi-disciplinary design optimisation problem. A flip chip design model was constructed using finite element methods. The deformations, strain and stress of the solder balls were evaluated subject to thermal cyclic changes. This example illustrates the reliability of materials to its life-time by observing the damage of materials. The materials were then assessed with its environmental impacts. A toxic index was used to rank the hazardous impact of the materials by mass in the flip chip package. The toxic index of unleaded type of solder such as Sn-Ag-Cu solder and various underfills were calculated to assess the degree of their environmental impacts.

With reliability requirements, environmental constraints required by the government on materials together with the consideration of package costs, a multi-dimensional design task was formulated. A *multi-disciplinary optimisation* problem was established to aid optimal decisions with respect to various types of criteria as oppose to a single objective. An optimal value of design variable solder joint stand-off-height was identified such that the life span of solder joint was maximised and fulfilled cost requirements. The best underfills were also identified among all available types without violating the constraints i.e. an environmental standard. Optimisation techniques were applied in this study. The approach can act as a tool that helps design engineer account for product design simultaneously in terms of reliability (e.g. damage and life time), cost (e.g. fabrication, materials, labour, shipping and disposal) and environmental requirements (eco-friendly designs and easy to dispose). The study on flip chip has helped select the best design among alternatives before any real prototyping and reduces time to market.

To sum up, the proposed methodology and its associated techniques are integrated in a systematic approach suitable for different industrial processes. It is designed as generic as possible to provide convincing decisions support based on strong underlying physics and theories. The methodology provides a design routine in handling uncertainties issues for miniaturised products manufacturing in order to meet certain system objectives such as reliability requirements and environmental compliances. The methodology also enhances the understanding of engineers, researchers, and decision makers about their system and researching fields. It can provide a useful tool that can assist decision making and may be tailored to industrial user needs.

8.2. Research Findings and Its Impact

The research work has been developed to provide decision makers a decision support tool with the aid of computational approaches for micro/ nano manufacturing. Achievements in this research work can be organised into three main categories:

(1) Methodology development for risk analysis in micro and nano manufacturing;

(2) Optimal process control of focused ion beam for micro-machining of nano features;

(3) Simulation driven approaches for risk analysis and optimal electronics package design with reliability, cost and material related specifications.

In the application of focused ion beam, a modified computational model is developed for the material sputtering using focused ion beam. Process control including adjusting process parameters to predict product shape overcomes the dependence on trial-and-error method. The major achievements in the research work with regards to optimal process control of focused ion beam are:

- The model allows analysis of sputtered nano features with FIB machines controlled through multiple beam scans and different beam overlapping;

- Integration of a re-deposition FIB model with the sputtering model

- Experimental validation of the FIB model;

- A tool that aids FIB users producing nano-features with enhanced accuracy. FIB manufacturing can be less dependent on the trial-and-error approach.

The novelty of the research work in the area of electronics package design is in the model driven multi-disciplinary design approach. Optimisation techniques are introduced to provide design engineers with the ability to account for cost related constraints and also to assess environmental impact of the design. Main achievements can be detailed as follows:

- Proposed approach to rank the hazardous impact on the environment of different electronics product materials. This approach has utilised the efficiency of conducting environmental assessment on design instead of a real end product;

- Environmental assessment allows the products design to be evaluated at the early design stage to compare to the new standards and regulations imposed against electronic products;

- Impacts on product characteristics - damage (as an reliability requirement) arises due to design variables uncertainties are quantified;

- Optimisation problem formulations for package design that includes reliability requirements, the cost aspects and the environmental impact of the problem;

- Demonstration of this approach to the design of a flip chip package. That helps to select the best design among alternatives before any real prototyping and reduces time to market.

With a thorough explanation of the techniques and tools, the risk analysis methodology was implemented using two innovative industrial applications. The two examples were carefully selected in order to represent a holistic perspective for both the products design and process fabrication during their development. The process fabrication concerns were identified through a focused ion beam (FIB) sputtering process control. The product design issues were characterised by a flip chip package fabrication. The importance of the research findings and its impact are summarised as follows:

- **<u>Better FIB Process Control for Sputtered Shape</u>**

  In the first applications, an identified computational focused ion beam (FIB) model provides a better understanding in the control of the advanced micro-machining process. The original models are modified by adding additional process parameters in its constitutive equation. The process parameters integrated with re-deposition effect in simulation has enhanced the accuracy to predict the final shape against the expected shape. The modelling results are validated and well-agreed with experiments. The modelling study has also been developed in a way to accounts for number of beam scans. This approach is completely different to the existing models in many current studies which only predict time or milling depth variation. The new model approach utilises the setup control of FIB machines. Adjusting FIB machines process parameters to obtain a pre-defined shape is no longer following on trial-and-error method. In summary, the whole simulation work has provided a better process control for the real FIB machining process to achieve accurate nano-structures fabrication. It also allows more flexibility to interact with FIB machines since every FIB machine operation style can be very different.

- **<u>Robust Flip Chip Design and Enhanced Decision for Materials Selection</u>**

  In the second applications, the research work has exploited a novel way to account for environmental impacts of materials numerically. This method has utilised the

efficiency of conducting a full products life cycle assessment to evaluate its environment impacts. This also allows the end products be compared to environmental standards for meeting the new regulations imposed against electronic products. The multi-disciplinary optimisation (MDO) design problem with the use of a computational model by finite element methods addresses the issues of identifying an optimal product from different design alternatives and material selections. The MDO design problem provides a holistic and unified design approach where reliability, environmental impacts and economic aspects used to be considered in only mono-disciplinary optimisation problem study.

- **Uncertainty Propagation for Quality Improvement**

  The risk mitigation framework has addressed the impacts of uncertainties, the stochastic behaviour of process. Prediction of a parameter value for optimum design and process is longer adequate to deal with process randomness or undetectable errors. The propagation of risk here has accounted for how *accurate* to obtain such a deterministic process output due to process variability. The risk analysis methodology provided a probabilistic approach for achieving a robust design. It is crucial to couple with the risk inherent systems especially during the new technologies development where historic data and fabrication knowledge are very limited. Certain process capability indices are applied allowing the process to be compared with the *'six-sigma'* design practice and relevant standards.

- **Optimising Process with Uncertainty**

  Minimising the deviation of process output from target requirements or enhancing the process capability in an optimisation problem are still lack of depth in current researches and studies. Optimisation routines using advanced optimisation

algorithms are illustrated here of how to derive a robust optimal design and process via the constructed reduced order model.

- **<u>Fast Reduced Order Modelling for Risk Analysis and Optimisation</u>**

  The computational model provides a virtual prototyping which hugely reduces the cost of real prototype or experiment to generate accurate process responses and to allow flexible adjustment of process setup efficiency. Reduced order model such as Kriging model is brought into micro-electronics without much loss of details from its original full model. It has greatly enhanced the evaluation of process responses since there are always trade-off between the computational resources and accuracy. This virtual prototype using reduced order modelling provides an efficient way to perform risk analysis and optimisation with enhanced accuracy.

8.3. Recommendations for Future Work

The future works are outlined as follows:

(1) <u>Model enhancement</u>

Some process parameters in the FIB model needs further adjustment. For example, a Gaussian bi-variate density function is used to represent the beam intensity profile. In fact, the centre and the tail part of the ion beam intensity profile can be modelled with a Gaussian distribution and exponential distribution respectively to improve the accuracy of ion flux estimation.

(2) <u>Further investigation and validation on other predefined shapes</u>

Re-deposition is not prominent in a *shallow* shape (small milling depth compared to the width of the shape). Since the desired milling depth of the investigated test case is not

deep enough, the re-deposition is not implemented here. However, re-deposition model can be implemented on other test case to refine the depth variation. Then the re-deposition model integrated with the developed model can be verified against new experiment setup. This motivates the need for investigation on any other shape such as a sine wave and a parabolic shape, and to further validate the process control capability of the developed models.

(3) Extension of risk analysis methodology

Advance techniques for response surface modelling, risk analysis and optimisation can be embedded into the design modelling as alternative tools. For example, other interpolations methods such as radial basic interpolations, spline interpolation, or even extrapolation methods can fit in the framework. Uncertainties propagation can be achieved through more accurate method such as second order third moment method and point estimation method that account for skewness of distribution. From optimisation perspective, *reliability based design optimisation* by analytical method such as *first order reliability method* and *second order reliability method* can greatly reduced the computational time using *Monte Carlo Sampling* based approach during iterative optimisation process.

(4) Software development

The framework is being established in parallel with our research group software - ROMARA (Reduced Order Modelling And Risk Analysis software). It captures the development of micro-integrated products and processing activities from design perspective. The underlying mathematical models and theories can also be programmed into this software as a decision support tool.

References

[1] WEEE, "Directive 2002/96/EC of the European Parliament and of the council on waste electrical and electronic equipment," 2002.

[2] RoHS, "Directive 2002/95/EC of the European Parliament and of the council on the restriction of the use of certain hazardous substances in electrical and electronic equipment," 2002.

[3] Bailey, C., "Exploiting Virtual Prototyping for Reliability Assessment," in *International Conference on the Business of Electronic Product Reliability and Liability*, 2003, pp. 2-3.

[4] Lee, D.J. and Thornton, A.C., "The Identification and Use of Key Characteristics in the Product and Development Process," in *ASME Design Engineering Technical Conference and Computer in Engineering Conference*, California, 1996.

[5] "Probabilistic Risk Assessment Procedures Guide for NASA Managers and Practitioners," *NASA, Version 1.1*, August, 2002.

[6] Tang, Y. K., Stoyanov, S., Ridout, S., Bailey, C., N. Sailesh, Eshahawil, T., Gindyl, N., "Risk Mitigation Framework for a Robust Design Process," in *The 2nd Electronics System-Integration Technology Conference*, London, 2008, pp. 1075-1080.

[7] Tang, Y.K., Stoyanov, S., Bailey, C., Chan, Y.C. , "'Risk Analysis and optimisation for models in Advanced Micro-system Electronics Manufacturing," in *The 2nd Electronics System-Integration Technology Conference*, London, 2008, pp. 941-946.

[8] Stoyanov, S., Tang, Y.K., Bailey, C., Evans, R., Marson, S. and Allen, D.M., "Modelling and Process Capability Analysis of Focused Ion beam," in *The 32nd International Spring Seminar on Electronics Technology*, Brno, Czeh Republic, 2009.

[9] Tang, Y.K., Stoyanov, S., Bailey, C., Chan, Y.C., "Optimisation Methodology for Risk Mitigation in Advanced Micro-system Electronics Manufacturing," in *International Conference on Engineering Optimization*, Rio de Janeiro, 2008.

[10] Stoyanov, S., Tang, Y.K., Bailey, R., Marson, S., Dyer, A., and Allen, D.M., and Desmulliez, M., "Computational modelling and optimisation of the fabrication of nano-structures using focused ion beam and imprint forming technologies," in *Journal of Physics: Conferences Series 253 (2010) 012008, doi: 10.1088/1742-6596/253/1/012008* , 2010, pp. 1-10.

[11] Germany -TPI Fraunhofer IZM, http://www.izm.fraunhofer.de/Images/Description_TPI_Calculator_tcm358-133298.pdf.

[12] ROMARA, "http://cmrg.gre.ac.uk/software/romara/".

[13] Kaplan, S. and Garrick, B.J, "On the quantitative definition of risk," *Risk Analysis,* vol. 1, no. 1, 1981.

[14] Modarres, M., *Risk Analysis in Engineering*, Raton Boca. FL, Ed.: CRC Press, 2006.

[15] Dezfuli, H., Youngblood, R., Reinert, J., "MANAGING RISK WITHIN A

DECISION ANALYSIS FRAMEWORK," in *the Second IAASS Conference*, Chicago (USA), 2007.

[16] NUREG/CR-2300, "IEEE/ANS Procedures Guide," 1983.

[17] Vesely, W.E. and Rasmuson, D.M., "Uncertainties in Nuclear Probabilistic Risk Analyses," *Risk Analysis*, vol. 4, no. 4, pp. 313-322, 1984.

[18] Haldar, A. and Mahadevan, S., *Probability, reliability and statistical methods in engineering design*. New York: John Wiley and Sons, 2000.

[19] Wang, J.X. and Roush, M.L. , *What Every Engineer Should Know About Risk Engineering And Management*, Marcel Dekker, Ed., 2000.

[20] "Guidance on the Treatment of Uncertainties Associated with PRAs in Risk-Informed Decision Making," *U.S. Nuclear Regulatory Commission [NUREG-1855]*, vol. 1, 2009.

[21] "Procedure for performing a failure mode effect and criticality analysis," United States Military Procedure [MIL-STD-1629A], U.S., November 24, 1980.

[22] Stamatis, D.H., *Failure mode and effect analysis: FMEA from theory to execution*, 2nd ed.: ASQ Quality Press, 2003.

[23] Clausing, D. and Simpson, B.H., "Quality by design ," *Quality Progress*, vol. 23, no. 1, pp. 41-44, 1990.

[24] NASA, "Risk Management Procedures and Guidelines," NPG 8000.4, April 25, 2002.

[25] The Responsive Manufacturing Group, "http://www.rmgn.org/,".

[26] Mankins, J.C., "Technology Readiness Levels," Advanced Concepts Office, Office of Space, NASA, White paper 1995.

[27] Narania, S and Tang, Y.K., "Risk Mitigation Framework for a Robust Design Process," in *2nd Electronics System-Integration Technology Conference*, London, 2008, pp. 1075-1080.

[28] "Advanced Quality System," Boeing Commerical Airplane Group, D1-9000-1, Novemeber, 1998.

[29] Du, X., Chen, W., "Towards a Better Understanding of Modeling Feasibility Robustness in Engineering Design," *ASME Journal of Mechanical Design*, vol. 122, no. 4, pp. 385-394, Dec 2000.

[30] Kim, B. S. and Leleur, S., "Appraisal of Airport Alternatives in Greenland by the use of Risk Analysis and Monte Carlo Simulation," in *Winter Simulation Conference*, 2007, pp. 1986-1993.

[31] Wilde, J. and Zukowski, E., "Probabilistic Analysis of the Influences of Design Parameter on the Reliability of Chip Scale Package," in *7th International Conference on Thermal, Mechanical and Multiphysics Simulation and Experiments in Micro-Electronics and Micro-Systems,EuroSimE2006*, Como, Italy, 2006, pp. 1-8.

[32] Helton, J.C., Davis, F.J., "Latin hypercube sampling and the propagation of uncertainty in analyses of complex systems," *Reliability Engineering and System Safety*, vol. 81, no. 1, pp. 23-69, Feb 2003.

[33] Tong, C., "Refinement strategies for stratified sampling methods," *Reliability Engineering and System Safety*, vol. 91, pp. 1257-1265, Jan 2006.

[34] Zhang. Y, Yoon, H.S., Koh, C.S., "Global Optimization of Electromagnetic Devices Combining Latin Hypercube Sampling Experiement and Adaptive

Response Surface Method," in *International Conference on Electrical Machines and Systems 2007*, Seoul, 2007, pp. 1414-1418.

[35] Wu, H., Xu, Y.,Liang, L, "The probability design for wire bonding process by finite element and Monte Carlo method," in *11th Int. Conf. on Thermal, Mechanical and Multiphysics Simluation and Experiments in Micro-Electronics and Micro-Systems, EuroSimE2010*, Bordeaux, 2010, pp. 1-9.

[36] Fenton, G.A.and Griffiths, D.V., *Risk Assessment in Geotechnical Engineering*.: Hoboken, N.J.: Wiley; Chichester: John Wiley; ISBN: 9780470178201, 2008.

[37] Rajaguru, P., Stoyanov,S., Tang, Y.K., Bailey, C., Claverley, J., Leach, R. and Topham, D., "Numerical Modelling Methodology for Design of Miniaturised Integrated Products – an Application to 3D CMM Micro-probe Development," in *11th International Conference on Thermal, Mechanical & Multi-Physics Simulation, and Experiments in Microelectronics and Microsystems (EuroSimE*, Bordeaux France, 2009, pp. 1-8.

[38] Du, X., Chen, W., "A most Probable Point Based Method For Uncertainty Analysis," in *ASME 2000 Design Engineering Technical Conferences*, Maryland, 2000, pp. 1-8.

[39] Hohenbichler, M., Gollwitzer, S., Kruse, W., Rackwitz, R., "New light on first- and second-order reliability methods," *Structural Safety*, vol. 4, no. 4, pp. 267-284, 1987.

[40] Haldar, A., Mahadevan, S., *Probability, reliability and statistical methods in engineering design*. New York: John Wiley and Sons, 2000.

[41] Deb,K., Gupta, S.,Daum, D., Branke, J., Mall, A. K.and Padmanabhan, D., "Reliability-Based Optimization Using Evolutionary Algorithms," *IEEE Transactions on Evolutionary Computation*, vol. 13, no. 5, pp. 1054-1074, Oct 2009.

[42] Qi, C., Wu, J., "Reliability Analysis Using Artificial Neural Networks," in *Sixth International Conference on Natural Computation (ICNC 2010)*, Valcencia, Spain, 2010, pp. 1783-1787.

[43] Duan, W., Wang, Z. , "Vibration Reliability Analysis of Turbine Blade Based on ANN and Monte Carlo simulation," in *6th Int. Conf. on Natural Computation ICNC2010*, Valencia, Spain, 2010, pp. 1934-1939.

[44] Shafer, G., *A mathematical theory of evidence*. NJ: Princeton, 1976.

[45] Zadeh, L.A., "Fuzzy sets. Information and Control 81," pp. 338-353, 1965.

[46] Thacker, B. and Huyse, L., "Probabilistic assessment on the basis of interval data," in *AIAA/ASME/ASCE/AHS Structures, Strcutural Dynamics, and Matreial Conference, AIAA-2003-1753,* Norfolk, Virginia, 2003.

[47] Tang, L. C., *Six sigma: advanced tools for black belts and master black belts*.: John Wiley and Sons; IBSN: 0470025832, 2006, pp. 131-132.

[48] Gerber, S. B. and Finn, K. V., "Sampling Distribution of a Sum and of a Mean," in *Using SPSS for Windows: data analysis and graphics*.: Springer, ISBM: 0387400834, 9780387400839, 2005, ch. 9, pp. 102-104.

[49] Björck, Å., *Numerical methods for least squares problems*, 2nd ed. U.S.: SIAM, 1996.

[50] Chatterjee, S. and Hadi, A.S., *Regression analysis by example*, 4th ed.: A John Wiley & Sons Inc. Publication, 2006, pp 86-88.

[51] MobileReference, *Statistics Quick Study Guide for Smartphones and Mobile Devices*.: MobileReference, Ch9, 2007.

[52] Saunders, S.C., *Reliability, life testing and the prediction of service lives: for engineers*. U.S.: Springer, 2007, ch 8.

[53] Mair, P., *Interpreting Standard and Nonstandard Log-Linear Models*. Germany: Waxmann Verlag, 2006.

[54] Härdle, W., *Applied nonparametric regression*. U.K.: Cambridge University Press, 1990.

[55] Baxter, B.J.C., "The interpolation Theory of Radial Basis Functions," Cambridge University, UK, Dissertation thesis of Doctor of Philosophy 1992.

[56] Matheron, G., "Principles of geostatistics, Economic Geology," vol. 58, no. 8, pp. 1246-1266, 1963.

[57] Stoyanov, S., Rajaguru, P., Tang, Y.K., Bailey, C., Claverley, J., Leach, R. , "Reduced order modelling for risk mitigation in design of miniaturised/integrated products," in *33rd International Spring Seminar on Electronics Technology (ISSE)*, Wars, 2010, pp. 402-407.

[58] Lall, P., Shirgaokar, A., Drake, L., Moore, T., Suhling, J. and Shah, M., "Principal component regression models for life prediction of plastic ball grid arrays on copper-core and no-core assemblies," in *11th Intersociety Conference on Thermal and Thermomechanical Phenomena in Electronic Systems*, Orlando, USA, 2008, pp. 770-785.

[59] Li, L., Ma, X.S. and Zhou, X., "Thermal stress analysis and structural optimization of ultra-thin chip stacked package device," in *International Conference on Electronic Packaging Technology & High Density Packaging, 2009. ICEPT-HDP '09.*, Beijing, 2009, pp. 1190-1194.

[60] You, H., Yang,M., Wang, D. and Jia,X., "Kriging Model combined with latin hypercube sampling for surrogate modeling of analog integrated circuit performance," in *10th International Symposium on Quality of Electronic Design*, San Jose, CA, USA, 2009, pp. 554-558.

[61] Hawe, G. and Sykulski, J., "Considerations of accuracy and uncertainty with kriging surrogate models in single-objective electromagnetic design optimisation," *IET Science, Measurement & Technology*, vol. 1, no. 1, pp. 37-47, Jan 2007.

[62] Simpson, T.W., Mauery, T.M., Korte, J.J. and Mistree, F., "Comparison of Response Surface and Kriging Models for Multidisciplinary Design Optimization," in *7th AIAA/USAF/NASA/ISSMO Symposium on Multidisciplinary Analysis & Optimization, AIAA, Vol. 1, AIAA-98-4755.*, St. Louis, MO, 1998, pp. 381-391.

[63] Bang, K.Il., Dong, S.H. and Geun, J.H., "Structural optimization for a jaw using iterative Kriging metamodels," *Journal of Mechanical Science and Technology*, vol. 22, no. 9, pp. 1651-1659, jun 2008.

[64] Husain, A. and Kim, K.Y., "Shape Optimization of Micro-Channel Heat," *IEEE Transactions on Components and Packaging Technologies*, vol. 31, no. 2, pp. 332-330, June 2008.

[65] Wikipedia, "http://en.wikipedia.org/wiki/Plenty_of_Room_at_the_Bottom,".

[66] Zheng, C., *Nanofabrication: principles, capabilities and limits*. China: Springer, 2008, ch. 1, pp. 1-4.

[67] Fu, Y. and Bryan, N.K.A., "Fabrication of three-dimensional microstructures by two-dimensional slice by slice approaching via focused ion beam milling," *J. Vac. Sci. Technol. B*, vol. 22, no. 4, pp. 1672-1678, Aug 2004.

[68] Vasile, M.J., Niu, Z., Nassar, R., Zhang, W. and Liu, S., "Focused ion beam milling: Depth control for three-dimensional," *J. Vac. Sci. Technol. B*, vol. 15, no. 6, Nov/Dec 1997.

[69] Vasile, M.J., Nassar, R.,Xie, J. and Guo,H., "Microfabrication techniques using focused ion beams and emergent," *Micron*, vol. 30, no. 3, pp. 235-244, 1999.

[70] Ali, M.Y. and Hung, N.P., "Surface Roughness of Sputtered Silicon. II. Model Verification," *Materials and Manufacturing Processes*, vol. 16, no. 3, pp. 315-329, 2001.

[71] Nassar, R., Vasile, M. and Zhang, W., "Mathematical modelling of focused ion beam microfabrication," *J. Vac. Sci. Technol. B*, vol. 16, no. 1, pp. 109-115, 1998.

[72] Itoh, F., Shimase, A. and Haraichi, S., "Two-dimensional profile simulation of Focused Ion Beam milling of LSI," *Journal of the Electrochemical Society*, vol. 137, pp. 983-988, 1990.

[73] Fu, Y. and Bryan, N.K.A., "Investigation of 3D microfabrication characteristics by focused ion beam technology in silicon," *Journal of Materials Processing Technology*, vol. 104, no. 1-2, pp. 44-47, April 2000.

[74] Beuer, S., Rommel M., Lehrer, Ch., Platzgummer, E. and Kvasnica, S., "Accurate parameter extraction for the simulation of direct structuring by ion beams," in *International Conference on Micro- and Nano-Engineering (MNE)*, vol. 84, Barcelona, 2007, pp. 810-813.

[75] Fu, Y., Bryan, N.K.A. Shing, O.N., Wyan, H.N.P., "Influence analysis of dwell time on focused ion beam micromachining in silicon," *Sensors and Actuators A: Physical*, vol. 79, no. 3, pp. 230-234, 2000.

[76] Hung, N.P., Ali, M.Y., Fu, Y.Q., Ong, N.S. and Tay, M.L., "Surface Integrity and Removal rate of Silicon Sputtered with Focused Ion Beam," *Machining Science and Technology*, vol. 5, no. 2, pp. 239-254, 2001.

[77] Hung, N.P., Fu, Y.Q. and Alil, M.Y., "Focused ion beam machining of silicon," *Journal of Materials Processing Technology* , vol. 127, no. 2, pp. 256-260, 2002.

[78] Assayag, G.B., Vieu, C., Gierak, J., Sudraud, P. and A.Corbin, "New characterization method of ion current-density profile based on damage distribution of Ga+ focused-ion beam omplantation in GaAs," *J.Vac.Sci.Technol B*, vol. 11, pp. 2420-2426, 1993.

[79] Kim, C.S., Park, J., Chu, W.S., Jang, D.Y., Kim, S.D. and Ahn, S.H., "Fabrication of silicon micro-mould for polymer replication using focused ion beam," *Microelectronic Engineering*, vol. 86, no. 4-6, pp. 556-560, 2009.

[80] Fu, Y. Q., Bryan, N.K.A., Shing, O.N. and Hung, N.P., "Influence of the Redeposition effect for Focused Ion Beam 3D," *International Journal of Advanced Manufacturing Technology*, vol. 16, no. 12, pp. 877-880, 2000.

[81] Tseng, A.A, Leeladharan, B., Li, B. and Insua, I.A., "Fabrication and modelling Microchannel Milling using Forcused Ion Beam," *International Journal of Nanoscience*, vol. 2, no. 4 & 5, pp. 375-379, 2003.

[82] Ishitani, T. and Ohnishi, T., "Modeling of Sputtering yield redeposition in focused-ion-beam trench milling," *J. Vac. Sci. Technol. A*, vol. 9, pp. 3084-3089, 1991.

[83] Kim, H.B., Hobler, G., Lugstein, A. and Bertagnolli, E., "Full three-dimensional simulation of focused ion beam micro/ nanofabrication," *Nanotechnology*, vol. 18, no. 24, 2007.

[84] Baldwin, D.F., *Electronic Packaging and Interconnection Handbook, ch.8*, 4th ed., C. A. Harper, Ed.: McGraw-Hill Professional, 2005.

[85] Miessner, R. and Haeussermann, T., "Use of Flow Simulation for Design and Process Optimisation for Flip Chip Underfill," in *5th International Conference on Polymers and Adhesives in Microelectronics and Photonics*, Wroclaw, Poland, 2005, pp. 171-175.

[86] Khor, C.Y., Mujeebu, M.A., Abdullah, M.Z.and Ani, F.C., "Finite volume based CFD simulation of pressurized flip chip underfill," *Microelectronics Reliability*, vol. 50, no. 1, pp. 98-105, January 2010.

[87] Lau, J.H., Lee, S.W.R. and Chang, C., "Effects of underfill material properties on the reliability of solder bumped flip chip on board with imperfect underfill encapsulants," *IEEE Transactions on Components, Packaging and Manufacturing Technology*, vol. 23, no. 2, pp. 323-333, January 2002.

[88] Ho, P.S., Wang, G.T., Ding, M., Zhao, J.H. and Dai, X., "Reliability Issues for Flip-Chip Packages," *Journal of Microelectronics Reliability*, vol. 44, pp. 719-737, 2004.

[89] Chiu, C.C., Huang, C.J., Yang, S.Y., Lee, C.C., Chiang, K.N. , "Investigation of the delamination mechanism of the thin film dielectric structure in flip chip packages," *Microelectronic Engineering*, vol. 87, no. 3, pp. 496-500, March 2010.

[90] Kim, J.W. and Jung, S.B., "Optimization of shear test for flip chip solder bump using 3-dimensional computer simulation," *Microelectronic Engineering*, vol. 82, no. 3-4, pp. 554-560, December 2005.

[91] Blanchard, B.S., *Logistics Engineering and Management*, 4th ed., Englewood Cliffs, Ed. New Jersey, U.S.: Prentice-Hall, Inc., 1992.

[92] Che, F.X. and Pang, J.H.L., "Vibration reliability test and finite element analysis for flip chip solder joints," *Microelectronics Reliability*, vol. 49, no. 7, pp. 754-760, July 2009.

[93] Wunderle, B., Nüchter, W., Schubert, A., Michel, B. and Reichl, H., "Parametric FE-approach to flip-chip reliability under various loading conditions," *Microelectronics Reliability*, vol. 44, no. 12, pp. 1933-1945, Decemeber 2004.

[94] Zhang, Y.L., Shi, D.X.Q. and Zhou, W., "Reliability study of underfill/chip interface under accelerated temperature cycling (ATC) loading," *Microelectronics and Reliability*, vol. 46, no. 2-4, pp. 409-420, February-April 2006.

[95] Shubert, A., "Fatigue Life Models of SnAgCu and SnPb Solder Joints Evaluated by Experiments and Simulations," in *53th Electronic Components and Technology Conference*, 2003, pp. 197-206.

[96] Li,X. and Wang, Z., "Thermo-fatigue life evaluation of SnAgCu solder joints in flip chip assemblies," *Journal of Materials Processing Technology*, vol. 183, no. 1, pp. 6-12, March 2007.

[97] Syed, A., "Accumulated Creep Strain and Energy Density Based Thermal Fatigue Life Prediction Models for SnAgCu Solder Joints," in *Electronic Components and Technology Conference*, 2004, pp. 737-746.

[98] Chiu, C.C., Wu, C.J., Peng, C.T., Chiang K.N., Ku, T., Cheng, K., "Lead-Free Flip Chip Package Reliability and the Finite Element-Factorial Design

Methodology," in *International Microsystems, Packaging, Assembly Conference Taiwan*, Taiwan, , 2006, pp. 1-4.

[99] Nissen, N.F., Griese, I., Middendorf, A., Muller, J., Potter, H., Reichl, H., "An environmental comparison of packaging and interconnection technologies," in *The IEEE International Symposium on Electronics and the Environment. ISEE - 1998*, Oak Brook, IL, 4-6 May, 1998, pp. 106-111.

[100] Muller, J., Griese, H., Nissen, N.F., Potter, H., Reichl, H., "Environmental aspects of PCB microintegration," in *International Symposium On Environmentally Conscious Design and Inverse Manufacturing*, Tokyo, 10-11 Dec, 1999, pp. 216-220.

[101] Nissen, N.F.; Griese, H., Middendorf, A., Muller, J., Potter, H., Reichl, H. , "Environmental assessments of electronics: a new model to bridge the gap between full life cycle evaluations and product design ," in *IEEE International Symposium on Electronics and the Environment*, New Jersey, 5-7 May, 1997, pp. 182-187.

[102] ISO, http://www.iso.org/, 1997.

[103] MSDSSEARCH, http://www.msdssearch.com/, 2003.

[104] Yen, S.B. and Chen, J.L., "The Development of Taiwan's Toxic Potential Indicator (TPI)," in *International Symposium on Environmentally Conscious Design and Inverse Manufacturing*, Toyko, Japan, 2003, pp. 632-635.

[105] Chung, J., Lee, H., Middendorf, A., Zuber, K.H., "A Study on the Trace of Appropriate Ecodesign Strategies," in *3rd International Symposium on Environmentally Conscious Design and Inverse Manufacturing*, Tokyo, Japan, 2003, pp. 291-296.

[106] Lau, J.H, "Cost Analysis: Solder Bumped Flip Chip Versus Wire," *IEEE Transactions on Electronics Packaging Manufacturing*, vol. 23, no. 1, pp. 4-11, Jan 2000.

[107] Palesko, C. A.; Vardaman, E. J, "Cost comparison for flip chip, gold wire bond, and copper wire bond packaging ," in *60th Electronic Components and Technology Conference (ECTC)*, Las Vegas , Nevada , 2010, pp. 10-13.

[108] Suwa, T. and Hadim, H., "Multidisciplinary Electronic Package Design and Optimization Methodology Based on Genetic Algorithm," *IEEE Transactions on Advanced Packaging*, vol. 30, no. 3, pp. 402-410, 2007.

[109] Hrennikoff, A., "Solution of Problems in Elasticity by the Framework Method," *J. Appl. Mech.*, vol. 8, pp. 169-175, 1941.

[110] McHenry, D., "A Lattice Analogy for the Solution of Plane Stress Problems," *J. Inst. Civil Eng.*, vol. 21, no. 2, pp. 59-82, 1943.

[111] Nellis, G.F. and Klein, S.A., "The Galerkin Weighted Residual Method," in *Heat Transfer*. UK: Cambridge University, ch. 2.7.

[112] Zienkiewicz, O.C., Taylor, R.L., Taylor, R.L. and Zhu, J.Z., "Standard and hierarchical element shape functions: some general family of C0 continuity," in *The finite element method: its basis and fundamentals*.: Butterworth-Heinemann, 2005: ISBN 0750663200, 9780750663205, 2005, ch. 4, pp. 103-130.

[113] "Advanced Quality System D1-9000-1," Boeing Commercial Airplane Group, November, 1998.

[114] Montgomery, D.C., *Design and Analysis of Experiments (third ed.)*.: John Wiley

& Sons, Inc., 1991.

[115] Box, G.E.P. and Wilson, K.B., "On the Experimental Attainment of Optimum Conditions," *Journal of the Royal Statistical Society Series* , vol. B13, no. 1, pp. 1-45, 1951.

[116] Vanderplaats Research and Development, Inc, 2004. VisualDOC, "http://www.vrand.com/visualDOC.html,".

[117] Montgomery, D.C., *Design and Analysisof Experiments*, 3rd ed. New York: John Wiley & Sons, Inc., 1991.

[118] Matheron, G., "Traité de géostatistique appliquée, Tome I.," *Mémoires du bureau de recherches géologiques et minières principles. Paris: Editions Technip,* vol. 14, p. 333, 1962.

[119] Cressie, N., *Statistics for Spatial Data*. New York: John Wiley & Sons, Inc., 1991.

[120] Stapenhurst, T., "Putting SPC into Practice," in *Mastering Statistical Process Control*.: Butterworth-Heinemann, 2005, ch. 3, pp. 59-68.

[121] Oakland, J.S., "Process Variability," in *Statistical Process Control*. UK: Butterworth-Heinemann, 2008, ch. 2, pp. 61-102.

[122] Rose, P.D., Brown, S.J., Jones G.A.C. and Ritchie, D.A., "A method to profile ion beam line exposures in situ using STM," *Microelectronic Engineering*, vol. 41-42, pp. 229-232, 1998.

[123] Tanaka, M., Furuya, K. and Saito, T., "In-situ Observation of Focused Ion Beam Micromilled Si, SiO2 and GaAs," in *International Conference on Ion Implantation Technology*, Tsukuba, Japan, 1999, pp. 1039-1042 (vol:2).

[124] Kirk, E.C.G., McMahon, R.A., Cleaver, J.R.A. and Ahmed,H., "Scanning ion microscopy and microsectioning of electron beam," *J. Vac. Sci. Technol. B*, vol. 6, no. 6, pp. 1940-1943, 1988.

[125] Smith, S., Walton, A.J., Bond, S., Ross, A.W.S, Stevenson, J.T.M., and Gundlach, A.M., "Electrical Characterization of Platinum Deposited by Focused Ion Beam," *IEEE Transactions on Semiconductor Manufacturing*, vol. 16, no. 2, pp. 199-206, May 2003.

[126] Stewart, D., Casey, J. and Choudhury P.R., "Handbook of Microlithography, Micromachining, and Micro-fabrication," vol. 2, Chapter 4, 1997.

[127] Prewett, P.D. and Heard, P.J., "Repair of opaque defects in photomasks using focused ion beams," *J. Phys. D: Appl. Phys.*, vol. 20, pp. 1789-1805, 1987.

[128] Santschi, C., Jenke, M., Hoffman, P. and BurggerJ. , "Interdigitated 50 nm Ti electrode arrays fabricated using XeF2 enhanced focused ion beam etching," *Nanotechnology*, vol. 17, p. 2722, 2006.

[129] Volkert, C.A. and Minor, A.M., "Focused ion beam microscopy and micromachining," *MRS Bulletin*, vol. 32, no. 5, pp. 389-399, 2007.

[130] Kubena, R.L. and Ward, J.W., "Current-density profiles for a Ga+ ion microprobe and their lithographic implications," *Applied Physics Letter*, vol. 51, no. 23, pp. 1960-1962, Dec 1987.

[131] Yamamura, Y. and Tawara, H., "Energy Dependence of Ion-Induced Sputtering Yields from Monatomic Solids at Normal Incidence," *Atomic Data and Nuclear Tables*, vol. 62, pp. 149-253, 1996.

[132] Ziegler, F., "SRIM Instruction Manual," http://www.srim.org, 2003.

[133] Moeller, W. and Posselt, M., "TRIDYN_FZR User Manual (Forschungszentrum Rossendorf)," 2002.

[134] H.B, Hobler, G., Lugstein, A. and Bertagnolli, E. Kim, "Simulation of ion beam induced micro/nano fabrication," *Journal of Micromechanics and Microengineering*, vol. 17, pp. 1178-1183, 2007.

[135] Taniguchi, J., Ohno, N., Takeda, S., Miyamoto, I. and Komuro, M., "Focused ion beam assisted etching of diamond in XeF2," *J. Vac. Sci. Technol*, vol. 16, no. 4, pp. 2506-2510, 1998.

[136] Kalburge, A. ,Konkar, A. ,Ramachandran, T. R. , Chen, P. and Madhukar,A., "Focused ion beam assisted chemically etched mesas on GaAs(001) and the nature of subsequent molecular beam," *Journal of Applied Physics*, vol. 82, no. 2, pp. 859-864, 15 July 1997.

[137] Itoh, F., Shimase, A. and Haraichi, S., "Two-Dimensional Profile Simulation of Focused Ion Beam Milling of LSI," *J. Electrochem. Soc.*, vol. 137, no. 3, pp. 983-988, 1990.

[138] Orloff, J., Utlaut, M. and Swanson, L., *High Resolution of Focused Ion Beam: FIB and its applications*. New York: Kluwer Academic/ Plenum Publishers, 2003, ch. 6.

[139] James, W., *Software engineering*.: PHI Learning Pvt. Ltd. ISBN: 8120335899, 9788120335899, ch. 10, p. 257.

[140] Coelho, L., "Gaussian quantum-behaved particle swarm Optimization approaches for constrained engineering design problems," *Expert Systems with Applications*, vol. 37, pp. 1676-1683, 2010.

[141] Suganuma, K., *Lead-Free Soldering in Electronics: Science,Technology and Environmental Impact*.: CRC Press, ISBN: 0824758595, 9780824758592, 2003, ch. 1, p. 7.

[142] Stoyanov, S. and Bailey, C., "Optimisation Modelling for Design of Advanced Interconnects," in *Electronics Systemintegration Technology Conference*, 2006 vol.2, pp. 1108-1117.

[143] ANSYS, "http://www.ansys.com/,".

[144] Tang, Y.K., Stoyanov, S., Bailey, C., Lu, H. , "Decision Support Systems for Eco-friendly Electronic Product," in *The 8th International Conference on Electronic Materials and Packaging*, Hong Kong, 2006, pp. 1-8.

[145] Meddendorf, A., "EE-Toolbox-a modular assessment system for the environmental optimisation of electronics," in *Electronics and Environment*, 2000, pp. 166-171.

[146] Chung, J., "A study on the trace of appropriate ecodesign strategies applying "Instep-DfE" and "IZM-EE toolbox" on a PDA," in *Environmentally Conscious Design and Inverse Manufacturing*, 2003, pp. 291-296.

[147] Yen, S.B., "The development of Taiwan's Toxic Potential Indicator (TPI)," in *Environmentally Conscious Design and Inverse Manufacturing*, 2003, pp. 632-635.

Appendix

Experiments for the focused ion beam sputtering process

Schematic of the FIB patterns

- 7 lines (Experiments 1-7)
- 2 trenches (Experiments 8 and 9)
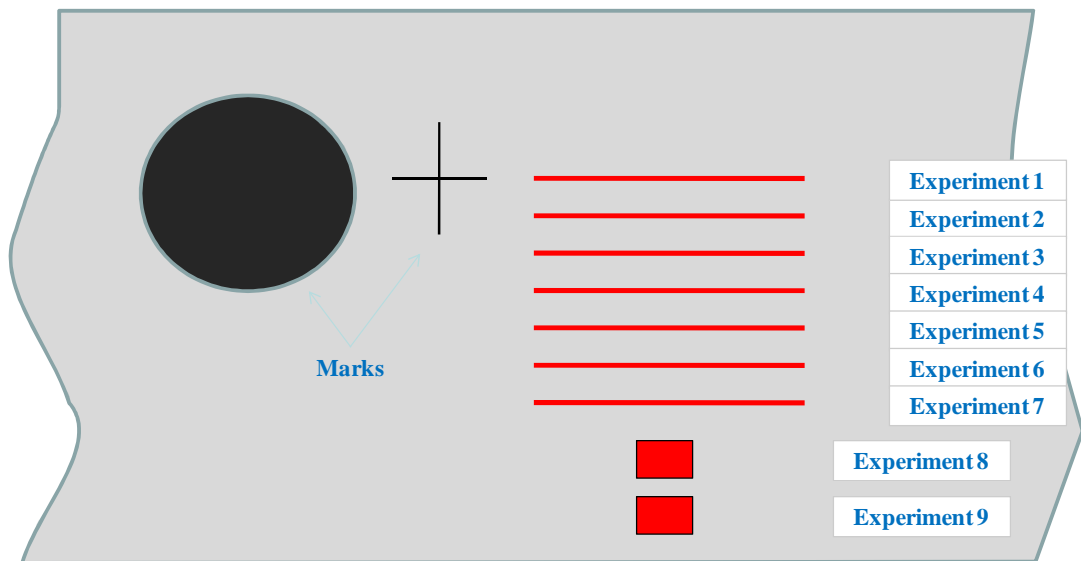
Schematic of the relative location of milled lines and trenches with respect a large circle mark and an accurate + mark

Specification of undertaken experiment

Experiment	Pattern	Size (mm)	Set depth Z (mm)	Current (pA)	Overlap (%)	Dwell time (ms)	Total Time (mm : ss)	Sputtering Yield (μm³/nC)
1	Line	100	2	70	0	1	6:58	0.15
2 (nominal)	Line	100	2	70	0	1	3:32	0.3
3	Line	100	2	70	0	2	3:32	0.3
4	Line	100	2	70	50	1	3:32	0.3
5	Line	100	2	150	0	1	2:35	0.3
6	Line	100	2	350	0	1	1:42	0.3
7	Line	100	4	70	0	1	7:03	0.3
8	Trench	10 x 5	1	350	0	1	7:19	0.3
9	Trench	10 x 5	1	350	50	1	7:40	0.3

Experimental results
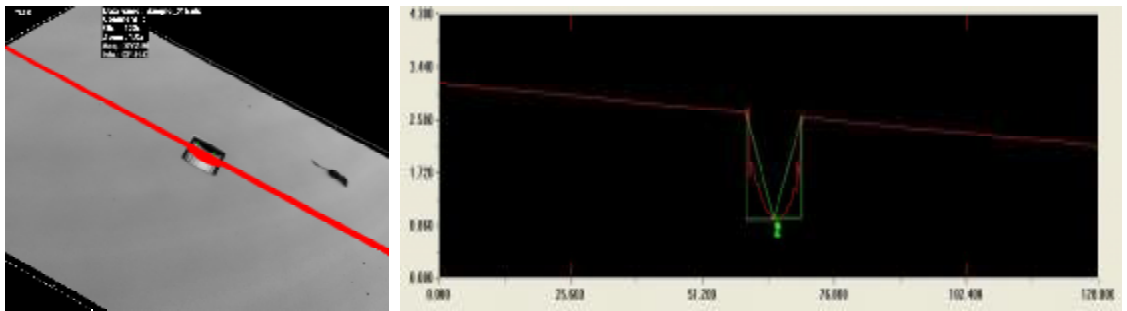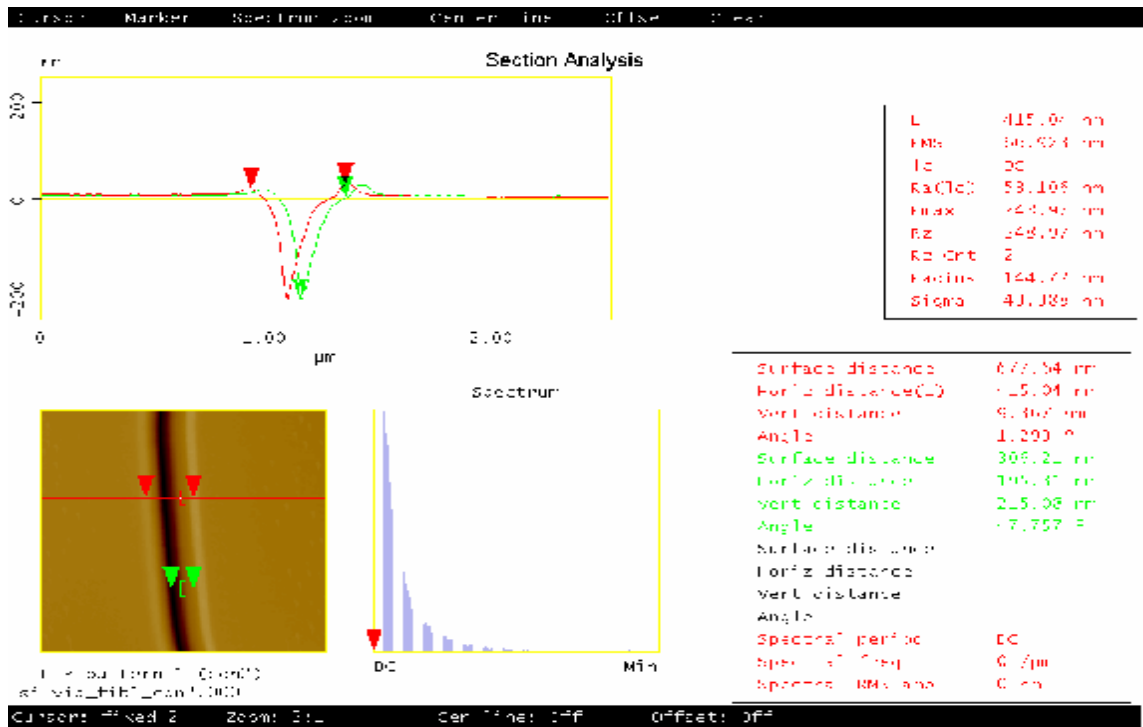
Confocal microscope image of the milled structure. The red line depicts the analysed cross section.